Fatigue Reliability of Concrete Elements in Bridges and Wind Turbines

Mankar, Amol

DOI (link to publication from Publisher):
10.54337/aau455432943

Publication date:
2021

Document Version
Publisher's PDF, also known as Version of record

FATIGUE RELIABILITY OF CONCRETE ELEMENTS IN BRIDGES AND WIND TURBINES

BY
AMOL MANKAR

DISSERTATION SUBMITTED 2021

AALBORG UNIVERSITY
DENMARK

FATIGUE RELIABILITY OF CONCRETE ELEMENTS IN BRIDGES AND WIND TURBINES

PH.D. DISSERTATION

Amol Mankar

AALBORG UNIVERSITY
DENMARK

DISSERTATION SUBMITTED JUNE 2021

Dissertation submitted: June 3rd, 2021

PhD supervisor: Prof. John Dalsgaard Sørensen,
Aalborg University

PhD committee: Associate Professor Christian Frier (chairman)
Aalborg University

Professor Bernt Leira
NTNU

Professor Dimitri Val
Heriot-Watt University (HWU)

PhD Series: Faculty of Engineering and Science, Aalborg University

Department: Department of Civil Engineering

ISSN (online): 2446-1636
ISBN (online): 978-87-7210-551-2

Published by:
Aalborg University Press
Langagervej 2
DK – 9220 Aalborg Ø
Phone: +45 99407140
aauf@forlag.aau.dk
forlag.aau.dk

Printed in Denmark by Rosendahls, 2021

AUTHOR CV

Name	**Amol Mankar**
E-mail	amol.mankar@hotmail.com
Birthday	1st May 1983
Work Experience	
Dec 2016-	**Ph.D. Fellow, MSCA (INFRASTAR)**
	Department of Civil Engineering, Aalborg University, Denmark
April 2014-Nov 2016	**Senior Structural Engineer**
	Technical Advisory Services, DNV GL, Abu Dhabi, UAE
Feb 2012-April 2016	**Senior Structural Engineer**
	Oil & Gas, DNV GL, Mumbai, India
Dec 2009-Feb 2012	**Assistant Manager Structural**
	Oil and Gas & Special Projects (OGSP), Larsen & Toubro (LnT), India

Sept 2006-Dec 2009	**Senior Engineer** Ocean Engineering Department, Engineers India Limited (EIL), New Delhi, India
Education	
2004-2006	**Masters of Technology: Structural Engineering** Department of Civil Engineering, Indian Institute of Technology Roorkee (IITR) Roorkee, Uttaranchal, India
2001-2004	**Bachelors in Civil Engineering** Department of Civil Engineering, Veer Mata Jijabai Technological Institute (VJTI), Mumbai, India
1998-2001	**Diploma in Civil and Rural Engineering** Department of Civil Engineering, Institute of Civil and Rural Engineering (ICRE), Gargoti, India

SUMMARY

Fatigue life prediction and fatigue safety verification of new and existing reinforced concrete structures are gaining substantial importance especially for two types of structures namely bridges and wind turbine foundations & support structures (onshore as well as offshore).

For wind turbine structures with an increase in the capacity of energy production, there is an increase in the size of the rotor, nacelle and assembly. This imposes higher load fluctuations, amounting to fatigue cycles of about 10^9 in a lifetime of 20 years. Thus fatigue verification becomes important for assessing the safety of these structures.

Similarly, for bridges initially with normal strength concrete dead loads stresses were high while live load fluctuations were relatively low. With the use of high strength concrete and an increase in the magnitude of vehicle loads, this situation is reversed. Further slabs of a bridge can experience more than 10^7 cycles during service life and fatigue verification becomes important for safety.

Fatigue life prediction for these types of structures is not a trivial task as both actions/ loads and fatigue resistance are stochastic in nature. Wind loads, wave loads on wind turbines and vehicle loads on bridges, vary in magnitude and frequency with time. Similarly, on the resistance side, fatigue tests on the concrete show a large scatter of fatigue life for the same test conditions.

A probabilistic approach can help to quantifying and handling the uncertainties in loads and resistances. Thus a probabilistic reliability framework is a tool that can be implemented in order to estimate fatigue safety of these structures.

Further estimating fatigue life for a reinforced concrete structure needs estimating the compression fatigue of concrete in the compression zone and estimating tension fatigue strength of the reinforcement in the tension zone. A literature study shows that for the bending failure mechanism, it is the reinforcement, which fails first. While there is a possibility of failure of the concrete in compression-fatigue when pre-stressing is used to avoid tension in concrete.

Based on the above aspects the current Ph.D. work focuses on the development of a probabilistic fatigue resistance model for compression fatigue of concrete, using a large database of fatigue test campaigns collected from literature and also probabilistic fatigue model for reinforcement based on fatigue tests conducted in past by other researchers.

The probabilistic reliability framework is exercised by using these newly developed probabilistic resistance models on three case studies by probabilistic modelling corresponding actions/ action effects on these structures. The three case studies are a reinforced concrete composite viaduct in Switzerland, an onshore wind turbine in Sweden and a gravity-based foundation of an offshore wind turbine in the Belgian part of the North Sea.

The outcome of these studies using a probabilistic framework is the probability of failure against fatigue/ fatigue reliability. This outcome can be compared against the requirements set forth in international standards. Further, it is important to keep these structures safe during the entire lifetime by maintaining the reliability levels above the limit set by the codes. For this purpose inspection and maintenance of the structure is performed. Thus a relation between inspection for the fatigue of concrete and fatigue reliability framework is established in order to update the reliability based on information obtained through the inspections. Finally, an approach for probabilistic design optimisation and reliability-based inspection planning for the fatigue of concrete structure is presented.

DANSK RESUME

Forudsigelse af udmattelseslevetid for nye og eksisterende armerede betonkonstruktioner er vigtig især for to typer af konstruktioner, nemlig broer og vindmøllefundamenter (både på land og offshore).

For vindmøller, hvor der i disse år sker en stor forøgelse i kapaciteten til energiproduktion, er der en stigning i størrelsen på rotor, nacelle, tårn og fundamenter. Dette medfører større variationer i lasterne, svarende til udmattelsescyklusser på ca. 10^9 i en levetid på 20 år. Således bliver eftervisning mht. udmattelse vigtig for at vurdere sikkerheden af disse konstruktioner.

Tilsvarende for broer, der oprindeligt er projekteret med normalstyrke beton, er spændinger fra egenlast relativt høje, mens belastningsvariationer fra trafiklast er relativt lave. Med øget brug af højstyrkebeton og en stigning i størrelsen og antal af køretøjsbelastninger ændres denne situation således at en bro kan opleve mere end 10^7 lastcyklusser i levetiden, og eftervisning mht. udmattelse bliver mere vigtig for sikkerheden.

Forudsigelse af udmattelseslevetid for disse typer af konstruktioner er ikke en triviel opgave, da både belastninger og udmattelsesstyrke er stokastiske. Vindbelastninger, bølgelast på vindmøller og køretøjsbelastninger på broer varierer i størrelse og frekvens med tiden. Tilsvarende på modstandssiden viser udmattelsesforsøg med beton en stor spredning af udmattelseslevetiden under de samme testbetingelser.

En probabilistisk tilgang kan hjælpe med at kvantificere usikkerheden i belastninger og styrker. Således er pålidelighedsbaseret analyse og design et værktøj, der kan benyttes med henblik på at modellere usikkerheder og estimere pålideligheden med hensyn til udmattelse for disse konstruktioner.

Endvidere vil det for estimering af udmattelseslevetid for en armeret betonkonstruktion være nødvendigt at estimere udmattelseslevetid for beton i tryk af beton og at estimere udmattelseslevetid af armering i områder med træk. Et litteraturstudie viser, at for bøjningssvigt i udmattelse er det armeringen, der først svigter. Når der benyttes forspænding mhp. at undgå træk, er der mulighed for udmattelsessvigt i betonen i tryk.

Baseret på ovennævnte fokuserer dette PhD studie på udvikling af en probabilistisk udmattelsesmodel for beton i tryk, baseret på en stor database over udmattelsesforsøg indsamlet fra litteraturen og også en probabilistisk udmattelsesmodel for armering baseret på udmattelsesforsøg udført af andre forskere.

Den probabilistiske pålidelighedsmodel benyttes i tre case-studier med probabilistisk modellering af belastninger på disse konstruktioner. De tre case-studier er en armeret betonkomposit-viadukt i Schweiz, en vindmølle på land i Sverige og et gravitationsfundament for en havvindmølle i den belgiske del af Nordsøen.

Resultatet af disse undersøgelser ved anvendelse af en pålidelighedsbaseret tilgang er sandsynligheden for svigt i udmattelse. Disse resultater sammenlignes med krav i internationale standarder. Det er således vigtigt at disse konstruktioner i hele levetiden opretholder at pålidelighedsniveau over det acceptable sikkerhedsniveau, der er angivet i normer og standarder. Med henblik herpå kan der udføres inspektion og vedligeholdelse af konstruktionerne. Således er der etableret en forbindelse mellem inspektioner for udmattelse af beton og kravene for sikkerhed mode udmattelse ved at opdatere pålideligheden baseret på information opnået gennem inspektioner. Endelig præsenteres metoder for probabilistisk designoptimering og pålidelighedsbaseret inspektionsplanlægning for udmattelse i betonkonstruktioner.

PREFACE

This Ph.D. research has received funding from the European Union's Horizon 2020 research and innovation programme under the Marie Skłodowska-Curie grant agreement No. 676139.

I started my Early Stage Research (ESR) position at the INFRASTAR project in December 2016 together with 11 other ESR fellows. The aim of the INFRASTAR project is to explore the effects of fatigue loads on concrete structures, namely bridges and wind turbines. The subject is looked at from a broad viewpoint; thus, the project is divided into three work packages. First work package deals with development of new monitoring and auscultation techniques for estimating and detecting fatigue phenomenon in concrete. Second work package deals with development of new and refinement of existing structure and load models for better estimation of fatigue life. Third work package where the author is employed deals with applying theoretical basis for reliability analysis and risk based optimal decision making along with coupling of monitoring information with structural reliability models. INFRASTAR project is spread across Europe (five countries) and based in eight different universities, research groups or four industrial partners. This project was a wide learning horizon on different aspects by well-managed Training weeks, Implementation days and Spring School.

For the entire three years duration of my Ph.D. I was based at Civil Engineering Department of Aalborg University, under the able guidance of Professor John Dalsgaard Sørensen. With initial work and literature study by John on the subject, I got insight in to the subject of fatigue reliability of concrete structures very quickly; and I could work further to develop my own research work efficiently.

As part of agreement with INFRASTAR, I was seconded at three institutes namely, EPFL, BAM and COWI for a total duration of six months.

First secondment was at EPFL (École Polytechnique Fédérale de Lausanne), Lausanne, Switzerland, where I got opportunity to work with second work package leader Professor Eugen Brühwiler, for efficient monitoring of bridges as well as understanding behaviour of UHPFRC (Ultra High Performance Fibre Reinforced Composite).

Second secondment was at BAM (Federal Institute for Materials Research and Testing) where I got opportunity to work with first work package leader Dr. Ernst Niederleithinger, for understanding different NDT techniques.

Third secondment was at COWI A/S, Aarhus Denmark, where I got opportunity to work with Claus Kramhøft and his group working with offshore wind turbines, for understanding aero-elastic simulation tool HAWC-2.

ACKNOWLEDGEMENTS

When I look back three years from now, I had a high paying job in the Gulf, at the same time I had a dream of undertaking a Ph.D. which got prolonged for about ten years and when I look at this opportunity everyone in my family was very supportive to me to leave that job and opt for this Ph.D. position. I am very happy while writing concluding words of my thesis, these three years passed very quick; out of which almost 10 months I was out of Denmark travelling the world for various secondments, training weeks, conferences, implementation days. I would say this Ph.D. is the highest level of international exposure where I got an opportunity to meet a lot of peers, friends and mentors.

I am very much thankful to my wife Revati and my father for constantly supporting me to undertake this challenging task. I am also very much thankful to my little four-year daughter Titiksha, who was a constant source of inspiration and learning to me, not to give up for any failure. I am also very much thankful to my mother for her support with her best wishes and prayers. I am also very much thankful to my sisters and their spouses for their encouragement during entire duration.

I would like to say thank you very much…

…to my supervisor, mentor and guide, Professor John Dalsgaard Sørensen. He was always supportive to all my stupid ideas with his great experience in the field of structural reliability. With his initial support and study of relevant literature, I could get easily into the narrow subject of fatigue reliability of the concrete structure. Despite of his very busy schedule, he was always available to me whenever possible at his office or at jds@civil.aau.dk. He was always quick in understanding different situations explained through writing and he was very quick with his motivational suggestions, answers and also very quick with each of the reviews.

...to the INFRASTAR project team: especially to the project manager Dr. Hakim Ferria and the project coordinator Dr. Odile Abraham, for great management of the project such that, every ESR could feel complete involvement and as part of the project, physically being away from the project management team.

…to Sima Rastayesh my fellow ESR and colleague at Aalborg University. She joined her Ph.D. just one month after me, she was always a supportive colleague and one of the best friends during my Ph.D.. We completed Ph.D. courses together. We exchanged a lot of ideas and wrote a few research articles together.

…to EPFL for hosting me for a period of three months special thanks to Prof. Eugen Brühwiler for his fruitful discussions which help me understand the monitoring of bridges and special new material UHPFRC.

… to Imane Bayane who was my fellow ESR at EPFL. I enjoyed her company exchanging great research ideas during my stay in Switzerland and also during her secondment at Aalborg University. She introduced me to the monitoring of bridges using electrical strain gauges and we visited one of the viaducts in Switzerland for gathering monitoring information. We studied different research areas together and wrote a couple of research article together.

…BAM and special thanks to Dr. Ernst Niederleithinger and Xin Wang who is my fellow ESR at BAM, for hosting me for a period of one month which help me understand different NDT for concrete structures.

…to COWI and special thanks to Claus Kramhøft for hosting me and giving me access to COWI systems for a period of two months where I could learn HAWC2 software.

… to Joey Velarde who was my fellow ESR at COWI. During my secondment at COWI, Joey was very supportive, he introduced me to HAWC-2 simulation tool and helped me understand basic concepts in aero-elastic modelling of wind turbines to learn during short period of time. We shared a lot of ideas for design optimization and calibration of safety factors for offshore wind turbines. I enjoyed breakfast and lunch with Joey during my COWI secondment.

…to Gianluca Zorzi who was my fellow ESR at GUD. We started to exchange ideas of implementing probabilistic approaches in foundation engineering along with Joey, as a result, Gianluca opted for a secondment at Aalborg University. I enjoyed being part of his work to apply probabilistic theory to geotechnical engineering.

…to Antoine Bassil who was my fellow ESR at IFSTTAR. We never got the opportunity to be together except for some training weeks or implementation days. However, Antoine shared great ideas about his research in the development of new techniques for detecting fatigue in concrete. We had several skype meetings during the afternoon to share ideas and finally we come up with the Probability of Detection Curves for Distributed Fiber Optics Sensors. This is complete novel research.

The thesis has been performed within the framework of the European project INFRASTAR (infrastar.eu), which has received funding from the European Union's Horizon 2020 research and innovation programme under the Marie Skłodowska-Curie grant agreement No 676139. The grant is gratefully acknowledged.

Thanks to all of you for making it possible.

Sincerely,

Amol Mankar

Thesis Title:

Fatigue reliability of concrete elements in bridges and wind turbines

Ph.D. Fellow:

Amol Mankar

Supervisor:

John Dalsgaard Sørensen

List of Published Papers:

Papers included in appendices of the thesis:

1. Mankar, A., Bayane, I., Sørensen, J. D., & Brühwiler, E. (2019). Probabilistic reliability framework for assessment of concrete fatigue of existing RC bridge deck slabs using data from monitoring. *Engineering Structures, 201*. doi:https://doi.org/10.1016/j.engstruct.2019.109788

2. Bayane, I., Mankar, A., Bruhwiler, E., & Sørensen, J. D. (2019). Quantification of traffic and temperature effects on the fatigue safety of a reinforced-concrete bridge deck based on monitoring data. *Engineering Structures, 196*. doi:https://doi.org/10.1016/j.engstruct.2019.109357

3. Mankar, A., Rastayesh, S., & Sørensen, J. D. (2019). Fatigue reliability analysis of Crêt de l'Anneau viaduct: a case study. *Structure and Infrastracture Engnieering*. doi:https://doi.org/10.1080/15732479.2019.1633361

4. Mankar, A., & Sørensen, J. D. (2019). Probabilistic fatigue design of reinforced-concrete wind turbine foundations. *13th International Conference on Applications of Statistics and Probability in Civil Engineering (ICASP).* Seoul, South Korea. doi:https://doi.org/10.22725/ICASP13.025

5. Sørensen, J., & Mankar, A. (2019). Probabilistic Design of WInd Turbine Concrete Components subject to fatigue. SMMS 2019 A RILEM spring convention and sustainable materials, systems and structures co*nference.* Rovinj, Croatia.

6. Mankar, A., Velarde, J., & Sørensen, J. (2019). Reliability-based design optimization and inspection planning of wind turbine concrete structures subjected to fatigue. Engineering Structures Journal (Submitted).

7. Velarde, J., Mankar, A., Kramhøft, C., & Sørensen, J. (2019). Probabilistic Calibration of Fatigue Safety Factors for Offshore Wind Turbine Concrete Structures. Reliability Engineering and System Safety Journal (Submitted).

Other papers

8. Mankar, A., Sørensen, J., Velarde, J., & Kramhøft, C. (2019). Optimisation of pre-stressing in gravity based foundation of an offshore wind turbine using reliability framework. *Wind Energy Science Conference 2019 (WESC).* Cork, Ireland.

9. Velarde, J., Mankar, A., Kramhøft, C., & Sørensen, J. (2019). Uncertainty Modeling and Fatigue Reliability Assessment of Offshore Wind Turbine Concrete Structure. International Journal of Offshore and Polar Engineering, 165-171. doi:https://doi.org/10.17736/ijope.2019.il54

10. Zorzi, G., Velarde, J., & Mankar, A. (2019). Reliability analysis of offshore wind turbine foundations under lateral cyclic loading. Wind Energy Science Conference 2019 (WESC). Cork, Ireland.

11. Rastayesh, S., Sørensen, J., Mankar, A., Nielsen , J., Konalki , K., & Kim, H. (2019). Bayesian networks for risk-based decision making. The 38th International Conference on Ocean, Offshore and Arctic Engineering (OMAE). Glasgow, Scotland.

12. Mankar, A., & Sørensen, J. (2018). Fatigue reliability analysis of onshore wind turbine foundations. 14th EAWE Ph.D. seminar on Wind Energy. Brussels, Belgium.

13. Mankar, A., Rastayesh, S., & Sørensen, J. (2018). Fatigue reliability analysis of Cret de l'Anneau viaduct a case study. The Sixth International Symposium on Life-Cycle Civil Engineering (IALCCE). Ghent, Belgium.

14. Mankar, A., Rastayesh, S., & Sørensen, J. D. (2018). Sensitivity and Identifiability Study for Uncertainty Analysis of Material Model for Concrete Fatigue. 5th International Reliability and Safety Engineering conference, IRSEC2018 (p. B3). Shiraj, Iran: Arzhang Printing.

15. Rastayesh, S., Mankar, A., & Sørensen, J. D. (2018). Comparative Investigation of Uncertainty Analysis with Different Methodologies on the Fatigue Data of Rebars. IRSEC2018.

16. Zorzi, G., Mankar, A., Velarde, J., Sørensen, J. D., Arnold, P., & Kirsch, F. (2019). Reliability analysis of offshore wind turbine foundations under lateral cyclic loading. Wind Energy Science (WEC).

17. Rastayesh, S., Mankar, A., Bahrebar, S., & Sørensen, J. D (2019). Development of Stochastic Fatigue Model of Reinforcement for Reliability of Concrete Structures. Applied Sciences (MDPI) Journal, (Submitted).

The submitted thesis for partial fulfilment of Ph.D. degree is based on published or/and submitted scientific papers enlisted above. Scientific content of the above listed papers is used directly or indirectly in text of the thesis for to establish the link in research. Co-author statements are submitted at the faculty. As this thesis contains some copyright material for which permission from respective journals is not available so it is not acceptable for open publication in its present form.

TABLE OF CONTENTS

Chapter 1

Introduction

Throughout the world, many efforts are directed to produce ever-increasing amounts of energy for social and industrial needs while trying to keep the environmental impact as low as possible. One of the most rapidly growing sources of sustainable energy is wind energy. To cope up with energy demands by use of wind energy a trend of rapid growth in rotor size and rated power generation capacity of wind turbines intended for offshore as well as onshore installations is also clearly visible. In recent years, the use of concrete has proved to be a very economical solution to minimize the Levelised Cost Of Energy (LCOE).

Traditionally, civil engineers did not pay attention to the fatigue of reinforced concrete, since dead loads are very high (for normal strength concrete) while live loads are comparatively small and thus to very small stress fluctuations during the service life of the structure [1], [2], . However, wind turbines structures push the limits of structural engineering and enter more into the mechanical domain, mostly due to the dynamic behaviour and the ratio of live loads to dead loads. With the use of concrete for the support structure of the ever-increasing sizes of wind turbines, understanding the fatigue process in concrete has gained attention [3]. In addition, with the trend of using mechanical properties of the material to the highest extent, the importance of studying fatigue in concrete is pronounced. Similar to wind turbine structures, for bridge structures, use of high strength concrete is increased further with an increase in magnitude and intensity of traffic loads, fatigue verification of these concrete structures is an important aspect concerning safety.

Although concrete is widely used as construction material, the understanding of fatigue failure in cementitious material is lacking as a comparison to ferrous materials. The fatigue properties of reinforced and pre-stressed concrete structures are dependent on the fatigue properties of the concrete, the steel reinforcement and the pre-stressing steel. The inhomogeneous and complex structure of concrete, along with large spatial variations, the steel reinforcement and pre-stressing, initial defects in the concrete and the interaction between the steel and concrete, introduce significant uncertainties. These can be modelled to some extent in a similar way as for welded steel structures by using SN-curves and the Miner rule for linear damage accumulation, or alternatively, fracture mechanics approach.

To optimize the fatigue design of reinforced and pre-stressed concrete structures, it is important that every possible uncertainty (both resistance and action side) is estimated and considered while designing the structure. This can be achieved by implementing a probabilistic design philosophy where the structure is designed for a target reliability level. Further, fatigue reliability can be estimated by quantifying the stochastically

modelled uncertainties related to each parameter influencing the fatigue strength. The fatigue limit state may result in being the governing limit state for bridges or wind turbine kind of structures; especially due to the fact that these structures are subjected to a very high number of fatigue cycles per year and also high concentrated stresses in critical locations e.g. for wind turbines the connection between tower and foundation.

The work conducted in the present Ph.D. thesis will be applied to wind turbine foundations and tower, and the fatigue loading conditions for wind turbines will be modelled considering typical large onshore and offshore wind turbines. Further, pre-normative calibration of partial safety factors for application in design standards will be performed as well as considerations of the effect of inspection and monitoring during operation using a life-cycle approach. The work conducted will also be applied to road bridges/ viaducts.

1.1 Objective of the thesis

"The main aim of the Ph.D. thesis is to develop a probabilistic framework for reliability assessment of reinforced concrete structures with respect to compression fatigue of the concrete. This includes application within the wind turbine industry where reinforced concrete structures are widely used not only for onshore foundations but also for new, innovative designs of concrete towers both for onshore and offshore applications. The probabilistic framework is also applicable to concrete bridges", these objectives are set by EU MCSA project, INFRASTAR. The following objectives are considered in the thesis:

- Development of a probabilistic framework for reliability assessment of reinforced concrete structures with respect to fatigue.
- Application for wind turbines: foundations and innovative concrete towers.
- Application for concrete bridges.
- Calibration of partial safety factors including considerations of the effect of inspections and monitoring.

The thesis focuses mainly on the fatigue of concrete in compression and quantification of uncertainties related to resistance part (concrete fatigue resistance) thus generic uncertainty models for the action side are used from literature. The following three case studies are covered through different papers.

- Case Study #A, a composite steel box girder and reinforced concrete deck viaduct in Switzerland, see Figure 1-1: Data (construction drawings and long term monitoring data) related to this case study was available from MCS department of EPFL, Lausanne, Switzerland.

- Case Study #B, an onshore wind turbine foundation in Sweden, see Figure 1-2: Data related to this case study was available from thesis available at Lund University, [4], [5].
- Case Study #C, a Gravity Based Foundation (GBF) of an Offshore Wind Turbine (OWT) foundation in the Belgian North Sea, see Figure 1-3: Data (Construction details and Simulations) for this case study was available from COWI A/S, as COWI A/S has done the design of this GBF for C-Power.

Transfer of results from the case studies is highly dependent on the type of structure and the governing failure-mode/ limit-state (tension-fatigue, compression-fatigue, ultimate, etc.) for the structure; however, the presented probabilistic reliability framework along with reliability updating using inspections is applicable for similar wind turbines as well as bridges.

Figure 1-1. Crêt De l'Anneau: a steel-concrete composite viaduct [6]

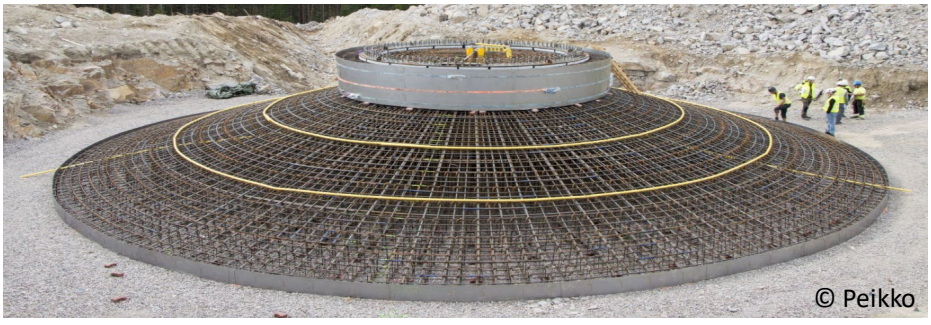

Figure 1-2. A typical foundation of an onshore wind turbine, © Peikko

Figure 1-3. GBF Thornton bank, © C-Power

1.2 Thesis outline

The current Ph.D. thesis is organised as collection of papers. Thus, the main text of the Ph.D. thesis presents links between all the papers while the papers are presented in the appendices. Figure 1-4 provides overview covering links between appendix (paper) and each chapter. Chapter 1 introduces the research work and thus the thesis. Chapter 2 presents basic theory of structural reliability assessments in probabilistic way. Chapter 3 focuses on physical understanding of the concrete fatigue and quantification of uncertainties (epistemic and aleatory) in the fatigue resistance model. Chapter 4 focuses on quantification of uncertainties on action side for different types of concrete structures subjected to fatigue, e.g. bridge decks, onshore wind turbine foundations and offshore wind turbine support structures. This chapter also gives a short example for probabilistic framework for cyclic loading on monopile foundation including soil structure interaction. Chapter 5 presents a probabilistic framework for reliability assessments using inputs from Chapter 3 for resistance part and from Chapter 4 for action/ load part. Chapter 5 also discusses about modelling of design parameters and calibration of safety factors. Chapter 6 presents reliability updating and reliability-based inspection planning along with a short overview of techniques available for inspection of concrete structures. Chapter 7 presents the conclusions and outlook. As state of the art and a literature review are presented in respective chapter for maintaining the ease in reading.

The following aspects are covered in different papers written by the author during his Ph.D. work:

- Uncertainty quantification for concrete fatigue resistance, which forms a major part of a reliability assessment (Papers 1, 3, 13 & 14).
- Uncertainty quantification for action/ load side for different concrete structures (Papers 1, 2, 3, 4, 5, 6, 7, 8, 11 and 12).
- Uncertainty quantification for foundation soil (Paper 10 & 16)
- A probabilistic framework for fatigue reliability assessment (Papers 1, 3, 12, 13 & 16)
- Structural design optimisation using a reliability framework (Papers 4 & 5)
- Uncertainty quantification of the information available through inspections and reliability updating using information from the inspections (Paper 6)

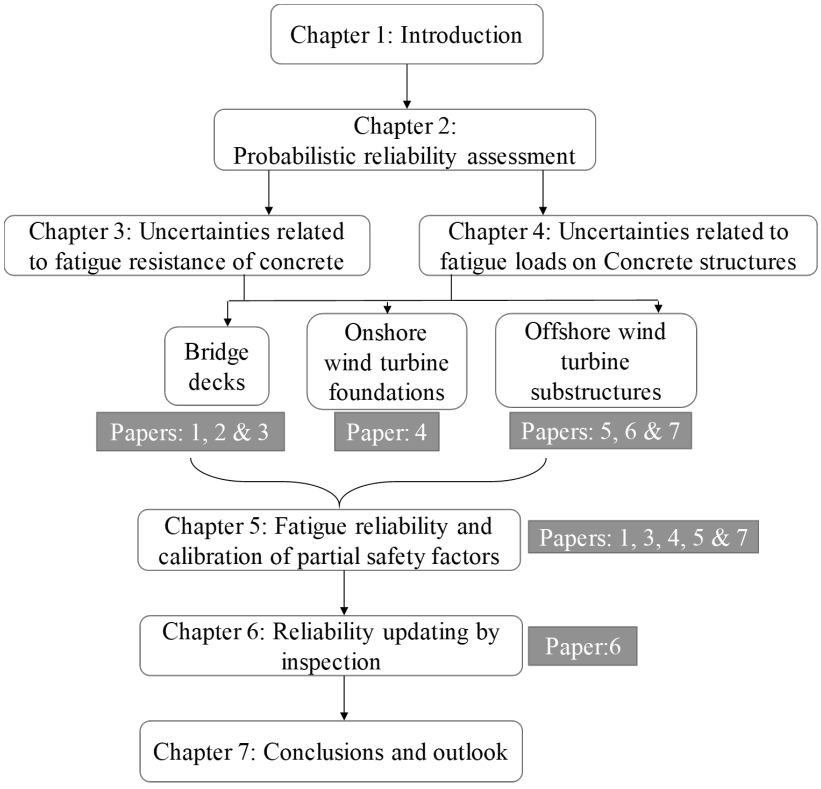

Figure 1-4. Graphical outline of the thesis

Chapter 2

Probabilistic reliability assessment

Structural engineers considered the problem of the design of structures as mainly being deterministic until the mid-twentieth century, using mean values of all loads and material strengths ignoring their dispersion or variance. The safety of structures was achieved by choosing strength of materials higher than all possible assumed load levels by a certain margin, thereby an implicit safety consideration is made accounting for the uncertainty The margin between loads and material strength was known as the safety factor and this factor served the safety of the structure or ultimately the so-called reliability of the structure. The values of these safety factors were decided based on experience and engineering judgement of similar built successful structures [7], [8].

Structural engineers during that time did not consider that it could be economically justifiable to spend some money on collecting the data regarding dispersion and uncertainties in material strength and loads on the structure [7], [8].

Later, with more knowledge on the variability of the random quantities, classical reliability theory was introduced with some initial resistance by professional engineers. Reliability considerations and methods were mainly introduced as a basis for Structural design codes which evolved by using methods of probabilistic design concepts deviating from the initial paradigms of deterministic design concepts. These codes introduced partial safety factors, which, are applied to loads and material strengths. Again, these partial safety factors were based on experience or calibrated to maintain certain levels of reliability. These target reliabilities were decided based on the type of structure and the consequence of failure. The consequences can be an economic, environmental, risk to human lives or combinations of these [7], [8] & [9].

The reliability of a structure or a structural component (structural reliability) can be defined as the probability that the structural component or the whole structure under consideration will perform its intended function throughout its planned lifetime. In addition, reliability analysis can be defined as a probabilistic technique used to estimate the probability of failure of the structure within its planned lifetime by modelling all associated uncertainties in a probabilistic way based on available information.

Structural reliability methods are divided into four groups based on a different level of idealizations/ assumptions and combinations of these to suit a particular design problem. Basically the four groups are based on the extent of information available about the problem, and how detailed the reliability assessment is [7].

- *Level I methods:* A characteristic/design value is used for modelling uncertain parameter, as for example code based partial safety factor concept.
- *Level II methods:* The mean values, the standard deviations and the correlation coefficients between stochastic variables are used to describe the uncertain parameters. These uncertain parameters are indirectly assumed to be Normally distributed. The reliability index method is an example of a level II method.
- *Level III methods:* Joint distribution functions are used to model the uncertain parameters. The reliability is measured by probability of failure.
- *Level IV methods:* In this method consequence is taken into account and risk is defined as a product of consequence and probability of failure. This method is used to compare different risk scenarios and also for cost benefit analysis.

For using these reliability methods in design, they need to be calibrated for getting consistent reliability levels. *Level I* methods can be calibrated using *Level II* methods and *Level II* methods can be calibrated using *Level III* methods so on. Most of the work in the current Ph. D. thesis uses *Level III* reliability methods.

Basic theory along with overview of probabilistic structural reliability assessment is furnished in [7], [8], [9] & [10]. Figure 2-1 shows steps in a typical probabilistic reliability assessment, once the target reliability level of the structure is defined and significant failure modes are identified. Each identified failure mode can be modelled using a limit state equation $g(x)$ along with uncertainties using the stochastic variables $X = \{X_1, X_2, \dots\}$.

$$M = g(x) = R(x) - S(x) \tag{2-1}$$

where M is the safety margin, $R(x)$ the resistance (typically material strength) and $S(x)$ the load effects. Design point is considered where the limit state equation is satisfied i.e. resistance is equal to load effects.

When the limit state equation $g(x)$ is linear then the reliability index is a ratio of expected value of the safety margin 'M' over the corresponding standard deviation, which is also known as simple reliability index or Cornell's reliability index [11].

Probability of failure can be obtained from reliability index in the following way, Table 2-1 shows most commonly used reliability indices with corresponding failure probabilities:

$$p_f(X) \approx \Phi\big(-\beta(X)\big) \tag{2-2}$$

$\Phi()$ is defined as the standard normal distribution.

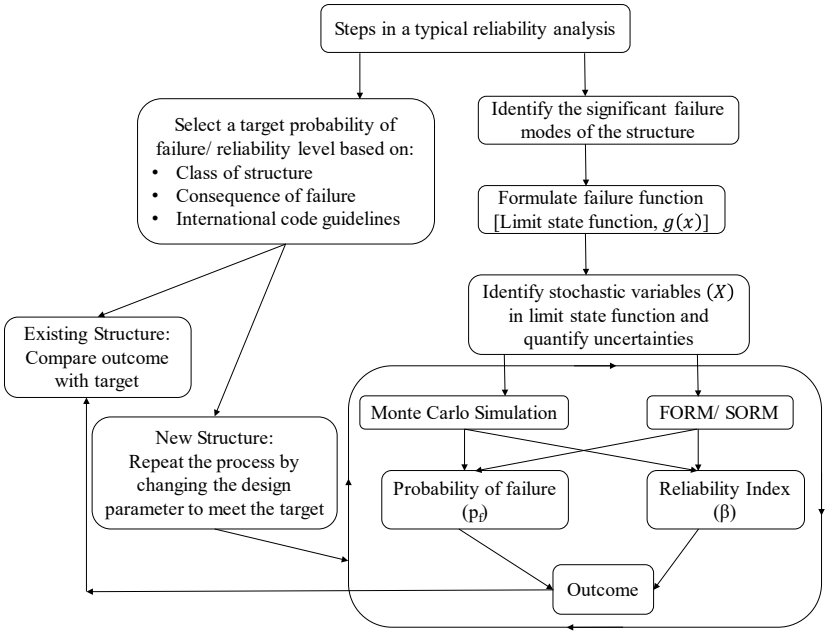

Figure 2-1. Steps in a typical reliability analysis

Table 2-1 Relation between failure probability p_f and β

p_f	10^{-6}	10^{-5}	10^{-4}	10^{-3}	10^{-2}
β	4.7	4.3	3.7	3.1	2.3

The probabilistic design of wind turbine components or reliability assessments is being initiated within the wind turbine industry. Wind turbines are basically designed based on the IEC 61400 series of standards where the new IEC 61400-ed. 4 [12] indicates a target reliability level which can be used for a probabilistic design. This standard also describes the basis for the calibration of material partial safety factors to the given target reliability level. Details on probabilistic design and reliability assessment of wind turbines can be found in [13], [14], [15] and [16], all these studies are limited to steel support structures.

Probabilistic design is not very common in the bridge industry; the design is based on design standards with partial safety factors. However, for assessment of existing bridges for safety or with life extension purposes, probabilistic reliability assessments

are performed to optimize the infrastructure from economic and ecological perspectives. Eurocode EN1990 [17] provides some aspects for assessment of new structures by a probabilistic approach and presents an indicative target accumulated reliability index for a lifetime of 50 years against fatigue, also some countries have codes e.g. Swiss codes SIA-261, [18] for new structures and SIA-269, [19] for existing structures. Most designers apply a code-based verification using partial safety factor approach, while few researchers e.g. [20], [21], [22], [23], [24], [25] [26] and [27] have demonstrated fatigue reliability of bridges using probabilistic approaches. However, again most of the studies are limited to steel bridges or its components.

The current Ph.D. thesis is limited to considering the fatigue limit state (failure mode) for concrete components of wind turbines and bridges. Fatigue resistance modelling of the concrete material is presented in Chapter 3, while, fatigue loads on bridges and wind turbines are presented in Chapter 4. Both chapters also cover modelling of corresponding uncertainties.

Chapter 3

Modelling of fatigue resistance of concrete and related uncertainties

3.1 Overview

Before modelling of uncertainties associated with the fatigue resistance of concrete a few basic concepts are presented e.g. the relation between static strength and fatigue strength, uncertainties associated with static strength of concrete, different ways to model fatigue resistance, and changes in properties of concrete during cyclic loading. All these aspects are explained in sections 3.2 to 3.2.4 of this chapter based on a literature review. Section 3.2.5 deals with modelling of uncertainties associated with fatigue resistance of concrete based on a compiled database from literature while the final stochastic fatigue resistance model is presented in Paper 1 of Appendix A. Section 3.2.6 shows the relative importance of uncertainty associated with concrete fatigue based on a case study of a GBF of an OWT.

For fatigue of reinforced concrete, it can, in general, be relevant to consider the following cases: fatigue of concrete in compression and fatigue of reinforcement in tension. Therefore, section 3.3 explains important issues of fatigue of reinforcement, and behaviour of reinforced concrete. Section 0 presents a stochastic fatigue resistance S-N model for reinforcement bars based test data available in the literature. Section 3.3.2 presents details about a stochastic fatigue resistance model for linear elastic fracture mechanics for reinforcement which is also presented in detail in Paper 3 of Appendix C.

3.2 Fatigue of concrete

3.2.1 Static strength vs fatigue strength of concrete

Fatigue strength of concrete is assumed to be relatively reduced as the compressive strength increases due to brittle behaviour of the concrete; relation between the fatigue strength and the compressive strength is presented in equation (3-1). The fatigue strength is related to the age of concrete at the time of fatigue loading and a corresponding reduction factor α_{fact} was proposed in [28], which is later modified in [29] based on [30] stating that this reduction factor leads to uneconomical design.

$$f_{cd,fat} = f_{cd}\,\alpha_{fact} = \underbrace{0.85\ \beta_{cc}(t)\ \frac{f_{ck}}{\gamma_c}}_{f_{cd}} \underbrace{\left(1 - \frac{f_{ck}}{40\ f_{ck0}}\right)}_{\alpha_{fact}} \tag{3-1}$$

where

$$\alpha_{fact} = \begin{cases} Eurocode: 1 - \frac{f_{ck}}{250} \\ MC\ 1990: 1 - \frac{f_{ck}}{25 \cdot f_{ck0}} \\ MC\ 2010: 1 - \frac{f_{ck}}{40 \cdot f_{ck0}} \end{cases}$$

f_{ck} is characteristic compressive strength.

f_{cd} is design compressive strength.

f_{ck0} is fatigue reference strength equal to 10 MPa.

$\beta_{cc}(t)$is a factor describing development of strength of concrete with time.

γ_c is partial safety factor on static strength of concrete.

Figure 3-1 shows the reduction of the fatigue strength compared to the compression strength imposed by different international codes on fatigue strength, the Eurocode [31] curve is not visible since it overlaps with MC 1990 [28]. Eurocode [31] and MC1990 [28] curves get regressive after a characteristic compressive strength of 125 MPa and thus adds an additional safety which is explicitly not mentioned in these codes. They are applicable for strengths up to 125 MPa only. MC 2010 [29] is applicable up to f_{ck} 200 MPa. Similar strength reduction is exercised by the DNV code [32] by the use of a factor 'C2'.

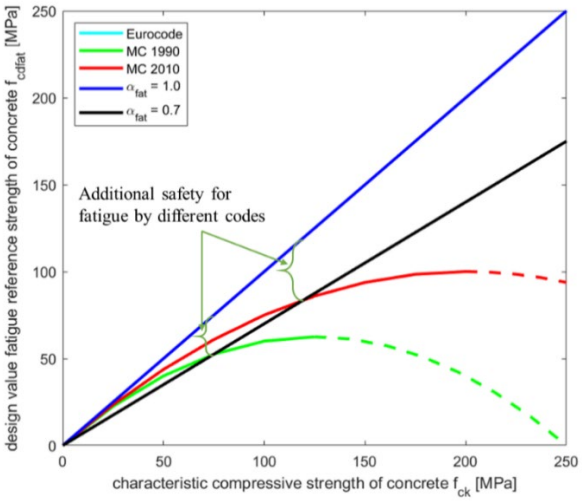

Figure 3-1 Static strength vs fatigue strength (Blue line represent compression strength)

3.2.2 Time dependent (cycle dependent) properties of concrete

Concrete changes mechanical properties during the lifetime, e.g. under uniaxial cyclic stresses permanent strain gets increased with a reduction in stiffness, see Figure 3-2. This happens mostly due to continuous micro-cracking process that results in a macroscopic behaviour as shown in Figure 3-2, [33], [34]. By representing the strain and stiffness evolution as a function of the number of cycles, typical three-stage curves are obtained. In the first stage degradation rate is high but decreasing, for the second stage is this rate is stable and constant, in the third stage degradation grows very quickly until failure is reached [33], Figure 3-3. Figure 3-3 further shows the degradation process in the form of development of micro and macro cracks in concrete. The left figure at the bottom shows pre-damaged material structure (small black lines indicate micro-cracks) even at the initial no loading stage. These cracks get further developed during fatigue lifespan; figures to the right show cracking patterns at 10%, 50%, 90% and 100% of the fatigue life.

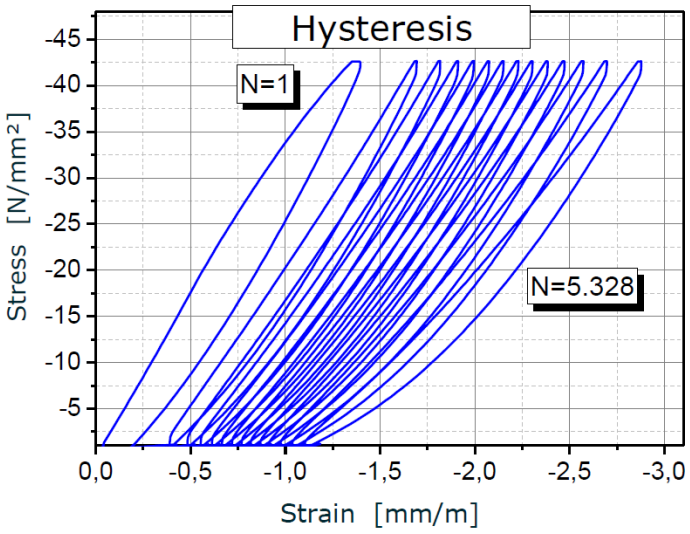

Figure 3-2 Development of stress-strain-behaviour [34]

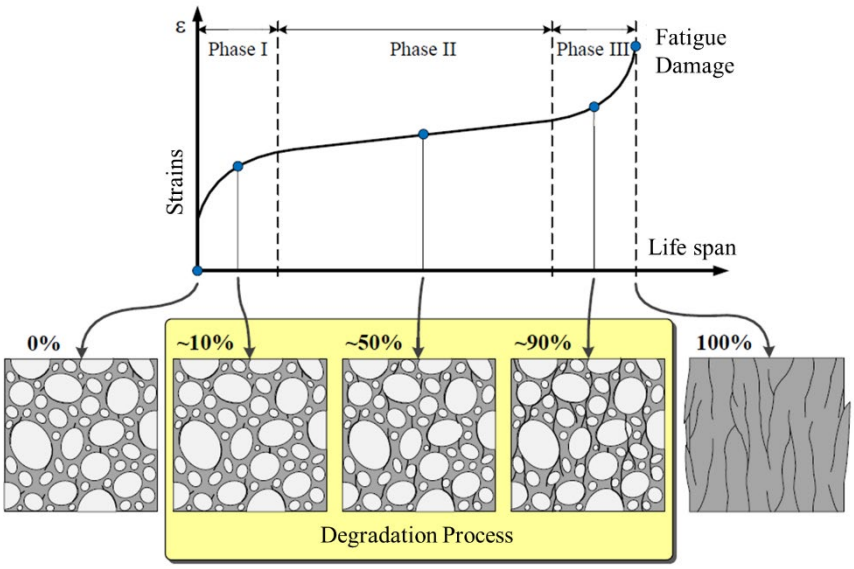

Figure 3-3 Fatigue cracks development during lifetime within concrete [34]

3.2.3 Modelling of fatigue resistance: Concrete

Current section describes theory behind the modelling of fatigue-resistance, especially for concrete material. For fatigue, which is characterised by cyclic loading, three different aspects/models are in use to describe fatigue of concrete. First aspect focuses on an empirical approach using Wöhler curves [35] or so-called SN (stress versus number of cycles) curves along with Palmgren-Miner rule [36], [37] of linear damage accumulation; this model is widely used and described in various international standards (e.g. [32], [28], [29], [31], [38] etc.), which is also the current focus of thesis. Second approach is based on fracture mechanics' principles, which considers crack propagation, a natural way to study material like concrete. Few researchers [39] explain about the application of the concept of fracture mechanics in concrete using principle of energy dissipation but typically limited to the ultimate limit state and not cyclic loading i.e. fatigue limit state. There is one way to describe fatigue behaviour is by using strain-stiffness relationship [40], as shown in Figure 3-3, however, prediction of fatigue failure using this approach is still underway.

S-N relations are obtained through laboratory tests on concrete cylinders typically 100mm diameter and 300mm height (1:3 proportion), with multiple stress cycles between upper and lower stress limits. These stress limits are expressed as a fraction of the concrete compressive strength and can be written as $S_{max} \cdot f_{ck}$ and $S_{min} \cdot f_{ck}$. The value of S_{max} and S_{min} are thus between 0 and 1.

Results of the laboratory tests ([41], [42], [43], [30] etc.) on concrete cylinders/ cubes show an almost linear relation between the logarithm of the number of cycles to failure and fraction of static compressive strength S_{max} to which the element is subjected. Further, it is observed that the number of cycles to failure is dependent on the fraction of static compressive strength S_{min} as well. An increase in S_{min} results in an increase in the number of cycles to failure since the increase in S_{min} results in a reduction in the amplitude of the stress cycles. Finally, the number of cycles to failure for concrete elements is not only dependent on stress range but also on the mean level of the stress. Thus fatigue resistance of concrete cannot be completely defined by S-N curves and a Goodman diagram [44] is needed.

3.2.4 Uncertainty associated with static strength of concrete

The compressive strength of concrete, f_c, at the age of 28 days from a cylinder of 300mm height and 150mm diameter (standard test specimens in standard conditions), [45] and [46]. All other properties of concrete are (e.g. tensile strength, modulus of elasticity, compressive strain and fatigue strength) derived based on f_c.

This compressive strength of concrete encompasses uncertainties (both aleatory and epistemic). Modelling of f_c stochastically is described in literature e.g. [10], [47], [31] and [48] et al.

The stochastic modelling explained in Dansk standard [47] is adopted for this thesis and related all papers. Based on [47], the concrete compression strength is modelled as lognormal distributed with a mean value of f_{cm} and a standard deviation σ_{fc}. The associated Coefficient of Variation is $V_{fc} = 0.14$.

3.2.5 Modelling of uncertainty in fatigue resistance of concrete

SN-curves for concrete fatigue are presented in various international codes and standards e.g. [32], [28], [29], [31], [38] and are generally developed based on data from test campaigns e.g. [41], [43], [30], [42]. All researchers, codes and standards accept scatter in the concrete fatigue test data and typically propose characteristic SN-curves and partial safety factors to obtain design SN-curves. Review of the literature shows that there is a lack of probabilistic / reliability-based assessment of the concrete structures subject to fatigue failure and thus a lack of stochastic models for fatigue resistance of concrete. With the aim to obtain such stochastic models a large database of tests conducted for compression fatigue on concrete is collected and compiled from literature namely, [49], [30], [43], [50] and [34]; it consists of 600+ laboratory tests, from 10-11 experimenters. These tests cover the following variables:

- compressive strength from 26 MPa - 226 MPa,
- stress range from 5% to 95% of static compressive strength,
- load cycle frequency from 1-65 Hz covering up to 15 million cycles.

Analysis of the data shows that none of these variables has a significant influence on the fatigue life of the concrete (number of cycles to failure) when the stress ranges for tests are expressed as fractions of the static compressive strength. Thus all variations in the data set for the same testing conditions are assumed to represent the variability/ uncertainty of the fatigue life prediction of an SN-curve model and is modelled as:

$$\log N_F \Rightarrow f\{S_{max} \& S_{min}\} + \epsilon \tag{3-2}$$

where, N_F is the number of cycles required for failure which is a function of S_{max} and S_{min}. ϵ models the model-uncertainty which is assumed to be unbiased and Normally distributed. With Normally distributed un-biased error (ϵ), the regression analysis and the parameter estimation is performed using Maximum Likelihood Method (MLM) and one of the parameter is the standard deviation of the error (σ_ϵ) itself. MLM provides us with the option to include runouts present in the dataset, [8]. Equation (3-3) shows a typical MLM function, which takes care of runouts in parameter estimation and provides a better fitting, compared over other methods e.g. least square fitting where runouts cannot be directly included.

$$\min_{A,\sigma_\epsilon} \mathrm{L}(A, \sigma_\epsilon) = \min_{A,\sigma_\epsilon} \left(\prod_{i=1}^{N_F} P(N_i(A, \sigma_\epsilon) = n_i) \cdot \prod_{i=1}^{N_R} P(N_i(A, \sigma_\epsilon) \geq n_i) \right) \tag{3-3}$$

where L is the likelihood function, A is the set of parameters to be estimated, N_F = number of observations where fatigue failure of the specimen was observed and N_R = number of observations where runouts (no failure) were observed. In addition, MLM provides us with statistical / parameter (epistemic) uncertainty associated with each parameter, which can be directly used in reliability analysis. Paper 1 of Appendix A presents the stochastic fatigue resistance model obtained from the database and procedure mentioned above.

3.2.6 Relative importance of uncertainty related to fatigue resistance of concrete

An uncertainty modelling and fatigue reliability assessment of an offshore wind turbine concrete foundation is performed (Paper 9, [51]) considering the uncertainties associated with:

- Structural model (steel resistance, concrete resistance, the mass of nacelle, hub mass, tower thickness & damping ratio)
- Soil (shear modulus & Poisson's ratio)
- Metocean parameters (wind speed, turbulence intensity, wind shear, wave height, wave period, water depth, drag and inertia coefficients for hydrodynamic calculations)
- Fatigue damage (model, stress, post-tension, damage ratio, concrete)

The study (Paper 9, [51]) concluded that uncertainties related to fatigue resistance of concrete (X_m) play a very important role compared to all other uncertainties in a fatigue limit state assessment [51]. A similar conclusion forms part of Paper 7 of Appendix G. Figure 3-4 shows variance decomposition [52] of fatigue damage (D_f) for two cases Stochastic Load Stochastic Resistance (SLSR) and Stochastic Load Deterministic Resistance (SLDR). Variance decomposition factor (β) have similar properties as α factors in reliability analysis. These factors are calculated by normalising the simple regression coefficients with the ratio of standard deviations of output to input parameters. They vary from -1.0 to +1.0, where an absolute value close to 1.0 shows high importance of the input parameter while a value close to zero shows low importance of the input parameter, [53].

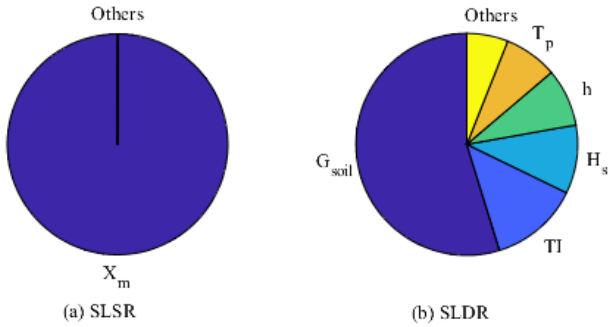

Figure 3-4 Variance decomposition of D_f at interface based on linearized damage models (taken from [51])

3.3 Fatigue of reinforcement

A special wear process occurs between contact areas of two materials due to relative motion under vibration or some other similar force [54]. This phenomenon is known as fretting fatigue. For eccentric fatigue loading on the reinforced-concrete specimen, this results in an increase in the number of load cycles to failure, showing re-distribution of the stresses in the concrete part. Such a process sheds off the load from most initially damaged compression zone to less damaged zones in the vicinity while at the same time the total and permanent strains are increasing. This large re-distribution capacity within concrete results into brittle fatigue-fracture of reinforcement [33].

Partially pre-stressed concrete (PPC) is widely used for bridges and marine structures. The fatigue behaviour of PPC shows that tensile non-pre-stressed reinforcement governs the fatigue life of PPC. This may typically be due to differences in bond behaviour of non-pre-stressed reinforcement as compared to pre-stressed reinforcement with concrete and also large redistribution of stresses within concrete. Different codes specify the concept of cracked section analysis and the plane section

concept such that the ratio of the strain range between pre-stressed reinforcement to normal reinforcement shall be close to unity. However, measured strain range ratio of pre-stressing steel to normal steel is less than unity which is caused by the respective difference in bond behaviour with concrete [55].

In a reinforced-concrete element fatigue failure of concrete is unlikely to occur if the concrete is in good condition i.e. concrete is not suffering from any deterioration mechanism (cracking) due to rebar corrosion, frost or aggregate-alkali reaction [56], [57]. In most cases, the failure of reinforcement governs the fatigue life of a reinforced concrete element.

Different researchers [58], [59] tested reinforcing bars for fatigue in the laboratory and found that the number of cycles to failure is proportional to stress range when plotted on a log scale, similar to welded steel details. A stochastic fatigue resistance model is developed based on data available and presented in Paper 15 and section 0. Further [57] showed that the Linear Elastic Fracture Mechanics (LEFM) approach can be used to estimate the fatigue life of reinforced concrete elements by estimating the life of a fatigue critical reinforcement bar, a stochastic model for the LEFM approach is presented in Paper 3 of Appendix C and in section 3.3.2.

3.3.1 Stochastic fatigue resistance model (S-N) for reinforcement

For steel reinforcement bars used in concrete, SN curves are recommended by various international codes e.g. [28], [29], [32], [31]. Fatigue behaviour of reinforcement is similar to that of steel in welded offshore structures, mainly described by only one slope in SN curves. The relation between the number of cycles required for failure and the stress range is expressed as:

$$\begin{gathered} N_i = K\Delta S_i{}^m \\ \text{or} \\ \log(N_i) = \log(K) - m\log(\Delta s_i) \end{gathered} \tag{3-4}$$

where N_i is the number of cycles to failure with stress range Δs_i in test number i. K and m are fatigue parameters to be fitted by MLM here using test data [58] & [59]. A stochastic fatigue resistance model was proposed in by [60]; however, it includes only data from only one laboratory test, [58]. The uncertainties in fatigue life (N) can be taken care of by an error term ϵ and equation (3-4) can be rewritten as:

$$\log(N_i) = \log(K) - m\log(\Delta s_i) + \epsilon \tag{3-5}$$

where ϵ represents the model uncertainty of the fatigue life model and is Normally distributed with mean value equal to zero and standard deviation σ_{ϵ}. As these parameters are estimated using a limited number of data; consequently they are subject to epistemic uncertainty. The covariance matrix of these parameters can be

obtained as negative inverse of the Hessian matrix being obtained from the second-order derivatives of the log-likelihood function, [61]. From the covariance matrix, it is typically observed that the parameters K and m are highly correlated with correlation coefficient (ρ) larger than 0.98; so, there will be multiple solutions to the problem of parameter estimation. Therefore the slope parameter m is generally fixed to 5.0 and the parameter K is estimated along with the model uncertainty/ the standard deviation of the error (σ_ϵ). The estimated value of σ_ϵ is in the study described in (Paper 15, [62]) observed to be equal to 0.39 which represents a quite large uncertainty compared to typical SN-curves for the fatigue of e.g. welded details.

3.3.2 Stochastic fatigue resistance model (LEFM) for reinforcement

[57] presented a case study for fatigue safety of a railway bridge by estimating the fatigue life of critical reinforcement bars by LEFM, this study is limited to the deterministic domain. The author further developed a similar model using the Paris-Erdogan Law [63] in the stochastic domain. Further, the LEFM approach is calibrated to the probabilistic S-N model explained in section 0 by matching the annual probability of failure, [9]. The attempted LEFM approach works well along with calibration, and detailed results are presented in Paper 3 of Appendix C.

Chapter 4

Reliability of bridges, wind turbines and soil foundations

Safety of the bridges and wind turbines can be governed by different limit states e.g. extreme/ ultimate limit state (extreme wind, extreme wave, extreme vehicle loads), fatigue limit states and maybe also accidental limit states. As the current Ph.D. thesis focuses only on the fatigue limit state of concrete structures, this chapter describes the importance of fatigue safety of existing bridges in section 4.1, describing fatigue critical elements in a typical road bridge. Further, section 4.1 explains a need for realistic load models for estimating reliability, such a load model for Case Study#1 is proposed in Paper 2 in the Appendix B. Similarly section 4.2 of this chapter gives an idea about wind load on wind turbines support structures and how industry perform the fatigue design of the support structure. Further critical components in wind turbines from a fatigue point of view are listed. Lastly, an example of the cyclic behaviour of foundation and reliability estimation by probabilistic modelling of soil is presented in section 4.3.

4.1 Fatigue reliability of existing bridges

A large proportion of today's bridges have been in service for more than sixty years and now experience traffic loading and volume far in excess of original design assumptions [64]. Although many of these structures have outlived their originally intended design lives, they are often sufficiently safe, especially if they are adequately maintained. While user safety is paramount, cases arise where over-conservative load models, coupled with simplistic dynamic amplification factors, result in the unwarranted condemnation of adequate bridges. These conservative load models are justified for new construction, with the argument that providing significant load-carrying reserves is necessary for the case of higher traffic loads in the future and strengthening of existing bridges is extremely expensive [65]. This implies that many existing bridges have a much larger load-bearing capacity than required and this is often due to conservative calculation models. This also implies that there is a potential for extending the use of these bridges.

With aim to maintain ecological balance (limit CO2 emissions), structural engineers need to justify the safety of available infrastructure by using the capacity of the mechanical/ strength properties of the materials to the extent possible; then traditional methods (use of the code defined load models and the partial safety factor approach) of safety verification are no longer adequate for efficiently maintaining bridges [66]. Therefore, load models and assessment techniques more appropriate to existing bridges are required. One of the recent codes in Switzerland is dedicated to existing

bridges with a reduction factor for loads to estimate the safety of existing bridges, [19]. However, again these reduction factors are general and a further reduction in the loads is possible with the use of site-specific measurements/ monitoring performed during the service life the bridges. An inverse engineering study/ a generic method to arrive at a load model from monitoring is proposed in Paper 2 of Appendix B.

4.1.1 Fatigue critical components in reinforced-concrete bridges

Stress variations imposed by vehicle loading on the deck slab of bridges are relatively larger compared to stress variations in support structures, piers and girders [64]. Thus, most critical elements with respect to fatigue of these bridges turn out to be the deck slabs. These slabs may experience more than 10^7 cycles during their service life [57].

4.1.2 Action model for a viaduct bridge

As stated in section 4.1 there is a need to use correct loads for estimating the safety of the bridge, one way is to long term monitor the behaviour of the bridge, which directly yields action effects. However, in such case it is not possible to compare these action effects with load models available in different international codes. Paper 2 of Appendix B presents an inverse study to obtain the load model from the monitored action effects model by using Peak Over Threshold (POT) method to filter vehicles from data. Further to understand the behaviour of the bridge a simple calibration test is performed by moving a truck of known axle weights. This calibration test is used to train the model for the inverse study, lastly, the obtained load model is compared with Weight In Motion (WIM) data and found close proximity. Using such a load model and Finite Element (FE) model of the bridge it is possible to estimate fatigue safety of other components where monitoring is not performed. Further Paper 1 of Appendix B uses this developed load model along with a FE model to estimate fatigue reliability of an existing bridge viaduct in Switzerland, Case Study #A.

4.2 Fatigue load on wind turbines

Offshore wind turbines can be subjected to very high number of cycles generating from waves alone further it would experience wind load cycles which are almost 10 times wave cycles [67], [68]. An integrated analysis of the complete structure including foundation with time history of loads is not normally carried out in the industry. Foundation designer generally passes super element of the foundation representing mass, stiffness in the form of matrices. Instead of performing a complete dynamic analysis, normally simplified approach is adopted for design using these Super elements along with Markov matrices, [69] i.e. selected load bins gathered using suitable counting method generally, rain-flow counting. A complete dynamic integrated analysis of the structure is performed only in limited cases since a large amount of numerical efforts are required.

4.2.1 Fatigue critical components in wind turbines

The fatigue components in onshore wind turbines and offshore wind turbines are studied through different papers which are part of Appendices of this thesis:

- Paper 4 of Appendix D discusses the design optimization and probabilistic fatigue design by identifying the foundation of an onshore wind turbine (Case Study #B) as a fatigue critical component.
- Paper 5 of Appendix E discusses the probabilistic design of components by identifying the interface between cone and shaft of a gravity based foundation of an offshore wind turbine (Case Study #C) as a fatigue critical location.

4.2.2 Fatigue of grouted connections

For more than 40 years offshore oil and gas structures have used grouted connections to connect the foundation pile to the pile sleeves/ jacket legs in fixed offshore jacket kind of structures. The annulus between the jacket sleeve and the pile is filled with grout, further to enhance the performance of the grouted connection shear keys or weld beads are used by industry in grouted connection region on both outside of piles and inside of sleeves. The same concept is used by the wind industry for offshore jacket structure as well as mono-pile structures [70]. However, these structures experience rather severe dynamic loading compared to oil and gas structures. The dynamic loading includes axial loads as well as moments. For monopile kind of structures high pressure zone gets developed in grouted connections locally in both ends of grout connection locally. Due to this high-pressure zone there is local fracture and crushing of grout. As these bending stresses repeat periodically the fatigue performance of the grout becomes essential [50].

4.3 Reliability analysis of an offshore wind turbine foundations under lateral cyclic loading

The behaviour of offshore wind turbine foundations is to a large extent governed by Soil-Structure Interaction (SSI) and thus influenced by the large uncertainty in modelling the soil parameters and the soil behaviour. A probabilistic framework could be helpful for geotechnical engineers to assess the performance of the foundation within operational tolerance prescribed by wind turbine manufactures, certification agencies, underwriters or insurance companies. Such a framework estimating, the reliability not exceeding the tilting allowance of 0.25° for an offshore foundation in the form of monopile supporting a 10 MW wind turbine, is outlined in Figure 4-5 and proposed in Paper 15 [71]. An important aspect related to modelling and quantification of uncertainties is also part of the work during this Ph.D. is explained here.

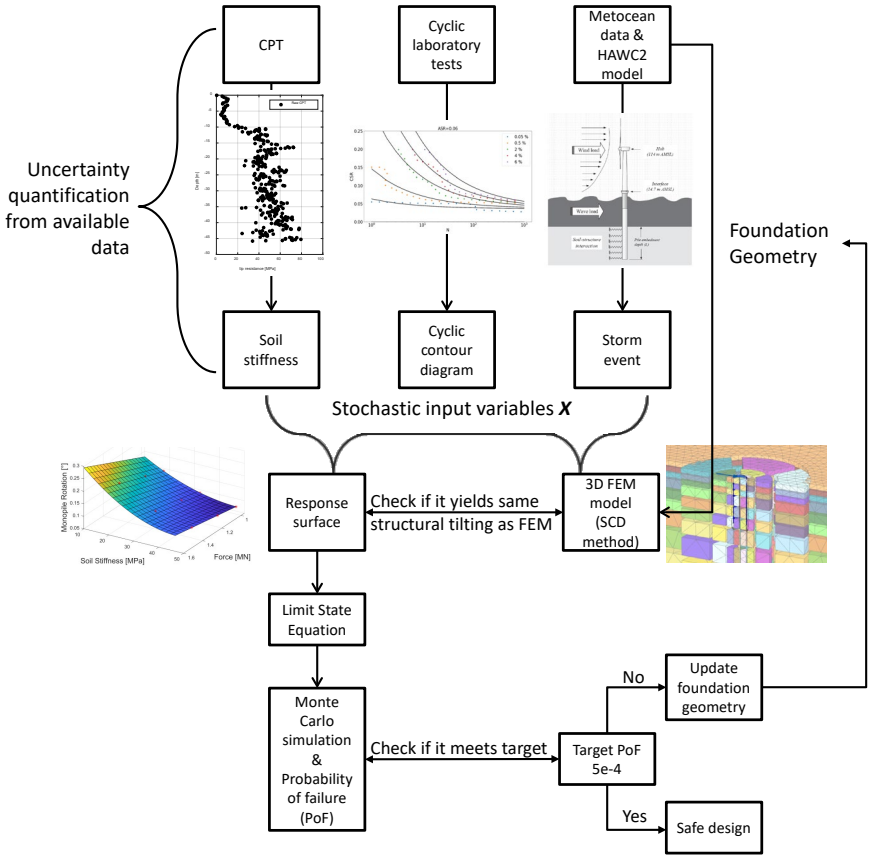

Figure 4-5 Methodology for reliability analysis (taken from [71])

A limit state equation can be formulated to be used to estimate the probability of exceedance of the tilting allowance often equal to 0.25° [72] which can be compared against reliability requirements set forth in international standards e.g. [12].

$$g(X) = \theta_{max} - \theta_{calc}(X)$$
$$P_f = \mathrm{P}[g(X) \leq 0] = P[\theta_{max} \leq \theta_{calc}(X)] \quad (4\text{-}1)$$

where, θ_{max} is maximum tilting allowance often equal to 0.25° [72]

$\theta_{calc}(X)$ is estimated tilting of pile after extrement event

(X) are stochastic parameters related to soil, loading, cyclic contour diagram based on which $\theta_{calc}(X)$ is calculated.

There could be different types of uncertainties associated with this problem, namely natural/ physical uncertainty associated with soil properties, model uncertainties associated with understanding the behaviour of soil. Such sources of physical and model uncertainty associated with this framework are estimated based on available data for three methods namely:

- Cone Penetration Test (CPT) using an empirical relationship between tip resistance and Elastic modulus, [73].
- Cyclic Counter Diagrams (CCD), a relation between the number of cycles required to attain specific plastic strain for a specific level of mean stress and amplitude stress, [74]
- Metocean & aero-servo-elastic model, [75]

Out of these three, CCD is quite similar to the fatigue failure surface for concrete. The contour diagram aims to estimate the amount of plastic/ permanent strain in the soil as a function of the Average Stress Ratio (ASR) or the mean level of stress, the Cyclic Stress Ratio (CSR) or the stress amplitude and the number of cycles with specific ASR & CSR. In order to obtain an accurate CCD a large database of test campaign is required which would cover different average and cyclic amplitude of stresses. So a test campaign of undrained single stage two-way cyclic simple shear tests are carried out in Technical University of Berlin's Soil Mechanics Laboratories, [71]. A power-law function is used to relate cyclic behaviour of soil to the data, see equation (4-2):

$$CSR = \mathrm{X}_c \, N^{X_d} + X_e + \varepsilon \tag{4-2}$$

The parameter d represents the shape of the curve, c is a scaling factor, e is the intersection with the CSR axis, while X_d, X_c & X_e are corresponding stochastic parameters respectively and ε is the fitting error. MLM is used estimate the standard deviation of all these parameters. The shape parameter d is assumed deterministic during fitting procedure. Figure 4-6 shows a slice of fitted CCD along with dots representing the original test data.

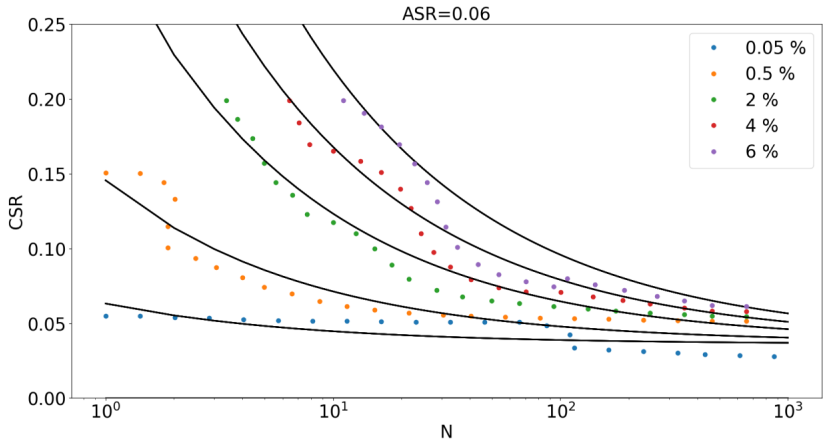

Figure 4-6: A Slice of the cyclic contour diagram at ASR = 0.06.(taken from [71])

Further, using these three input parameters a FE model of an offshore wind turbine with monopile (with a diameter equal to 8m) is prepared in PLAXIS 3D [76] to estimate the tilting of the foundation for different load parcels. Each load parcel basically represents time history load in the form of equivalent load with the same number of cycles producing the same plastic strain in soil. However, this model is computationally intensive and expensive to use for different realizations to estimate the probability of failure; therefore a response surface is established using the theory of design and analysis of experiments & linear regression [77]. This response surface is trained to yield the same tilting (θ°) as the PLAXIS 3D FE model, keeping it as a black box. Further, it was observed that the uncertainty associated with the response surface itself has a negligible impact on the final probability of failure/ reliability index. Figure 4-7 shows the obtained response surface, where red dots are simulations obtained from the 3D FE model while surface shows fitted response surfaces to the simulations. For the fitted function, the R-squared value is 0.9984 underlining a good fit of the function to the data.

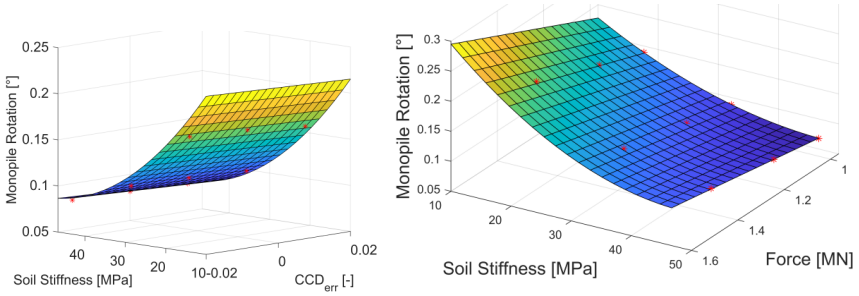

a) b)

Figure 4-7: Response surface (taken from [71])

For the current case, a reliability index of 4.03 is obtained, which is higher than the generally acceptable reliability index for an offshore wind turbine. Further, the reliability index is found to be sensitive to uncertainty in soil stiffness and uncertainty in lateral loading. It is also to be noted that the reliability index is not sensitive to uncertainty in the cyclic contour diagram and fitting error for the response surface.

Chapter 5

Fatigue reliability and calibration of partial safety factors

5.1 General safety format

"*A limit state can be defined as a state beyond which the structure as a whole or its component no longer satisfies the design performance*", [78], [79]. These limit states can be separated as follows:

- Ultimate Limit State (ULS) is a state related to failure due to reaching the ultimate capacity
- Fatigue Limit State (FLS) is a state related to the failure due to the repetitive/ cyclic loading
- Accidental Limit State (ALS) is a state related to failure due to an accidental event during operations
- Serviceability limit state (SLS) is a state related to aesthetics or durability or normal use

The safety format used in limit state standards is schematically illustrated in Figure 5-1 showing the probability density function for load in blue and for resistance in red. As the current work is limited to the FLS, the loads are the fatigue loads (e.g. wind & wave on wind turbines and vehicle & wind loads on bridges) and the resistance is the fatigue resistance. The distinction between the load and the load effect is important for the cases with nonlinear behaviour see section 5.3. For illustration in Figure 5-1 this relation is assumed linear. As shown in Figure 5-1 the load and the resistance are modelled as stochastic variables and described by their probability density functions (here Normal distributions for illustration). Then each quantity (load and resistance) will vary around its mean value and the first step in introduction of safety is to use corresponding characteristic value. Characteristic values are typically the 98^{th} percentile of the load and the 5^{th} percentile of the resistance. The second level of safety measure is the limit state format and its use of safety factors on both load and resistance. These safety factors will increase characteristic load to design load and reduce characteristic resistance to design resistance and limit state requirement is decided based on these design quantities, e.g. γ_c explained in section 3.2 is a safety factor on the resistance side. The probability of failure is estimated, based on integral as follows, [80], see also Figure 5-1:

$$P_F = P(R \leq S) = P(R - S \leq 0) = \int_{-\infty}^{\infty} F_R(x) f_S(x) dx \tag{5-1}$$

where $F_R(x)$ is the cumulative distribution function for resistance while $f_S(x)$ illustrates the probability density function for loads/ load effects. It should be noted that the probability of failure is not determined as the overlap of the two curves.

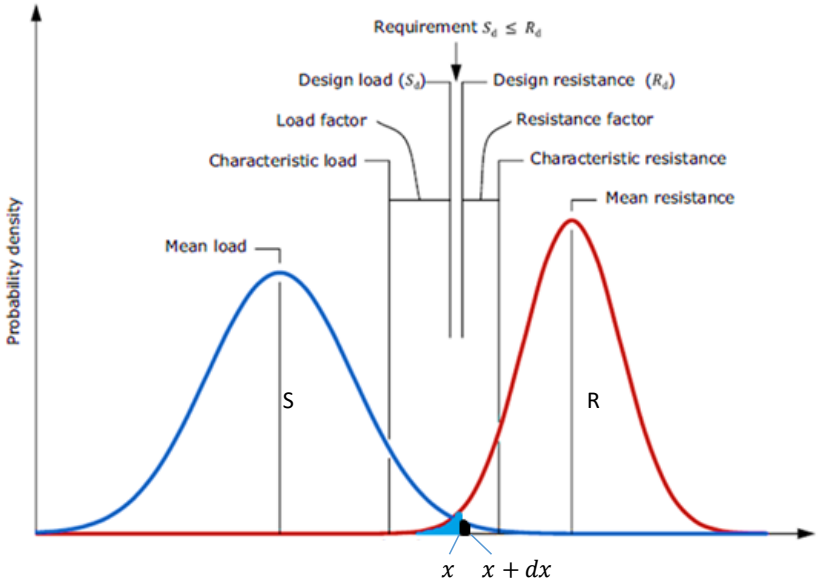

Figure 5-1 Design principles: estimating probability of failure

5.2 Target Reliability Level

For a reliability-based design approach, the structural reliability acceptance criteria typically is expressed by a *target reliability* level. The requirements for the safety of structural elements/ failure modes/ systems are often represented in terms of *a target reliability level* or *a target probability of failure,* based on an economic optimization considering initial building costs and consequence of failure costs, [10]. Additionally, minimum reliability levels may be required to be fulfilled. The target reliability can be used as a control parameter for optimisation of the structure. For e.g. wind turbines these target reliability values are derived based on an assumption that of systematic rebuild or repair in case of failure.

Joint Committee on Structural Safety (JCSS) [10] proposes such target reliability indices for a reference period of one year (annual reliability indices) for ultimate limit states based on the relative cost of the safety measure and the consequence of failure. Similarly, Swiss standard SIA-269 [19] for existing structures specify the requirement of structural safety through target reliability values for a reference period of one year. These target values are again dependent on the consequence of failure. These are

estimated by a coefficient ρ representing the consequence of structural failure which is calculated as follow:

$$\rho = {}^{C_F}/_{C_w} \tag{5-2}$$

According to SIA-269 C_F refers to all direct costs in the event of failure and C_w to costs of restoration of the structure following a failure, [19]. Further, the proportionality of safety-related interventions is assessed on the basis of their efficiency taking into consideration the following aspects:

- Safety requirements with respect to individuals and society
- Availability of a structure and installation
- The extent of damage to persons, material goods and the environment
- Preservation of cultural values

The efficiency of interventions is assessed again with the coefficient EF_M which is expressed as follows:

$$EF_M = {}^{\Delta R_M}/_{SC_M} \tag{5-3}$$

where, ΔR_M represents the reduction in risk as a result of interventions and $\mathrm{SC_M}$ represents the safety costs associated with making the structure safe. A safety-related intervention is regarded as proportionate if $\mathrm{EF_M} \geq 1.0$ and considered as dis-proportionate if $\mathrm{EF_M} < 1.0$. Based on the efficiency of intervention and consequence following table summarises target reliability indices.

Table 5-2 Target values of annual reliability index

Efficiency of interventions ($\mathbf{EF_M}$)	Consequence of structural failure		
	minor $\rho < 2$	moderate $2 < \rho < 5$	Serious $5 < \rho < 10$
Low: $\boldsymbol{EF_M < 0.5}$	3.1	3.3	3.7
Medium: $\boldsymbol{0.5 < EF_M < 2.0}$	3.7	4.2	4.4
High: $\boldsymbol{EF_M > 2.0}$	4.2	4.4	4.7

As the current Ph.D. thesis is limited to reliability-based approaches, detailed financial calculations are avoided and for the Case Study #A it is assumed to have a low EF_M and serious consequences of failure; and thus the target reliability index is set as 3.7 which corresponds to a probability of failure as 10^{-4}. However, in case of wind turbines, the risk of loss of human lives in case of failure of structural elements are generally small. Therefore, an appropriate target reliability level corresponding to an

annual probability of failure is considered to be $5 \cdot 10^{-4}$ (annual reliability index equal to 3.3), see [12] and [81].

5.3 Calibration of the partial safety factors

5.3.1 Design parameter

The relation between loads and load effects is dependent on the design parameter (z) chosen for the optimisation of the structure. For performing a reliability analysis this relationship (between loads and load effects) needs to be established using a simple mechanics or detailed FE model based on the complexity of the problem and accuracy needed. A design load effect S_d is the most unfavourable combined load effect. Taking the load effect to be a single quantity derivable by the load effect function $\psi(\cdot)$, the design load effect from say n design loads $F_{d,i}$ may be expressed as, [82]:

$$S_d = \psi\left(F_{d,1}, F_{d,2} \ldots . , F_{d,n}\right) \tag{5-4}$$

The load effect function $\psi(\cdot)$ is established for bridges, onshore wind turbine foundations, offshore wind turbine gravity-based structures and offshore wind turbine foundations including SSI during the current Ph.D. work for code calibration and optimization of the structures. Note that for wind turbines typically characteristic values of loads are used as input to the numerical calculation model and a partial safety factor is applied to the obtained load effect. The effect of changing the design parameter is studied and applied in the following case studies:

1. Case Study #A, a Swiss viaduct: A FE model of the viaduct is prepared in ANSYS and the effect of changing the following design parameters is studied and presented in Paper 1 and Paper 2 of Appendix A and B respectively:
    a. The thickness of the deck slab
    b. Tensile reinforcement in the deck slab
2. Case Study #B, an onshore wind turbine foundation: A simple structural mechanics model is used to obtain action effects from actions on a wind turbine (represented by a Markov matrix for overturning moment received from M/S Siemens, [4]) based on the theory presented in [5]. The following design parameters are studied and presented in Paper 4 of Appendix D:
    a. Thickness change of foundation slab
    b. Tensile reinforcement in the foundation slab
3. Case Study #C, a GBF for an OWT: A simple structural mechanics model is used to obtain action effects from actions on wind turbines (Markov matrix obtained by from aero-hydro-servo-elastic model prepared in HAWC-2, [51]) based on the theory presented in [67]. The following design parameters are studied and presented in Paper 5, Paper 6 and Paper 7 of Appendix E, Appendix F and Appendix G respectively:

   a. The thickness of the vertical shaft of GBF
   b. Reinforcement in the shaft of GBF
   c. Pre-stressing in the shaft of GBF
4. An OWT foundation including SSI: A PLAXIS-3D-FE model is prepared and the effect of change of soil parameters is studied and a response surface is created to account for this variation considering an FE model as a black box as explained in section 4.3, and presented in Paper 16.

Out of four cases presented above the first two cases are almost similar since the governing failure mode in fatigue is bending of the slab and the effect of change of mean stress is not prominent; however for the third case study where the structure is pre-stressed (pre-stressing has a direct effect on mean stress) the modelling of the effect of change of design parameters is not trivial, which is presented in detail in Paper 7 in Appendix G.

5.3.2 Calibration of the partial safety factor

Calibration of partial safety factors by the judgement was the main method until 20-30 years ago. Reliability-based calibration of partial safety factors is applied to calibrate a lower level reliability method by a superior level reliability method, see Chapter 1. A general procedure for code calibration is presented in Paper 7 in the Appendix G and in [80]. The recommended value for the partial safety factor on resistance ($\gamma_m \; or \; \gamma_c$) for the fatigue limit state for concrete is 1.50 and could be understood as follows:

$$\gamma_m = \gamma_c = \frac{f_{ck,fat}}{f_{cd,fat}} \tag{5-5}$$

This partial safety factor (γ_m) is calibrated by varying the design parameter as explained in section 5.3, in different case studies:

1. Case Study #A (Paper 1 of Appendix A).
2. Case Study #B (Paper 4 of Appendix D).
3. Case Study #C (Paper 7 of Appendix G)

Comparison of three case studies is shown in Figure 5-2. For the case of a bridge (Case Study #A) the variation of the annual reliability index is shown for three values of the CoV of live loads due to vehicle CoV_{X_L}; similarly for the case of onshore (Case Study #B) and offshore (Case Study #C) wind turbines the variation of annual reliability index is shown for three CoVs of the wind fatigue loads CoV_{X_W}.

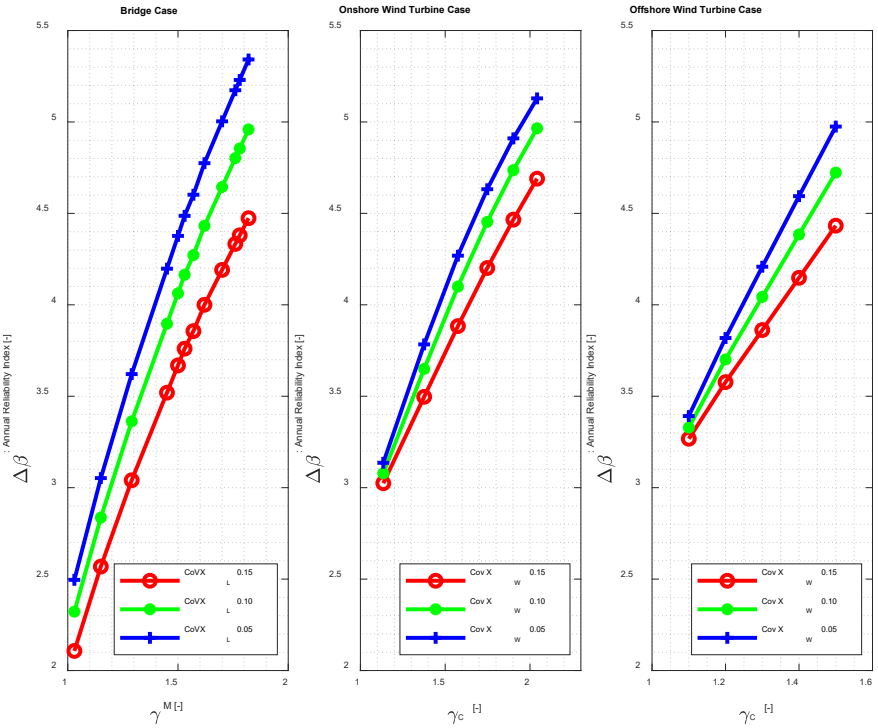

Figure 5-2 Comparison of code calibration for a viaduct bridge an onshore wind turbine and an offshore wind turbine

It can be seen from Figure 5-2 that, comparison cannot be made as the results are dependent on each structures' stress levels, for the case of the bridge it can be seen that, annual reliability value is very sensitive to partial safety factor compared to other two cases of wind turbines.

Chapter 6

Reliability updating by information from inspection

This chapter gives an overview of updating the reliability of a bridge or a wind turbine structure by information obtained from inspections. Section 6.1 gives a generic description of the steps in structural damage inspection. Section 6.2 gives an overview of some methods or potential methods for inspection of concrete for identifying and quantifying fatigue damage. Further section 6.3 estimates the uncertainty associated with an inspection technique by the Probability of Detection (PoD) approach. Section 6.4 explains the use of Bayes rule for updating probability of failure/ reliability of the structure from equality or non-equality type of information.

6.1 Structural damage inspection

Whenever a structure experience damage, it is reflected in changes in properties of the structure or with a change in the behaviour of the structure. This could be the change in mass, damping and/or stiffness, [83]. The damage characterisation process can be described as follows, [84]:

- Detection of damage: is damage present?
  Damage can be detected by identifying the change in the behaviour of the structure. The change in behaviour of a structure could be identified by a trained algorithm of a monitoring technique by means of the outlier identification process.
- Localisation of damage: where is the damage located?
  Localisation of damage needs an understanding of the behaviour of the structure in the intact state as well as in the damaged state. The localisation can be performed to some extent by understanding the critical elements identified during the design process of the structure.
- Quantification of damage: what is the size of the damage?
  Once the damage is localised, an appropriate inspection technique can be employed in order to quantify the damage.

Once all above three steps of diagnosis (damage characterisation) are over then it comes to prognosis (the consequence of the damage).

The current Ph.D. thesis work is limited to step 3) quantification of damage assuming the two other stages are already performed. Further the current work identifies uncertainties associated with the damage quantification process.

6.2 Overview of available methods for inspection of concrete

6.2.1 Ultrasonic Technique (UT)

The velocity of a UT signal changes with change in elastic modulus of the material it is passing through. Thus the UT signal can be used as an indicator as it can indicate changes in elastic modulus of concrete which may be due to damage in the concrete. Use of UT signals to detect and quantify the damage and compare with Miner's damage and further update the probability of failure based on information obtained from such a UT inspection is presented as Paper 6 of Appendix F.

6.2.2 Acoustic Emission (AE) measurements

Acoustic Emission (AE) is a passive technique that records the elastic waves generated when a local internal micro-displacement occurs in materials. The frequencies of the recorded waves range between 20Hz and 1MHz. This technique was first introduced by Joseph Kaiser in 1950 [85] and was applied latter to determine the characteristics of plain concrete in 1977 [86].

In recent decades, this technique has been used in many laboratory tests, e.g. [87], as well as in real-time monitoring to estimate the fatigue damage of concrete [88].

An AE system comprises sensors to be fixed to the concrete surface in order to convert the elastic waves into an electrical signal. The signal is then amplified with embedded or external amplifiers and transmitted with cables to the data acquisition system, where it is digitized, treated and stored. A good signal requires an appropriate coupling between sensors and concrete and well-defined filters. The signal is affected generally by the characteristics of the AE source to the sensor, the characteristics of the sensor and the measurement system [89].

To evaluate the fatigue damage of concrete structures, two methods can be used: parametric AE and signal based AE. The first method focuses on extracting parameters such as AE hits, signal strength, amplitude and energy from the filtered signal. One parameter is generally not enough to investigate a structure. Therefore, a fusion of different parameters is investigated. The second method requires analysing the waveform, and provides quantitative information about the damage.

The changes in velocity can give an idea about the relative changes of the Young modulus. The velocity of longitudinal waves V_L, and transverse waves V_t are linked to the Young modulus E of concrete and its density ρ according to equation:

$$V_L = \sqrt{\frac{EK}{\rho}} \text{ and } V_T = \sqrt{\frac{E}{2\rho(1+\nu)}} \tag{6-1}$$

If the AE signal is not attenuated, the changes in wave velocities can give a good indication about the relative changes in the Young modulus, like the UT technique.

AE provides also the possibility to detect [90], [91], [92] classify [92] and localize [93], [94] cracks in concrete. It is, therefore, a promising technique for the bridge industry and for the wind turbine industry to assess fatigue of concrete of e.g. support structures like onshore foundations and offshore gravity-based foundations.

6.2.3 Coda Wave Interferometry technique (CWI)

The traditional UT is the UPV (Ultrasonic Pulse Velocity) method, which determines the velocity by measuring the TOF (Time of Flight). UPV technique does not work well when the change in the medium is small (i.e. fatigue damage is very small) generating the same TOFs of the signals (e.g. Figure 6-3 [0.15ms 0.35ms]). When UT measurements are performed in a frequency range higher than 50 kHz, the waves interact with the heterogeneities and the wave path becomes longer and more complicated than the direct waves. Coda wave means the later arrivals of the signal (e.g. Figure 6-3 [1.5ms 1.7ms]). Different from TOF, the velocity change is considered as a dilation or compression in time [95]. CWI has a high sensitivity to subtle changes (strain, temperature, humidity, crack, etc.) in heterogeneous materials.

The basis of CWI is the velocity change and the correlation coefficient which measures the similarity of the signals. To compare with damage in the structure, the temperature and stress-induced velocity changes are very small. The opening of cracks near the sensors normally causes a velocity change of more than 1 % [8]. Thus, it is very easy to separate the cause of this change.

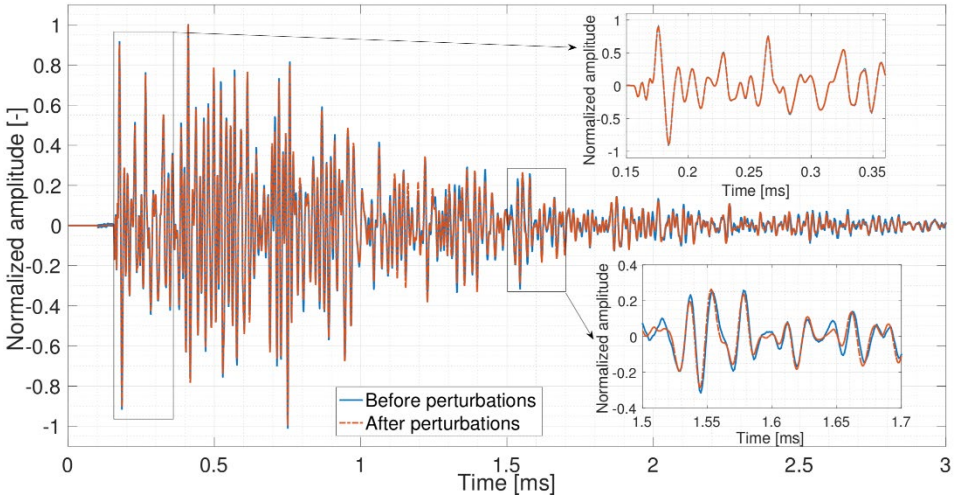

Figure 6-3 Signal recorded before and after small perturbation in the medium [96]

The classical way to do UT monitoring is to glue UT sensors on the surface of the structure (Figure 6-4 (a)). To reduce the influence of near-surface change and focus on the interior of the structure, a new type of embedded ultrasonic sensors 'SO807' is

invented [97]. These sensors can be installed inside concrete structures easily before (Figure 6-4 (b)) or after the construction.

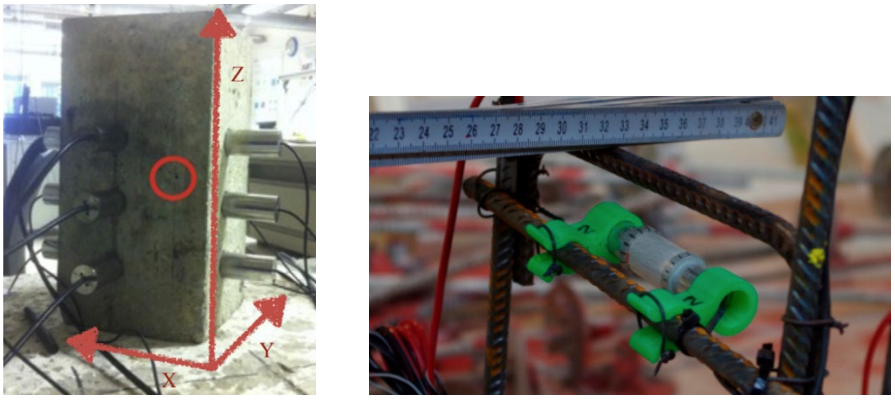

(a) (b)

Figure 6-4: (a) UT sensors are glued on the surface of the specimen [98]

(b) Embedded sensor installed on the rebar before casting the concrete [99]

Thus, the CWI method is an emerging technique for periodic inspections or continuous monitoring of concrete structures. This is a very helpful tool for an early indication of damage in the structure and works better when fused with other techniques. Further research is required to relate the outcomes of this method to fatigue damage in concrete for its commercial use. Moreover, a Probability of Detection (PoD) curve for the CWI technique can be obtained by similar to the UT technique. It is expected to have a higher probability of detection for the same crack sizes compared to UT, as this technique is very sensitive to subtle changes. Currently sufficient test results are not available to construct a reliable PoD curve.

6.2.4 Distributed Fiber Optic Sensing technique (DFOS)

Recently, Distributed Fiber Optic Sensing (DFOS) techniques showed their capacity to monitor strain all over a tiny optical fiber. This fiber is able to cover a large part of the structure, and thus replace the traditional big number of discrete strain gauge sensors. Aiming to monitor the health of a reinforced concrete structure and follow a long-term phenomenon like fatigue, DFOS sensors can follow strain in the reinforcements (Figure 6-5a) and in the concrete material in tension and compression zones. For this purpose, the optical fiber has to be surrounded by protective layers. Then, the packaged optical cable can be fixed to rebars during the construction works or glued on the surface of the structure after casting of concrete (Figure 6-5b).

(a) **(b)**

Figure 6-5: **(a)** Gluing an optical fiber on the reinforcement bars. **(b)** Packaged optical cable fixed to rebars and glued on the surface of concrete.

DFOS techniques based on the Rayleigh backscattering phenomenon can reach high spatial resolutions (in the order of millimetres) and therefore become sensitive to tiny micro-cracks in the concrete material. These discontinuities disturb the spatial strain distribution and therefore allow the detection of cracks (Figure 6-6) without being dependent on the location of the sensor contrary to discrete and long gauge sensors [100]. Recently, [95] showed that this technique can be as sensitive as CWI to micro-cracks while providing their locations and monitoring their openings [101]. As a result, this novel technique forms the only Non-Destructive-Technique (NDT) capable of following the in-depth cracks propagation. On the other hand, laying the fiber at different height can also provide information about the crack depth [102].

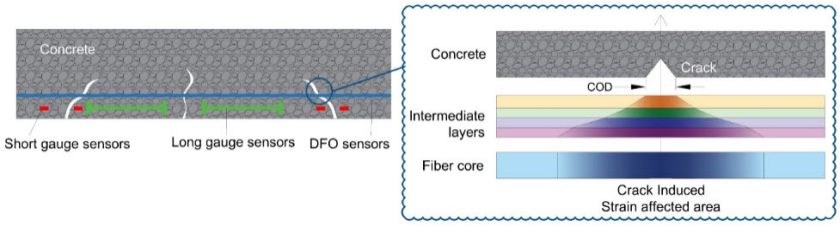

Figure 6-6: Crack detection using Distributed Fiber Optics Sensing technique [95].

6.3 PoD for DFOS technique

In order to update the information about the structure or its components, the crack detection ability of the DFOS technique for a range of crack sizes is investigated by developing a Probability of Detection (PoD) curve. The PoD is developed based on test data of three-point-bending tests performed at IFSTTAR (the French Institute of Science and Technology of Transport, Development and Networks) for 7 beams and a total of 27 DFOS lines, [95]. The PoD can be calculated based on equation (6-2) and [103]. Monte-Carlo simulations of the fitted distribution of the signal (Figure 6-7 & Table 6-1) are used to obtain the PoD [104]. In Table 6-1 ‘a’ is the crack width in mm

and 'μ and σ' represent the mean value and standard deviation of the DFOS strain signal in μm/m conditioned on the crack width 'a'. Figure 6-7 shows the relation between strain in DFOS and crack width measured by a Linear Variable Differential Transformer (LVDT). It is seen that uncertainty in the measured strain by DFOS increases with an increase in crack width. This may be dependent on the change of bond between the coating material and the concrete (due to fatigue degradation and development of micro-cracks) or change of shear lag parameter, which governs the strain in the DFOS, [95].

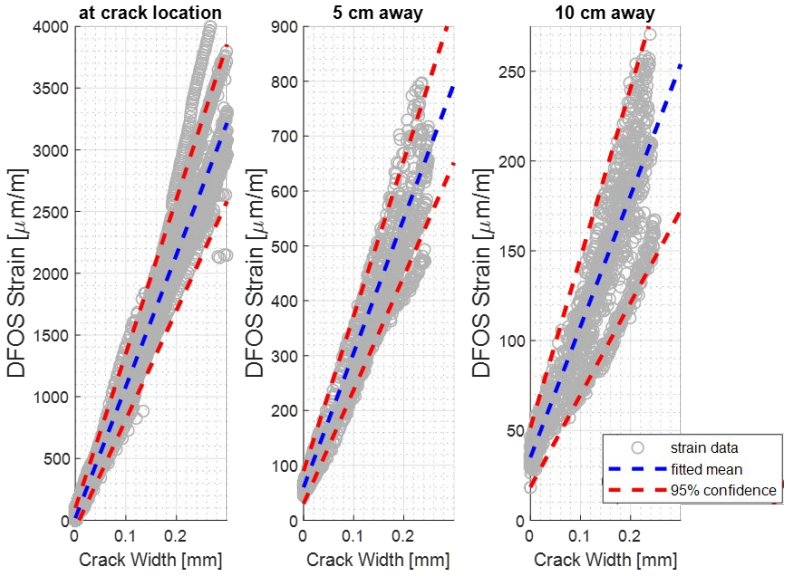

Figure 6-7 Linear regression analysis of strain data.

Table 6-1 Distribution of the signal at crack location, 5 cm and 10 cm away from crack location

Location	Mean (μ) [μm/m]	Standard Dev (σ) [μm/m]
0 cm	$10670 \cdot a + 17$	$1116 \cdot a + 50$
5 cm	$2450 \cdot a + 60$	$230 \cdot a + 18$
10 cm	$730 \cdot a + 35$	$131 \cdot a + 10$

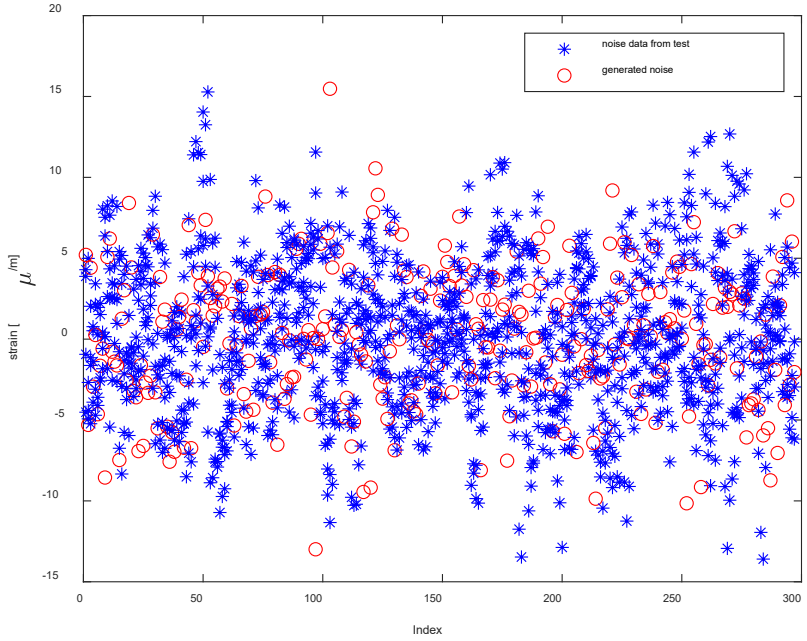

Figure 6-8 Noise in DFOS

A study of the noise at zero load level or no crack stage (see Figure 6-7) shows a normal distribution, see Figure 6-8. Thus, the noise in the system is modelled as Normal distributed with a mean of 0.24 µm/m and a standard deviation of 4.41 µm/m. Test data from a damaged structure of known crack sizes are compared to decide a threshold value. A threshold value ('t' in equation (6-2)) is generally chosen such that the probability of false alarm (Type-1 error) is minimised, [103]. For the current study, it is chosen equal to 100 µm [95], such that a very low probability of false alarm based on the study of noise is obtained. It is to be noted that the PoD is highly sensitive to the threshold. Figure 6-11 shows the sensitivity of the PoD for different threshold values for a DFO strain at 10 cm away from the crack location.

$$P(I|a) = \int_{t}^{\infty} f(s|a)ds \tag{6-2}$$

where

t is the threshold value chosen in 'µm'

a is the crack size in 'mm'

$f(s|a)$ is the conditional distribution of the signal size s, given the crack size a

$P(I|a)$ is the probability of indication or probability of detection for a given crack size.

Mean values and standard deviations of $f(s|a)$ are shown in Table 6-1.

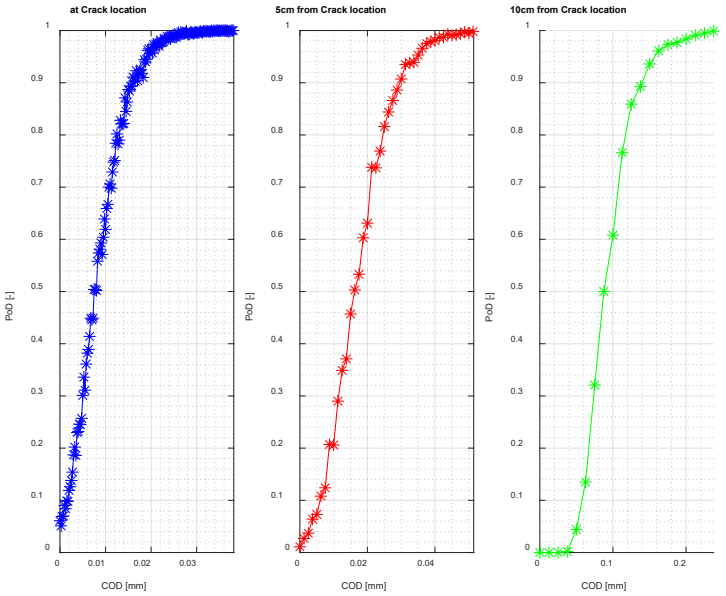

Figure 6-9 PoD for DFOS at different locations measured from the crack.

The DFOS technique can detect very low crack sizes when the strain is measured at the crack location. As a result, PoD for this method is equal to 1.0 for all sizes of the cracks of practical importance in structural engineering. For a real structure, it is difficult to know accurately the location of the crack prior to the installation of SHM and thus, DFOS strain measurements may not be captured at the crack location. Therefore, the detection of cracks is also dependent on gauge distance chosen for the DFOS measurements, e.g. if a gauge distance of 10 cm is chosen, then the maximum distance of crack from any measurement is 5 cm and PoD corresponding to 5 cm should be used. The current study uses such information of DFOS strain measured being away from the crack location and uses a PoD curve based on a maximum 5 cm distance from the damage. Figure 6-10 shows strain in DFOS at different locations: at crack, 5 cm and 10 cm away from the crack (i.e. gauge distance of 10 cm and 20 cm respectively). It is observed that the strain at crack location starts crossing the threshold at a very early stage < 1 µm. The strain at 5 cm starts detecting the crack when its size is ~12 µm, while the strain at 10 cm starts detecting the crack only when the crack size is more than ~90 µm. This also can be observed from the PoD curves

presented in Figure 6-9, e.g. at crack location, 5 cm and 10 cm, the detection starts at ~5 µm, ~20 µm ~60 µm respectively.

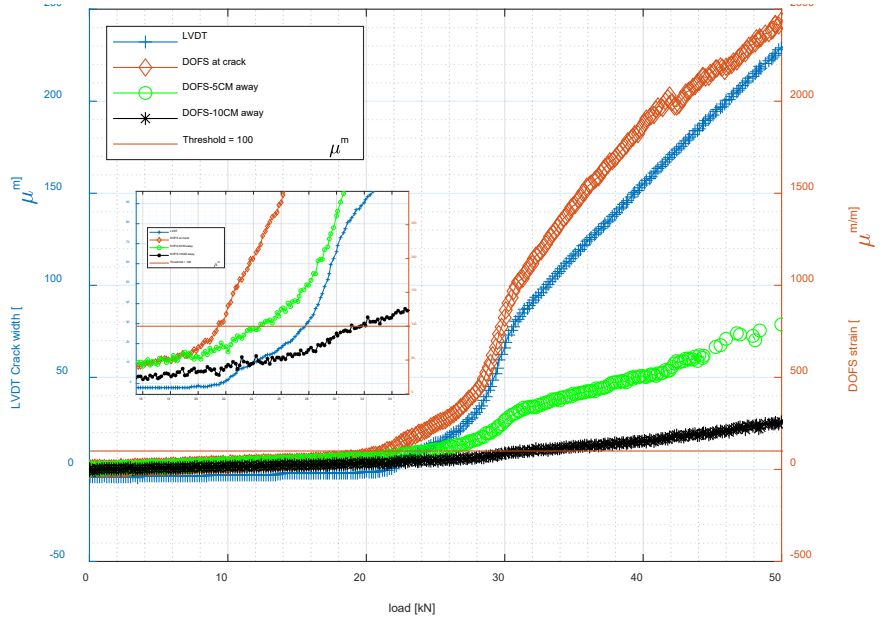

Figure 6-10 DFOS strain as function of LVDT crack width

(Small figure below legend shows a zoom-in view around the crossing threshold)

Figure 6-9 shows PoD curves obtained for different Crack-Opening-Displacements (COD) at three locations (crack location, 5 cm and 10 cm away). The first plot (at crack location) has the highest PoD as expected, whereas, at 5 cm, the PoD is slightly lower and at 10 cm, it is the lowest among the three.

DFOS techniques aim at localizing the cracks and quantifying the crack size, treating the cracking phenomenon locally. However, it is very difficult to relate this information of local crack size to the global behaviour of the structure, for concrete structures. This could be a very useful tool for materials like Ultra-High-Performance-Fibre-Reinforced-Cementitious material (UHPFRC) where discrete cracks are formed like steel. Then, for such structures with UHPFRC materials, reliability updating can be performed by using a Probability of Detection (PoD) curve developed above.

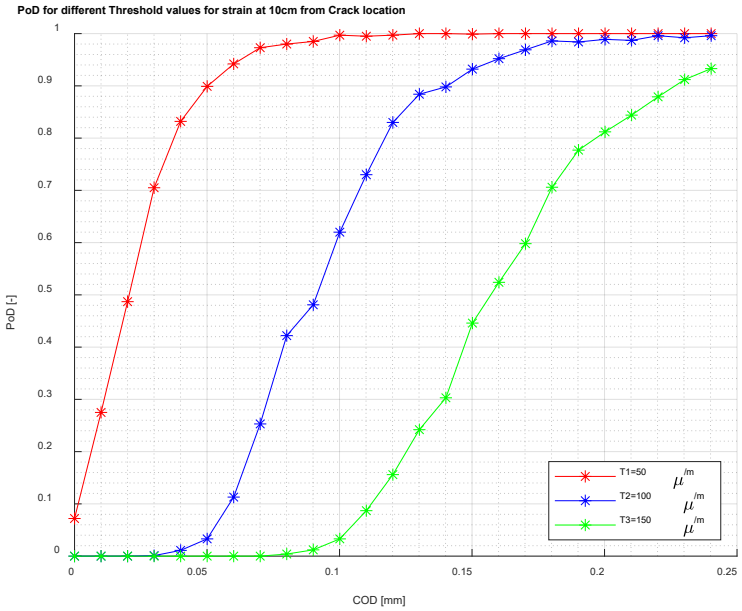

Figure 6-11 PoD for DFOS at 10 cm from crack location for different threshold values

6.4 Updating the reliability based on new information

Regular inspections or structural health monitoring checks are performed in order to assess the current state/ health of the structure. With each of such inspections, new information about the structure is available which can be used to obtain updated failure probability of the structure based on Bayes' rule. This aspect is explained in detail for a case study of an offshore wind turbine gravity-based structure in Paper 6 of Appendix F. This paper presents updating failure probability using both cases of inspection using UT when damage is found (equality type of information) and when no damage is found (in-equality type of information).

Chapter 7

Conclusions and outlook

7.1 Conclusions

The current Ph.D. thesis work is focused on fatigue reliability concrete structures with a specific focus on the fatigue of concrete in compression and quantification of uncertainties related to the resistance part (concrete fatigue resistance). The following key aspects are presented through various research papers on different case studies.

- Identification and quantification of uncertainties along with the development of a stochastic resistance model using the S-N approach for compression fatigue of concrete using a large database collected from the literature.
- Identification and quantification of uncertainties of vehicular traffic in terms of weight of vehicle and location of vehicles on the deck of a bridge. Further development of a stochastic load model by using an inverse engineering study.
- Development of a probabilistic framework for reliability estimation using stochastic resistance models, stochastic load models developed earlier and a new way of modelling the design parameter for existing structures.
- Probabilistic fatigue design and design optimisation are investigated in different case studies using different design parameters for onshore as well as offshore wind turbines.
- Code calibration of material partial safety factor for fatigue resistance of concrete.
- Development of a stochastic resistance model using the S-N approach for tension fatigue of reinforcement bars.
- Development of a stochastic resistance model using the LEFM approach for tension fatigue of reinforcement bars and calibration of the LEFM approach with the S-N approach by matching the annual probability of failures for both approaches.
- Development of PoD curve for two inspection techniques namely DFOS and UT.
- Updating the fatigue reliability of concrete structure using PoD curves.
- Development of a probabilistic framework for the assessment of a limit state related to tilting of monopile foundations by probabilistic modelling of soil stiffness.

Probabilistic models related to compression fatigue of concrete have been applied to reinforced concrete bridges, onshore wind turbine foundations and gravity-based offshore wind turbine support structures.

7.2 Outlook

The author believes that the current work can be further developed on a few more fronts:

- More fatigue test experiments should be planned not only at the material level but at the structural level or subcomponent level for a better physical understanding of fatigue phenomenon.
- Few fatigue test experiments for UPHFRC material are available at material level as well as at component level, development of stochastic resistance model should be planned based on these experiments.
- The current study is limited to component level reliability; however, an approach considering system level reliability would be relevant e.g.
    - for Case study 'A', the current study is limited to failure of just one rebar, an approach with failure entire deck slab could be relevant to study by looking at rebars as a parallel system.
    - for Case study 'C', only concrete compression failure at extreme fibre is considered; it would be relevant to consider the failure of surrounding concrete and estimate the time to failure for through-thickness failure or failure of component based on re-distribution of forces within concrete.
- Current tests on tension fatigue show only one slope of the SN-curve; more fatigue tests should be planned to investigate if there is any change in slope for high cycle fatigue at lower stress levels, see section 7.2.1.
- Vibration-based monitoring by measuring natural frequency could be a good option to estimate fatigue damage in concrete for a wind turbine; should be explored further, see section 1.16.2.1.
- Most of the current work is limited to one limit state, namely FLS; it would be very relevant to study all applicable limit states together for holistic design optimisation.

The author studied two of the abovementioned aspects during his Ph.D. which could be developed further and may be of interest to the bridge and the wind turbine industry. They are briefly described in the following section.

7.2.1 Tension fatigue of concrete

Tension fatigue of concrete was studied by researchers in the 1980s, e.g. [42], by testing beams under flexure or by concentric tension tests or by splitting tension tests. Each employed method has its own influence on the outcome in terms of the number of cycles for failure. The current Ph.D. work is limited to the study of compression fatigue of concrete; however, while comparing the data from tension and compression fatigue tests it was observed that tension fatigue varies largely from compression fatigue presenting inability of the material to take up tension fatigue. Also, no

endurance limit (some stress range and/ or mean stress, at which concrete can take up an infinite number of cycles) was found for tension fatigue of concrete, [2, p. 95/305].

The left-hand side of Figure 7-1 shows the data for tension fatigue and a thin line represent code model; similarly a MLM fit to the data is shown by a thick line. Similarly the right-hand side of Figure 7-1 shows data for compression fatigue along with its S-N curve proposed in [29] and a MLM fit proposed by the author in [6], Paper 1 of Appendix A.

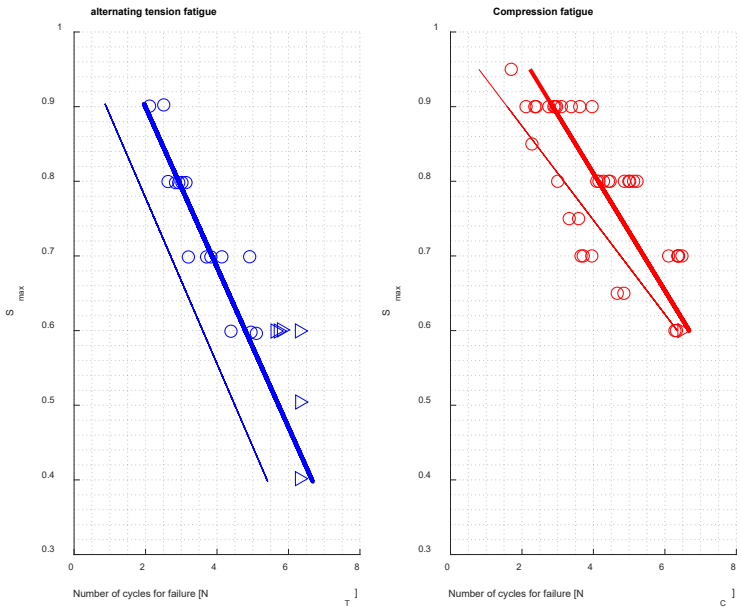

Figure 7-1 Fatigue data and different fits (code [thin] and MLM [thick])

Figure 7-2 also shows a comparison of tension and compression fatigue strength described in [29] by presenting a ratio of the number of cycles required for failure. It is also interesting to see that when Smin is increasing then the stress range gets reduced and performance in compression fatigue gets better. However, this effect is not seen on tension fatigue so the ratio of the number of cycles to failure gets increased with increasing Smin.

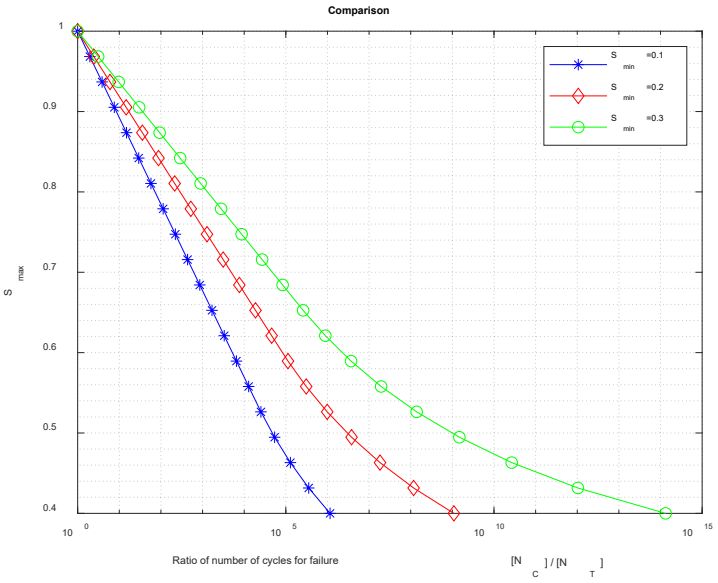

Figure 7-2 Comparison of number of failure cycles for tension and compression fatigue

6.2.1 Vibration based SHM: Frequency measurement for damage detection

HAWC-2 simulations are performed by changing Young's modulus of concrete in a GBF in order to estimate if there is any relation to the natural frequency, see Figure 7-3. This relation shows that the natural frequency is a very good indicator of normalised damage of concrete. It is to be noted that when damage level is increased by 30%, the corresponding relative change in frequency is 5% and with current measurement techniques, it is easy to measure this 5% change with great accuracy. However, it should be noted that the current results are deterministic and do not cover any uncertainties. Uncertainties need to be accounted in order to use this indicator to update the reliability of the structure, e.g. uncertainty associated with Young's modulus of concrete, uncertainty associated with variation of damage along the shaft/ cone length, uncertainty associated with structural damping assumed.

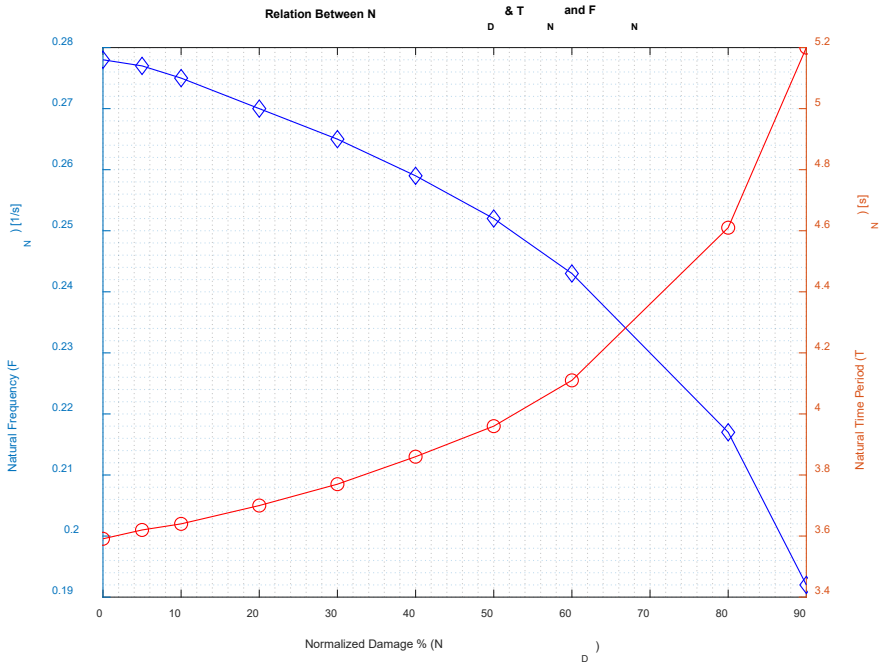

Figure 7-3 Relation between normalised damage and natural frequency/natural time period

Bibliography

[1] G. P. Mallet, Fatigue of Reinforced Concrete (State of the Art Review), Stationery Office Books (TSO), 1991.

[2] CEB 1988, "Fatigue of concrete structures - State of Art Report," CEB, Zurich, 1989.

[3] J. D. Sørensen and A. Mankar, "Probabilistic Design of WInd Turbine Concrete Components subject to fatigue," in *SMMS 2019 A RILEM spring convention and sustainable materials, systems and structures conference*, Rovinj, Croatia, 2019.

[4] F. Görasson and A. Nordenmark, "Fatigue Assessment of Concrete Foundations for Wind Power Plants," Göteborg, Sweden, 2011.

[5] H. Svensson, "Design of Foundation for Wind Turbines," Lund, Sweden, 2010.

[6] A. Mankar, I. Bayane, J. D. Sørensen and E. Brühwiler, "Probabilistic reliability framework for assessment of concrete fatigue of existing RC bridge deck slabs using data from monitoring," *Engineering Structures,* p. Submitted (ENGSTRUCT_2019_3_R1), 2019.

[7] Madsen, H. O., Krenk, S. & Lind, N. C., Methods of Structural Safety, New Jersey: Prentice-Hall, 1986.

[8] J. D. Sørensen, Notes in Structural Reliability Theory and Risk Analysis, Aalborg University, 2011.

[9] DNVGL RP 0001, "Probabilistic methods for planning of inspection for fatigue cracks in offshore structures," DNVGL, Oslo, 2015.

[10] JCSS, "JCSS PROBABILISTIC MODEL CODE," JCSS, 2000.

[11] C. A. Cornell, "A Probability-Based Structural Code," *ACI-JOurnal,* vol. 66, pp. 974-985, 1966.

[12] IEC 61400-1, Wind turbine generator systems – Part 1: Safety requirements, 4th edition ed., Geneva: International Electrotechnical Commission, 2019.

[13] J. D. Sørensen and H. S. Toft, "Probabilistic Design of Wind Turbines," *Energies,* vol. 3(2), pp. 241-257, 2006.

[14] J. D. Sørensen, "Reliability-based calibration of fatigue safety factors for offshore wind turbines," *International Journal of Offshore and Polar Engineering,* vol. 22, no. 3, pp. 234-241, 2012.

[15] H. S. Toft, "Probabilistic Design of Wind Turbines," PhD thesis, Aalborg University, 2010.

[16] D. Veldkamp, "Chances in Wind Energy - A Probabilistic Approach to Wind Turbine Fatigue Design," PhD thesis, DUWIND Delft University, Wind Energy Research Institute, Delft, 2006.

[17] EN 1990, "EN 1990 Basis of structural Design," European committee for standardisation, Brussels, 2002.

[18] SIA-261, "SIA 261 - Action on Structures," Swiss Society of Engineers and Architects, PO Box, CH-8039 Zurich, 2003.

[19] SIA-269, "Existing structures – Bases for examination and interventions," Swiss Society of Engineers and Architects, P.O. Box, CH-8027 Zurich, 2016.

[20] L. Yang, X. Xinhui, L. Naiwei, D. Yang and T. Tai, "Fatigue Reliability Assessment of Orthotropic Bridge Decks under Stochastic Truck Loading," *Shock and Vibration,* vol. 2016, p. 10 Pages, 2016.

[21] K. Kwon and D. M. Framgopol, "Bridge fatigue reliability assessment using probability density functions of equivalent stress range based on field monitoring data," *International Journal of Fatigue,* vol. 32, p. 1221–1232, 2010.

[22] M. R. Saberi, A. R. Rahai, M. Sanayei and R. M. Vogel, "Bridge fatigue service-life estimation using operational strain measurements," *Journal of Bridge,* vol. 21(5), 2016.

[23] Z. Wei and C. S. Cai, “Reliability-Based Dynamic Amplification Factor on Stress Ranges for Fatigue Design of Existing Bridges,” *Journal of Bridge Engineering,* vol. 18, no. 6, pp. 538-552, 2013.

[24] Y. Liu, H. Zhang, D. Li, Y. Deng and N. Jiang, “Fatigue Reliability Assessment for Orthotropic Steel Deck Details Using Copulas: Application to Nan-Xi Yangtze River Bridge,” *Journal of Bridge Engineering ,* vol. 23, no. 1, 2018.

[25] L. Huile, D. M. Frangopol, M. Soliman and X. He, “Fatigue reliability assessment of railway bridges based on probabilistic dynamic analysis of a coupled train bridge system,” *Journal of Bridge Engineering,* vol. 142, no. 3, 2016.

[26] Z. W. Chen, Y. L. Xu and X. M. Wang, “SHMS-Based Fatigue Reliability Analysis of Multiloading Suspension Bridges,” *Journal Structural Engineering,* vol. 138, no. 3, 2012.

[27] M. Krejsa, “Probabilistic reliability assessment of steel structures exposed to fatigue,” *Safety, Reliability and Risk Analysis: Beyond the Horizon,* 2014.

[28] fib MC1990, “FIB Model Code for concrete structures 1990,” Berlin, 1993.

[29] fib MC2010, “FIB Model Code for concrete structures 2010,” Ernst & Sohn, Berlin Germany, 2013.

[30] L. Lohaus, N. Oneschkow and M. Wefer, “Design Model for fatigue behaviour of normal-strength, high-strength and ultra-high-strength concrete,” *Structural Concrete,* 2012.

[31] EN 1992-1, “Design of concrete structures - Part 1-1: General rules and rules for buildings,” European committee for standardisation, Brussels, 2004.

[32] DNV OS C 502, “DNV OS C 502, Offshore concrete structures,” DNVGL, Høvik, 2012.

[33] C. Zanuy, L. Albajar and P. d. l. Feunte, “Sectional Analysis of Concrete Structures under Fatigue Loading,” *ACI Structural Journal,* pp. 667-677, September-October 2009.

[34] M. Thiele, “Experimentelle Untersuchung und Analyse der Schädigungsevolution in Beton unter hochzyklischen Ermüdungsbeanspruchungen,” BAM, Berlin, 2016.

[35] A. Wöhler, “Über die Festigkeitsversuche mit Eisen und Stahl (About the strength tests with iron and steel),” *Zeitschrift für Bauwesen (Journal of Construction),* pp. 73-106, 1870.

[36] A. Palmgren, “Die lebensdauer von kugellagern (The life of ball bearings),” *Zeitschrift Des Vereins Deutscher Ingenieure,* vol. 68, no. 14, pp. 339-341, 1924.

[37] M. A. Miner, “Cumulative damage in fatigue,” *American Society of Mechanical Engineers - Journal of Applied Mechanics,* vol. 12, no. 3, pp. 159-164, 1945.

[38] NEN 6723, “Regulations for concrete - Bridges - Structural requirements and calculation methods,” Netherlands, 2009.

[39] E. Brühwiler, “FRACTURE MECHANICS AND FATIGUE OF CONCRETE STRUCTURES,” MCS, EPFL, Lausanne, Switzerland, 2017.

[40] N. Oneschkow, “Fatigue behaviour of high-strength concrete with respect to strain and stiffness,” *International Journal of Fatigue,* vol. 87, pp. 38-49, 2016.

[41] K. Waagaard, “Fatigue strength of offshore concrete structures,” Det Norske Veritas, Hovik, Norway, 1981.

[42] H. A. W. Cornelissen, “Fatigue failure of concrete in tension,” Stevinweg 4, P.O. Box 5048, 2600 GA Delft, The Netherlands, 1986.

[43] G. Petkovic, H. Stemland and S. Rosseland, “Fatigue of High strength Concrete,” *American Concrete Institute (International Symposium),* pp. 505-525, 1992.

[44] J. Goodman, “Mechanics Applied to Engineering,” *Longman, Green & Company,* 1899.

[45] ISO 1920, "Testing of Concrete," International Organisation for Standardisation, 2004.

[46] ISO 3893, "Concrete--Classification by compressive strength," International Organization for Standardisation, 1977.

[47] DS-INF 172, "Background Studies in connection with the preparation of National Annexes to EN 1990 and EN 1991," DS-publikationen er på dansk., København, Danmark, 2009.

[48] MC2010, "FIB Model Code for concrete structures 2010," Ernst & Sohn, Berlin Germany, 2013.

[49] E. Lantsought, "Fatigue of Concrete under compression Database and proposal for high strength concrete," TU-Delft, Delft, 2014.

[50] E. V. Sørensen, "Fatigue life of high performance grout in dry and wet environment for wind turbine grouted connections," *Nortic Concrete Research,* vol. 44, pp. 1-10, 2011.

[51] J. Velarde, A. Mankar, C. Kramhøft and J. D. Sørensen, "Uncertainty Modeling and Fatigue Reliability Assessment of Offshore Wind Turbine Concrete Structure," *IJOPE,* 2018.

[52] G. Sin, K. V. Gernaey, M. B. Neumann, M. C.M. van Loosdrecht and W. Gujer, "Global sensitivity analysis in wastewater treatment plant model applications: Prioritizing sources of uncertainty," *Water Research,* vol. 45, no. 2, pp. 639-651, 2011.

[53] J. Velarde, C. Kramhøft and J. D. Sørensen, "Global sensitivity analysis of offshore wind turbine foundation fatigue loads," *Renewable Energy,* vol. 140, no. Sept 2019, pp. 177-189, 2019.

[54] ASM Handbook Volume 19, Fatigue and Fracture, USA: ASM International Handbook Committee, 1996.

[55] J. Han, Y. Song, L. Wang, S. Song and B. Lei, "Steel Stress Redistribution and Fatigue Life Estimation of Partially Prestressed Concrete Beams under Fatigue Loading," *Advances in Structural Engineering,* vol. 17, no. 2, pp. 179-196, 2014.

[56] M. Plos, K. Gylltoft, K. Lundgren, L. Elfgren, J. Cervenka, E. Brühwiler, S. Thelandersson and E. Rosell, "Structural assessment of concrete railway bridges: non-linear analysis and remaining fatigue life," in *IABMAS'06: 3rd International Conference on Bridge Maintenance, Safety and Management*, Porto, Portugal, 2006.

[57] M. Rocha and E. Brühwiler, "Prediction of fatigue life of reinforced concrete bridges using Fracture," *Bridge Maintenance, Safety, Management, Resilience and Sustainability,* 2012.

[58] L. P. Hansen and G. Heshe, "Fibre Reinforced Concrete and Ribbed Bars," *Nordic Concretre Research,* vol. 26, no. 2001, pp. 17-37, 2001.

[59] M. Rocha, "Fatigue Behaviour of Steel Reinforcement Bars at Very High Number of Cycles," École Polytechnique Fédérale De Lausanne, Lausanne, Switzerland, 2014.

[60] S. M´arquez-Dom´ınguez, Reliability-Based Design and Planning of Inspection and Monitoring of OffshoreWind Turbines, Aalborg: Aalborg University, 2013.

[61] D. V. Lindley, Introduction to Probability and Statistics from a Bayesian Viewpoint Vol 1+2, Cambridge: Cambridge University Press, 1976.

[62] S. Rastayesh, A. Mankar and J. D. Sørensen, "Comparative Investigation of Uncertainty Analysis with Different Methodologies on the Fatigue Data of Rebars," *IRSEC2018,* 2018.

[63] P. Paris and F. Erdogan, "A critical analysis of crack propagation laws," *J Basic Engineering,* vol. 85, pp. 528-534, 1963.

[64] M. Schläfli and E. Brühwiler, "Fatigue of existing reinforced concrete bridge deck slabs," *Engineering Structures,* vol. 20, no. 11, 1998.

[65] E. Brühwiler and J.-P. Lebet, "Updating of traffic loads on existing bridges," in *IABSE-fib Conference on 'Codes in Structural Engineering'*, Cavat, Croatia, 2010.

[66] M. A. Treacy and E. Brühwiler, "A direct monitoring approach for the fatigue safety verification of construction joint details in an existing post-tensioned

concrete box-girder bridge," *Engineering Structures,* vol. 88, no. 2015, pp. 189-202, 2015.

[67] J. Grünberg and J. Göhlmann, Concrete Constructions for Wind Turbines, Hamburg, Gernamy: Ernst & Sohn, 2013.

[68] ASTM E1049-85(2017), "Standard Practices for Cycle Counting in Fatigue Analysis," ASTM International, West Conshohocken, PA, 2017.

[69] Sandia National Laboratories, "On the Fatigue Analysis of Wind Turbines," Sandia National Laboratories, New Mexico, US, 1999.

[70] I. Lotsberg, "Structural mechanics for design of grouted connections in monopile wind turbine structures," *Marine Structures,* vol. 32, pp. 113-135, 2013.

[71] G. Zorzi, A. Mankar, J. Velarde, J. D. Sørensen, P. Arnold and F. Kirsch, "Reliability analysis of offshore wind turbine foundations under lateral cyclic loading," *Wind Energy Science (WEC),* 2019.

[72] DNV GL RP C212, "Offshore soil mechanics and geotechnical engineering," DNV GL, Høvik, 2017.

[73] T. Lunne and H. P. Christoffersen, "Interpretation of Cone Penetrometer Data for Offshore Sands," in *Offshore Technology Conference*, Houston, Texas (USA), 1983.

[74] K. H. Andersen, "Cyclic soil parameters for offshore foundation design," *The 3rd McClelland Lecture, Forntiers in Offshore Geotechnics III, ISFOG,* vol. 1, pp. 5-82, 2015.

[75] J. Velarde, J. D. Sørensen, C. Kramhøft and G. Zorzi, "Fatigue reliability of large monopiles for offshore wind turbines," *International Journal of Fatigue,* no. Submitted, 2019.

[76] PLAXIS 3D, "Reference Manual, Edited by Brinkgreve, R.B.J., Kumarswamy, S., Swolfs, W.M., and Foria F.," 2017.

[77] D. C. Montgomery, Designa and Analysis of Experiments, Westford, USA: John Wiley & Sons, Inc., 1013.

[78] DNVGL ST 0126, Support Structures for wind Turbines, Copenhagen: DNVGL, 2018.

[79] ISO 2394, “General Principles on Reliability for Structures,” International Standardisation Organisation, Geneva, Switzerland, 1998.

[80] M. Faber and J. D. Sørensen, “Reliability-Based Code Calibration: The JCSS Approach,” in *ICASP: 9th International Conference on Application of Statistics and Probability in Civil Engineeering*, Millpress, 2003.

[81] J. D. Sørensen and H. S. Toft, “Safety Factors IEC 61400-1 background document,” DTU Wind Energy, Aalborg, Denmark, 2014.

[82] DNV GL RP 0419, Analysis of grouted connections using finite element method, Høvik, Norway: DNV GL AS, 2016.

[83] M. D. Ulriksen, “Damage localization for structural health monitoring: An exploration of three new vibration-based schemes,” Aalborg University, PhD Thesis, Aalborg, 2018.

[84] A. Rytter, “Vibration Based Inspection of Civil Engineering Structures,” Aalborg University,, Aalborg, 1993.

[85] M. Ohtsu and H. Watanabe, “Quantitative damage estimation of concrete by acoustic emission,” *Construction Building Material,* vol. 15, no. 5, pp. 217-224, 2001.

[86] R. Meltzer, K. Lieb, R. Horstman, I. Moore, J. Nielsen and D. Griffin, “Acoustic Emission of Plain Concrete,” *Journal of Testing and Evaluation,* vol. 5, no. 6, p. 476, 1977.

[87] S. Urban, A. Strauss, R. Schütz, K. Bergmeister and C. Dehlinger, “Dynamically loaded concrete structures - mointoring-based assessment of the real degree of fatigue deterioration,” *Structural Concrete,* vol. 14, no. 4, 2014.

[88] M. N. Noorsuhada, “An overview on fatigue damage assessment of reinforced concrete structures with the aid of acoustic emission technique,” *Construction building Materials,* vol. 112, no. June 2016, pp. 424-439, 2016.

[89] “Nondestructive Testing Handbook, Third Edition: Volume 6, Acoustic Emission Testing (AE),” [Online]. Available:

https://www.asnt.org/Store/ProductDetail?productKey=fab658bd-d953-431f-8143-b3cfb1164886.

[90] T. Shiotani, H. Ohtsu, S. Momoki, H. K. Chai, H. Onishi and T. Kamada, "Damage Evaluation for Concrete Bridge Deck by Means of Stress Wave Techniques," *Journal of Bridge Engineering,* vol. 17, no. 6, pp. 847-856, 2012.

[91] C. Wang, Y. Zhand and A. Ma, "Investigation into the Fatigue Damage Process of Rubberized Concrete and Plain Concrete by AE Analysis," *Journal of Materials in Civil Engineering,* vol. 23, no. 7, pp. 953-960, 2011.

[92] A. Benavent, E. Castro and A. Gallego, "Evaluation of low-cycle fatigue damage in RC exterior beam-column subassemblages by acoustic emission," *Construction and Building Materials,* vol. 24, no. 10, pp. 1830-1842, 2010.

[93] S. Shahidan, R. Pulin, N. Muhamad Bunnori and K. M. Holford, "Damage classification in reinforced concrete beam by acoustic emission signal analysis," *Construction Building Material,* vol. 45, no. Aug 2013, pp. 78-86, 2013.

[94] K. M. Holford, "Acoustic Emission in Structural Health Monitoring," *Key Engineering Materials,* 2009.

[95] A. Bassil, X. Wang, X. Chapeleau, E. Niederleithinger, O. Abraham and D. Leduc, "Distributed Fiber Optics Sensing and Coda Wave Interferometry Techniques for Damage Monitoring in Concrete Structures," *Sensors,* p. 19, 2019.

[96] X. Wang and E. Niederleithinger, "Coda Wave Interferometry used to detect loads and cracks in a concrete structure under field conditions," in *European Workshop on Structural Health Monitoring Series*, Manchester, UK, 2018.

[97] E. Niederleithinger, J. Wolf, F. Mielentz, H. Wiggenhauser and S. Pirskawetz, "Embedded ultrasonic transducers for active and passive concrete monitoring," *Sensors,* pp. 9756-9772, 2015.

[98] F. Xie, L. Moreau, Y. Zhang and E. Larose, "A Bayesian approach for high resolution imaging of small changes in multiple scattering media," *Ultrasonics,* pp. 106-114, 2016.

[99] E. Niederleithinger, X. Wang, M. Herbrand and M. Müller, "Processing ultrasonic data by coda wave interferometry to monitor load tests of concrete beams," *Sensors,* p. 1971, 2018.

[100] B. Glisic, D. L. Hubbell, D. H. Sigurdardottir and Y. Yao, "Damage detection and characterization using long-gauge and distributed fiber optic sensors," *Optical Engineering,* vol. 52, no. 8, p. 087101, 2013.

[101] A. Bassil, X. Chapeleau, D. Leduc and O. Abraham, "Quantification of cracks in reinforced concrete structures using distributed fibre optic sensors," in *9th European Workshop on Structural Health Monitoring* , Manchester, United Kingdom, 2018.

[102] G. Rodriguez, J. R. Casas Rius, S. Villalba Herrero and A. J. d. S. Barrias, "Monitoring of shear cracking in partially prestressed concrete beams by distributed optical fiber sensors," in *Maintenance, Monitoring, Safety, Risk and Resilience of Bridges and Bridge Networks*, CRC Press Taylor, 2016.

[103] S. Thöns, M. Döhler and L. Long, "On damage detection system information for structural systems," *Structural Engineering International,* vol. 28, no. 3, pp. 255-268, 2018.

[104] MIL-HDBK-1823A, Nondestructive evaluation system reliability assessment, Department of Defence Handbook, 2009.

[105] M. Rosenblatt, "Remarks on a multivariate transformation," *The annals of Mathematical Statistics,* vol. 23, no. 3, pp. 470-472, 1952.

[106] A. Nataf, "Détermination de distributions de probabilités planes dont les marges sont données," *Comptes Rendus Académie des Sciences,* no. 225, pp. 42-43, 1962.

[107] A. Hasofer and N. Lind, "An Extract and Invariant First Order Reliability Format," *Journal of Engineering Mechanics,* pp. 111-121, 1974.

[108] A. Ang and W. Tang, Probability Concepts in Engineering: Emphasis on Applications in Civil and Environmental Engineering, New York: John Wiely & Sons, 2007.

[109] P. Bjerager, "Probability integration by directional simulation," *Journal of Engineering Mechanics,* vol. 114, no. 8, pp. 1285-1302, 1988.

[110] O. Ditlevsen, P. Bjerager, R. Olesen and A. Hasofer, "Direcdtional Simulation in gaussian processes," *Probabilistic Engineering Mechanics,* vol. 127, no. 5, pp. 296-300, 1988.

[111] R. Melchers, "Radial importance sampling for structural reliability," *Journal of Engineering Mechanics,* vol. 116, no. 1, pp. 189-203, 1990.

[112] P. Bernard and M. Fogli, "Une méthode de monte carlo performante pour le calcul de la probabilité de ruine," *Construction Métallique,* vol. 4, pp. 23-39, 1987.

[113] C. Bucher, "Asymptotic sampling for high-dimensional reliability analysis," *Probabilistic Engineering Mechanics,* vol. 24, no. 4, pp. 504-510, 2009.

[114] S. Au and J. Beck, "First excursion probabilities for linear systems by very efficient importance sampling," *Probabilistic Engineering Mechanics,* vol. 16, no. 3, pp. 193-207, 2001.

[115] J. D. Sørensen, "Program for Reliability Analysis and Design of Structural Systems," Aalborg University, Aalborg, 1991.

[116] FERUM, "Finite Element Reliability Using Matlab," 2010.

[117] RCP Consult GmbH - Strurel, [Online]. Available: http://www.strurel.de/.

[118] DNV GL: Proban, [Online]. Available: https://projects.dnvgl.com/sesam/download/windows/programs.html.

[119] E. V. Sørensen and B. Aarup, "Mechanical Properties of UHPFRC materials for FORIDA Wind Turbine Towers," 2012.

[120] S. Márquez-Domínguez and J. D. Sørensen, "Fatigue Reliability and Calibration of Fatigue Design Factors for Offshore Wind Turbines," *Energies,* vol. 5, pp. 1816-1834, 2012.

[121] B. Efron, "Bootstrap Methods: Another Look at The Jackknife," *The annals of Statistics,* vol. 7, no. 1, pp. 1-26, 1979.

[122] M. Seidel, “Auslegung von Hybridtürmen für Windenergieanlagen [Design of hybrid towers for wind turbines],” *Beton- und Stahlbetonbau,* vol. 11, no. 97, pp. 564-575, 2002.

[123] C. Kesseler-Kramer, “zur degradation von stahlbetonbauteilen unter ermüdungsbeanspruchung [for the degradation of reinforced concrete components under fatigue stress],” Institut für Massivbau und Baustofftechnologie (IMB), Karlsruhe, Germany, 2002.

[124] I. Lotsberg, Fatigue Design of Marine Structures, New York: Cambridge University Press, 2016.

[125] API RP 2A-WSD, “Planning, Designing, and Constructing Fixed Offshore Platforms—Working Stress Design,” American Petroleum Institute, 2014.

[126] NORSOK N-004, “Design of steel structures,” Norwegian petroleum industry, Lysaker, Norway, 2004.

APPENDICES

Appendix A.

Paper 1

Probabilistic reliability framework for assessment of concrete fatigue of existing RC bridge deck slabs using data from monitoring

Amol Mankar

Imane Bayane

John Dalsgaard Sørensen

Eugen Brühwiler

This papar has been published online (with Golden Open Access) in Engineering Structures Journal

doi:https://doi.org/10.1016/j.engstruct.2019.109788

Engineering Structures 201 (2019) 109788

Contents lists available at ScienceDirect

Engineering Structures

journal homepage: www.elsevier.com/locate/engstruct

Probabilistic reliability framework for assessment of concrete fatigue of existing RC bridge deck slabs using data from monitoring

Amol Mankar[a,*], Imane Bayane[b], John Dalsgaard Sørensen[a], Eugen Brühwiler[b]

[a] Aalborg University, Thomas Manns Vej, 23, 9220 Aalborg, Denmark
[b] EPFL ENAC IIC MCS, Ecole Polytechnique Fédérale de Lausanne, Switzerland

ABSTRACT

Assessment of existing bridge structures for inherent safety level or for lifetime extension purposes is often more challenging than designing new ones. With increasing magnitude and frequency of axle loads, reinforced concrete bridge decks are susceptible to fatigue failure for which they have not been initially designed. Fatigue verification and prediction of remaining service duration may turn out to be critical for civil infrastructure satisfying the required reliability. These structures are exposed to stochastic loading (e.g. vehicle loads, temperature loads); on the resistance side, reinforced concrete also behaves in a stochastic way. This paper presents a probabilistic reliability framework for assessment of future service duration, which includes probabilistic modelling of actions based on large monitoring data and probabilistic modelling of fatigue resistance based on test data. A case study for the steel - reinforced concrete slab of the Crêt de l'Anneau Viaduct is presented along with calibration of resistance partial safety factors for lifetime extension.

1. Introduction

Most of the reinforced-concrete bridges in Switzerland are more than ~60 years old. Deck slab is the high fatigue loaded part of such bridges due to the moving wheel loads [1–4]. However, such slabs may not be designed for fatigue [5]. Fatigue verification of reinforced concrete consists of (1) the verification of steel reinforcement in tension zone for tension fatigue, (2) the verification of concrete in compression zone for compression fatigue and (3) the fatigue verification of the bond between steel reinforcement and concrete [6].

Probabilistic fatigue reliability framework was used by many researchers [7–15], to estimate the fatigue safety of road and railway bridges. However these studies were limited to steel bridges or their components. They included different aspects e.g. [9] worked on the fitting of probability density functions over monitoring data for a steel bridge and concluded that, such approach worked well and produced reliable estimates of the probability of failure [13]. used six months operational strain measurement and extended the data by using Bootstrap Method [16]. [12] worked on reliability framework and replaced a complicated 3D finite element model by a response surface using theory of design and analysis of experiments & linear regression [17].

All the above-mentioned aspects related to the probabilistic modelling of actions or action effects can be used for reinforced-concrete bridge as well; e.g. the approach of fitting density functions, and response surface was used on a reinforced concrete bridge see, [18]. Quite a few researchers worked on the safety verification of reinforced-concrete and pre-stressed concrete bridges, by studying the response of reinforced-concrete material to fatigue loads. Schläfli and Brühwiler [5] conducted experimental campaign of testing 27 slab like beams (without shear reinforcement) and concluded that fatigue failure can only be observed when the fatigue load exceeds 60% of static ultimate loads. Failure was always observed on tensile reinforcement due to fracture of reinforcement and no failure on compression fatigue of concrete was observed. S-N relations of reinforcement bars were valid for estimating the life of the structures. A similar conclusion was obtained by testing corrugated steel plates and orthotropic reinforced-concrete decks under four point bending test where the failure was always observed in the welded parts of the corrugated steel plates and the corresponding S-N relations were valid for the estimating life [19]. Using the above conclusions [20], performed fatigue safety checks of a post-tensioned box-girder-road bridge. This work was limited to the deterministic domain and did not consider the compression fatigue of concrete. The safety of reinforced-concrete bridges were estimated by other approaches e.g. estimating the remaining life of bridges by linear elastic fracture mechanics of reinforcing bars [21]. [22] focused on the fretting fatigue of pre-stressing reinforcement, which occurs at the contact between pre-stressing tendons and inner surface of duct. Fatigue safety was studied using S-N curves similar to the ones of steel reinforcement.

On the other side [1–4], illustrated that, fatigue cracks in the compression side of concrete were possible. Firstly, flexural cracks get formed in the tension side of reinforced concrete and later these tensile

* Corresponding author.
E-mail address: ama@civil.aau.dk (A. Mankar).

https://doi.org/10.1016/j.engstruct.2019.109788
Received 1 January 2019; Received in revised form 7 October 2019; Accepted 10 October 2019

flexural cracks get progress into the compression side due to the twisting action when a moving wheel load passes these tensile flexural cracks. This reduces shear rigidity and it further degrades deck slabs if rain water ingresses these cracks. CEB Bulletin 188 [23], illustrated seventeen case histories concerning the failure of reinforced-concrete bridge structures. For most of the cases, fatigue was the main factor contributing to the failure combined with other factors. Case histories of bridges in Holland and Japan cover failure of concrete in compression zone where reinforcement was in an intact condition. [24] conducted compression fatigue tests on cubic specimens and three point bending fatigue tests on full-scale pre-cast reinforced-concrete slabs for railway tracks.. In this study, a relation between fatigue life and secondary strain rate was developed based on test campaign. [25] covered numerical validation of tests conducted by [24]. However this study was limited to the deterministic domain. [26] considered using an artificial neural network to estimate the fatigue life of reinforced-concrete decks based on crack patterns. This study had an issue that, the training of an artificial neural network needs to cover all kind of crack patterns covering all possible failure mechanisms.

With potential fatigue damaging over time and the increase in axle loads in both aspects magnitude and frequency, the reinforced-concrete bridges often need strengthening to continue using the infrastructure with the required reliability level. Before any intervention, an assessment is necessary [5]. However, the assessment of existing bridge structures for inherent safety level or for lifetime extension purposes is often more challenging than designing new bridges. This may include updating all the uncertainties on both the action and resistance sides based on information obtained from inspections, structural interventions and monitoring campaigns conducted during the service duration of the structure. Uncertainties on the action side may include variation in vehicle weights and positions on carriageway-width of deck slabs, velocity of vehicles, number of vehicles crossing the bridge from each traffic direction, uncertainties related to temperate and related temperature induced strains. Uncertainties on the resistance side are in the form of large scatter in fatigue test data even for same conditions of test campaigns. Uncertainties in resistance also include structural response to these actions in the form of variation in action effects. Uncertainty in compressive strength of concrete relates to the gain in concrete strength over time due to continued cement hydration. To cover these wide ranges of uncertainties, the probabilistic reliability method proves to be efficient for assessing the fatigue safety of structures.

This paper presents a probabilistic reliability framework for assessment of future service duration, which includes a probabilistic modelling of actions based on monitoring data collected for a period of one year; probabilistic modelling of the fatigue resistance based on large fatigue test data compiled from literature. The probabilistic modelling of actions includes the identification and quantification of uncertainties associated with the weight of vehicles, position of vehicles and temperature inducing strain variations. This modelling is limited to the verification of the fatigue limit state only and is based on a monitoring campaign conducted for the Crêt de l'Anneau Viaduct for a period of one year and the weigh in motion (WIM) data obtained from Swiss authorities, see [18] for details about monitoring and WIM data. The probabilistic load modelling is described in Section 3. The probabilistic modelling of resistance includes a stochastic fatigue resistance model based on a wide fatigue test database available in literature; see Section 2 for details about probabilistic fatigue resistance modelling. Thus, the novelty of the paper lies with presenting a generic technique to model relation of design parameter for existing structures to calibrate partial safety factors, based on newly developed stochastic-fatigue-resistance-material-model. In addition, a case study for the Crêt de l'Anneau Viaduct is presented along with calibration of resistance partial safety factors. Calibration of resistance material partial safety factors turns to be useful for existing structures, where structural engineers can meet reliability requirements, simply by using the calibrated partial safety factors with a code-based design without performing complex reliability analyses.

2. S-N relations for concrete fatigue

2.1. Introduction

S-N relations for concrete fatigue are generally developed using data from testing campaigns. Waagaard, [27] in 1981 tested concrete for axial and flexural fatigue under different confining conditions in the presence of water (for offshore concrete foundations), see Det Norske Veritas (currently DNVGL) [27]. Cornelissen in 1986 tested concrete under tension fatigue at TU Delft, Netherlands [28]. Petkovic in 1990 tested high strength concrete during that time, which is less than 100 MPa compressive strength, for axial compression fatigue [29]. Lohaus and others tested ultra-high strength concrete with compressive strength of 180 MPa [30]. As outcome of all this research works, international codes e.g. DNV-OS-C502 [31], NEN 6723 [32], EN 1990 [33], *fib* MC1990 [34] and *fib* MC2010 [35], have proposed models for predicting fatigue service duration of concrete structures. These codes use the Palmgren-Miner (PM) rule [36,37] of linear damage accumulation where the fatigue strength is represented by a combination of Goodman Diagrams [38] and Wöhler Curves also known as S-N curves. Fatigue behaviour of concrete is governed not only by the stress range but also by the mean level of stresses. Use of the Goodman diagram to describe the fatigue behaviour accounts for the importance of the mean level of stresses.

All research papers, reports, international codes and standards agree that scatter in concrete fatigue test results has to be accounted for and proposed characteristic design curves/surfaces together with the partial safety factor concept. In order to obtain both reliable and cost-competitive design of reinforced and pre-stressed concrete structures, it is important that the uncertainty of the individual parameters is estimated and taken into account in the design process. This can to some degree be done by applying the partial safety factor approach but a much more elaborate approach can be obtained by adopting a probabilistic design approach where the structure is designed to meet a target reliability level. For this purpose uncertainty related to each parameter influencing the fatigue strength should be quantified and modelled by stochastic variables in order to estimate fatigue reliability. Thus, application of structural reliability theory could be an efficient way, to adequately-account for all these uncertainties while predicting fatigue service durations and future service durations of concrete structures [39].

2.2. Compilation- and statistical-analysis- of fatigue test data

The stochastic material model for fatigue of concrete presented in this paper is developed from a large database of concrete fatigue tests, collected from the literature, namely [40,30,29,41,42]. All compiled data and thus the developed model focuses on axial compression-compression fatigue of concrete. The database used for development of the material model consists of 600 + laboratory tests, from 10 to 11 experimenters. These tests cover a wide range of variables. For example, normal-strength concrete with compressive strength from 26 MPa to ultra-high-strength concrete with compressive strength of 226 MPa. The stress range varies from 5% to 95% of static compressive strength, tested under different range of frequencies 1–65 Hz and cover very high cycles of fatigue up to 15 million cycles. Normalized data is plotted (asterisks) see Fig. 1. A statistical analysis of the above database is performed using the fatigue strength model presented by Lohaus et al. [30], also adopted by [35]. This statistical analysis is performed using the Maximum Likelihood Method (MLM) for fitting the data to the model. Compared to other methods like least square fit, MLM has the advantage that, runout cases in fatigue tests can be included. Furthermore, it is easier to obtain Fisher information matrix and thus the parameter uncertainty associated with estimated parameters along with

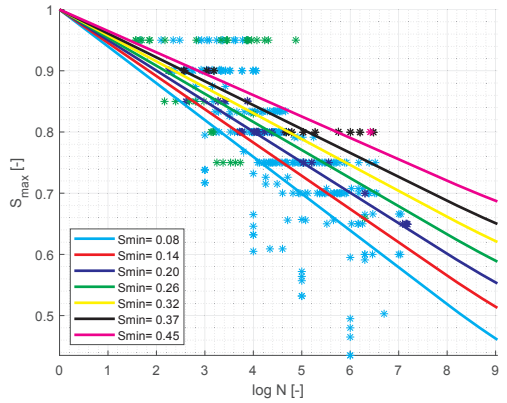

(a) fib MC2010 material model and fatigue test data

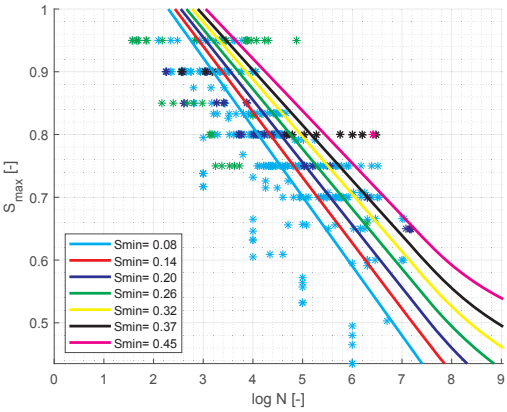

(b) Probabilistic material model (mean curves) and fatigue test data

Fig. 1. (a&b) Probabilistic material model fit comparison with fib MC2010 fit for all fatigue test campaigns.

their correlations. This information can be directly used in reliability analysis [43,44]. A local sensitivity and identifiability analyses were performed to obtain a unique set of parameters from available data, see [45], for other models, reference is also made to [46,47]. This dataset is used for obtaining a probabilistic fatigue-strength model as explained in Section 2.3, which forms as stochastic input of resistance side for reliability analysis.

2.3. Modification of existing S-N relations for better fit to the data

The *fib* MC2010 [35], is used as basis for modification to new SN-curves. The fib MC2010 [16], is used as basis since the S-N relations are formulated covering high-strength- and ultra-high-strength- concrete fatigue tests. Also fib MC2010 uses asymptotic second slope of S-N relations without any kink. The number of cycles required for failure ($\log N_{D,ij}$)at a specific maximum ($\sigma_{c,\max,i}$) and minimum ($\sigma_{c,\max,j}$) level of stress is given by:

$$\log N_{D,ij} = \frac{8}{(Y-1)}\cdot(S_{cd,max,i}-1), \quad \text{if } \log N_{D,ij} \le 8$$

$$\log N_{D,ij} = 8 + \frac{8\cdot\ln(10)}{(Y-1)}\cdot(Y - S_{cd,min,j})\cdot\log\left(\frac{S_{cd,max,i}-S_{cd,min,j}}{Y-S_{cd,min,j}}\right), \quad \text{if } \log N_{D,ij} > 8 \tag{1}$$

where

$$Y = \frac{0.45 + 1.8\cdot S_{cd,min}}{1 + 1.8 S_{cd,min} - 0.3\cdot S_{cd,min}^2}$$

$$S_{cd,max,i} = \frac{\gamma_{ED}\cdot|\sigma_{c,max}|\cdot\eta_c}{f_{cd,fat}}$$

$$S_{cd,min,j} = \frac{\gamma_{ED}\cdot|\sigma_{c,min,j}|\cdot\eta_c}{f_{cd,fat}}$$

γ_{ED} partial safety factor for fatigue load. For sufficiently accurate stress analysis γ_{ED} can be 1.0 otherwise a value of 1.1 is recommended in [35]. For current case, γ_{ED} is considered as 1.0 as direct strain measurements are available.

η_c averaging factor for concrete stresses in the compression zone considering stress gradient.

$f_{cdfat} = \beta_{c,sus(t,t0)}\cdot\beta_{cc(t)}\cdot f_{cd}\cdot(1 - f_{cd}/400)$, is the design reference fatigue strength.

$f_{cd} = f_{ck}/\gamma_c$, in MPa.

$\sigma_{c,\max,i}$ & $\sigma_{c,\max,i}$ are max. and min. stresses used to obtain $S_{cd,max,i}$&$S_{cd,min,j}$.

γ_c partial safety factor for material, 1.5 is recommended in [35]

$\beta_{cc(t)}$ factor considered for strength gain over time due to continued hydration.

$\beta_{c,sus(t,t_0)}$ coefficient which takes into account the effect of high mean stresses during loading. For fatigue loading it may be taken as 0.85.

Eq. (1) presents a design equation, while the corresponding characteristic equation can be obtained by setting the resistance partial safety factor $\gamma_c = 1.0$.

Eq. (1) is slightly modified and stochastic variables are introduced in order to capture various uncertainties. The basic change adopted to Eq. (1) is that $S_{cd,max,i} = 1$ is not bound to be at $\log N_{D,ij} = 0$. This is done by replacing 1.0 with a stochastic variable X_1. This enables the failure curves to capture the data points more accurately. However, this introduces a limitation to the failure curves and the curves cannot be used for low cycle fatigue (number of cycles in order of 1000 i.e. $\log N_{D,ij} \le 3$) coupled to ultimate strengths.

Further, the assumption about the sustained compressive strength of concrete linearity until $\log N_{D,ij} = 8$ is changed in the model and instead, a stochastic variable (X_2) is introduced to take care of this linearity limit of curves. The fatigue strength reduction factors proposed ($\beta_{c,sus}$ and $1 - f_{cd}/400$) in [30,35] are not included in the probabilistic modelling since they are not supported by any test evidence, [35] & [47].

Also an un-biased error term ϵ normally distributed $N(0, \sigma_\epsilon)$ is added to take care of model uncertainty with the proposed model. All these three parameters (X_1, X_2&σ_ϵ) are estimated by using MLM. See Table 1 for their estimated mean values, parameter uncertainties and correlation coefficients among each other. See Eq. (2) which is used in MLM for fitting the curves.

$$\log N_{S,ij} = \frac{X_2}{(Y-X_1)}\cdot(S_{c,max,i} - X_1) + \epsilon, \quad \text{if } \log N_{S,ij} \le X_2$$

$$\log N_{S,ij} = X_2 + \frac{X_2\cdot\ln(10)}{(Y-X_1)}\cdot(Y - S_{c,min,j})\cdot\log\left(\frac{S_{c,max,i}-S_{c,min,j}}{Y-S_{c,min,j}}\right) \text{ if } \log N_{S,ij} > X_2 + \epsilon, \tag{2}$$

2.4. Comparison of new fit

Asterisks in Fig. 1 show the fatigue test results from the data base explained in Section 2.2 above. As explained in Section 2.1 fatigue test

Table 1
Stochastic parameters in limit state equation.

Area	Parameter	Distributiontype	MLE Estimation		Remark
			Mean	Std. Dev.	
Fatigue Strength Model, see Section 2.5	Δ	Lognormal	1.0	0.30	Uncertainty associated with PM rule concrete fatigue
	X_1	Normal	8.66	0.37	Limit for linearity of $logN_S$
	X_2	Normal	1.13	0.03	Value of $S_{max,i}$ at $\log N_S = 0$
	ε	Normal	0.00	σ_ε	Error assumed N(0, σ_ε), Unbiased
	σ_ε	Normal	0.88	0.07	Std. Dev of Errorε
	$\rho_{X_1,\sigma_\varepsilon}$	–	0.01		Correlation coefficient obtained by MLE
	$\rho_{X_2,\sigma_\varepsilon}$	–	−0.01		Correlation coefficient obtained by MLE
	ρ_{X_1,X_2}	–	−0.84		Correlation coefficient obtained by MLE
	X_{fc}	Log-Normal	1.00	0.20	Assumed uncertainty associated with strength of concrete f_c ++
Fatigue Load Model	X_L	Log-Normal	1.00	0.05	Uncertainty associated with stress from monitoring and obtained from ANSYS through FEM*
	ε_{temp}	Normal	10.00	15.00	Fitted distribution to observed temperature strain +
Evolution of traffic see Section 3.2.1	B_{CFT}	Normal	0.02	0.00**	Slope parameter obtained by MLM, see Section 3.2.1 for details.
	ε_{CFT}	Normal	0.00	0.05	Error parameter obtained by MLM, see Section 3.2.1 for details.
	$\rho_{B_{CFT},\varepsilon_{CFT}}$	NA	0.14	–	Correlation coefficient between B_{CFT} and ε_{CFT}

* A very low value of uncertainty is assumed as this FEM model is calibrated to monitoring data, ** A very low value but not zero, + normal distribution is fitted to the temperature strain values obtained from monitoring of one year data, + + mean strength of concrete at age of 60 years is unknown, construction drawings specify 40 MPa strength during construction, now fcm is assumed as 50 MPa.

data has three main variables namely, mean-stress, stress-range and number of cycles required for fatigue-failure for a particular level of stress-range and mean-stress. Based on same, the data is plotted depicting number of cycles (log$N$) as function maximum level of stress in test campaign (S_{max})and different value of minimum level of the stress in same test campaign(S_{min}) shown in different colours. Further, Fig. 1 (a) shows fib MC2010 deterministic curves, while Fig. 1 (b) shows probabilistic mean curves obtained from new model explained Section 2.3. $S_{c,max,i}$ & $S_{c,min,j}$ are normalized with respect to f_{ck}(not $f_{ck,fat}$ as the fatigue strength reduction factors proposed ($\beta_{c,sus}$ and $1 - f_{cd}/400$) in [30,35] are not included in the probabilistic modelling since they are not supported by test evidence, [35] & [47]) as the mean values of concrete static strength for the tests conducted are not known. Comparison shows modified S-N curves are better fit to the data compared to *fib* MC2010 fit, and as expected they pass through centre of the data points which achieved by MLM.

Fig. 2 and Fig. 3 show a comparison of the new modified fitted curve with international codes, e.g. [31,48,34,35] for mean and characteristic strengths respectively. Fatigue tests data are also plotted (asterisks) for getting a better idea about associated strength curves. Two values of the characteristic compressive strengths (f_{ck}) are chosen for illustration such that they represent normal-strength (38 MPa) and ultra-high-strength (170 MPa) concretes.

Comparing characteristic curves is an easy task as these characteristic curves are directly shown in all codes; however, obtaining mean curves is not a trivial task, as not all assumptions made by these codes while producing the curves are known. For illustration purpose, it is assumed that the mean curves can be obtained by replacing all characteristic values of material strength in codes by the corresponding mean values. It is to be noted that, this assumption results in conservative curves, as all other constants used for obtaining the curves are kept same. The other constants mentioned before consists of constants used in formulation of S-N relations in different codes (e.g. 8, 1.8 0.45, 0.3 in *fib* MC2010 formulations, C1 in DNV formulation, 14 proposed in EN1992 or 12, 16, 8 in *fib* MC1990 formulations), are not touched upon, there are conservatism built-in these constants.

Observations from Fig. 2 (a & b): the mean SN-curves of all standards remain the same for all strengths of concrete (shown for two strengths) as they are normalized with respect to strength of concrete, see assumptions presented above. The mean SN-curves of all standards appear to be away from the fatigue test data while the modified curve passes through the data and the new fitted mean curves change for each strength of concrete as it is based on related fatigue tests. The test data is available until 15 million cycles (max), the extended part of the curves (tail of S-N curves) asymptotically reaches minimum compressive stress value, which basically shows when stress range is reduced very high number of cycles are required for failure.

Observations from Fig. 3 (a & b): Characteristic failure curves is highly influenced by the static compressive strength of concrete. All international codes are very conservative, especially with increased static strength of concrete. The proposed curves by all codes are far away from the data predicting a very low number of cycles to failure. This conservatism increases with increase in static strength of concrete as it can be seen that the SN-curve for f_{ck} of 170 MPa is much more conservative than the SN-curve obtained for f_{ck} equal to 38 MPa. DNVOSC502 is a bit less conservative compared to all other codes. Change of formulation for fatigue strength reduction based on static strength of concrete in *fib* MC2010, compared to *fib* MC1990 is reflected as large deviation in curves for high strength concrete compared to other standards [48] & [34]. EN1992, [48] and *fib* MC1990, [34] looks similar to each other.

The new characteristic SN-curve is obtained as $\log N_{SC} = \log N_S - 1.65 * \sigma_\varepsilon$, where $\log N_S$ and σ_ε are defined by Eq. (2). While obtaining characteristic curves the uncertainty related to compressive strength is not accounted as variation in compressive strength of concrete is not available for the database considered in this study.

2.5. Specific to the Crêt de l'Anneau Viaduct

As seen in Fig. 2, the mean fitted curves vary based on the strength of the concrete. To obtain a stochastic model for fatigue of concrete for the current case study of the Crêt de l'Anneau Viaduct, fatigue test data within the range of compressive strength varying from 20 MPa to 60 MPa are used. This is considered to represent the variability in viaduct's compressive strength, which was ~40 MPa, 60 years ago. The material model formulation is detailed in Section 4.2. The stochastic parameters used to obtain the strength curves shown in Fig. 4 are listed in Table 1.

3. Stochastic action model for the Crêt de l'Anneau viaduct

Fig. 5 shows view of Crêt De l'Anneau bridge viaduct, it was commissioned in year 1957. It has eight spans with total length of 194.8 m, each span is connected to each other by articulation of steel box girder

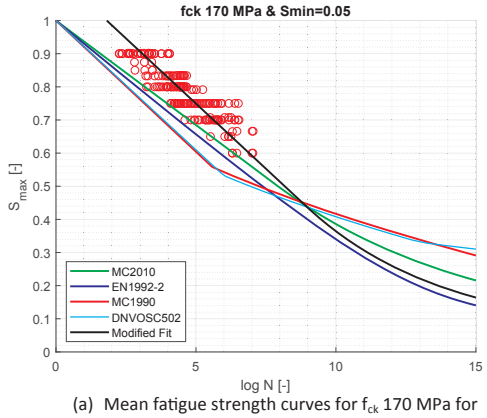

(a) Mean fatigue strength curves for f_{ck} 170 MPa for tests with S_{min}=0.05

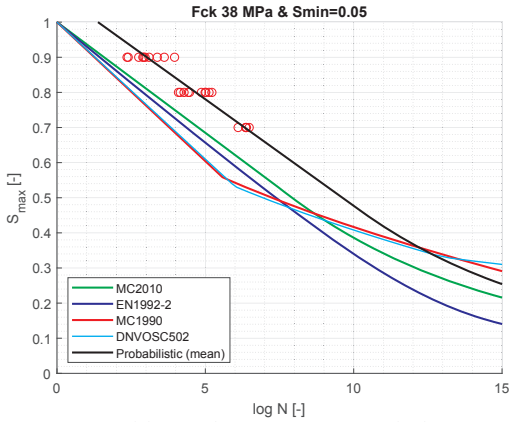

(b) Mean fatigue strength curves for f_{ck} 38 MPa for tests with S_{min}=0.05

Fig. 2. (a & b) Comparison of mean failure curves with different international codes (red dots represent corresponding fatigue test campaign) shown for two static strengths.

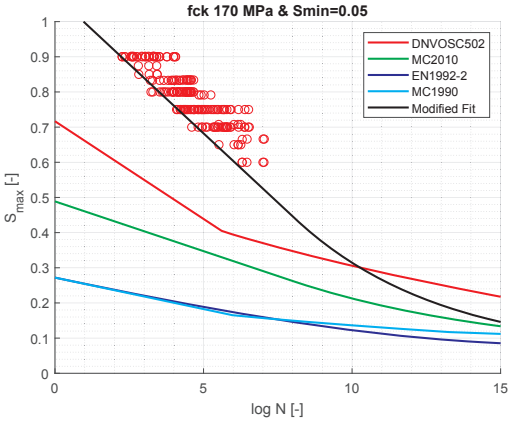

(a) Characteristic fatigue strength curves for f_{ck} 170 MPa for tests with S_{min}=0.05

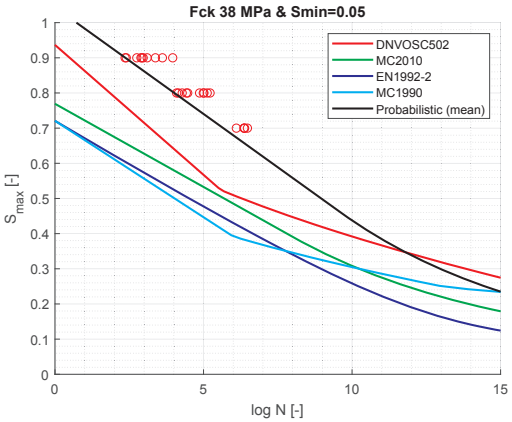

(b) Characteristic fatigue strength curves for f_{ck} 38 MPa for tests with S_{min}=0.05

Fig. 3. (a & b) Comparison of Characteristic failure curves with different international codes (red dots represent corresponding fatigue test campaign) shown for two static strengths.

beams. The carriage-way width of the deck is 12.7 m is supported transversely between two box girder beams. The deck slab has orthogonal grid reinforcement serving for double bending behaviour in transverse and longitudinal direction. The reinforcement consists of different diameters ranging from Φ10 mm, Φ14 mm and Φ18 mm forming grid in both compression and tension zone.

Strain gauges are installed on the Crêt de l'Anneau Viaduct. Continuous measurements are performed for a period of one year (from July 2016 to July 2017) with frequency of 50, 75 and 100 Hz for strains and 1 Hz for temperature and humidity. Data obtained from these continuous measurements is presented shortly in Section 3.1. Further, a stochastic load model is developed from these strain measurements, which includes stochastic variation of live load (vehicles) and stochastic variation of temperature load, is presented in Sections 3.2 and 3.3. Monitoring data obtained and development of stochastic load model are detailed in [18]. The reinforced concrete deck slab of the viaduct is governed by its transverse bending behaviour and found critical in fatigue after code-based re-calculation [49]. The action effects and stochastic model studied in further sections are limited to transverse stresses in concrete at mid-span of the viaduct in compression zone.

3.1. Action effects (Monitoring data-Strain)

Highest stresses due to live load are expected at mid-span (in the transverse direction) of the deck slab based on influence line diagram for longitudinal section of the viaduct. At this same location, strain gauges are installed on longitudinal and transverse reinforcements for the strain measurements. Strain is measured at a frequency of 50–100 Hz that captures responses due to every vehicle passing the viaduct. Along with this high frequency response of traffic, strain gauges also capture change in structural response due to ambient temperature variation [18,50].

Neutral axis for reinforced concrete section of deck slab is obtained [18] and a Markov Matrix for stresses is obtained from monitored strain in concrete for a period of one year is presented in Fig. 6.

3.2. Live load (vehicles)

Monitoring data presented in Section 0 is used to obtain weight of vehicle and its position along the carriageway width. The vehicle

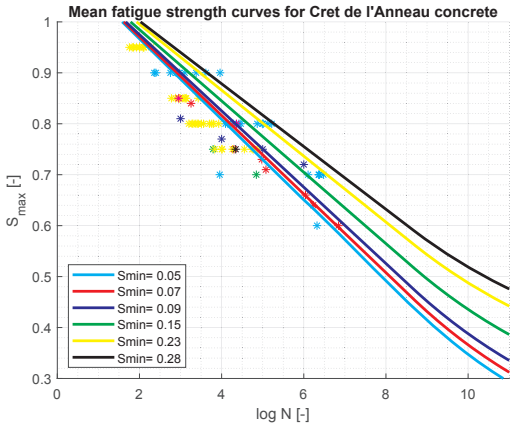

Fig. 4. Mean fatigue failure curves for concrete for the RC slab of the Crêt De l'Anneau Viaduct.

weight and the position is back calculated based on the calibration test performed for the viaduct with a truck of 40 Metric Tonne (MT) of known axle weights, [49]. The logic behind back calculation is detailed in [18].

The stochastic variation of live loads is presented in the form of weight distributions of vehicles and vehicle positions on carriageway width of the viaduct, see Fig. 7. A vehicle is described by its weight and position and both these variables are correlated to each other. However, to cover more possibilities which might not been captured in one year of measurements, these variables are modelled as un-correlated. Then, the probability of vehicle with specific weight (W) at specific position (P) can be calculated as simple product of these two probabilities, see Eq. (3).

$$P_{ij} = P\left[\left(P_{BC,i} - \frac{P_{B_W}}{2}\right) \le P \le \left(P_{BC,i} + \frac{P_{B_W}}{2}\right)\right] \cdot P\left[\left(W_{BC,j} - \frac{W_{B_W}}{2}\right) \le W \le \left(W_{BC,j} + \frac{W_{B_W}}{2}\right)\right] \quad (3)$$

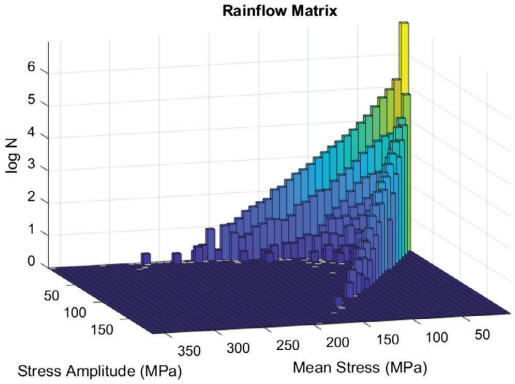

Fig. 6. Markov matrix for strain in concrete at mid-span of the viaduct.

where $P_{BC,i}$ is i^{th} bin-centre for the position with bin width of P_{B_W} while $W_{BC,i}j^{th}$ bin-centre for the weight with bin width of W_{B_W}.

Eighty-five bins of 100 mm size each are used for description of vehicle positions while sixty-four bins of 1.0 MT each are used for description of vehicle weight.

Finite Element (FE) model in ANSYS is used to obtain the response of the structure for each position and weight of the vehicle covering all possibilities i.e. 5440 (85 × 64). The FE model is detailed in [18].

3.2.1. Evolution of traffic with time

Traffic data are obtained from two Swiss authorities for the years from 2002 to 2016 and plotted as shown in Fig. 8, see [18] for details. Traffic growth is plotted as the ratio of number of vehicles versus years in which the traffic is observed. This ratio is normalized with respect to the number of vehicles observed in year 2016. A MLM estimate is obtained using the linear model shown in Eq. (4).

$$traffic(t) = A_{CFT} + B_{CFT} \cdot t + \epsilon_{CFT} \quad (4)$$

where t is the lifetime of the structure, A_{CFT} is an intercept parameter and B_{CFT} is a slope parameter. ϵ_{CFT} models the error in estimate and its unbiased estimate so ϵ_{CFT} $N(0, \sigma_{\epsilon_{CFT}})$. All the three parameters $(A_{CFT}, B_{CFT} and \sigma_{\epsilon_{CFT}})$ are modelled as uncertain parameters describing the trend of the traffic. However, it was observed that, A_{CFT} and B_{CFT}

Fig. 5. Crêt De l'Anneau: the investigated steel-concrete composite viaduct.

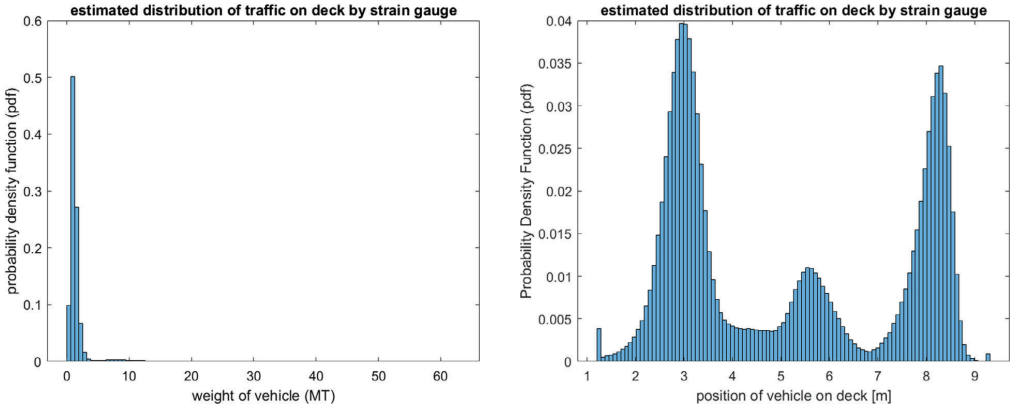

(a) Traffic weight distribution (b) Traffic position distribution along the width of viaduct

Fig. 7. Weight and Position Distribution (along carriageway width) of vehicular traffic on the Crêt de l'Anneau Viaduct.

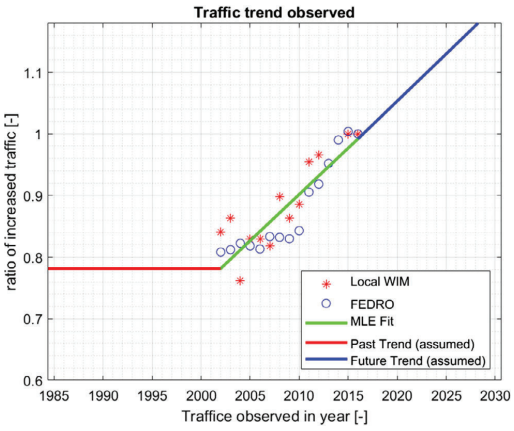

Fig. 8. Traffic trend modelled based on available data for the Crêt de l'Anneau Viaduct*.

are highly correlated with correlation coefficient close to unity so A_{CFT} is fixed and B_{CFT} & $\sigma_{\epsilon_{CFT}}$ are obtained from MLE (see Table 1).

Traffic trend is assumed to follow same growth in number of vehicles after year 2016 with the same level of uncertainty, while past traffic is assumed with the same number of vehicles as of year 2002 with the same level of uncertainty (this is a conservative assumption due to lack of data on past traffic), see Fig. 8.

3.3. Action model for temperature variation

The stochastic variation of temperature is captured by thermometers installed in concrete part of the viaduct and related temperature strains derived from monitoring data (see Fig. 9). The temperature strain can be easily separated from observed monitoring data as vehicles have very high frequency change in strain compared to temperature, see [18]. A normal distribution fits well for temperature strain and it can be easily used in a reliability analysis.

4. Assessment equation and limit state equation

Reliability analyses are performed for two load models: (1) strains obtained from monitoring (action effects, Section 0) are used directly; (2) strains obtained from the numerical model (ANSYS) is used for the stochastic load model described in Section 3.2. Rain-flow counting of stress history (see Markov matrix Section 0) based on strain obtained from monitoring is performed in order to estimate the number of cycles, stress-range and mean-stress levels. These form input for assessment Eq. (5). Strains observed in monitoring are assumed to be very accurate information with COV 5% and is modelled as lognormal distribution; see Table 1, this stochastic variable is an input for limit sate Eq. (6). The vehicle position and weight are input parameters for ANSYS model to obtain stresses/strains for that particular position and weight. As the ANSYS model is calibrated to yield the same results as those obtained by monitoring, it is assumed that ANSYS results have same uncertainty of COV = 5% and is modelled by a lognormal distribution, see Table 1. For both the cases, the assessment equation and limit state equation remain the same with just with the change of stress inputs.

4.1. Assessment equation

An assessment Eq. (5) is formulated using the Miner's rule of linear damage accumulation and Eq. (2).

$$G(T_L) = 1 - Damage = 1 - \sum \frac{n}{N} = 1 - \sum_{i=1}^{N_{smax}} \sum_{j=1}^{N_{smin}} \frac{C_{FT} \cdot n_{ij} \cdot T_L}{N_{Dij}} \quad (5)$$

where

T_L service duration of the structure.

N_{Smax} and N_{Smin} are the number of bins for $S_{Cd,max}$ and $S_{Cd,min}$ respectively.

n_{ij} experienced/observed number of stress cycles of $S_{Cd,max,i}$ and $S_{Cd,min,j}$ in each bin (i, j) per year.

$N_{D,ij}$ required number of stress cycles of $S_{Cd,max,i}$ and $S_{Cd,min,j}$ in each bin (i, j) per year for failure calculated deterministically based on Eq. (1).

C_{FT} Section 3.2.1.

$\sigma_{c,max,i}$ and $\sigma_{c,min,j}$ are maximum and minimum stresses.

$\sigma_{c,max,i} = DPR_{DL} \cdot \sigma_{DL} + DPR_{LL} \cdot X_L \cdot \sigma_{LL,max} + DPR_{temp} \cdot \sigma_{temp}$.

$\sigma_{c,min,j} = DPR_{DL} \cdot \sigma_{DL} + DPR_{LL} \cdot X_L \cdot \sigma_{LL,min} + DPR_{temp} \cdot \sigma_{temp}$.

σ_{DL} the stress due to dead load of the viaduct.

σ_{LL} the stress due to vehicle load on the viaduct and is obtained for two cases first for case of monitoring and second for stochastic load model input to FEM.

σ_{temp} is the stress due to temperature effect on the viaduct,

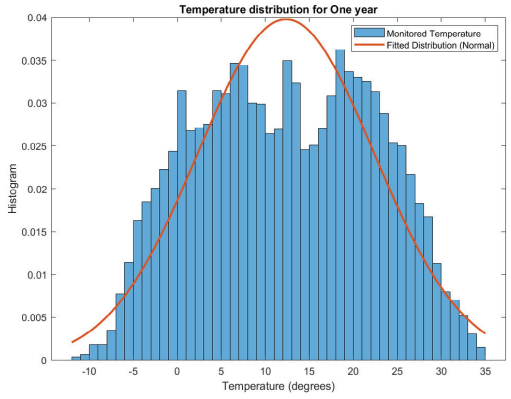

(a) Temperature data for one year observed to follow normal distribution

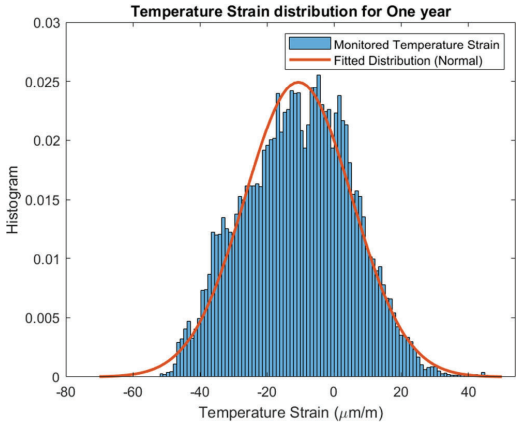

(b) Temperature strain data for one year observed to follow normal distribution

Fig. 9. Temperature variation and temperature strain variation in concrete part of the Crêt de l'Anneau Viaduct.

$\sigma_{temp} = \epsilon_{temp} \cdot E_c$.
ϵ_{temp} is the measured strain due to temperature.
E_c is the modulus of elasticity of concrete in MPa, $Ec = 4700\sqrt{f_{ck}}$.
f_{ck} is the characteristic static compressive strength of concrete in MPa.
DPR a coefficient that models relation between stress ratio and design parameter, see Section 4.3.

4.2. Limit state equation

A limit state Eq. (6) corresponding to the assessment Eq. (5) and Eq. (2) can be formulated by introducing stochastic variables.

$$g(t) = \Delta - \sum_{i=0}^{N_{Smax}} \sum_{j=1}^{N_{Smin}} \frac{C_{FT} \cdot n_{ij} \cdot t}{N_{S,ij}} \tag{6}$$

where

Δ model uncertainty associated with PM rule.
t time in years $0 < t < T_L$.

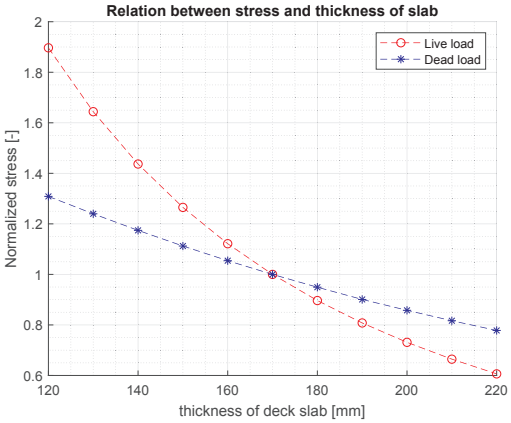

Fig. 10. Variation in stresses (due to dead load and live load) vs variation in Design parameter (Thickness of Deck Slab).

4.3. Modelling relation between design parameter and stresses

Modelling the relation between the stress values (mean and amplitude or minimum and maximum) and the design parameter is not trivial as changing the design parameter has different effects on mean level of the stresses and amplitudes of the stress history. To model the effect of change of a design parameter, maximum and minimum stresses are further decomposed to dead load, live load and temperature load. The effects of change of the design parameter on each of the stresses (σ_{DL}, σ_{LL} & σ_{temp}) are modelled individually. The principle of superposition can be assumed satisfied here and sequence of load application does not matter as all these loads are still in linear range, as this was verified during the calibration tests of the viaduct by MCS department of EPFL, Lausanne by load testing using a 40 MT truck with no permanent deformations observed [49]. The design parameter considered in the current study is the thickness of deck slab. Fig. 10 shows the relation between change in design parameter and change of stresses. Fig. 10 depicts also that, increasing the thickness of the slab reduces the live load stresses and the dead load stresses, but at a different rate. The increase in thickness increases of the bending stiffness of the deck slab, which reduces the stresses. However, for dead load the rate of decrease in stresses is lower as increase in thickness has also the opposite effect that it increases the weight of the slab. The effect on temperature stresses of changing the design parameter is assumed the same as the live load stresses. It is also possible to consider other design parameters e.g. tensile reinforcement in the deck slab, and then its relation with changes of stresses will generally be different from that of thickness of the deck slab.

5. Reliability analysis

Current viaduct was commissioned for public use in 1957 (~60 years back) and in this paper, it is assumed to be used for 60 more years, i.e. in total of 120 years of service duration. The reliability of reinforced concrete deck slab is assessed for fatigue failure of concrete in compression and the results are presented below. Current work focuses on reliability of viaduct for fatigue failure of concrete in compression only, as fatigue reliability of reinforcement in tension is already investigated [50]. The First Order Reliability Method (FORM) is used for calculation of probability of failure, [44] & [43]. An open source Matlab-based toolbox namely, the FERUM (Finite Element Reliability Using Matlab) is used for performing all FORM calculations [51].

The cumulative (accumulated) probability of failure in time interval [0,t] is obtained by Eq. (7):

$$P_F(t) = P(g(t) \le 0) \tag{7}$$

The probability of failure is estimated by FORM, see (Madsen et al., 2006). The corresponding reliability index $\beta(t)$ is obtained by Eq. (8):

$$\beta(t) = -\Phi^{-1}(P_F(t)) \tag{8}$$

where, Ð¤() is standardized normal distribution function.

The annual probability of failure is obtained based on cumulative probability of failure, see Eq. (9):

$$\Delta P_F(t) = P_F(t) - P_F(t-\Delta t), \quad t > 1 \ \ year \tag{9}$$

where $\Delta t = 1$ year. The corresponding annual reliability index is denoted $\Delta\beta$.

5.1. Code requirements for reliability

The Swiss standard (SIA-269, 2016), [52], provides guidelines for assessing the safety of existing structures. It uses a probabilistic approach and presents a target reliability level in the form of reliability indices based on consequence of failure and efficiency of interventions. Efficiency of safety-related interventions, expressed as the ratio of risk reduction to safety costs, which is similar to relative cost of safety measure explained in probabilistic model code JCSS, [53]. Low efficiency of intervention is assumed considering cost to rehabilitate an existing structure as very high and consequences of structural failure are assumed to be serious which leads to a target annual reliability of 3.7.

5.2. Effect of different uncertainties on reliability index

Uncertainty considered in Miner's rule is 0.3 is based on test data for fatigue of steel, [46,47], as a reference value, however this value for concrete may be different. A sensitivity study shows that, uncertainty on Miner's rule (Δ) is not important.

5.3. Calibration of resistance partial safety factor:

fib MC2010 recommends a partial safety factor (γ_{ED}) on fatigue loads as 1.1 and for sufficiently accurate stress analysis, this may be taken as 1.0; see section 4.5.2.3 of *fib* MC2010 [35]. For current case, very accurate strain measurements are available, so γ_{ED} it considered as 1.0.

The partial safety factor for resistance (concrete compression strength) γ_c for persistent or transient loading is recommended as 1.5 in *fib* MC2010, [35]. The definition of this partial safety factor in case of fatigue design is the ratio of design-fatigue-reference strength to characteristic-fatigue-reference strength obtained as follows see Eq. (10); see also equations 5.1–110 and 7.4–4 in *fib* MC2010, [35].

$$\gamma_M = \gamma_C = \frac{f_{ck,fat}}{f_{cd,fat}} \tag{10}$$

Relationship between the partial safety factor for material strength $\gamma_c$and annual reliability index $\Delta\beta$ can be obtained by using the design equation, see Eq. (5) and the limit state equation, see Eq. (6). The design parameter is the only connection between these two equations, which for the current case is thickness of the deck slab. To obtain different values of γ_c each time design parameter is set to a value such that, design-Eq. (5) is exactly fulfilled.

Thus, the relation between annual reliability index and resistance partial safety factor is presented in Fig. 11. Target reliability indices indicated in (*fib*, MC2010) [35], (SIA-269, 2016), [52] and (EN 1990, 2002), [33] can be compared to have an idea about resistance partial safety factor behind these requirements. The results shown in Fig. 11 correspond to $CoV_{X_L}$of 0.05 for T_L of 120 years. The uncertainty

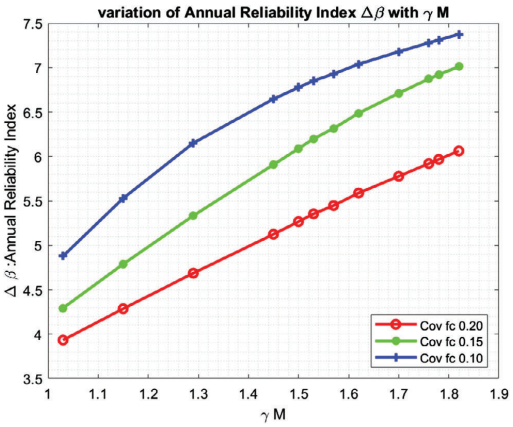

Fig. 11. Variation in annual reliability index with γ_M for TL 120.

associated with stress values obtained also plays an important role in reliability of the structure similar to uncertainty on compressive strength of concrete and therefore γ_{ED}can depend on CoV_{X_L}.

From Fig. 11 it can be seen that, a resistance partial safety factor of ~1.0 is required to achieve an annual reliability index of 3.7 when $CoV_{f_c}$is 0.2. It is further reduced to value less than 1.00 to achieve same criteria when, a more accurate information on concrete strength is available. It is to be noted that these conclusions are assuming a very accurate information (due to direct strain monitoring) on action effects is available (CoV_{X_L} = 0.05). The reliability index is equally sensitive to uncertainty associated with stresses (action effects) i.e. CoV_{X_L}.

5.4. Comparison for two load models

Reliability analysis is performed for the two load models as described in Section 0, 3.2 and 4. The results are compared to see the effect of non-correlation between vehicle weight and position as described in Section 3. The difference between the two models is that model 1 uses direct strains obtained from monitoring for vehicles (for a specific weights and specific positions), while model 2 uses back calculated weight of vehicles by FEM [18] at every possible position of carriage-way width of the viaduct. Fig. 12 shows the variation of annual

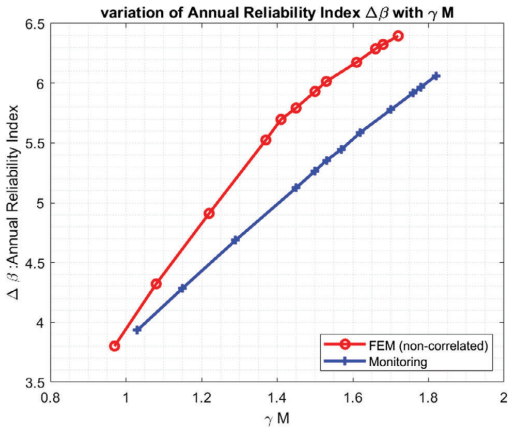

Fig. 12. Annual reliability index as function of γ_M for TL 120 and CoV_{f_c} 0.2.

reliability index ($\Delta\beta$) for both cases. There is a large difference between the reliability indices, as the characteristic stresses obtained in both cases in same way and also uncertainty with FEM is also assumed same as monitoring (since FEM is calibrated to monitoring), the reason for this variation in reliability indices may be that the current position of the vehicles (model 1, monitoring) are more critical as they pass near the centre of carriageway width while for non-correlated model (model 2, FEM) they are distributed over entire carriageway, which is yielding lower stresses and thus higher reliability. In Fig. 12 it can be seen that, for the same value of resistance partial safety factor a higher annual reliability can be obtained for FEM case. Thus distributing the weight of vehicle over entire carriageway width does not produce critical results for this case and considered fatigue critical location.

5.5. Scientific contribution, conclusion and future work

The current study proposes a methodology for the fatigue reliability assessment of existing reinforced concrete structures which includes a new stochastic SN model for fatigue of concrete, two different traffic models (action effect models), a new concept of modelling of relation between assessment parameter and stresses in concrete for existing structures. The new stochastic SN model captures fatigue test data (Section 2.2) more accurately and thus reduce model uncertainty.

Two factors play a very important role in assessment of the reliability level for fatigue of concrete structures namely the accuracy in estimating the fatigue action effects and the uncertainty related to the static compressive strength of concrete. For the considered case a very accurate information on action effects is available. However, accurate information on the static compressive strength is lacking. Also, static compressive strength of the concrete improves over the years. The accurate information about this gain in strength of concrete is unknown, unless a Non Destructive Test (NDT) is performed. It is recommended that a NDT should be performed to obtain the static compressive strength of the concrete before exercising lifetime extension decisions based on assessment of the reliability with respect to fatigue failure of the concrete.

Current study focuses on component level reliability, however an approach considering the system reliability would be helpful for inspection planning and maintaining a consistent safety of the whole structure throughout planned fatigue service duration.

Declaration of Competing Interest

The authors declare that they have no known competing financial interests or personal relationships that could have appeared to influence the work reported in this paper.

Acknowledgments

Current work is carried out under the project INFRASTAR (infrastar.eu), which has received funding from the European Union's Horizon 2020 research and innovation programme under the Marie Skłodowska-Curie grant agreement No 676139. The grant is gratefully acknowledged.

References

[1] Okada K, Okamura H, Sonoda K. Fatigue failure mechanism of reinforced concrete bridge deck slabs. Transport Res Record 1978.
[2] Perdikaris PC, Beim S. RC bridge decks under pulsating and moving load. Struct Eng 1988;114(3):591–607.
[3] Maekawa K, Gebreyouhannes E, Mishima T, An X. Three-dimensional fatigue simulation of RC slabs under traveling wheel-type loads. Adv Concr Technol 2006;4(3):445–57.
[4] Gebreyouhannes E, Chijiwa N, Fujiyama C, Maekawa K. Shear fatigue simulation of RC beams subjected to fixed pulsating and moving loads. Adv Concr Technol 2008;6(1):215–26.
[5] Schläfli M, Brühwiler E. Fatigue of existing reinforced concrete bridge deck slabs. Eng Struct 1998;20(11):pp.
[6] Mallet GP. Fatigue of Reinforced Concrete (State of the Art Review), Stationery Office Books (TSO), 1991.
[7] Chen ZW, Xu YL, Wang XM. SHMS-based fatigue reliability analysis of multiloading suspension bridges. J Struct Eng 2012;138:3.
[8] Krejsa M. Probabilistic reliability assessment of steel structures exposed to fatigue. Safety, Reliability and Risk Analysis: Beyond the Horizon; 2014.
[9] Kwon K, Frangopol DM. Bridge fatigue reliability assessment using probability density functions of equivalent stress range based on field monitoring data. Int J Fatigue 2010;32:1221–32.
[10] Ye XW, Ni YQ, Wong KY, Ko JM. Statistical analysis of stress spectra for fatigue life assessment of steel bridges with structural health monitoring data. Eng Struct 2012;45(2012):166–76.
[11] Li H, Frangopol DM, Soliman M, Xia H. Fatigue reliability assessment of railway bridges based on probabilistic dynamic analysis of a coupled train bridge system. J Bridge Eng 2016;142:3.
[12] Liu Y, Xiao X, Lu N, Deng Y. Fatigue reliability assessment of orthotropic bridge decks under stochastic truck loading. Shock Vib 2016;2016:10.
[13] Saberi MR, Rahai AR, Sanayei M, Vogel RM. Bridge fatigue service-life estimation using operational strain measurements. J Bridge 2016;21(5).
[14] Zhang W, Cai CS. Reliability-based dynamic amplification factor on stress ranges for fatigue design of existing bridges. J Bridge Eng 2013;18(6):538–52.
[15] Liu Y, Zhang H, Li D, Deng Y, Jiang N. Fatigue reliability assessment for orthotropic steel deck details using copulas: Application to nan-Xi yangtze river bridge. J Bridge Eng 2018;23:1.
[16] Efron B. Bootstrap methods: another look at the jackknife. Ann Statist 1979;7(1):1–26.
[17] Montgomery DC. Designa and analysis of experiments. westford, USA: John Wiley & Sons, Inc.; 2017. 1013.
[18] Bayane I, Mankar A, Bruhwiler E, Sørensen JD. Quantification of traffic and temperature effects on the fatigue safety of a reinforced-concrete bridge deck based on monitoring data. Eng Struct 2019;196.
[19] Ahn J-H, Sim C, Jeong Y-J, Kim S-H. Fatigue behavior and statistical evaluation of the stress category for a steel–concrete composite bridge deck. J Constr Steel Res 2008;65(2009):373–85.
[20] Treacy MA, Brühwiler E. A direct monitoring approach for the fatigue safety verification of construction joint details in an existing post-tensioned concrete box-girder bridge. Eng Struct 2015;88(2015):189–202.
[21] Rocha M, Brühwiler E. Prediction of fatigue life of reinforced concrete bridges using fracture. Bridge Mainten Saf, Manage, Resilien Sustain 2012.
[22] Casas JR, Crespo-Minguillon C. Probabilistic response of prestressed concrete bridges to fatigue. Eng Struct 1998;20(11):940–7.
[23] CEB. Fatigue of concrete structures - State of Art Report. CEB Zurich; 1988. p. 1989.
[24] Tarifa M, Zhang X, Ruiz G, Poveda E. Full-scale fatigue tests of precast reinforced concrete slabs for railway tracks. Eng Struct 2015;100(2015):610–21.
[25] Poveda E, Yu RC, Lancha JC, Ruiz G. A numerical study on the fatigue life design of concrete slabs for railway tracks. Eng Struct 2015;100(2015):455–67.
[26] Fathalla E, Tanaka Y, Maekawa K. Remaining fatigue life assessment of in-service road bridge decks based upon artificial neural networks. Eng Struct 2018;171(2018):602–16.
[27] Waagaard K. Fatigue strength of offshore concrete structures. Hovik, Norway: Det Norske Veritas; 1981.
[28] Cornelissen HAW. Fatigue failure of concrete in tension. Stevinweg 4, P.O. Box 5048, 2600 GA Delft, The Netherlands, 1986.
[29] Petkovic G, Stemland H, Rosseland S. Fatigue of high strength concrete. American Concrete Institute (International Symposium). 1992. p. 505–25.
[30] Lohaus L, Oneschkow N, Wefer M. Design Model for fatigue behaviour of normal-strength, high-strength and ultra-high-strength concrete. Struct Concr 2012.
[31] DNV OS C 502, DNV OS C 502, Offshore concrete structures. DNVGL, Høvik, Sept, 2012.
[32] NEN 6723. Regulations for concrete - Bridges - Structural requirements and calculation methods. Netherlands; 2009.
[33] EN 1990. EN 1990 Basis of structural Design," European committee for standardisation, Brussels; 2002.
[34] fib MC1990. FIB Model Code for concrete structures 1990. Berlin; 1993.
[35] fib MC2010. FIB Model Code for concrete structures 2010. Ernst & Sohn, Berlin Germany; 2013.
[36] Palmgren A. Die lebensdauer von kugellagern (The life of ball bearings). Z Ver Dtsch Ing 1924;68(14):339–41.
[37] Miner MA. Cumulative damage in fatigue. Am Soc Mech Eng – J Appl Mech 1945;12(3):159–64.
[38] Goodman J. Mechanics applied to engineering. Longman, Green & Company; 1899.
[39] Byung HO. Fatigue analysis of plain concrete in flexure. Struct Eng 1986;112(2):273–88.
[40] Lantsought E. Fatigue of Concrete under compression Database and proposal for high strength concrete. Delft: TU-Delft; 2014.
[41] Sørensen EV. Fatigue life of high performance grout in dry and wet environment for wind turbine grouted connections. Aalborg: AAU; 2011.
[42] Thiele M. Experimentelle Untersuchung und Analyse der Schädigungsevolution in Beton unter hochzyklischen Ermüdungsbeanspruchungen. Berlin: BAM; 2016.
[43] Sørensen JD. Notes in Structural Reliability Theory and Risk Analysis. Aalborg University; 2011.
[44] Madsen HO, Krenk S, Lind NC. Methods of Structural Safety. New York: Dover Publications; 2006.
[45] Aankar M, Rastayesh S, Sørensen JD. Sensitivity and Identifiability Study for Uncertainty Analysis of Material Model for Concrete Fatigue. In: IRSEC 2018,

Shiraj, 2018.
[46] Marquez-Domínguez S, Sørensen JD. Probabilistic Fatigue Model for Reinforced Concrete Onshore Wind Turbine Foundations. In: Safety, Reliability and Risk Anaysis: Beyond the Horizon ESREL 2013, Amsterdam, 2013.
[47] Slot RMM, Andersen T. Fatigue behavior and reliability of high strength concrete. Denmark: Aalborg; 2015.
[48] EN 1992-1. Design of concrete structures - Part 1-1: General rules and rules for buildings. European committee for standardisation, Brussels; 2004.
[49] MCS. Surveillance du Viaduc du Crêt de l'Anneau par un monitoring à longue durée. MSC, Lausanne; 2017.
[50] Mankar A, Rastayesh S, Sørensen JD. Fatigue Reliability analysis of Cret De l'Anneau Viaduct: a case study. Struct Infrastruct Eng 2019.
[51] FERUM. Finite Element Reliability Using Matlab; 2010.
[52] SIA-269. Existing structures – Bases for examination and interventions. Swiss Society of Engineers and Architects, P.O. Box, CH-8027 Zurich; 2016.
[53] JCSS. JCSS PROBABILISTIC MODEL CODE. JCSS; 2000.

Appendix B.

Paper 2

Quantification of traffic and temperature effects on the fatigue safety of a reinforced-concrete bridge deck based on monitoring data

Imane Bayane

Amol Mankar

Eugen Brühwiler

John Dalsgaard Sørensen

This papar has been published (with Golden Open Access) in Engineering Structures Journal

doi:https://doi.org/10.1016/j.engstruct.2019.109357

Engineering Structures 196 (2019) 109357

Contents lists available at ScienceDirect

Engineering Structures

journal homepage: www.elsevier.com/locate/engstruct

Quantification of traffic and temperature effects on the fatigue safety of a reinforced-concrete bridge deck based on monitoring data

Imane Bayane[a,*], Amol Mankar[b], Eugen Brühwiler[a], John Dalsgaard Sørensen[b]

[a] EPFL ENAC IIC MCS, Ecole Polytechnique Fédérale de Lausanne, Switzerland
[b] Aalborg University, Thomas Manns Vej, 23, 9220 Aalborg, Denmark

ARTICLE INFO

Keywords:
Fatigue
Reinforced Concrete (RC)
Existing road bridge
Traffic
Temperature
Inverse method
Monitoring

ABSTRACT

For assessment of existing reinforced-concrete bridges, only few rules and recommendations are available, and engineers meanwhile apply design codes for new bridges to evaluate the fatigue safety of existing bridges leading to non-realistic approaches and conclusions. Design codes for new structures are often based on the worst scenarios, and they are not made to assess existing structures with specific loadings and material properties. Direct monitoring provides an important source of information about the actual structural loading and response. This article presents an integral approach to identify fatigue damage of a reinforced-concrete deck as a function of the relevant actions for fatigue using monitoring data. This includes a long-term monitoring system to measure strain and temperature in the most loaded parts, an inverse method using monitoring data to reconstruct traffic actions from the structural response, and a simulation of traffic loading and its effects using a compiler and a finite element model to estimate fatigue damage. The presented approach can be used as a base on how to monitor and analyze recorded data to evaluate the fatigue safety of existing reinforced-concrete slabs in road bridges.

1. Introduction

Reinforced Concrete (RC) is a composite material in which concrete is designed to resist compression stresses and steel reinforcement is designed mainly to resist tensile stresses. Fatigue verification of reinforced-concrete elements requires the examination of both materials, concrete, and steel.

For steel, the fatigue phenomenon has been known as a possible failure cause since the 19th century. Fatigue design rules were introduced particularly with the findings of Wöhler (1867) [1], who recognized that repeated loading far below the ultimate static resistance of a structural element could induce failure [2]. Knowledge about fatigue in metals and other materials has evolved since then.

A century later, fatigue design rules for concrete and reinforced-concrete were introduced in Concrete VB (1974), FIP (1975), TNO-IBBC procedures (1974), DNV rules (1977), NPD regulations (1985), the draft Rules of Concrete Bridges (1988) [3], and SIA (1989) [4].

Most of today's RC bridges were constructed before introducing these rules, and fatigue was not considered during design as a possible failure cause. In Europe, around 75% of RC bridges were constructed before 1988 and in Switzerland, most of them before 1976 [5]. Therefore, there is a need to develop methodologies and approaches to verify the fatigue safety of existing RC bridges.

In the findings of State of the Art Report 188 [6], 17 cases of RC structural elements mainly bridge decks from all around the world (Japan, Sweden, Holland, Germany, United Kingdom, and the United States), were reported where fatigue was the main factor contributing to the deterioration of the structural elements.

For road bridges, RC decks are the most fatigue vulnerable part due to the pronounced effect of axle loads [7–11]. Different experiments and simulations were conducted on reinforced-concrete slabs under moving loads to investigate the fatigue failure mode [12–17]. Fatigue life prediction of RC decks was found to be a challenging task because it is affected by various sources of uncertainties, including material properties, vehicle loads, structural responses and environmental conditions. Therefore, one effective way to cover all these uncertainties comprises the direct monitoring on structures. Structural analysis implementing load-models from standards is not a reliable approach to examine existing RC decks. The load models of the standards are conservative since they do not rely on actual loading and actual structural conditions. In contrast, monitoring provides explicit information about the structural response and thus reduces most uncertainties of parameters related to fatigue safety investigation.

This paper presents a probabilistic methodology to verify the fatigue

* Corresponding author. Tel.: +41 021 693 32 93.
E-mail address: imane.bayane@epfl.ch (I. Bayane).

https://doi.org/10.1016/j.engstruct.2019.109357
Received 21 December 2018; Received in revised form 27 June 2019; Accepted 28 June 2019

safety of existing RC slabs, based on data obtained from monitoring. The originality of this work includes:

- The development of an inverse method to identify the position and load of traffic from long-term monitoring data.
- The quantification of the effect of vehicle position and load, as well as temperature variations on the fatigue damage of a RC bridge-deck slab.
- The combination of monitoring data, numerical simulations, and probabilistic assessments to define a procedure for fatigue safety verification.

The methodology can be used as a base on how to monitor existing reinforced-concrete decks and how to process data to evaluate their fatigue safety. It will be illustrated by considering an existing bridge, the Crêt de l'Anneau viaduct, in Switzerland.

2. Monitoring

2.1. Description of the monitored structure

Crêt de l'Anneau viaduct built in 1959 is located in Switzerland on the cantonal road 10, 20 km away from the French border (Fig. 1). It is a composite steel-concrete structure with seven typical spans of 25.6 m and one 15.8 m approach span, for a total length of 195 m. The viaduct is composed of a reinforced-concrete slab fixed on two steel-box-girder beams of 1.3 m height and of variable thickness ranging in the transverse direction from 24 cm near the supports to 17 cm at mid-span. The spans linked to each other by hinges and supported by the piers located 5 m away from each hinge (Fig. 2).

The RC slab was cast with concrete containing 350 kg of cement per m^3; its cube strength was equal to 45 N/mm^2 at 28 days. The deck slab has orthogonal grid reinforcements in both tensile and compression zones with diameters of 10 mm, 14 mm, and 18 mm. A single layer of reinforcement consisting of 25 ϕ10 @200 was provided in the longitudinal direction and 5 ϕ10 @240 in the transverse direction on the compression side. On tensile side, a single layer of reinforcement consisting of 5 ϕ14 @l/3 and 20 ϕ14 @6/m was provided in the longitudinal direction, 10 ϕ14 @106.66 and 2 ϕ18 @l/3 in the transverse direction. A compression-tensile strength of 300 N/mm^2 is assumed for rebars and 235 N/mm^2 for the steel girder.

2.2. Description of the monitoring system

The monitoring system used to investigate the fatigue safety of the RC slab is a system of non-destructive measurements, composed of strain gauges and thermocouples. It is cost-effective, easy to install, use and maintain. It is accessible to any engineering company.

The monitoring system implements recent technologies in data storage and high-frequency acquisition to perform continuous real-time monitoring of the structural response due to action effects mainly traffic loading and temperature. It is implemented for occasional inspections as well as for long-term monitoring. The bridge structure was instrumented in June 2016 with the monitoring system to measure strain and temperature histories at two main spans 2 and 4 (Fig. 2).

Transverse strains were measured by means of two strain gauges installed in the transverse rebars at the mid-span of Slabs 2 and 4 (Fig. 2). Longitudinal strains were measured by two strain gauges installed in the longitudinal rebars at mid-span of the same Slabs 2 and 4 and via one strain gauge installed in the steel girder beam at the mid-span of Slab 4. To monitor the variation of temperature, three thermocouples were installed, namely in the concrete of the slab, on the steel girder and in the air (Fig. 3).

The monitoring system has been operating since June 2016. 44 GB of data were collected and analyzed during the first year of monitoring. The data were recorded continuously with a sampling frequency of 50 and 100 Hz for strain and 2 and 1 Hz for temperature. Every 24 h a binary file was created and stored in the server. It was converted afterward to a Matlab file to process the data.

2.3. Description of the load test

A load test was carried out after the instrumentation of the structure using a five-axle truck with the maximum legal load of 400 kN. LVDT (Linear Variable Differential Transformer) sensors were installed in the instrumented slabs to evaluate the deflection of the cross-section. Four truck passages per direction were performed. The truck speed was varying from 80, 40, 35 to 10 km/h. The five axles of the truck were separately weighted and their actions on the viaduct identified.

Transverse rebars were under tensile stresses during the passage of the truck. In the longitudinal direction, the girder and the longitudinal rebars showed the expected stress reversal, i.e., both tensile and compressive stresses due to vehicle passage (Fig. 4). The five peaks in the longitudinal response represent the passage of the five axles of the truck. The measured strains were mainly influenced by the truck position and by the slab slenderness that accentuates local strains under the wheels.

Identical structural responses were obtained from passages that follow the same trajectory.

The axle configuration of the load-test truck does not have any

Fig. 1. View of the investigated steel-concrete composite viaduct.

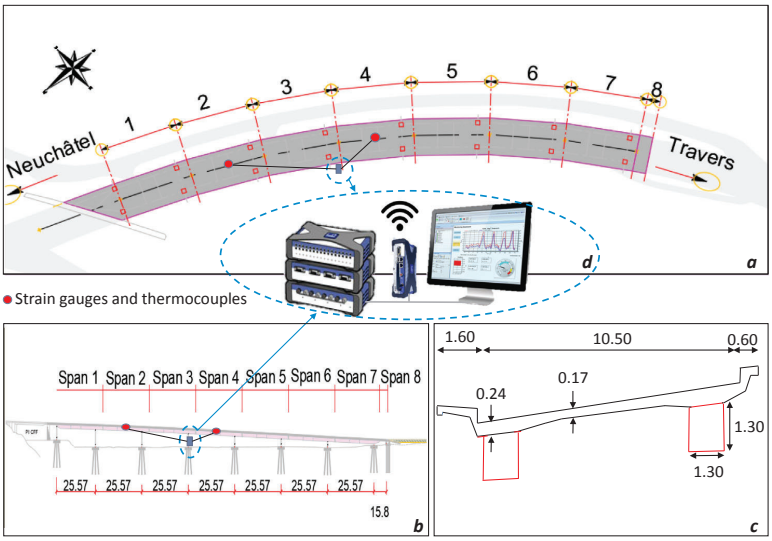

Fig. 2. Drawing of the viaduct (a) plan view; (b) elevation side; (c) typical cross-section; (d) data acquisition and storage unit; dimensions in [m].

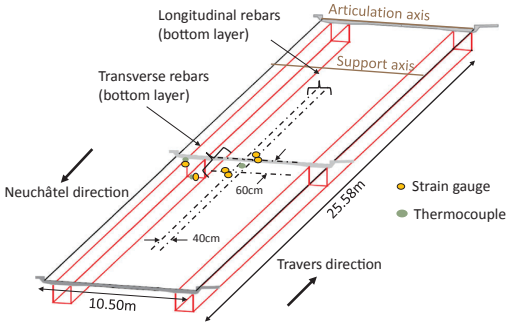

Fig. 3. Location of the sensors in span 4.

influence on the response of the transverse reinforcement and the steel girder, which means that the effect of vehicles can be directly related to their total load when analyzing the structural response of the cross-section.

The results of the load test serve as a base for performing an inverse method to identify traffic features from the recorded strain.

3. Relevant fatigue actions

3.1. Traffic

3.1.1. Approach

An inverse method was developed to identify traffic features from the recorded strain. The results of the load test were used to correlate the strain with the position and the load of the vehicles. Weight In Motion (WIM) data, collected from the same road about 1 km away from the viaduct was used to confirm the results of the inverse method and to evaluate traffic loads in the past and future [18,19]. The long-term statistical distributions of the load and position of all the vehicles crossing the bridge-structure were then established for an assumed 120 years of service duration.

3.1.2. Identification of vehicles

A Peak Over Threshold (POT) approach was applied to the recorded strain to identify all light vehicles and heavy trucks crossing the bridge. Minimum peaks to be included in the dataset were chosen to be above the measurement error, which is 1 μm/m, and the minimum time between each peak was set to 3 s such that, only one peak is identified per vehicle (Fig. 5). The threshold of 1 μm/m eliminates motorbikes and very light cars that are not relevant for structural safety.

This method was applied to strain measurements of the

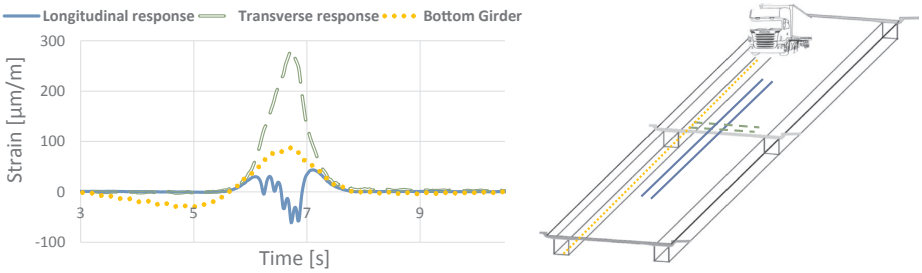

Fig. 4. Strain variations due to a moving load (35 km/h).

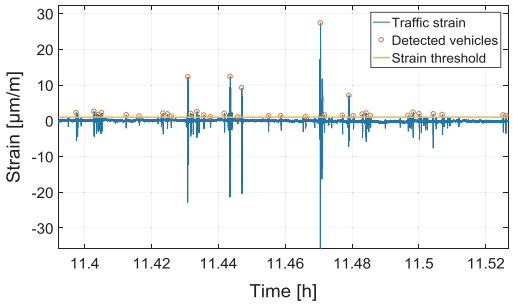

Fig. 5. POT for vehicle identification.

instrumented longitudinal and transverse rebars. A comparison between the identified peaks in each case showed that the longitudinal response has a better representation of the vehicles when comparing with WIM data. The identification of the vehicles was thus performed based on the longitudinal response.

3.1.3. Identification of vehicle position

The roadway width of the viaduct has two lanes, one for respectively the Neuchâtel and Travers directions. To quantify the position of the vehicles, the coordinates of their gravity centre over the width of the roadway are defined as being 0 m for the end of the lane in the Neuchâtel direction, 5.25 m in the centre of the road and 10.5 m for the end of the lane in the Travers direction, as shown in Fig. 6.

During the load test, the truck passed over the viaduct at five positions with respect to the roadway width. Strains in the rebars (transverse and longitudinal) and the girder versus the five positions of the truck are analyzed to determine an explicit correlation between recorded strains and vehicle positions.

It was found that the strain in the transverse rebars was the most sensitive to the position of the vehicles. To quantify this sensitivity, different combinations between transverse strains versus the positions of the test-truck were analyzed and compared to the measured data. The ratio r of strains $\varepsilon_{transverserebar1}$ and $\varepsilon_{transverserebar2}$ in the two instrumented transverse rebars was the parameter directly related to the position, giving similar values for passages with the same position (Eq. (1)). This ratio is approximately unity when the vehicle is located at the centre of the roadway.

$$r = \frac{\varepsilon_{transverserebar1}}{\varepsilon_{transverserebar2}} \tag{1}$$

The ratio r as a function of the vehicle position was fitted with a

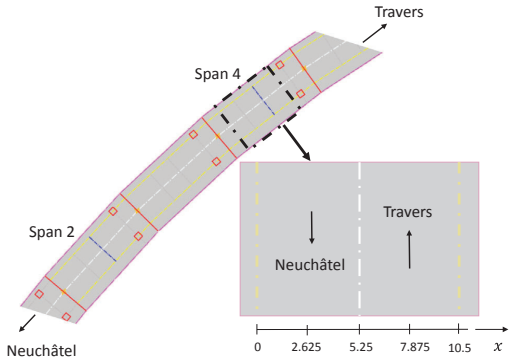

Fig. 6. Vehicle positions in [m] over the roadway width.

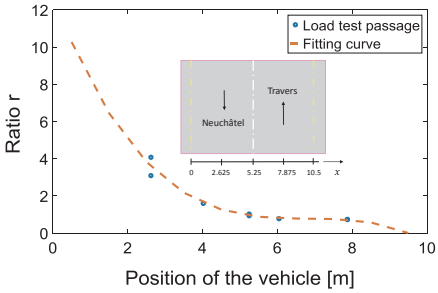

Fig. 7. Fitting curve to calculate the position of the vehicles across the roadway width.

third degree polynomial equation:

$$r = ax^3 + bx^2 + cx + d \tag{2}$$

where x is the position of the vehicle, and a, b, c and, d are the polynomial coefficients, defined from the load-test data. Fig. 7 illustrates the fit of this ratio versus the position of the 400 kN test-truck used to calculate the positions of the detected vehicles.

To obtain the long-term statistical distribution of truck positions, the vehicles were first identified using the peak over threshold approach applied to the longitudinal recorded strains. The corresponding peaks of strains in the two-instrumented transverse rebars were identified, and the ratio r between the peaks was calculated. The real solution of the polynomial $ax^3 + bx^2 + cx + d - r = 0$ corresponds to the position.

The roadway width of the viaduct is 10.5 m, and the wheels of the vehicles can have extreme positions such as 0 m and 10.5 m. The maximum width of the vehicles was assumed as 2 m (Section 3.1.6) and then, in this case, the centre of gravity of the vehicles cannot be less than 1.2 m and cannot be more than 9.3 m. When the calculated position was not in the defined interval, the centre of gravity was directly set at 1.2 m and 9.3 m for the vehicles in the Neuchâtel and Travers directions respectively. The possible positions were then defined in the interval [1.2 m, 9.3 m].

Fig. 8 presents the normalized long-term distribution of vehicle positions over the roadway width.

An increment of 0.1 m was used to define this discrete distribution for the possible positions in the interval [1.2 m, 9.3 m]; as such, 82 positions were defined with their normalized probability of occurrence.

There are three clear peaks for vehicle positions. The peak in the middle represents the vehicles crossing the road from the centre, which can be due to the important slab-slope of 7% and the bend in the road creating a centrifugal force toward the centre for the light vehicles in the Travers direction. Moreover, the vehicles crossing simultaneously the instrumented slab from different directions can create a ratio r near to unity; accordingly, they are also counted in the middle peak.

The two other peaks represent the vehicles crossing the viaduct from the middle of the lane respectively in the Neuchâtel and Travers directions.

The algorithm is well predicting the position of the vehicles since their number in each direction corresponds to the number of vehicles provided by the WIM data (Section 3.1.5). The vehicles that are not included in the interval [1.2 m, 9.3 m], are not frequent.

3.1.4. Identification of vehicle load

The loads are calculated after the identification of the vehicles and their positions. It is assumed that the load and the corresponding strain follow a linear relationship for a specific position.

This assumption of linearity is supported by the results of the load test, where the deflection and the strain values under the 400 kN test-

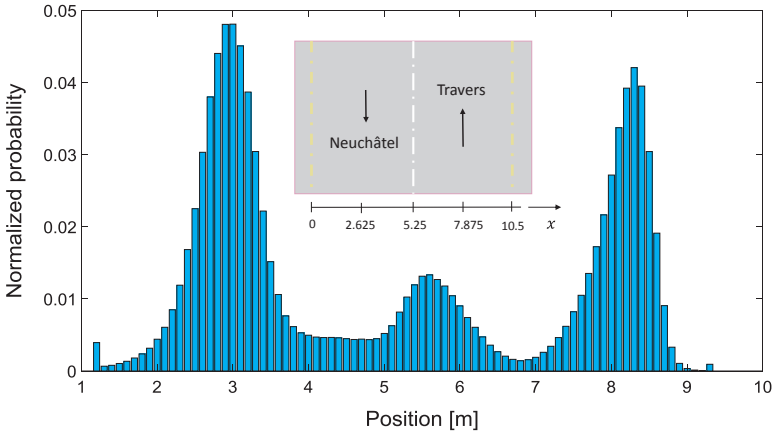

Fig. 8. Normalized annual distribution of vehicle positions.

truck (load limit) regained their initial values after each passage. Moreover, identical structural responses were obtained from passages that follow the same trajectory. The data of the load test contain one set of positions for the same load (400 kN), and they are used to estimate vehicle loads knowing their positions.

The distribution of strain over the roadway width was modeled by a third polynomial fitting of load-test results:

$$\varepsilon(L = 400 \text{ kN} \quad and \quad x = i) = ai^3 + bi^2 + ci + d \tag{3}$$

where ε is the strain due to the passage of vehicle with the load $L = 400$ kN and the position $x = i$, $i \in [1.2m, 9.3m]$.

The response of the girder and the transverse rebars was found to be the most sensitive to truck positions. Therefore, they were used to calculate the load distribution for the 400 kN truck and the identified vehicles according to equation (4).

$$L(x = i) = 400 \text{ kN} \frac{\varepsilon(x = i)}{\varepsilon(L = 400 \text{ kN} \ and \ x = i)} \tag{4}$$

where $\varepsilon(x = i)$ is the recorded strain at the position $x = i$.

Eq. (4) was applied to the recorded strain in the transverse rebars and the girder, and for each vehicle, three loads L were calculated to find the best estimate. Different combinations of the calculated loads were then compared to the WIM data to identify the actual load. Subsequently, the load of the vehicles in the Neuchâtel direction was set equal to the mean of the calculated loads using the strain measured in the girder and the transverse rebar at the mid-span (Eq. (5)). For the Travers direction, the load was directly calculated from the strain measured in the transverse rebar at the mid-span (Eq. (6)).

$$\begin{aligned} L(x = i)_{Neuchâtel} &= 400 \text{ kN} \frac{1}{2} \\ &\left(\frac{\varepsilon_{transverserebar}(x = i)}{\varepsilon_{transverserebar}(L = 400 \text{ kN} \ and \ x = i)} \right. \\ &\left. + \frac{\varepsilon_{girder}(x = i)}{\varepsilon_{girder}(L = 400 \text{ kN} \ and \ x = i)} \right) \end{aligned} \tag{5}$$

$$L(x = i)_{Travers} = 400 \text{ kN} \left(\frac{\varepsilon_{transverserebar}(x = i)}{\varepsilon_{transverserebar}(L = 400 \text{ kN} \ and \ x = i)} \right) \tag{6}$$

Eqs. (5) and (6) were applied to analyze one year of measurements and establish the normalized annual distribution of vehicle loads. An increment of 10 kN was used to represent this discrete distribution, and overall 64 load categories were identified with their normalized probability of occurrence, see (Fig. 9).

The developed algorithm is efficient for the identification of the composition of traffic based on the measured structural response. The resulting traffic distribution reveals that more than 96% of all detected vehicles are cars or small trucks, and 4% are heavy trucks (with a load more than 35 kN). Overloaded trucks exceeding the limit of 400 kN are identified with their position, their velocity and the time they crossed the viaduct. One hundred ten trucks did not respect the 400 kN legal limit over the first year of monitoring with the heaviest recorded load of 640 kN. The heavy trucks represent 8.10^{-5} of all detected vehicles and were frequent during October 2016 for the Neuchâtel direction and during June-July 2017 for the Travers direction, and almost absent during December and January. They were crossing the viaduct mostly from the centre of each lane.

The efficiency of the inverse method depends on the location of strain gauges and their number. It is important to design the position of the gauges over the longitudinal and the cross sections and to choose their numbers. The sensors should provide first, the strain in the most loaded parts to verify the structural safety (with respect to fatigue in the mid-span for the present study). Secondly, four aligned and separated strain gauges for the cross-section are necessary to detect the position of the vehicles in each lane, assuming that the road-bridge has two directions. Finally, two separated strain gauges in the longitudinal section are essential to detect the vehicles and calculate their velocity.

3.1.5. Validation and calibration using WIM data

The WIM-data collected from the local territorial development department [19] was used to validate and calibrate the results of the inverse method (Tables 1 and 2).

The WIM system was installed 1 km away from the viaduct, on the last week of September 2017 (from Monday 25 September to Sunday 1 October). It provided one week of continuous measurement of light and heavy traffic, which represents a solid database to verify the results of the inverse method.

The results of the inverse method were calibrated by the introduction of a calibration factor, equal to the ratio of the results of the inverse method and the WIM data. The weekly number of vehicles for each direction was used to calculate this factor, and accordingly, the number of daily vehicles was calibrated (Tables 1 and 2). An error estimate was calculated as the ratio of the difference between WIM data and calibrated results of the inverse method, and the WIM data.

Light vehicles such as cars of less than 35 kN and motorcycles identified by the established algorithm are not matching with WIM data because most of these vehicles have strain peaks in the domain of error of measurements, i.e., 1 μm/m. This number can easily be matched by

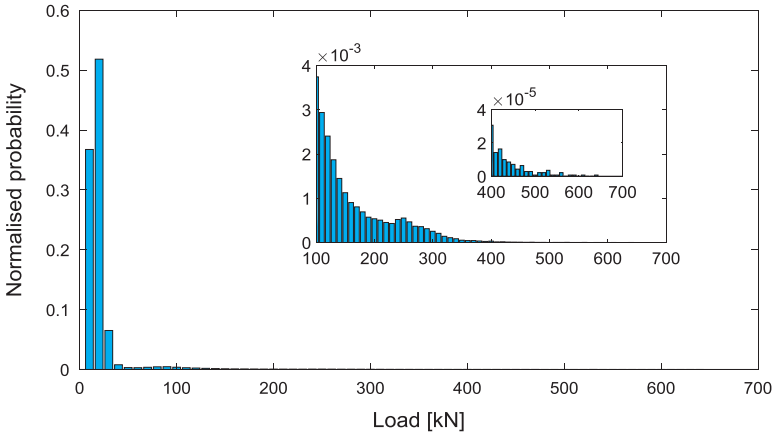

Fig. 9. Normalized annual distribution of vehicle load.

changing the threshold of the POT approach or simply by introducing the missing vehicles. These underestimated vehicles can be neglected compared to other vehicles for the following case study. This assumption is justified in the result section (Section 5).

The error in the estimation of the heavy trucks during the weekend is big. This is due to their small number leading to an increase in the ratio used to calculate the error. In fact, by comparing the detected number of trucks directly, the difference between the WIM data and the inverse method is not important. Moreover, verifying the load of these trucks showed that they are near 35 kN used to separate heavy trucks from light vehicles. Therefore, the error of detection can also be due to the WIM system during the classification.

The load and the position of the vehicles were evaluated by comparing the calculated and the measured numbers of heavy trucks for each direction. It was found that the inverse method provides the correct number of heavy trucks in the Neuchâtel direction, and overestimates the number in the Travers direction. This is mainly due to the use of only one strain gauge response to calculate vehicle loads in the Travers direction. In fact, a more reliable prediction can be achieved in the future by installing a strain gauge in the non-instrumented girder to obtain the transverse response of two aligned strain gauges for each direction. This overestimation was corrected by introducing a factor reducing the difference between the data of the model and the WIM data. The calculated and the measured daily number of heavy trucks in the Travers direction were evaluated, and the daily average of overestimation was identified as 42%. Therefore, the calculated number of heavy trucks ($N°$(heavytraffic))was reduced by introducing a factor of 0.7 (=1/1.42) (Eq. (7)).

$$N°(heavy\ \ traffic)_{corrected} = 0.7N°(heavy\ \ traffic)_{calculated} \quad (7)$$

After the calibration of the results using one week of local continuous WIM data, the robustness of the model was evaluated using continuous monthly WIM data and some daily data recorded during the same period of monitoring (July 2016 to July 2017). The data were collected from the Federal Roads Office FEDRO in Switzerland [18], where the WIM system was installed on the same road, few kilometers far away from the viaduct. To use the provided data, a coefficient of 1.47 was applied to reduce the difference between the FEDRO WIM data and the local WIM corresponding to the traffic crossing the viaduct, according to equation (8).

$$\frac{N°(traffic)_{localWIM}}{N°(traffic)_{FEDRO}} = 1.47 \quad (8)$$

The results of the inverse method were compared with the FEDRO WIM data. The calculated and the measured monthly averages of light vehicles and heavy trucks, and the daily averages of the most loaded days were similar. The calibrated model is efficient for predicting the load and the position of the vehicles.

3.1.6. Traffic growth

Local WIM data [19] and FEDRO data [18] were used to define traffic growth. The data provided the evolution of the annual traffic since 2002 for the same cantonal road X10. Fig. 10 includes the ratio of traffic evolution for the collected data with a linear fitting curve

Table 1
Detected light vehicles according to the WIM data and the inverse method.

Light vehicles								
	WIM data		Inverse method				Error	
			Before calibration		After calibration		After calibration	
Direction	Travers	Neuchâtel	Travers	Neuchâtel	Travers	Neuchâtel	Travers	Neuchâtel
Monday	4124	4217	2418	2439	4256	4293	−3%	−2%
Tuesday	4322	4384	2403	2531	4229	4455	2%	−2%
Wednesday	4408	4436	2508	2546	4414	4481	0%	−1%
Thursday	4544	4644	2538	2591	4467	4560	2%	2%
Friday	4678	4826	2618	2684	4608	4724	1%	2%
Saturday	3363	3477	2113	2250	3233	3443	4%	1%
Sunday	2574	2597	1744	1753	2668	2682	−4%	−3%
Total	28,013	28,581	16,342	16,794	27,875	28,638	0%	0%

Table 2
Detected heavy trucks according to the WIM data and the inverse method.

Heavy trucks								
	WIM data		Inverse method				Error	
			Before calibration		After calibration		After calibration	
Direction	Travers	Neuchâtel	Travers	Neuchâtel	Travers	Neuchâtel	Travers	Neuchâtel
Monday	126	119	122	191	122	125	3%	−5%
Tuesday	128	135	164	191	164	148	−28%	−10%
Wednesday	134	130	143	183	143	134	−7%	−3%
Thursday	138	138	141	185	141	137	−2%	1%
Friday	148	132	156	196	156	127	−5%	4%
Saturday	51	46	44	66	44	36	14%	22%
Sunday	29	26	13	23	13	7	55%	73%
Total	754	726	783	1035	783	714	−4%	2%

defining the annual ratio of traffic growth.

Traffic evolution between 2002 and 2016 was defined according to the ratio of the annual increase in traffic, equal to 1.8%. Since no information was available about the traffic in the past and the evolution of traffic in the future, the ratio 1.8% was used to define four traffic scenarios for 120 years of service, from 1957 to 2077 (Fig. 11).

Scenario 1: constant traffic before 2002 and after 2017 and a linear increase between 2001 and 2017.

Scenario 2: linear increase in traffic before 2017 and constant traffic after 2017.

Scenario 3: constant traffic before 2002 and linear increase in traffic after 2002.

Scenario 4: linear-increasing traffic.

The four scenarios of traffic evolution were used to define the annual statistical distribution of traffic based on the results of the inverse method. The normalized probability of the long-term distribution of vehicle positions and loads was assumed constant while changing the annual number of vehicles according to traffic-growth scenarios.

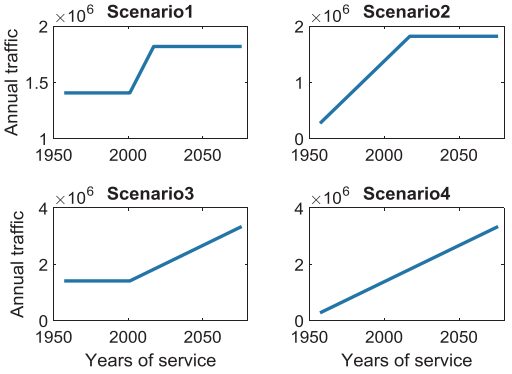

Fig. 11. Scenarios of traffic growth.

3.1.7. The contact surface of vehicles

Axle dimensions and contact surfaces were assumed similar because the local effect of axle dimension was small when simulating the stresses in the finite element model, and the applied loads were correctly diffused in the slab (Section 4). Moreover, the contact surface was modeled only by 2 or 5 axles, since there was not a big difference between the simulated stresses using 2, 3, 4 or 5 axles (Section 4.2).

The vehicles of traffic flow were classified into three categories according to their load to define their surface of contact, used to apply loads in the finite element model.

The first category represents the light vehicles less than 35 kN (cars and small trucks); it was modeled by two axles equally loaded. Heavy trucks more than 35 kN were divided into two categories, two and three. The second category of vehicles with the load range [35, 100 kN] was modeled by two axles loaded differently. The third and last category is for the vehicles heavier than 100 kN, it was modeled by five

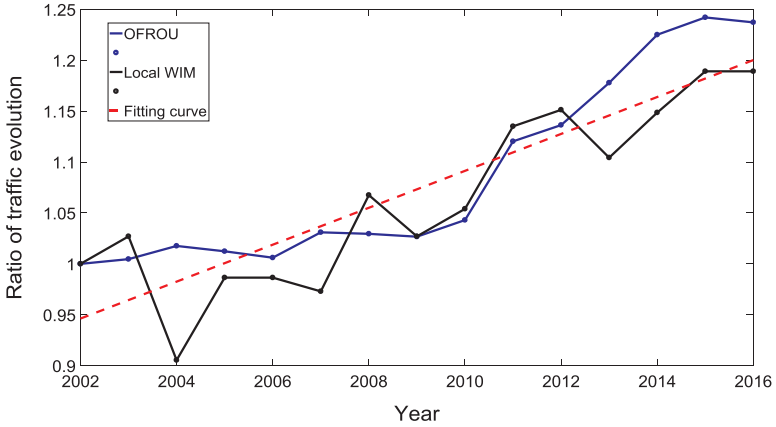

Fig. 10. Ratio of traffic growth from 2002 to 2016.

Table 3
Contact surface of the classified vehicles.

Category	Axles	Contact surface	Axle load distribution	Load category
Light vehicles	1 2	0.4*0.4 m	Equally distributed	[0,35 kN]
Heavy trucks	2 2	0.4*0.4 m	30% and 70%	[35,100 kN]
	3 5	0.4*0.4 m	15%, 15%, 20%, 25% and 25%	[100,700 kN]

axles loaded according to the truck model provided by the Federal Roads Office [20].

The legal limit load of a single axle is 100 kN; therefore, it was defined as the transition from 2 to 5 axles. The details of each category are summarised in Table 3.

The spacing of the axles was also taken from the updated traffic load for concrete deck slabs of existing bridges provided by the federal roads office, as shown in Fig. 12 [20].

The location of the centre of gravity of each category was calculated. This location corresponds to the position provided by the inverse method, used with the defined loads to distribute and load the surfaces of contact for each identified vehicle.

3.2. Temperature

3.2.1. Introduction

The thermal effect on concrete bridges has been widely studied in the literature showing that the contribution of temperature has a significant effect on damage evolution for concrete elements [8,21–24]. Many researches tried to model this effect, particularly [25–27,22]. However, the models were generally subject to many uncertainties, especially when applied to existing bridges, where the state of concrete is not well known. Besides, the thermal gradient is dependent on local conditions. Design codes, for example, present different requirements for each country [24].

Thermal response is, in fact, specific to each bridge and only precise monitoring of temperature and its effect with an explicit analysis of the measured parameters can reduce uncertainties and provide clear information about the structural response due to thermal variations.

For this aim, a detailed study of monitoring data was performed to define the distribution of temperature and thermal strains in the reinforced-concrete slab.

3.2.2. Temperature cycles

Temperature variation is a combination of two cycles, the daily and seasonal cycles. As such, the effect of temperature is a function of two parameters, the period of the day and the period of the year.

To separate these cycles and their effects, a moving average is used in the present case. The daily effect is directly presented with 24 h of measurements for a moving average with a subset of generally 10 min. The seasonal effect is deduced by the moving average with a subset of 30 days.

This processing is outlined in Fig. 13, where the combined, annual and daily cycles of concrete temperature are presented for the Crêt de l'Anneau viaduct.

3.2.3. Temperature effect

Temperature variations can have two direct effects, i.e., thermal diffusivity and thermal expansion.

Thermal diffusivity is the transfer of thermal energy from the warm side to the cold side of the structural element, producing a gradient of temperature that creates a gradient of thermal strain due to thermal expansion. Thermal expansion is presented by the contraction and expansion of materials and is characterized physically by the dilatation coefficient α (Eq. (9)).

$$\varepsilon = \alpha \Delta T \tag{9}$$

where $\Delta\varepsilon$ is the thermal strain variation, α the dilatation coefficient [$^{\circ}C^{-1}$], and ΔT the temperature variation [°C].

For concrete and steel, the dilatation coefficient is equal to $10^{-5}\,^{\circ}C^{-1}$.

During monitoring, the configuration of strain gauges is adapted to compensate for the thermal expansion of materials and measure the thermal expansion of structural elements. Stresses due to temperature are in fact, produced when thermal expansion or contraction is restrained in structural elements [26].

This effect is remarkable by its small frequency compared to traffic. Subsequently, the short-term fluctuations due to traffic action effects, and the long-term fluctuations due to temperature effects of time-series data for the recorded strain are separated using a moving average that creates a series of averages for each subset of 10-min. Three signals are resulting as presented in Fig. 14.

Raw data = recorded strain
Thermal strain = moving average of raw data each 10 minutes
Traffic strain = raw data − moving average

The subset of 10 min was chosen by a sensitivity analysis of the structural response. The parameter was modified until obtaining a signal with all the targeted features for traffic strain and thermal strain. Therefore, thermal strains are properly extracted from the recorded data and can be used to evaluate the effect of temperature on fatigue. The probability of occurrence of the recorded temperature and thermal strain within one year of monitoring is normalized, and the annual statistical distributions of temperature and its effect are presented in Fig. 15 for the transverse reinforcement in the mid-span of Slab 4. An increment of 2 μm/m was used to define this discrete distribution for the possible thermal strain of concrete, such that 51 strains were defined with their normalized probability of occurrence. The statistical distribution of temperature and its effect are used to define the mean stress relevant for fatigue reliability investigations for concrete.

4. Numerical simulations

4.1. Finite element model

4.1.1. Approach

A 2-dimensional Finite Element Model (FEM) was developed using the commercial program ANSYS R18.2 for one span of the viaduct, with the purpose of defining the statistical distribution of stresses in the slab

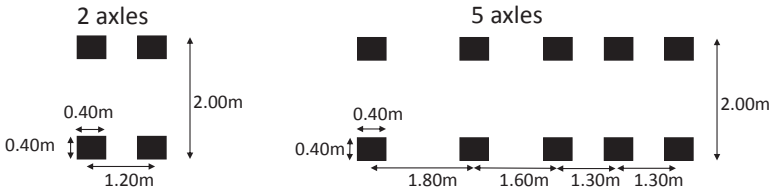

Fig. 12. Spacing of the axles.

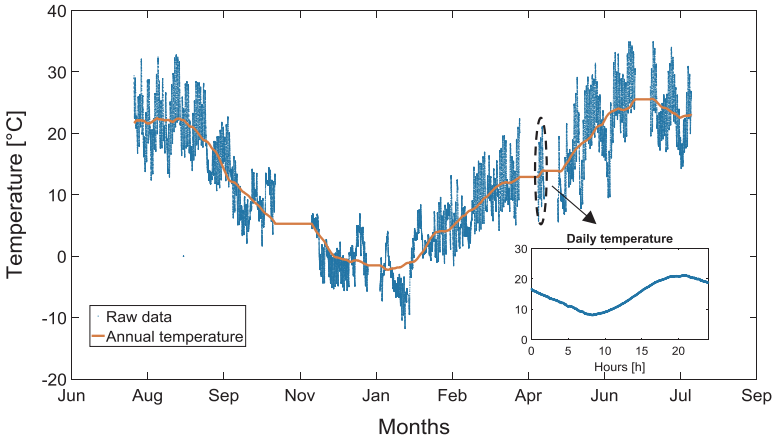

Fig. 13. Annual and daily cycles of concrete temperature.

due to traffic loading.

Numerical models of large civil engineering structures are disposed to uncertain system parameters, which affect the ability of such models to accurately predict the structural response [28]. It is then necessary to develop a detailed finite element model when analyzing the structural response to a specific loading. For this aim, the model was calibrated with monitoring data to reduce the difference between the finite element results and the real-time structural response as obtained by monitoring.

4.1.2. Description of the finite element model

Structural analysis of one span was performed since the seven spans are identical. The concrete and steel were modeled using their initial mechanical properties. To take into account the evolution of material properties during the 60 years of service, the model is calibrated by comparing the simulated strains with the results of the load test. The simulations were performed in the elastic domain.

The element Shell 181 in the ANSYS software was used to model the concrete slab and steel girder. For the slab, an elastic modulus of 35,000 N/mm^2, a Poisson ratio of 0.2, a density of 25 kN/m^3, a compressive strength of 35 N/mm^2 and tensile ultimate strength of 3 N/mm^2 were used.

For the steel girder, an elastic modulus of 210,000 N/mm^2, a Poisson ratio of 0.3 and a compression-tensile ultimate strength of 235 N/mm^2 were used. Material properties are grouped in Table 4.

Mesh density was checked in longitudinal and cross sections by comparing simulated strain for different element sizes. An optimal element size of 100 mm in the longitudinal section and 50 mm in the cross-section were found to give accurate results without time-consuming simulations.

The connection between the reinforced-concrete slab and the girder was assumed a total fixity.

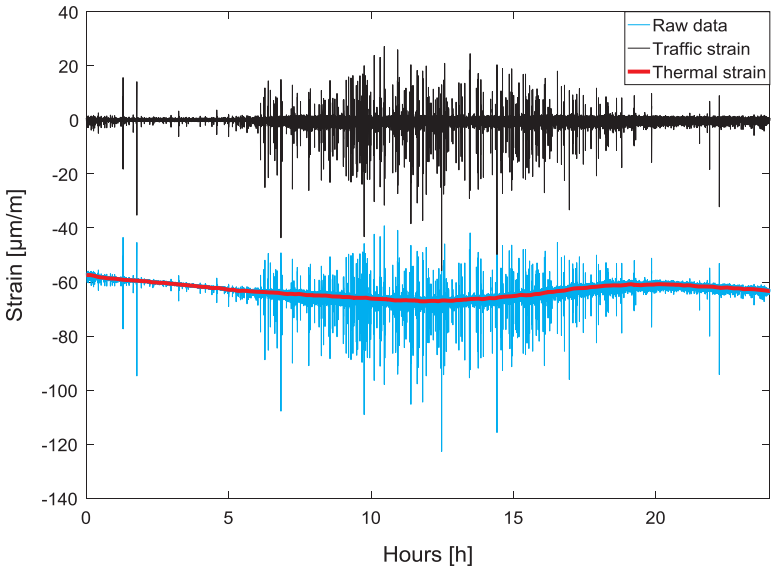

Fig. 14. Daily raw data, thermal strain, and traffic strain.

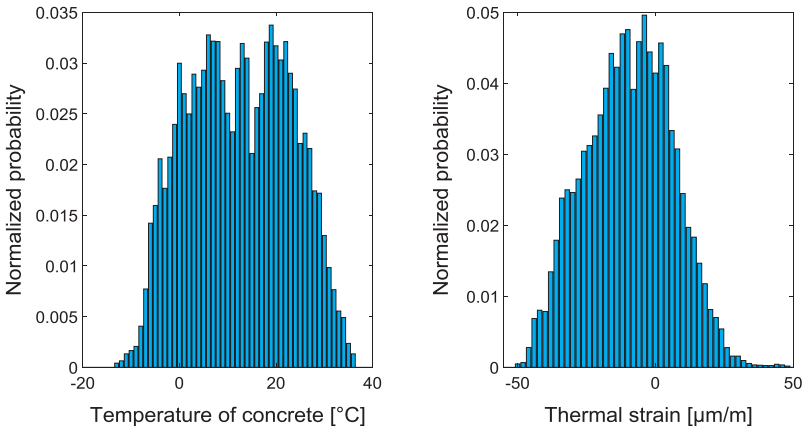

Fig. 15. Normalized annual probability of concrete temperature and thermal strain.

For the boundary conditions, the span was articulated from one side and simply supported as a continuous beam from the other side. The longitudinal displacement and rotations were thus free on one side, and all the displacements and rotations were restricted on the other side.

Fig. 16 includes simulation results for a 5-axle truck with a load of 640 kN on the mid-span.

4.1.3. Calibration of the FE model

The finite element model was calibrated using measured strains and deflections as obtained from the load test. The calibration included changes in material properties, the connections, and the boundary conditions to get the same measured parameters as in the load test [29].

For this case study, the calibration minimizing the difference between monitoring and finite element results was performed in two steps: calibrating strains of the longitudinal section by changing the stiffness, and then calibrating strains and deflection of the transverse section by introducing a calibration factor. Three models are defined: the initial theoretical model, the calibrated model with different stiffness, and the calibrated model with the new stiffness and the calibration factor.

The passages of the 400 kN truck in the centre of the roadway were used for the calibration. The longitudinal response was calibrated by taking the elastic modulus of the concrete as a parameter. It was modified to minimize the difference between the measured and the calculated longitudinal strains.

For the cross-section, a comparison between the results of the non-calibrated finite element model and the load-test model shows that the reinforced-concrete slab is not totally fixed in the steel girder. In fact, the simulated longitudinal strains are identical to monitoring data, but the transverse strains are different. To get closer to real-time measured strains, calibration was proceeded with modeling the elastic flexibility between the girder and the RC slab. This generated some convergence issues due to the use of nonlinear behavior. Therefore, the flexibility between the girder and the slab was introduced by a calibration factor that compensates the difference between the simulated and the measured transverse strain. The calibration factor was found equal to 1.5 to provide the same results as for those obtained by monitoring.

The 2D model was developed to run simulations faster and lighten the calculations while providing the same response of the reinforced-concrete slab as obtained by load test data.

4.2. Simulation and results

Traffic loads are simulated with the toolbox ANSYS_aaS in Matlab providing a direct link between the programs. A Matlab code is developed to run ANSYS commands and save the results for several simulations. Once the deck is modeled, the code generates a new vehicle with a specific load and position, calculates the loads and the positions of the axles, applies the calculated axle loads to the finite element model, runs the model and takes the transverse strain in the mid-span.

The results of the simulation provide the distribution of the strain in the deck for the possible 82 positions and 64 loads.

Fig. 17 includes the distribution of stress ranges in the transverse rebar at the mid-span as a function of vehicle positions and loads. Stress ranges are calculated from the simulated strains using the elastic modulus of steel, 210,000 N/mm^2, and the elastic modulus of concrete, 35,000 N/mm^2.

A small peak can be observed (surrounded by a dashed line), located for stresses under 100kN load, where the passage from two axles to five axles is performed. The peak is present due to the local effect of the applied loads and is more pronounced for two axles. However, this local peak stress is very small and represents less than 1 N/mm^2. As it was highlighted in Section 3.1.7, the number of axles does not induce a significant difference between the simulated stresses. The choice of two axles for loads smaller than 100 kN and five axles for loads higher than 100 kN is thus appropriate.

The simulated and the measured maximum stresses are alike, which proves that the finite element model is well calibrated for the structural response of heavy trucks.

The maximum stresses are due to the heavy trucks located at the mid-span. The trucks create two peaks, 1 m away from the mid-span, which corresponds to the location of the axles.

To define the annual statistical distribution of stresses due to traffic, the position and the load of the vehicles were considered as

Table 4
Material properties.

Material	Density [kN/m^3]	Young's Modulus [N/mm2]	Poisson's Ratio	Element
Reinforced concrete (slab)	25	35,000	0.2	Shell 181
Steel (girder)	78.5	210,000	0.3	Shell 181

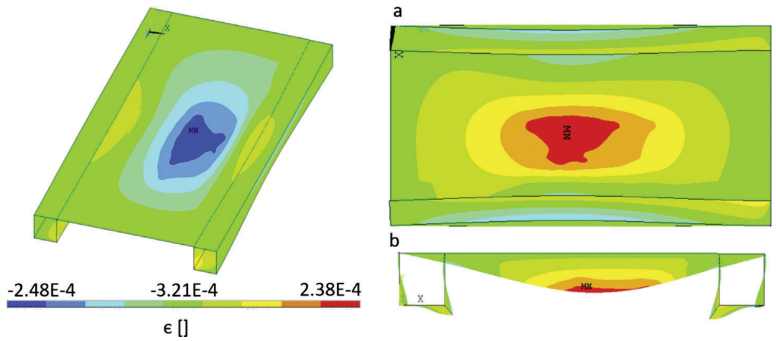

Fig. 16. FEM simulation results of the deck, bottom side (a) and cross-section side (b).

independent stochastic variables. The annual number of cycles with the strain range $\varepsilon_{i,j}$ generated by the vehicle with the position-load $[x_i, L_j]$, is defined from the distributions of the loads and positions (Fig. 8, Fig. 9), according to equation (10).

$$n_{i,j} = P_{x_i} P_{L_j} N \tag{10}$$

where $n_{i,j}$ is the number of vehicles with the position x_i and the load L_j creating the strain range $\varepsilon_{i,j}$

P_{L_j} is the probability that the vehicle has a load L_j

P_{x_i} is the probability that the vehicle is at position x_i

N is the total number of vehicles per year

Fig. 18 provides steps to identify the probabilistic distribution of stresses as a function of the load and the position of the vehicles.

5. Fatigue verification

In this study, the verification of the fatigue safety of the present reinforced concrete slab designed to resist predominantly in the transverse direction is focused on the bending failure mode, which may result either in compression failure of the concrete or tensile failure of the reinforcement.

The recorded strains in the transverse rebars were higher than the strain in the longitudinal rebars, which is mainly due to the distribution of the actual traffic loads on both the RC slab and the steel girder carrying in the longitudinal direction, while in the transverse direction only the 17 cm-thickness RC slab is acting. The mechanism of fatigue failure of reinforced-concrete slabs is complex and depends on many variables (stress ranges, reinforcement ratio, boundary conditions…).

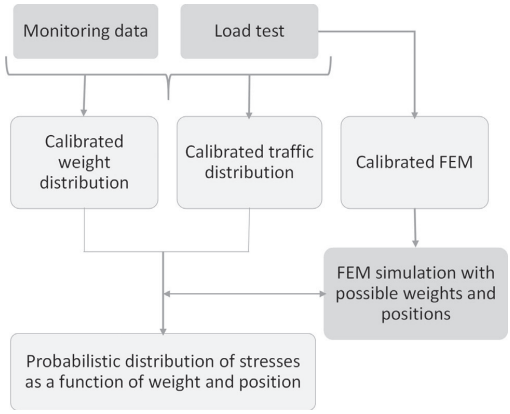

Fig. 18. Steps to define the statistical distribution of traffic stresses.

Previous studies show that the failure can be induced by the interaction of flexural-shear cracks of concrete [12–14] or rebar fracture when there is no longer stress transfer [30,15]. For this study, no concrete cracking was visible in the mid-span of the RC slab, the reversal stresses were present in the longitudinal response as shown in Fig. 4, but were lower than transverse stresses. Even under significant shear fatigue stress, this type of slabs were reported to fail due to fatigue failure of the

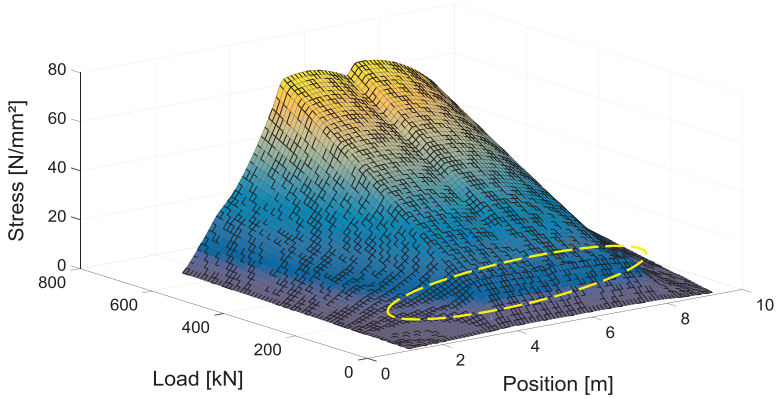

Fig. 17. 3D distribution of the simulated stresses at the mid-span transverse rebar.

rebars [30]. Therefore, the cross-section of the RC slab was defined as the critical section, and the fatigue stress is investigated using the transverse strains. The investigation of the effect of reversal stresses will be presented in future work.

5.1. Fatigue verification of steel reinforcement

Fatigue of steel reinforcement is verified at two levels. The first level requires the verification of the fatigue stresses to be below the endurance limit. Level 2 is performed when Level 1 is not conclusive, and it requires the calculation of the fatigue damage. In the Swiss standard SIA269/2, the fatigue resistance of straight rebars with a diameter less than 30 mm is equal to $\Delta\sigma_{sd,\ fat} = 150\ N/mm^2$ and the endurance limit is equal to 80% of the fatigue limit, i.e., $\Delta\sigma_{sD} = 120\ N/mm^2$, the slope of the S-N curve being equal to m = 4 [31].

The level one is fulfilled for the rebars at the mid-span since all the measured stress ranges are below $120\ N/mm^2$. Therefore, steel reinforcements do not present any fatigue problem based on the one-year monitoring data. The Level 2 of fatigue verification does not need to be performed in this case. However, to illustrate the damage as a function of the actions relevant to fatigue, the recorded stresses are arbitrarily amplified by a factor of 4 to obtain stress values higher than the endurance limit. Subsequently, the Level 2 verification is conducted with fictitious stress values that relate to real loading conditions.

Fatigue damage is quantified in terms of Miner's damage summation to deal with variable amplitude loading in the S-N approach. According to this rule, all stress cycles induce proportional fatigue damage, which is linearly additive. The scatter in the stress history may be neglected and the damage d due to n_i cycles for the stress range $\Delta\sigma_i$ is equal to:

$$d = \sum \frac{n_i}{N_i} \tag{11}$$

where

d	is the cumulative damage
n_i	is the number of cycles for the constant stress $\Delta\sigma_i$
N_i	is the total number of cycles to failure under the constant amplitude stress $\Delta\sigma_i$

The fatigue safety is fulfilled if the accumulated damage is less than 1:

$$d < 1 \tag{12}$$

The damage is calculated according to Eq. (11) using the annual statistical distribution of stresses and stress cycles defined in the previous section. Fig. 19 illustrates the annual distribution of damage for the first year of monitoring as a function of the position and load of vehicles.

The fatigue damage is zero for stresses lower than the endurance limit, which is the case for the vehicles lower than 300 kN, no matter their positions. Only heavy trucks are then relevant for fatigue damage, and the light vehicles can be neglected for the verification of the fatigue safety of steel reinforcement. This justifies the threshold used in the POT approach, discriminating the vehicles that create strain less than 1 μm/m.

Fig. 19 indicates that fatigue damage is more pronounced for the vehicles crossing the roadway from the middle.

The trucks with a load between 350 kN and 400 kN are the most frequent, which is mainly due to the legal load limit for vehicles fixed at 400 kN for this viaduct. The frequency of these trucks creates the highest annual fatigue damage.

The trucks heavier than 400 kN create high fatigue damage. However, they are not frequent, and their annual effect is less pronounced.

To evaluate the accumulated damage during the years of service of the viaduct, and to predict the total damage in the future, the four scenarios of traffic growth introduced in Section 3.1.6 are analyzed. Accordingly, the accumulated damage is calculated for 120 years of service as shown in Table 5.

Even by amplifying the stress ranges arbitrarily with a factor of four, the fatigue damage is small and does not present a significant damage value after 120 years of service, for different scenarios of traffic growth. Consequently, the service duration of the viaduct is very long, with the actual evolution of traffic considering fatigue safety.

The scenarios of traffic growth define the evolution of the accumulated damage. A difference of 40% is present between the non-conservative scenario (2) and the conservative scenario (3). Therefore, the consideration of different scenarios of traffic growth is necessary to quantify the fatigue damage, mainly when no information is available for the past and future traffic.

This inverse method allows evaluating the damage as a function of vehicle position and load. This information may be useful to make decisions about limiting or reducing a particular type of vehicles or imposing certain vehicle positions to restrain fatigue damage. Moreover, this information may also be useful to allow for a controlled increase in the number of vehicles and trucks and the legal vehicle load limit while limiting possible fatigue damage.

5.2. Fatigue verification of concrete

The fatigue of concrete is verified based on the *fib* Model Code [32]. The fatigue requirements under cyclic loading are met if the required lifetime (number of cycles) is lower than or equal to the number of

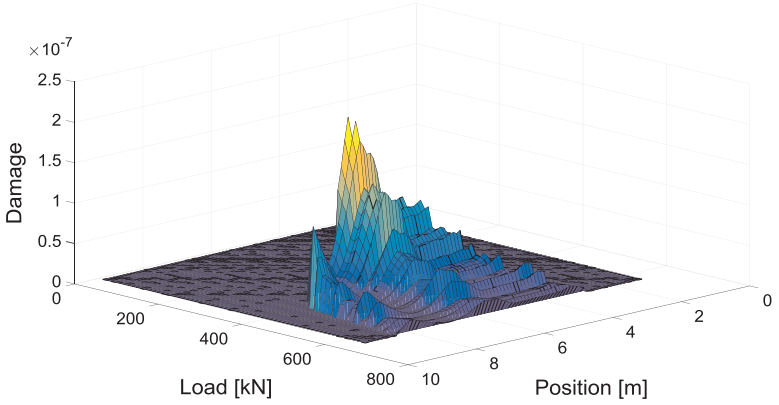

Fig. 19. Annual fatigue damage distribution for the transverse rebar at the mid-span (Monitored stresses are arbitrarily amplified by a factor of four).

Table 5
Accumulated fatigue steel damage for 120 years of service.

Scenario	1	2	3	4
Accumulated damage	4.80 10^{-03}	4.20 10^{-03}	5.90 10^{-03}	5.30 10^{-03}

cycles to failure.

$$n \leq N \tag{13}$$

n is the foreseen number of cycles during the service duration
N is the number of resisting stress cycles

The recorded strains in the transverse rebars were more than twice the strains of the longitudinal rebars. In fact, in the longitudinal section of the viaduct, the applied traffic loads were distributed across the RC slab and the steel girder, but for the cross-section, axle loads were directly distributed along the 17 cm RC slab. Therefore, the reinforced concrete is verified for the cross-section assuming uniaxial tensile stress in the steel reinforcement rebars, and uniaxial compression stress in the concrete. Assessment of fatigue damage for the concrete under compression is presented in the following.

Fatigue loading of concrete is expressed in [32] by the maximum compressive stress level $S_{c,max}$ and the minimum compressive stress level $S_{c,min}$. Such as, for $S_{c,min} > 0.8$, the S-N relations for $S_{c,min} = 0.8$ are valid, and for $0 < S_{c,min} \leq 0.8$, the following equations apply.

The number of cycles N to failure is obtained from

$$\log N = \log N1 \quad if \quad \log N1 \leq 8 \tag{14}$$

$$\log N = \log N2 \quad if \quad \log N1 > 8 \tag{15}$$

where

$$\log\ N1 = \frac{8}{Y-1}(S_{c,max} - 1) \tag{16}$$

$$\log\ N2 = 8 + \frac{8ln(10)}{Y-1}(Y - S_{c,min})\log\left(\frac{S_{c,max} - S_{c,min}}{Y - S_{c,min}}\right) \tag{17}$$

$$with\ Y = \frac{0.45 + 1.8S_{c,min}}{1 + 1.8S_{c,min} - 0.3S_{c,min}^2} \tag{18}$$

$$S_{c,max} = |\sigma_{c,max}|/f_{ck,fat} \tag{19}$$

$$S_{c,min} = |\sigma_{c,min}|/f_{ck,fat} \tag{20}$$

The fatigue reference compressive strength $f_{ck,fat}$ depends on the age of concrete at the beginning of fatigue loading and it may be estimated from [32]:

$$f_{ck,fat} = \beta_{cc}(t)\beta_{c,sus}(t,\ t_0)f_{ck}(1 - \frac{f_{ck}}{400}) \tag{21}$$

with

N	is the number of cycles to failure
$S_{c,max}$	is the maximum compressive stress level
$S_{c,min}$	is the minimum compressive stress level
$\sigma_{c,max}$	is the maximum acting compressive stress in [MPa]
$\sigma_{c,min}$	is the minimum acting compressive stress in [MPa]
f_{ck}	is the characteristic compressive strength
$f_{ck,fat}$	is the fatigue reference compressive strength
$\beta_{cc}(t)$	Is a coefficient which depends on the age of concrete at the beginning of fatigue loading
$\beta_{c,sus}$	Is a coefficient which takes into account the effect of high mean stresses during loading, for fatigue loading it may be taken as 0.85

β_{cc} represents the 'time-dependant' aspect and it is calculated according to equation (22).

$$\beta_{cc}(t) = \exp[s\left(1 - \sqrt{\frac{28}{t}}\right)] \tag{22}$$

such as s = 0.25, a coefficient which depends on the strength class of cement and t is the concrete age in days.

The RC slab is made with a special concrete CP350, with cube strength equal to 45 N/mm^2 at 28 days. f_{ck} is then equal to 35 N/mm^2 and the elastic modulus is equal to 35 000 N/mm^2 [32].

The maximum compressive stress is equal to the stress due to dead loads, temperature and traffic:

$$\sigma_{c,max} = \sigma_{traffic} + \sigma_{dd} + \sigma_{temperature} \tag{23}$$

The minimum compressive stress is equal to the stress due to dead loads and temperature:

$$\sigma_{c,min} = \sigma_{dd} + \sigma_{temperature} \tag{24}$$

where

$\sigma_{traffic}$	is the stress due to traffic loading
σ_{dd}	is the stress due to dead load
$\sigma_{temperature}$	is the stress due to temperature

Strain values in the concrete are deduced from the calculated strain in the transverse rebar at the mid-span with respect to the neutral axis location of the cross-section. For a non-cracked section, the neutral axis is located at a distance of 87.5 mm from the top. The concrete below the neutral axis is assumed to be cracked [30], and steel reinforcement is taking the tensile stress. Accordingly, the recalculation gives the new location of neutral axis at 45 mm below the top. This neutral axis is subsequently used to calculate concrete stresses due to traffic $\sigma_{traffic}$ as the highest stress at the top of the cross-section using measured strain values.

The stress due to dead loads σ_{dd} is obtained from the finite element model.

The stress due to temperature $\sigma_{temperature}$ is considered as a stochastic independent variable, with a discrete distribution defined from monitoring data (Section 3.2.3, Fig. 15).

Stresses are calculated from strain by multiplying them with the elastic modulus of concrete. To obtain significant fatigue stresses, an arbitrarily chosen multiplication factor of four is again used for the stress values of concrete. Each calculated stress corresponds to the passage of a vehicle with the transverse signature illustrated in Fig. 4, thus, for each calculated stress range corresponds ½ cycle.

The fatigue damage of concrete is calculated as a function of temperature variations and the position and the load of the vehicles.

Fig. 20 illustrates the fatigue damage of concrete as a function of vehicle positions and temperature for a load of$L = 320$ kN, as a function of vehicle load and temperature for the position$x = 2.2$ m, and as a function of the load and the position of the vehicles for the temperature $T = 820$ °C.

Temperature variations influence the fatigue damage of concrete, which takes the same distribution of temperature (Fig. 15) for a fixed load or position. The fatigue damage of concrete increases significantly for loads higher than 400 kN, which means that the heavy trucks create higher fatigue damage even if they are not as frequent as the light vehicles. The damage is higher in the Neuchâtel direction, where the heaviest trucks are more frequent. The accumulated fatigue damage according to the four scenarios of traffic growth is presented in Table 6.

The fatigue damage of concrete due to the past and future traffic is also very small, even after 120 years of service, although the values from monitoring were arbitrarily multiplied by a factor of four. Consequently and despite highly conservative assumptions, the

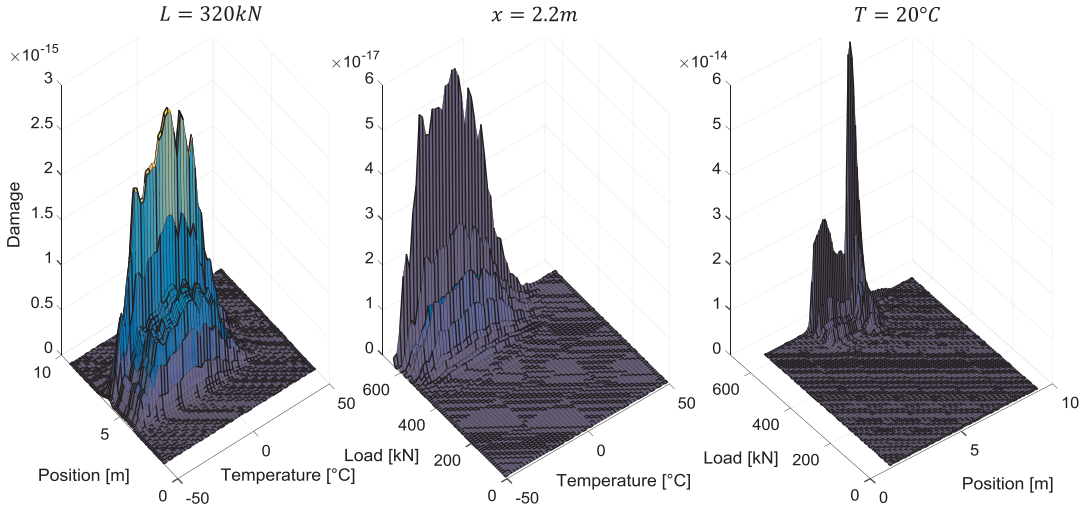

Fig. 20. Long-term fatigue damage distribution of concrete (L = 320 kN, x = 2.2 m, T = 20 °C) (Monitored stresses are arbitrarily amplified by a factor of four).

Table 6
Accumulated fatigue concrete damage for 120 years of service.

Scenario	1	2	3	4
Accumulated damage after 120 years of service	8.90 10^{-04}	7.74 10^{-04}	1.10 10^{-03}	9.81 10^{-04}

concrete of the RC slab does not show any fatigue problem in the present and will not present any notable fatigue issue in the future.

The calculated fatigue damage of concrete is 20% lower than the calculated fatigue damage of steel reinforcement. This means that under pure compression of concrete, the steel reinforcement can be expected to fail first due to tensile cyclic loading. This result coincides with the findings of [10,15,33] where steel rebars failed before concrete under fatigue loading.

5.3. Sensitivity analysis

To understand the interrelation between input parameters and fatigue damage and to identify the parameters that cause significant uncertainties in the calculations, a sensitivity analysis of the fatigue damage of steel and concrete is conducted.

The sensitivity of three main parameters involved in the fatigue damage d calculations is evaluated. The compressive strength of concrete f_{ck}, the stress factor and the annual traffic is varied such that 100% corresponds to their initial values, 35 MPa, 4, and 1 405 502 vehicles/year, respectively (Figs. 21 and 22).

The fatigue damage of steel and concrete presents a linear variation with the annual traffic in terms of vehicle number. In fact, while changing the annual traffic, the position and the load of the vehicles stay constant. The stress ranges are thus the same with different cycles. According to Eq. (11), the fatigue damage is linearly related to the number of stress cycles. Therefore, traffic growth under the same distribution of loads and positions will generate similar growth of fatigue damage.

The fatigue damage of steel is increasing exponentially with the stress factor, while the logarithm of concrete damage and the stress factor are linearly related. The stress factor presents the changes in the stress ranges due to the variation in load and position distributions. Fatigue damage is thus highly sensitive to heavy trucks and the most-loaded positions.

The increase of concrete compression strength creates an exponential decrease in the fatigue damage of concrete. It is then essential to assess the strength of concrete well when evaluating its fatigue safety because it is a critical parameter for fatigue damage.

6. Conclusion

The fatigue safety of the RC slab of a 60-year road viaduct is investigated based on monitoring data, considering the structural response, traffic loads, temperature effect, and their combinations. The main goal of this study is to develop a practical method to evaluate the fatigue safety of RC road bridges. This is particularly significant when using monitoring data that reduces the uncertainties in traffic and environmental load properties and structural response, which is a considerable advantage over design code estimates. For this purpose, the focus was to evaluate the fatigue damage of steel reinforcement and concrete and its evolution in time as a function of temperature variations and the positions and loads of vehicles.

Five main conclusions can be highlighted as follows:

1. The inverse method identifies precisely the loads and positions of all the vehicles that are crossing the RC slab, using data from only four strain gauges and a load test.
2. The combination of FE modeling and probabilistic assessment of monitoring data provides probabilistic distributions of stresses in the RC slab as a function of the load and the position of the vehicles.
3. The comparative verification of both steel reinforcement and concrete identifies the governing material in terms of fatigue safety. Steel reinforcement is governing.
4. Recording ambient temperature and thermal variations of concrete for one year provides reliable data to capture the effect of temperature on concrete fatigue.
5. The sensitivity of fatigue damage to different sources of uncertainties (associated with compressive strength, level of stress and magnitude of annual traffic) is clearly identified.

The results of the inverse method were compared to WIM data and found to be accurate. Hence, the presented methodology can be used to

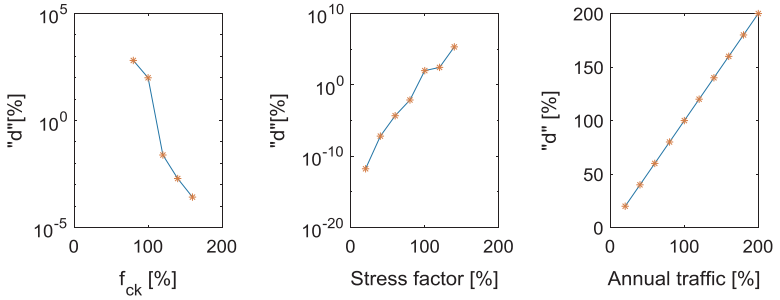

Fig. 21. Sensitivity of the fatigue damage of concrete.

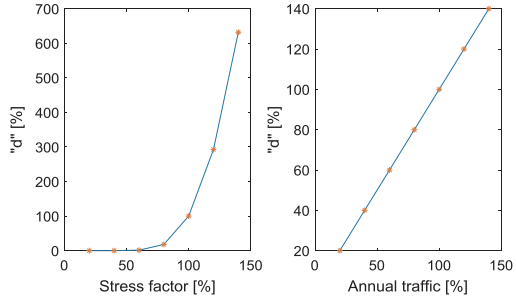

Fig. 22. Sensitivity of the fatigue damage of steel.

verify the RC slabs suspected to have a fatigue problem. The accuracy of the inverse method can be further improved by installing two strain gauges for each lane and direction and performing a load test with different positions, velocities and loads.

The combination of the calibrated finite element model and the probabilistic assessments is demanding. However, it can be updated and used to verify the fatigue safety of the structure for future service duration. Regarding the sensitivity analysis, an extension for the future is to consider it from a reliability point of view, accounting for the uncertainty of the fatigue load and fatigue strength and the influence of the reliability.

Acknowledgments

Current work is carried out under project INFRASTAR (Innovation and Networking for Fatigue and Reliability Analysis of Structures - Training for Assessment of Risk). The project INFRASTAR (infrastar.eu) has received funding from the European Union's Horizon 2020 research and innovation programme under the Marie Skłodowska-Curie grant agreement No 676139.

References

[1] Wöhler A. Wöhler's experiments on the strength of metals. In: Engineering, vol. 4, Lond.; 1867. p. 497–8.
[2] Schijve J. Fatigue of structures and materials. 2nd ed. Netherlands: Springer; 2009.
[3] Siemes AJM, TNO Institue for building materials and structures. Fatigue evaluation of concrete structures preliminary studies, procedure and examples. HERON 1988;33(3):75.
[4] S.I.A. SIA, Ermüdung von Betonbauten. SIA Dokumentation, no. D 0133; 1997.
[5] Fehlmann P. Zur Ermüdung von Stahlbetonbrücken. ETH Zurich; 2012.
[6] CEB, Comité Euro-International du Béton, Fatigue of concrete structures, state of the art, no. 188; 1988.
[7] Spathelf CA. Fatigue performance of orthogonally reinforced concrete slabs. Report: ETH Zurich; 2018.
[8] Treacy MA, Brühwiler E. Action effects in post-tensioned concrete box-girder bridges obtained from high-frequency monitoring. J. Civ. Struct. Health Monit. 2015;5(1):11–28.
[9] Fehlmann P, Vogel T. Experimental investigations on the fatigue behavior of concrete bridges. Sustainable infrastructure : IABSE Symposium, Bangkok 2009. 2009.
[10] Herwig A. Reinforced Concrete Bridges under increased Railway Traffic Loads - Fatigue Behaviour and Safety Measures, PhD Thesis Éc. Polytech. Fédérale Lausanne, no. 4010; 2008.
[11] Schläfli M, Brühwiler E. Fatigue of existing reinforced concrete bridge deck slabs. Eng Struct 1998;20(11):991–8.
[12] Fathalla E, Tanaka Y, Maekawa K. Remaining fatigue life assessment of in-service road bridge decks based upon artificial neural networks. Eng Struct 2018;171:602–16.
[13] Gebreyouhannes E, Chijiwa N, Fujiyama C, Maekawa K. Shear fatigue simulation of RC beams subjected to fixed pulsating and moving loads. J Adv Concr Technol 2008;6(1):215–26.
[14] Maekawa K, Gebreyouhannes E, Mishima T, An X. Three-dimensional fatigue simulation of RC slabs under traveling wheel-type loads. J Adv Concr Technol 2006;4(3):445–57.
[15] Schläfli M, Brühwiler E. Fatigue considerations in the evaluation of existing reinforced concrete bridge decks. IABSE Proc. IABSE Zurich. 1997. p. 76.
[16] Perdikaris PC, Beim S. RC bridge decks under pulsating and moving load. J Struct Eng 1988;114(3):591–607.
[17] Okada K, Okamura H, Sonoda K. Fatigue failure mechanism of reinforced concrete bridge deck slabs. Transp. Res. Rec. 1978.
[18] FEDRO (The Federal Roads Office), "Annual and monthly results of traffic 2002–2017." 2018 < https://www.astra.admin.ch/astra/en/home/documentation/traffic-data/data-and-publication/swiss-automatic-road-traffic-counts–sartc-/annual-and-monthly-results.html > .
[19] Road construction office (Service des ponts et chaussées), "Weekly traffic distribution, Road construction office. Department of territorial management, Neuchatel Canton."; 2018 (sitn.ne.ch).
[20] Stucki D, Meystre M, Lebet J-P. Updated traffic load for concrete deck slabs of existing bridges. Office fédéral des routes; 2014.
[21] Barr PJ, Stanton JF, Eberhard MO. Effects of temperature variations on precast, prestressed concrete bridge girders. J Bridge Eng 2005;10(2):186–94.
[22] Branco FA, Mendes PA. Thermal actions for concrete bridge design. J Struct Eng 1993;119(8):2313–31.
[23] Elbadry M, Ghali A. Nonlinear temperature distribution and its effects on bridges | heat transfer | convection. Scribd 1983.
[24] Priestley MJN. Thermal gradients in bridges, some design considerations. N Z Eng 1972;27(7):228–33.
[25] Zhu X, Dai Z, Ling J, Chen L. Thermal expansion prediction of cement concrete based on a 3D micromechanical model considering interfacial transition zone. Constr Build Mater 2018;171:891–900.
[26] El-Tayeb EH, El-Metwally SE, Askar HS, Yousef AM. Thermal analysis of reinforced concrete beams and frames. HBRC J 2017;13(1):8–24.
[27] Shen L, Ren Q, Zhang L, Han Y, Cusatis G. Experimental and numerical study of effective thermal conductivity of cracked concrete. Constr Build Mater 2017;153:55–68.
[28] Mottershead JE, Friswell MI. Model updating in structural dynamics: a survey. J Sound Vib 1993;167(2):347–75.
[29] Liu Y, Tan Z, Yang C. Refined finite element modeling of a damaged bridge with virtual distortion method coupling solid superelement. Mech Syst Signal Process 2017;93:559–77.
[30] Schläfli M, Brühwiler E. Test Report 'Fatigue of reinforced concrete elements without shear reinforcement; 1999.
[31] SIA 269, Existing structures – Concrete structures. Zurich: Swiss society of engineers and architects; 2013.
[32] CEB.FIP, fib Model Code for Concrete Structures 2010. Paul Beverly, U. K; 2010.
[33] Johansson U. Fatigue tests and analysis of reinforced concrete bridge. Deck Models 2004.

Appendix C.

Paper 3

Fatigue reliability analysis of Crêt de l'Anneau viaduct: a case study

Amol Mankar

Sima Rastayesh

John Dalsgaard Sørensen

This papar has been published online in

Structure and Infrastructure Engineering Journal

doi:https://doi.org/10.1080/15732479.2019.1633361

Amol Mankar

From: NSIE-production@journals.tandf.co.uk
Sent: 18 July 2019 08:28
To: Amol Mankar
Subject: Question about copyright agreement: NSIE 1633361 #TrackingId:4176896

Dear Dr. Amol Mankar,

I hope this email finds you well.

Yes, please include the published paper as part of your Ph.D. thesis.

Regards,

A.B. Indu

Structure and Infrastructure Engineering

From:cats@taylorandfrancis.com
Sent:17-07-2019 03:20
To:cats@taylorandfrancis.com
Cc:ama@civil.aau.dk
Subject: Question about copyright agreement: NSIE 1633361

The following message was sent to you by an author via CATS:

Journal: NSIE
Manuscript ID:1633361
Title:Fatigue reliability analysis of crÃªt de lâ€™Anneau viaduct: a case study

Author / From: Mr Amol Mankar
E-mail: ama@civil.aau.dk

hi, I would like to include my published paper n as part of my Ph.D. thesis, can you permit me to do the same.

STRUCTURE AND INFRASTRUCTURE ENGINEERING
https://doi.org/10.1080/15732479.2019.1633361

Fatigue reliability analysis of crêt de l'Anneau viaduct: a case study

Amol Mankar, Sima Rastayesh, and John Dalsgaard Sørensen

Department of Civil Engineering, Aalborg University, Aalborg, Denmark

ABSTRACT

Fatigue of reinforced concrete is often not considered for civil engineering structures since the self-weights of reinforced concrete structures are very high (in case of normal strength concrete) while live loads are relatively small, which leads to very small stress variations during service duration of the structure. However, particularly for bridge structures with increased use of high strength concrete and increase in traffic loads, this scenario is reversed and fatigue verification becomes much more important for the safety. This paper presents a probabilistic approach for reliability assessment of existing bridges along with reliability-based calibration of fatigue-design-factors based on the S-N approach, calibration of S-N approach with fracture-mechanics approach and reliability updating using inspections along with a case study for the Crêt de l'Anneau viaduct in Switzerland. It has been observed that, a designer needs to design the structure for fatigue life of 3.5–4.5 times the planned service life, in order to achieve the target annual reliability index of 3.7 at the end of the service life. Further, the presented framework can easily be extended to any other viaducts to estimate the fatigue reliability and maintain the safety level throughout the entire service duration.

ARTICLE HISTORY
Received 25 February 2019
Revised 23 May 2019
Accepted 7 June 2019

KEYWORDS
Reliability; fatigue; fracture mechanics; reinforced concrete; bridges; calibration

1. Introduction

Until 1960, it was believed to be impossible to get any fatigue failure in reinforced concrete structures with mild steel as reinforcement within the level of permitted stresses at that time, (Mallet, 1991). Most of the bridges in Switzerland built during the last 50 years are reinforced concrete bridges and they typically experience more than 100 million cycles of fatigue load during design lifetime. This is especially the case for reinforced concrete decks of such bridges exposed to traffic loads during their lifetime, which are not designed for fatigue (Schläfli & Brühwiler, 1998, p. 1).

Currently bridge engineers in the industry use Palmgren & Miner's rule of linear damage accumulation along with Wöhler curves from codes and standards (e.g. SIA-261, 2003) for new structures and (SIA-269, 2016) for existing structures. The result might often be the replacement of the existing bridge or atleast its deck. On strength side, the fatigue tests exhibit large scatter, and on action side, codes defining heavy vehicles as actions/loads may lead to non-economical and non-ecological solutions.

A better way forward could be the use of reliability methods (probabilistic approach) to assess the bridge, by quantifying all possible uncertainties in loads and resistance and thereby form a better basis for decision-making. This requires to formulate a stochastic material model from the fatigue test data and a stochastic load model using among others, the monitoring of strains in the structure at critical locations. By this approach, it is possible to quantify the level of damage and the remaining useful fatigue life of the structure. Further, in order to maintain the reliability above acceptable level throughout the service life, it can be important to perform inspections and use the outcomes of the inspections to update the reliability and proceed with mitigation actions, if necessary.

Fatigue reliability assessment of the steel components of bridges is studied in many references where Weight In Motion data (WIM) are used to estimate the reliability of orthotropic bridge decks (see e.g. Yang, Xinhui, Naiwei, & Yang, 2016). Kihyon and Dan (2010) focussed on fatigue reliability assessment of steel bridges by using probability density functions of the equivalent stress range based on the field monitoring data. Saberi, Rahai, Sanayei, and Vogel (2016) estimated the bridge fatigue service life using operational strain measurements. Furthermore, probabilistic reliability assessment of steel structures exposed to fatigue is studied by Krejsa (2014). Sain and Chandra Kishen (2008) presented a probabilistic approach for assessment of fatigue crack growth in Steel Reinforced Concrete (SRC). Petryna, Pfanner, Stangenberg, and Kratzig (2002) proposed a time variant reliability framework, at component level along with a material model for reinforced concrete; however, the obtained results show its inapplicability to system level.

Based on the literature review, it can be seen that, most of the research work for fatigue of bridges is limited to steel bridges or its components, very few researchers focus on concrete bridges. Further, most of the researchers limit to determinstic approaches, when using monitoring results. To estimate fatigue reliability of a reinforced concrete bridge by taking care of all possible uncertainties in load and fatigue

CONTACT Amol Mankar ama@civil.aau.dk

strength, in a probabilistic way, this paper presents a reliability-based framework for assessment with respect to fatigue failure of Crêt de l'Anneau viaduct as a case study. where the Labourator of Maintenance, Construction and Safety of the structures (MCS) department at École polytechnique fédérale de Lausanne (EPFL), Lausanne, Switzerland has installed a long-term monitoring system for estimating strains in the structure deck slab. As part of reliability-based framework, stochastic modelling of fatigue strength of reinforcing bars along with stochastic modelling of fatigue loads is presented as well as the calibration of fatigue safety factors. The reliability indices obtained are compared with target values indicated in SIA-269 (2016), the Swiss standard for existing structures.

Further, a probabilistic fracture-mechanics (FM) approach (damage evolution model) for the tensile reinforcement is developed based on Ayala-Uraga and Moan (2007), Lotsberg and Sigurdsson (2005), Madsen, Krenk, and Lind (2006), Moan, Hovde, and Blanker (1993) and Paris and Erdogan (1963). The FM approach is calibrated to the probabilistic S-N model using the annual probability of failure. To maintain the required target reliability level, a reliability-based-inspection-planning approach is presented.

2. Crêt de l'Anneau viaduct and its monitoring system

2.1. Salient features

Crêt de l'Anneau viaduct is an eight span composite bridge with a total length of 194.8 m, built in 1957. It has a reinforced concrete deck slab with a thickness of 170 mm at mid-span. The deck is supported by two parallel steel box girders, which have an average height of 1.3 m. These box girders are connected to each other by articulation at about 4 m from the support. The concrete used during construction had a cube strength of 40 MPa, which now may be estimated, approximately to 50 MPa (gain in strength due to continued hydration during ~60 years of life).

The deck slab has an orthogonal grid reinforcement serving for double bending (sagging) behaviour in transverse and longitudinal direction. An orthogonal grid is also present in the hogging bending section, near the longitudinal and transverse supports (near and above the box girders). The grid reinforcement consists of different diameters ranging from 10 mm, 14 mm and 18 mm. 18 mm at 500 mm and 14 mm at 100 mm reinforcement are used in the main transverse bending direction between two girders. Out of the two diameters, 18 mm reinforcement in transverse direction is considered in the current study, where strain gauges are installed. Clear cover to reinforcement is 20 mm.

2.2. Fatigue behaviour

The identified critical part of this composite bridge is the reinforced concrete slab (MCS, 2017, p. 41). The fatigue behaviour of the reinforced concrete deck slab is mainly governed by transverse bending between two girders; it contributes also to local longitudinal bending under vehicle rolling wheel loads, thus it is a double bending behaviour. The stress levels in the steel box girder are very low and below the endurance limit for the steel. Therefore, the current study focuses only on reinforced concrete deck slab, and especially on fatigue of the reinforcement in the tension zone, since fatigue of concrete in the compression zone is unlikely to occur (Rocha & Brühwiler, 2012, p. 1) if concrete is not suffering from any other deterioration mechanisms like frost or aggregate alkali reaction. The behaviour of the viaduct is studied considering:

- Fatigue of steel-reinforcement in tension zone and fatigue of concrete in compression zone, using deterministic approach (Bayane, Mankar, Brühwiler, & Sørensen, 2019).
- Fatigue reliability of concrete in compression zone, using probabilistic approach (Mankar, Bayane, Sørensen, & Brühwiler, 2019).

The results of these studies show that, for this particular viaduct, fatigue of steel-reinforcement in tension zone is critical compared to fatigue of concrete in compression zone.

2.3. Monitoring system

The MCS department at EPFL has installed eight electrical strain gauges on longitudinal and transverse reinforcement bars of two spans of the viaduct, at halfway between articulation and support. Two more strain gauges are installed to capture the response of the steel box girders. First, on the bottom side of the top flange and second, on the bottom side of the bottom flange. Furthermore, thermocouples are installed to measure temperature variations in concrete and steel parts of the viaduct. For details about monitoring system, reference is made to MCS (2017), as shown in Figures 1 and 2.

3. Results of monitoring and stochastic load model

3.1. Measurement of strain and calculation of stresses

A study of influence line diagram for the bridge shows that the maximum stress range for the live loads due to traffic can be expected at the mid-span between articulation and support. At the same location strain, gauges are installed to measure strain variations with a frequency of 50–100 Hz. This high frequency of the strain measurement captures all the vehicles and the associated peaks in the responses. Along with this high-frequency-traffic-strain measurements, the strain gauges also capture a low-frequency-strain change due to the temperature variation and the associated structural response. The two responses can be separated since their frequencies vary largely. Figure 3 depicts strain measurements and corresponding temperature effect.

Figure 1. Monitoring system installed on Crêt de l'Anneau viaduct, a view from bottom of viaduct. (Strain gauges locations are highlighted with explosions.)

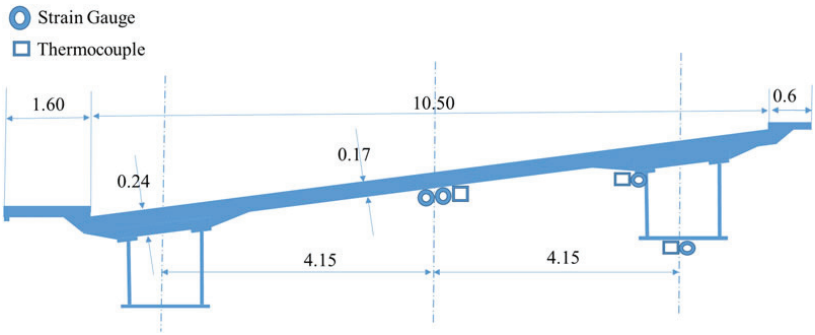

Figure 2. Crêt de l'Anneau viaduct cross section (all dimensions are in m).

The temperature effect can easily be removed from the total response in order to obtain the response due to vehicles only. Five to 10 min averaging time for calculating the mean temperature effect is generally sufficient. Moving average method can be employed using Equation (1) (National-Instruments, 2012). Once the temperature effect is removed from the strains, stresses in the steel-reinforcement can easily be obtained:

$$f(y_i) = \frac{1}{2n+1}\sum_{k=i-n}^{k=i+n} y_k \ \textit{for}\ N - n > i > n \qquad (1)$$

where

$f(y_i)$ = mean temperature effect,
n = averaging time chosen,
N = total number of data points.

3.2. Rain-flow counting and stress histogram

The stress histogram is obtained by rain-flow counting of the strain data for a monitoring duration of 303 days. The number of cycles required for failure are related only to the stress range (and not to the mean-stress), which is similar to the welded steel. The stress range histogram of transverse reinforcement is shown in Figure 4. The fatigue life of the

viaduct can be estimated using the stress range histogram (Figure 4) along with Equation (2) and Miner's rule. As the actual stresses (Figure 4) in the bridge are very low and the bridge has a very high fatigue life. The reliability analysis is illustrated through the actual histogram, which is scaled such that the design equation, with characteristic values and safety factors-DFF, presented in Section 4.2, is exactly fulfilled. The scaling is performed on the stress range as well as on the number of cycles.

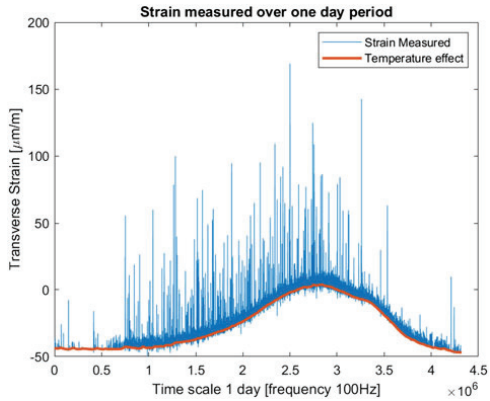

Figure 3. Effect of temperature on strain measurements.

3.3. Stochastic load model for reliability analysis

Uncertainty in the fatigue load (for this specific case, traffic load) covers different aspects and each of them can be modelled independently. These different aspects could be e.g. measurement uncertainty in the strain measurements, as these measurements are very accurate, a very small uncertainty associated with measurement is assumed and modelled as lognormal with a mean of 1.0 and a standard deviation of 0.05, see X_w in Table 1.

Other uncertainties can be related to:

- Extrapolation of results to another location in the structure based on measurement at a certain location (this is not considered here as strain gauges are installed at exactly the same location).
- Extrapolation of the available results to a full year fatigue load based on 303 days observations.
- Extrapolation of the results to the remaining life, which includes year-to-year variations and increase in traffic load and frequency with time.

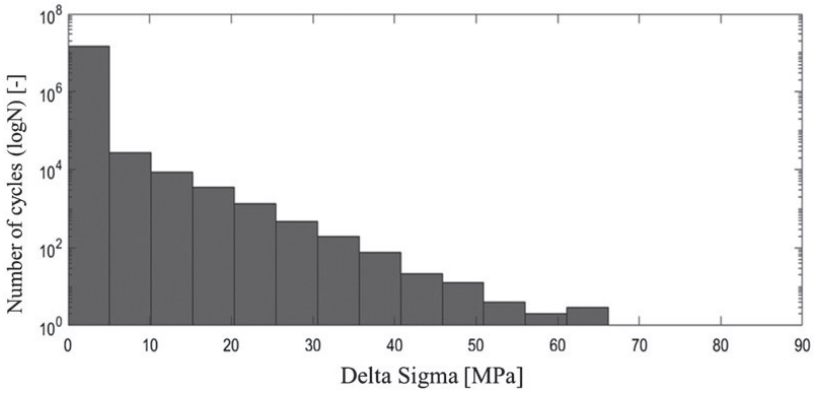

Figure 4. Stress histogram for transverse reinforcement.

Table 1. Stochastic model for Wöhler curve.

Parameter	Distribution	Mean	Standard deviation	Remark
Δ	Lognormal	1	0.30	Model uncertainty related to PM Rule*
X_w	Lognormal	1	0.05	Uncertainty in strain measurements
X_n	Lognormal	1	**0.01** –0.1^{++}	Uncertainty in number of vehicles
$logk$	Normal	18.77	0.07	Location parameter in Wöhler curve
m	Fixed	5	–	Slope of Wöhler curve fixed to 5^{+}
ϵ	Normal	0	$\sigma\varepsilon$	Standard deviation of the error term
σ_ε	Normal	**0.39**/0.20**	0.06	Standard deviation of the error term
$\rho_{logk,\sigma\varepsilon}$	Deterministic	0.06	–	Correlation coefficient between location and standard deviation of error

*Model uncertainty obtained by fitting lognormal distribution to test data in (CEB 1988, 1989).
$^{+}$slope of Wöhler curve fixed to 5 as logk and m are highly correlated with correlation coefficient equal to 0.9997.
$^{++}$Variation in reliability index as function of standard deviation of X_n values is studied.
**Variation in reliability index as function of standard deviation of *logK* values is studied.
Values in bold indicates base values used for reliability analysis.

Available traffic data for 303 days are extrapolated to the total life of the structure by making the assumption of a constant traffic over the entire completed life of 60 years; this is a conservative assumption, as the traffic in the early service duration of the structure is low compared to the present traffic. For the future life of the structure, which is 60 years, 1% increase in the traffic volume each year is assumed. Uncertainties associated with this extrapolation are modelled as lognormal with a mean of 1.0 and standard deviation of 0.10, see X_n in Table 1.

4. Reliability framework

The First Order Reliability Method (FORM) is used for the reliability analysis (Madsen et al., 2006; Sørensen 2011) through the open source Matlab-based toolbox FERUM (Finite Element Reliability Using Matlab) (FERUM, 2010).

4.1. Stochastic material reinforcement in reliability analysis

The deterministic Wöhler curves are recommended by various international codes for the verification of reinforcement fatigue (e.g. DNV OS C 502, 2012; (EN 1992-1, 2004; MC1990, 1993; MC2010, 2013, etc.). These are used as basis for establishing stochastic models together with statistical analysis of the available test data for reinforcement fatigue (Hansen & Heshe, 2001).

For reinforcement fatigue, the number of cycles required for fatigue failure can be calculated based on Wöhler curve, as follows:

$$N = k\Delta\sigma^{-m}$$

or

$$\log N = \log k - m \cdot \log\Delta\sigma + \varepsilon \tag{2}$$

where ε models the uncertainty related to the SN-curve and is assumed Normal distributed with the mean value and the standard deviation equal to 0 and σ_ε respectively. The values of $logk$, m, σ_ε are obtained by the Maximum Likelihood Method (MLM) (Sørensen & Toft, 2010). As these parameters are estimated based on limited set of the data there is a statistical uncertainty, which is presented in Table 1. The use of the MLM provides the option to include run-outs. For more details about probabilistic model for fatigue strength of reinforcing bars and associated uncertainties, reference is made to Rastayesh, Mankar, and Sørensen (2018).

4.2. Design equation and limit state equation

The design equation for reinforcement fatigue is developed based on Equation (2) and Miner's rule, as follows:

$$G = 1 - \sum_{i=1}^{j} \frac{n_i T_F}{k^c} \mathrm{R}_D \Delta\sigma_i^m = 0 \tag{3}$$

where
k^c is the characterisitc value of k;
$logk^c = logk^{mean} - 1.64 \cdot \sigma_\varepsilon$; $logk^c$ corresponds to 95% quantile;
n_i is the number of cycles experienced by the structure—for the i^{th} stress range bin $\Delta\sigma_i$;
j *is the total number of bins*;
T_F is the fatigue life; $T_F = FDF \cdot T_L$; FDF is the fatigue-design factor; T_L is the service life time of the structure;
R_D is modelling the ratio of design parameters, here the section modulus of the deck slab;
$\Delta\sigma_i$ is the stress range for the i^{th} bin.

Stress range for each bin is obtained directly by rain-flow counting of the strain gauge measurements, see Section 3.2. Stress range in each bin is multiplied by the ratio of the design parameters (New design parameter/Original design parameter). A specific value of Fatigue-Design Factor (FDF) can be obtained by changing the ratio of design parameter. The design equation (Equation (3)) can be transformed to a limit state equation by introducing the stochastic variables, as follows:

$$g(t) = \Delta - \sum_{i=1}^{j} \frac{X_n n_i t}{10^\epsilon \cdot k} (X_w R_D \Delta\sigma_i)^m = 0 \tag{4}$$

where t indicates the time $0 < t < T_L$ in years. All other terms in the limit state equation are explained in Table 1.

4.3. Calculation of reliability index

As explained in Section 3.2, the actual stresses in the bridge are very low and the bridge has a very high fatigue life. Therefore, the reliability analyses are performed using the scaled fatigue load. The cumulative (accumulated) probability of failure $P_F(t)$ in the time interval [0, t] is obtained:

$$P_F(t) = P\big(g(t) \le 0\big) \tag{5}$$

The probability of failure is estimated by FORM (see Madsen et al., 2006). The corresponding reliability index $\beta(t)$ is obtained:

$$\beta(t) = -\phi^{-1}(P_F(t)) \tag{6}$$

where $\Phi()$ is the standardised normal distribution function. The annual probability of failure is obtained based on the cumulative probability of failure:

$$\Delta P_F(t) = P_F(t) - P_F(t - \Delta t), t > 1 \text{ year} \tag{7}$$

where $\Delta t = 1$year. The corresponding annual reliability index is denoted $\Delta\beta$.

5. Reliability results with the S-N approach

The current age of the bridge is 60 years, and it is investigated if the bridge can be used for additional 60 years, i.e. a total of 120 years. The reliability is assessed for the reinforced concrete deck slab with respect to fatigue failure of the reinforcement.

Table 2. Stochastic parameters in FM Model.

Parameter	Distribution	Mean	Std-Dev	Remark
a_{cr}	Normal	10.8 mm	1.8 mm	Crack size at unstable fracture (SB)
a_d	Exponential	0.5, 1 ,5* mm	0.5, 1, 5* mm	PoD assumed for AE_Tomography
log$C$	Normal	−12.738	0.11	Material parameter C, (DNVGL)
X_S	LogNormal	1	0.05	Uncertainty in monitored stress
X_n	LogNormal	1	0.05	Uncertainty in number of vehicles

SB: Schläfli and Brühwiler, (1998); DNVGL: DNVGL RP 0001 (2015).
*A sensitivity study is performed for different values of PoD.

5.1. Code requirements for reliability analysis

The Swiss standard (SIA-269, 2016) provides guidelines for assessing the safety of existing structures by a probabilistic approach and presents a target reliability level in the form of reliability indices based on the consequence of failure and the efficiency of interventions (a unity value for the coefficient of efficiency of interventions is recommended by SIA-269 (2016), when it is not determined during the examination phase, see table 2 in Appendix B of SIA-269, 2016). In this study, a low efficiency of intervention is assumed considering that costs to rehabilitate an existing structure as very high and consequences of structural failure are assumed to be serious, which leads to a target annual reliability index of 3.7. Efficiency of safety-related interventions is expressed as the ratio of the risk reduction to the safety costs, which is similar to relative cost of safety measure as explained in probabilistic model code JCSS (2000).

EN 1990 (2002) provides some aspects for assessment of new structures by a probabilistic approach and presents an indicative target accumulated reliability index for life time of 50 years against fatigue. It provides a range of target reliability from 1.5 to 3.8, based on the degree of inspect-ability, repair-ability and damage tolerance (see table C2 in Appendix C of EN 1990, 2002).

5.2. Results of reliability analysis

Results of reliability analysis are presented for different values of Coefficient of Variation (CoV) of *logK*. CoV of *logK* represents the variability in fatigue performance of the steel-reinforcement. It may vary for different deliveries of the steel-reinforcement. Lower the quality control in production of the steel-reinforcement, larger the CoV and lower the fatigue reliability. For current reliability analysis, CoV of 0.39 is used, which is obtained from test results (Hansen & Heshe, 2001). While, CoV of 0.2 is standard CoV recommended by DNVGL RP C203 (2016).

The variation of the cumulative reliability index along the service life of the structure is presented in Figure 5 for the case where the uncertainty in the vehicle number X_n is 1% and CoV for *logK* is 0.39. The annual reliability index ($\Delta\beta$) as a function of the FDF for different CoV values of *logK* representing reinforcement from an arbitrary delivery is presented in Figure 6. It is observed that the CoV of *logK* has a large influence on the reliability index values. To meet a target annual reliability index of 3.7 with planned design life of 120 years, the required FDF is of the order of 3.8 for CoV of 0.2 for *logK*, while the needed FDF is of order of 4.4 for CoV of 0.39 for *logK*.

The annual reliability index (β) as a function of the FDF for different CoV values of *logK* is presented in Figure 7 for

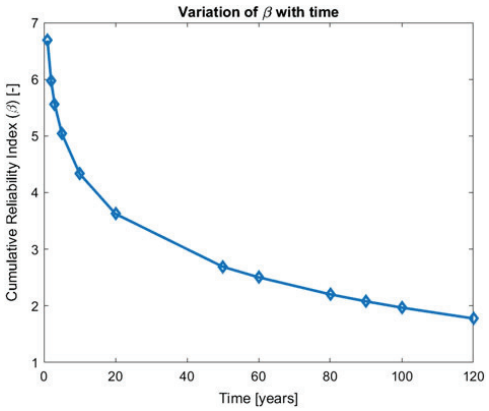

Figure 5. Variation in Cumulative reliability index along service duration of structure (FDF∼2 and T_L=120 years).

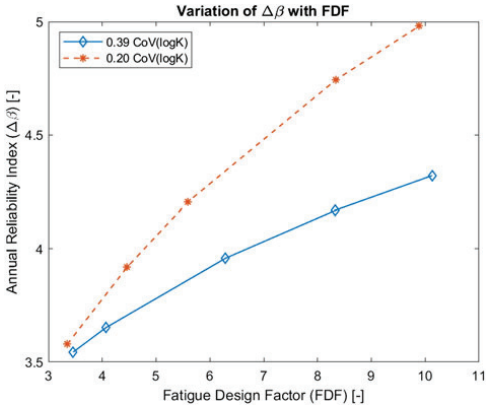

Figure 6. Annual reliability index as function of FDF.

120 years of design life. The cumulative reliability indices in Figure 7 can be compared to the target reliability indices indicated in EN 1990 (2002). A range of fatigue safety factors (FDF) required to achieve the accumulated target reliability index can be obtained from Figure 7.

6. Fracture-mechanics (FM) approach

6.1. FM model for crack growth

This section presents a generic crack growth model based on Paris-Erdogan law (Paris & Erdogan, 1963), for the main

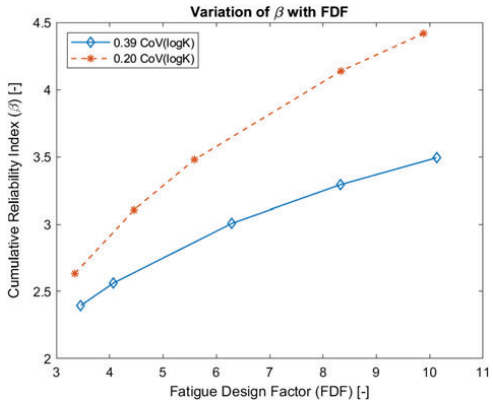

Figure 7. Cumulative reliability index as function of FDF ($T_L = 120$ years for mean values of σ_ε equal to 0.20 and 0.39).

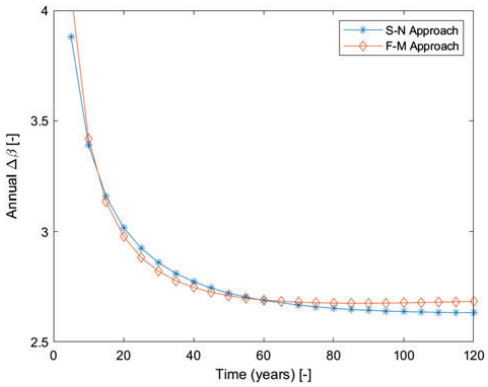

Figure 8. Calibration of FM approach with S-N approach (FDF = 1.5).

reinforcement of 18 mm, at a critical fatigue location. Experimental investigations show that the increment of crack per stress cycle can be approximated as follows:

$$\Delta a = C\left(\sqrt{\pi a}\Delta\sigma Y\right)^m \tag{8}$$

The crack length increment Δa is often very small compared to the variation of $a^{m/2}$, therefore Δa can be idealised to be the differential quotient da/dN, where N is the number of cycles considered as a continuous parameter and then, the solution $a_{(T)}$ is given by Equation (9) (Ditlevsen & Madsen, 1996). The geometry function or shape factor (Y) is assumed to be 1.0 in Equation (9) and it shows sufficiently accurate calibration with S-N approach (see Section 6.3):

$$a_{(T)} = \left[a_0^{\frac{(2-m)}{2}} + \left(\frac{2-m}{2}\right)\cdot C\cdot \pi^{\frac{m}{2}}\cdot \Delta\sigma^m \cdot n\cdot T\right]^{\left(\frac{(2-m)}{2}\right)^{-1}} \tag{9}$$

where
$a_{(T)}$ crack length at time T (years);
a_0 initial crack length back calculated based on calibration (see Section 6.3);
m & Cparameters in Paris' law;
n Number of stress cycles per year with stress range $\Delta\sigma$.

6.2. Limit state equation for FM

A limit state equation corresponding to FM model explained in Section 6.1 can be written as Equation (10). This limit state equation corresponds to the state when the crack size $(a_{(T)})$ in the year under consideration reaches the critical crack size (a_C). The critical crack size is the crack size where the unstable brittle fracture of reinforcement occurs or when rupture occurs. This critical crack size (a_C) can be calculated as the ultimate level of stress based on extreme value theory, however for this paper critical crack size is assumed as normal distributed with a mean value of 60% of the diameter of reinforcement and a CoV of 0.1 (see Table 2 and Rocha & Brühwiler, 2012):

$$g(T) = a_c - \left[a_0^{\frac{(2-m)}{2}} + \left(\frac{2-m}{2}\right)\cdot C\cdot\left(\sqrt{\pi}\cdot\Delta\sigma\right)^m\cdot n\cdot T\right]^{\left(\frac{2-m}{2}\right)^{-1}} \tag{10}$$

6.3. FM calibration

An outcome of an inspection cannot be related directly to the damage obtained from the S-N approach. Therefore, the FM approach with Paris-Erdogan law is used, where an inspection outcome can be related to the crack size, which is obtained from the FM approach. However, calculated fatigue lives based on S-N data are more reliable than those based on FM, as S-N data are derived directly from fatigue tests; while FM is based on calculations where additional parameters are required as input to the analysis. Thus, it is reasonable to make a calibration such that the probability of a fatigue failure based on fracture mechanics follows that of S-N data (test data) until the first in-service inspection. After the first inspection, the results will depend on the FM model and the reliability of inspection method. The calibration purpose, it is assumed that crack growth starts at the first stress cycle and then, the distribution of initial crack size (a_0) is calibrated such that probability of a fatigue failure at a given number of stress cycles is similar to S-N fatigue test data. Thus, this initial crack size is "fictitious" as it can hardly correspond to real physical crack sizes (DNVGL RP 0001, 2015).

Figure 8 presents the calibration of the FM approach with S-N approach. Calibration for the current study is performed such that the reliability index at the inspection year for FM approach is achieved as for the S-N approach. For the rest of the years, the calibration is performed, using a least square fitting method. Two parameters are used here for the calibration, namely the initial crack size (a_0) and the FM approach (m). The resulting amount of required in-service inspection is highly correlated with this calibration (Lotsberg, Sigurdsson, Fjeldstad, & Moan, 2016).

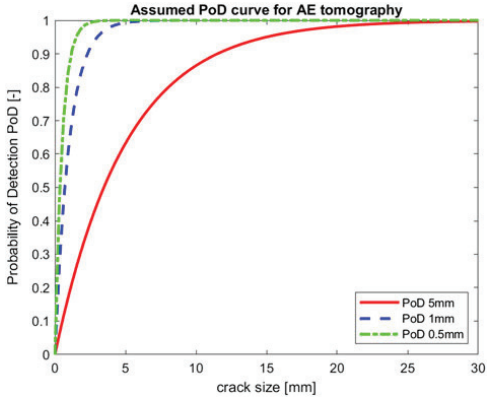

Figure 9. Assumed PoD for AE tomography.

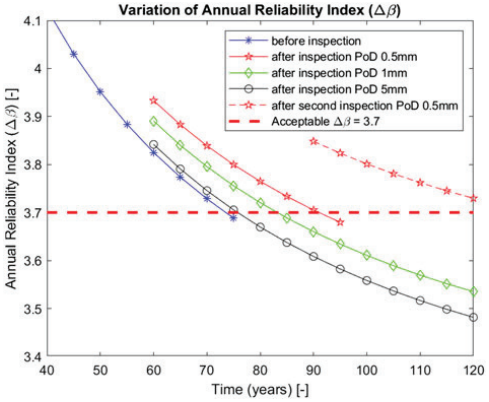

Figure 10. Reliability updating based on AE tomographic inspections for FM approach (FDF∼30).

6.4. Reliability updating using inspections

In order to maintain the reliability level, periodic inspections need to be performed. Information available through inspections can be used to assess the current 'health' of the structure as well as to predict its behaviour, by updating the future failure probabilities. Currently, researchers focus more on understanding fracture surface of reinforcement after failure to know the crack propagation over the diameter. Thus, these present techniques lack to measure the crack size in reinforcement. However, researchers believe that it is possible with Acoustic Emission (AE) tomography (which could be part of a future work for other researchers). In the current study, it is assumed that it is possible to measure the crack size with unknown uncertainty, for the purpose a sensitivity study is performed with different values of uncertainty ranging from 0.5 to 5 mm. The crack size obtained from inspection is used to update the reliability indices, similar to offshore steel structures (DNVGL RP 0001, 2015). It is assumed that the reliability associated with the AE tomography technique is described by a Probability of Detection (PoD) curve (Sergio & Sørensen, 2012), see Figure 9 and Equation (11), where a_d models the smallest detectable crack size:

$$POD(a) = F_{a_d}(a) = 1 - e^{\left(-\frac{a}{b}\right)} \tag{11}$$

where b is the expected value of a_d and is assumed to be equal to 0.5, 1 and 5 mm.

The limit state equation corresponding to an inspection event (h), where no cracks are observed (crack size is less than the detectable crack size a_d), is modelled (see Equation (12)). The inspection event (h) smaller than zero implies that crack size is smaller than the detection ability of inspection method, resulting in no detection of crack while (h) larger than zero implies that crack size is larger than the smallest detectable crack:

$$h\left(T_{insp}\right) = a(T) - a_d \leq 0 \tag{12}$$

The failure probability P_F after an inspection event is updated by calculating the conditional probability of failure, given the inspection event is performed. Bayes' rule is used to obtain the updated failure probability, P_F^U, as follows:

$$P_F^U = P\left(g(T) \leq 0 | h\left(T_{insp}\right) \leq 0\right)$$

$$P_F^U = \frac{P\left(g(T) \leq 0 \cap h\left(T_{insp}\right) \leq 0\right)}{h\left(T_{insp}\right) \leq 0} \tag{13}$$

The numerator in the above equation $P\left(g(T) \leq 0 \cap h\left(T_{insp}\right) \leq 0\right)$ is calculated as the probability of failure of a parallel system by FORM (Madsen et al., 2006). The corresponding updated annual reliability index can be obtained:

$$\Delta\beta^U(\mathrm{T}) = -\emptyset^{-1}\left(\begin{array}{c} P\left(g(T) \leq 0 | h\left(T_{insp}\right) \leq 0\right) - \\ P\left(g(T-1) \leq 0 | h\left(T_{insp}\right) \leq 0\right) \end{array}\right)$$
$$T > T_{insp} \tag{14}$$

Figure 10 illustrates the variation of annual reliability index along the service life the structure, at about 75 years of life the annual reliability index is lower than threshold value of 3.7 specified in SIA-269 (2016), thus it is assumed that an inspection of reinforcement near the critical fatigue location is performed at 60 years of life (current year) with AE tomography and no crack was found. The failure probability is updated after the inspection event at 60th year, and thus updated annual reliability after 60th year is obtained for remaining service life until planned future life of 120 years.

It is seen that for AE tomographic inspection with high uncertainty, i.e. mean value of 5 mm for PoD, there is no gain in the form of updated failure probability (P_F^U). The updated failure probability follows almost the same trend as if there is no inspection performed. While with reduction in the uncertainty for AE tomographic inspection to 0.5 mm, the gain in updated probability of failure (P_F^U) is significant. The updated failure probability (P_F^U) crosses the target reliability threshold at about 90 years of life instead of 75 years. Further, if a second inspection is performed at 90 years with

an assumed outcome of no crack detection, then for the remaining service life, the structure meets the requirement of the minimum acceptable level of annual reliability index of 3.7.

7. Conclusions

In this paper, the probabilistic framework for estimating fatigue reliability of bridges is presented. As a case study, fatigue reliability of Crêt de l'Anneau viaduct is presented by formulating the stochastic models for action effects (strain/stress) based on monitoring data and for fatigue resistance of steel-reinforcement based on fatigue test data of steel-reinforcement. It has been observed that the reliability indices for the structure are larger than the acceptable level. As the structure considered in the case study exhibits a very high reliability level with respect to fatigue failure of the reinforcement, the traffic load on the structure can be increased along with the life extension of the structure.

CoV of *logK* has been found to have a large influence on the reliability index values. To meet a target annual reliability index of 3.7 with a planned design life of 120 years, the required FDF is of the order of 3.8 for CoV of 0.2 for *logK*, while the needed FDF is of order of 4.4 for CoV of 0.39 for *logK*. FDF of 3.8 can be interpreted deterministically as the designer should consider designing the structure with a fatigue life of $3.8 * 120 = 456$ years to achieve a target annual reliability index of 3.7 at the end of 120 years of service life when CoV of *logK* is 0.2 while a fatigue life of $4.4 * 120 = 528$ years needs to be used if CoV of *logK* is 0.39.

No noticeable variation in the reliability index is observed for a sensitivity study of the uncertainty associated with vehicle numbers X_n with CoV ranging from 1% to 10%. However, it is seen that changes in uncertainty associated with *logK* result in large variations in the reliability index. Thus, focus should be on reducing the uncertainty in *logK* in order to take decisions. It is observed that calibration of FM approach with S-N approach works well for reinforcement as well similar to offshore oil and gas steel structures using Paris-Erdogan law.

Furthermore, updating the reliability using inspection information by the FM approach is a very useful tool to assess the reliability of the existing assets, however it should be noted that outcome of these updates in safety assessment (or failure probability) is highly dependent on the uncertainty associated with the inspection technique and more work is needed to develop inspection techniques for reinforcements, especially methods that can give indirect information on the fatigue damage state of the reinforcement. The current approach uses only fatigue limit state at the component level reliability, it would be interesting to see the results which include the system level reliability coupled with the ultimate failure of bridge decks.

Funding

The project INFRASTAR (infrastar.eu) has received funding from the European Union's Horizon 2020 research and innovation programme under the Marie Skłodowska-Curie grant agreement No. 676139.

ORCID

Amol Mankar 0000-0003-4015-041X
Sima Rastayesh 0000-0001-9536-3469
John Dalsgaard Sørensen 0000-0001-6987-6877

References

Ayala-Uraga, E., & Moan, T. (2007). Fatigue reliability-based assessment of welded joints applying consistent fracture mechanics formulations. *International Journal of Fatigue*, *29*, 444–456. doi:10.1016/j.ijfatigue.2006.05.010

Bayane, I., Mankar, A., Brühwiler, E., & Sørensen, J. D. (2019). Quantification of traffic and temperature effects on the fatigue safety of a reinforced-concrete bridge deck based on monitoring data. *Engineering Structures*, in press.

CEB 1988. (1989). *Fatigue of concrete structures - State of Art Report*. Zurich: CEB.

Ditlevsen, O., & Madsen, H. (1996). *Structural reliability methods* (1st ed.). Chichester, UK: John Wiley & Sons Ltd.

DNV OS C 502. (2012). *DNV OS C 502, Offshore concrete structures*. Høvik: DNVGL.

DNVGL RP 0001. (2015). *Probabilistic methods for planning of inspection for fatigue cracks in offshore structures*. Oslo: DNVGL.

DNVGL RP C203 (2016). *DNVGL RP C203 Fatigue design of offshore steel structures*. Høvik: DNVGL.

EN 1990 (2002). *EN 1990 Basis of structural design*. Brussels: European Committee for Standardisation.

EN 1992-1 (2004). *Design of concrete structures – Part 1-1: General rules and rules for buildings*. Brussels: European Committee for Standardisation.

FERUM. (2010). *Finite Element Reliability Using Matlab*. Berkeley: University of California.

Hansen, L. P., & Heshe, G. (2001). Fibre Reinforced Concrete and Ribbed Bars. *Nordic Concrete Research*, *26*, 17–37.

JCSS. (2000). *JCSS probabilistic model code*. Joint Committee on Structural Safety JCSS. ISBN: 978-3-909386-79-6.

Kihyon, K., & Dan, M. F. (2010). Bridge fatigue reliability assessment using probability density functions of equivalent stress range based on field monitoring data. *International Journal of Fatigue*, *32*, 1221–1232.

Krejsa, M. (2014). Probabilistic reliability assessment of steel structures exposed to fatigue. In *Safety, reliability and risk analysis: Beyond the horizon*. Boca Raton, London, New York, Lejden: CRC Press.

Lotsberg, I., & Sigurdsson, G. (2005). Assessment of input parameters in probabilistic inspection planning for fatigue cracks in offshore structures. In Proceedings of the 9th International Conference on Structural Safety and Reliability, ICOSSAR'05, Rome, Italy.

Lotsberg, I., Sigurdsson, G., Fjeldstad, A., & Moan, T. (2016). Probabilistic methods for planning of inspection for fatigue cracks in offshore structures. *Marine Structures*, *46*, 167–192. doi:10.1016/j.marstruc.2016.02.002

Madsen, H. O., Krenk, S., & Lind, N. C. (2006). *Methods of structural safety*. New York: Dover Publications.

Mallet, G. P. (1991). *Fatigue of reinforced concrete (state of the art review)*. Stationery Office Books (TSO). ISBN-10: 0115509798, ISBN-13: 978-0115509797

Mankar, A., Bayane, I., Sørensen, J. D., & Brühwiler, E. (2019). Probabilistic reliability framework for assessment of concrete fatigue of existing RC bridge deck slabs using data from monitoring. *Engineering Structures*, in press.

MC1990. (1993). *FIB model code for concrete structures 1990*. Berlin: Ernst & Sohn.

MC2010. (2013). *FIB model code for concrete structures 2010*. Berlin: Ernst & Sohn.

MCS. (2017). *Surveillance du Viaduc du Crêt de l'Anneau par un monitoring à longue durée*. Lausanne: MSC.

Moan, T., Hovde, G., & Blanker, A. (1993). *Reliability-based fatigue design criteria for offshore structures considering the effect of inspection and repair* (II, pp. 591–600). Houston, TX: 25th Offshore Technology Conference.

National-Instruments. (2012). *Smoothing functions*. Retrieved from http://zone.ni.com/reference/en-XX/help/370859K01/genmaths/genmaths/calc_smoothfunctions/

Paris, P., & Erdogan, F. (1963). A critical analysis of crack propagation laws. *Journal of Basic Engineering*, *85*, 528–534. doi:10.1115/1.3656900

Petryna, Y. S., Pfanner, D., Stangenberg, F., & Kratzig, W. B. (2002). Reliability of reinforced concrete structures under fatigue. *Reliability. Engineering and System Safety*, *77*, 253–261. doi:10.1016/S0951-8320(02)00058-3

Rastayesh, S., Mankar, A., & Sørensen, J. D. (2018). Comparative investigation of uncertainty analysis with different methodologies on the fatigue data of rebars. In *IRSEC2018*. Arzhang Printing: Shiraj, Iran.

Rocha, M., & Brühwiler, E. (2012). Prediction of fatigue life of reinforced concrete bridges using Fracture. In Bridge Maintenance, Safety, Management, Resilience and Sustainability. London: CRC Press.

Saberi, M. R., Rahai, A. R., Sanayei, M., & Vogel, R. M. (2016). Bridge fatigue service-life estimation using operational strain measurements. *Journal of Bridge Engineering*, *21*, 04016005. doi:10.1061/(ASCE)BE.1943-5592.0000860

Sain, T., & Chandra Kishen, J. M. (2008). Probabilistic assessment of fatigue crack growth in concrete. *International Journal of Fatigue*, *30*, 2156–2164. doi:10.1016/j.ijfatigue.2008.05.024

Schläfli, M., & Brühwiler, E. (1998). Fatigue of existing reinforced concrete bridge deck slabs. *Engineering Structures*, *20*, 991–998.

Sergio, M.-D., & Sørensen, J. D. (2012). Fatigue reliability and calibration of fatigue design factors for offshore wind turbines. *Energies*, *5*, 1816–1834. doi:10.3390/en5061816. doi:10.3390/en5061816

SIA-261. (2003). *SIA 261 – Action on structures*. Zurich: Swiss Society of Engineers and Architects.

SIA-269. (2016). *Existing structures – Bases for examination and interventions*. Zurich: Swiss Society of Engineers and Architects.

Sørensen, J. D. (2011). *Notes in structural reliability theory and risk analysis*. Denmark: Aalborg University.

Sørensen, J. D., & Toft, H. S. (2010). Probabilistic design of wind turbines. *Energies*, *3*, 241–257. doi:10.3390/en3020241

Yang, L., Xinhui, X., Naiwei, L., & Yang, D. (2016). Fatigue reliability assessment of orthotropic bridge decks under stochastic truck loading. *Shock and Vibration*, *2016*(3), 1–10.

Appendix D.

Paper 4

Probabilistic fatigue design of reinforced-concrete wind turbine foundations

Amol Mankar

John Dalsgaard Sørensen

This papar has been published online in

ICASP-13 (Open Access policy)

doi:https://doi.org/10.22725/ICASP13.025

13th International Conference on Applications of Statistics and Probability in Civil Engineering, ICASP13
Seoul, South Korea, May 26-30, 2019

Probabilistic fatigue design of reinforced-concrete wind turbine foundations

Amol Mankar
PhD Fellow, Dept. of Civil Engineering, Aalborg University, Aalborg, Denmark

John Dalsgaard Sørensen
Professor, Dept. of Civil Engineering, Aalborg University, Aalborg, Denmark

ABSTRACT: Probabilistic fatigue design of wind turbines is a new approach to optimize the design by reducing in a reliability- and cost-optimal way the amount of materials used for the construction, ultimately reducing the cost of energy. This paper presents such a probabilistic framework for reliability assessment of onshore wind turbine foundations with aim to optimize the design. This framework includes stochastic modelling of fatigue strength based on a large database of test results, stochastic modelling of the fatigue load (wind), modelling of the related epistemic and aleatory uncertainties, along with a case study showing how optimization could be exercised using the reliability-based framework.

1. INTRODUCTION

It is important to design wind turbine structures to a specific (target) reliability level, in order to avoid conservative designs and excessive use of materials with the overall aim to minimize the cost of such installations and ultimately the cost of energy (Sørensen & Toft, 2006).

Wind turbines are exposed to cyclic load from wind. This causes fatigue of all components of the wind turbine including the reinforced concrete foundation. In most of the cases, fatigue design governs the structural dimensions or the amount of reinforcement in the foundation of an onshore wind turbine, (Görasson & Nordenmark, 2011). However, estimating the level of damage in the foundation is complex and therefore prediction of the actual fatigue life is difficult. The current international codes use models for damage accumulation with respect to fatigue of concrete, which are generally conservative; they are not able to predict the real behavior accurately but can only predict the remaining useful life with uncertainty.

This paper presents a probabilistic framework for reliability assessment with respect to fatigue failure of an onshore reinforced concrete wind turbine foundation. This includes stochastic modelling of the fatigue strength, stochastic modelling of fatigue loads, uncertainties associated with strength and load modelling, and reliability-based calibration of material partial safety factors (γ_C) for design with respect to fatigue failure of the concrete. Examples of reliability assessment and optimization of design parameters will be presented.

2. DETAILS OF THE ONSHORE WIND TURBINE FOUNDATION

A gravity spread foundation is the most commonly used foundation for onshore wind turbines. This is due to ease of construction with little excavation and refill work. This foundation consists of a large slab, which could be square, octagonal or circular in plan, with or without thickness variation. Typically the reinforcement is placed at top and bottom layers of the slab with orthogonal grids and radial pattern through an embedded ring. This radial pattern can also be used for circular slabs. Typically, this kind of foundation transmits forces from wind turbine tower to soil to a larger area by a spreading action. The foundation slab transmits the forces from the tower to the soil by a cantilever bending action,

and thus the cross section of the slab experiences bending moment and bending stresses. These variations in the fatigue forces / stresses are modelled by force / stress ranges and mean values in the form of Markov Matrices (Sandia National Laboratories, 1999).

This paper deals with fatigue reliability assessment of a similar reinforced concrete foundation as described in (Svensson, 2010) along with a Markov-matrix based on 20 years of wind data for a Siemens wind turbine described in (Görasson & Nordenmark, 2011). The basic features of the wind turbine foundation is shown in Figure 1 and Table 1.

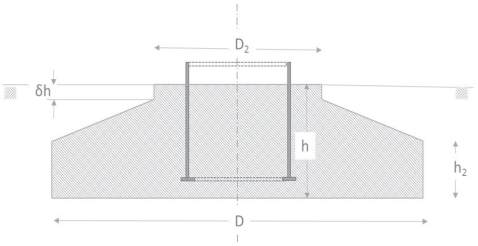

Figure 1: Principal geometry of the foundation

Table 1: Main Design characteristic of the wind turbine foundation.

Hub-height	99.5 m
Design wind speed at hub-height	8.5 m/s
Shape	Circular
Concrete class	C30/37
Diameter (D & D_2)	15.66 m, 6.0 m
Thickness (h & h_2)	3.0 m, 1.73 m
Pedestal height (δh)	0.27 m
Reinforcement type	B500B
Reinforcement	1540 mm^2/m

Part of the Markov matrix is shown in Table 2 and Figure 2. Heading in Table 2 shows the mean values of overturning moment. The values in Table 2 show amplitudes to be added or subtracted from mean values in the heading to obtain maximum and minimum overturning moments. The first column indicates the number of cycles observed during one year.

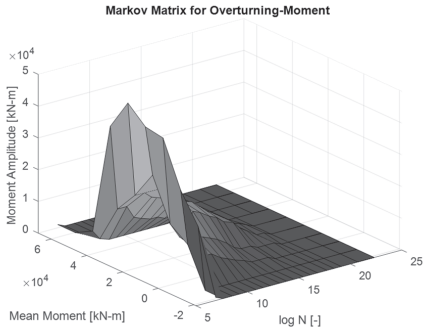

Figure 2: Markov matrix for overturning moment

3. MODELLING OF UNCERTAINTIES

The following uncertainties are considered in the current paper: concrete strength, fatigue strength model for linear damage accumulation (S-N) curves, wind load effects and Miner's rule. This includes modelling of all epistemic and aleatory uncertainties.

3.1. Concrete strength

The reference property of concrete is the compressive strength f_c of standard test specimens (cylinder of 300 mm height and 150 mm diameter), tested according to standard conditions at a standard age of 28 days (ISO 1920, 2004) and (ISO 3893, 1977). All other properties (e.g. tensile strength, modulus of elasticity, and compressive strain) are related to the reference strength of concrete.

However, the reference strength of concrete is subject to both aleatory and epistemic uncertainties. Stochastic modelling of f_c is explained in various international standards, guidelines and background documents e.g. (JCSS, 2000), (DS-INF 172, 2009), (EN 1992-1, 2004) and (MC2010, 2013).

The stochastic modelling applied in (DS-INF 172, 2009) is adopted here. Accordingly, the concrete compression strength is assumed to be lognormal distributed with a mean value of

f_{cm} and a standard deviation σ_{fc}. The associated Coefficient of Variation (CoV) becomes $V_{fc} = 0.14$.

Table 2: Fatigue overturning moment spectrum (Görasson & Nordenmark, 2011).

	Peak-to-peak fatigue load bins [kNm]									
	mean values of moment [kNm]									
(n_i)	-21300	-11450	-1600	8250	18100	27950	37800	47650	57500	67300
1.0E+9	0	0	0	0	0	0	0	0	0	0
5.0E+8	0	0	0	0	0	0	0	0	0	0
2.0E+8	0	0	0	5	5	5	0	0	0	0
1.0E+8	0	0	0	5	1000	1000	5	0	0	0
5.0E+7	0	0	5	1000	1000	2000	5	0	0	0
2.0E+7	0	0	5	1000	3000	3000	1000	0	0	0
1.0E+7	0	0	5	1000	4950	4950	2000	0	0	0
5.0E+6	0	0	1000	2000	6950	6950	3000	0	0	0
2.0E+6	0	0	1000	2000	7950	8900	4000	0	0	0
1.0E+6	0	0	1000	3000	9900	10900	4950	0	0	0
5.0E+5	0	0	2000	4950	10900	12900	5950	0	0	0
2.0E+5	0	0	3000	6950	12900	13850	5950	0	0	0
1.0E+5	0	0	4000	7950	13850	14850	6950	0	0	0
5.0E+4	0	0	4950	8900	6850	15850	6950	5	0	0
2.0E+4	0	0	6950	9900	17800	17800	7950	5	0	0
1.0E+4	0	0	6950	9900	19800	17800	8900	5	0	0
5.0E+3	0	0	9900	10900	23750	19800	12900	5	0	0
2.0E+3	0	5	11900	15850	28700	19800	12900	1000	0	0
1.0E+3	1000	20800	29700	43550	44500	49450	39600	4000	1000	1000

Number of cycles

3.2. Fatigue strength model

The FIB Model Code 2010, (MC2010, 2013), presents a model to estimate the number of fatigue cycles to failure by equation (2), see below, which then can be used to estimate the level of fatigue damage in concrete. For reliability analysis equation (2) is modified to equation (4) removing the safety factors and characteristic values applied in (MC2010, 2013). A few stochastic variables are introduced X_1, X_2 & ϵ. Here, X_1 corresponds to condition of $S_{max} = 1$ at $\log N = 0$, X_2 corresponds to limit of linearity of these curves presented, see Figure 3, and ϵ models the model uncertainty associated with the fatigue strength model. Using a large database complied from literature (Lantsought, 2014), (Lohaus, Oneschkow, & Wefer, 2012) & (Thiele, 2016) of fatigue laboratory tests, estimates of X_1, X_2 and σ_ε are obtained using the Maximum Likelihood Method (MLM), and corresponding parameter uncertainties (standard deviations and correlation coefficients) are estimated, see (Mankar, Bayane, Sørensen, & Brühwiler, 2018) & (Mankar, Rastayesh, & Sørensen, 2018). To obtain a stochastic model for fatigue of concrete for the wind turbine foundation, fatigue test data within the range of compressive strength varying from 20 MPa to 60 MPa from database (described above) are used. This range represents the variability of the compressive strength in the foundation concrete, which is class C 30/37. See Table 3 for stochastic parameters described and obtained by MLM for this wind turbine. Figure 3 shows the mean failure curves obtained using equation (4) for the chosen dataset within range of 20 MPa to 60 MPa.

3.3. Wind load

A model uncertainty related to fatigue load assessment X_W is introduced in order to capture the uncertainty related to the assessment of the fatigue load from wind turbine structure, controller, turbulence simulation and aero-elastic model, see (Toft, Svenningsen, Sørensen, Moser, & Thøgersen, 2016).

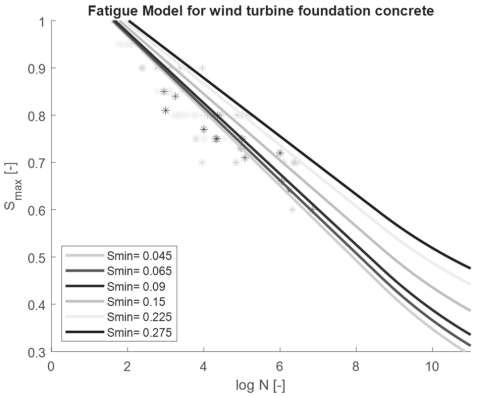

Figure 3: Fatigue strength model of concrete for onshore wind turbine foundation

4. DESIGN-EQUATION

A design-equation is formulated for fatigue failure of concrete based on Miner's rule of linear damage accumulation, as shown in equation (1).

$$G(T_L, Z) = 1 - Damage = 1 - \sum \frac{n}{N} = 1 - \sum_{i=1}^{N_{smax}} \sum_{j=1}^{N_{smin}} \frac{n_{ij} \cdot \mathrm{T_L}}{N_{Dij}} \quad (1)$$

where

T_L service life of the structure

N_{Smax} and N_{Smin} are the number of bins for $S_{Cd,max}$ and $S_{Cd,min}$ respectively

n_{ij} experienced / observed number of stress cycles of $S_{Cd,max,i}$ and $S_{Cd,min,j}$ in each bin (i,j) per year

$N_{D,ij}$ required number of stress cycles of $S_{Cd,max,i}$ and $S_{Cd,min,j}$ in each bin (i,j) per year for failure calculated deterministically based on equation (2).

Z design parameter, for current case it is tensile reinforcement area.

$$\log N_{D,ij} = \frac{8}{(Y-1)} \cdot \left(S_{cd,max,i} - 1\right), \text{if } \log N_{D,ij} \le 8$$

$$\log N_{D,ij} = 8 + \frac{8 \cdot \ln(10)}{(Y-1)} \cdot \left(Y - S_{cd,min,j}\right) \cdot \log\left(\frac{S_{cd,max,i} - S_{cd,min,j}}{Y - S_{cd,min,j}}\right), \text{if } \log N_{D,ij} > 8 \quad (2)$$

where

$Y = \frac{0.45+1.8 \cdot S_{cd,min}}{1+1.8 S_{cd,min} - 0.3 \cdot S_{cd,min}^2}$

$S_{cd,max,i} = \frac{\gamma_{ED} \cdot |\sigma_{c,maxi}| \cdot \eta_c}{f_{cd,fat}}$

$S_{cd,min,j} = \frac{\gamma_{ED} \cdot |\sigma_{c,min,j}| \cdot \eta_c}{f_{cd,fat}}$

γ_{ED} the partial safety factor for fatigue load. For this case, γ_{ED} is considered as 1.0 as direct strain measurements are available, (MC2010, 2013).

η_c the averaging factor for concrete stresses in the compression zone considering stress gradient. The recommended value 1.0 for uniform stress i.e. for the case of no stress gradient.

$f_{cdfat} = \beta_{c,sus(t,t0)} \cdot \beta_{cc(t)} \cdot f_{cd} \cdot (1 - f_{cd}/400)$, is the design reference fatigue strength.

$f_{cd} = f_{ck}/\gamma_c$

γ_c the partial safety factor for material; 1.5 is recommended in (MC2010, 2013).

$\beta_{cc(t)}$ factor considered for strength gain over time due to continued hydration.

$\beta_{c,sus(t,t_0)}$ is a coefficient, for fatigue loading it may be taken as 0.85.

$\sigma_{c,max,i}$ & $\sigma_{c,max,i}$ are max. and min. stresses used to obtain $S_{cd,max,i}$ and $S_{cd,min,j}$

$\sigma_{c,max,i} = \sigma_{DL}(Z) + \sigma_{WL,max}(Z)$

$\sigma_{c,min,j} = \sigma_{DL}(Z) + \sigma_{WL,min}(Z)$

σ_{DL} stress due to dead load

σ_{WL} stress due to wind load on the turbine

E_c modulus of elasticity of concrete in MPa, $E_c = 4700 \cdot \sqrt{f_{ck}}$

f_{ck} characteristic static compressive strength of concrete in MPa.

5. LIMIT-STATE-EQUATION

A limit-state-equation corresponding to design-equation (1) is formulated, see equation (3).

$$g(t,Z) = \Delta - \sum_{i=1}^{N_{Smax}} \sum_{j=1}^{N_{Smin}} \frac{n_{ij} \cdot t}{N_{S,ij}} \qquad (3)$$

where

Δ model uncertainty associated with PM rule

t time in years $0 < t < T_L$

$N_{S,ij}$ required number of stress cycles of $S_{Cd,max,i}$ and $S_{Cd,min,j}$ in each bin (i,j) per year for failure calculated using stochastic variables described in equation (4).

$$\log N_{S,ij} = \frac{X_2}{(Y - X_1)} \cdot \left(S_{c,max,i} - X_1\right) + \epsilon \,, \quad \text{if } \log N_{S,ij} \le X_2$$

$$\log N_{S,ij} = X_2 + \frac{X_2 \cdot \ln(10)}{(Y - X_1)} \cdot \left(Y - S_{c,min,j}\right) \cdot \log\left(\frac{S_{c,max,i} - S_{c,min,j}}{Y - S_{c,min,j}}\right) + \epsilon \quad \text{if } \log N_{S,ij} > X_2 \qquad (4)$$

where,

$S_{c,max,i} = |\sigma_{c,max,i}|/f_{cfat}$

$S_{c,min,j} = |\sigma_{c,min,j}|/f_{cfat}$

$\sigma_{c,max,i}$ and $\sigma_{c,min,j}$ are maximum and minimum stresses used to obtain $S_{c,max,i}$ and $S_{c,min,j}$

$\sigma_{c,max,i} = \sigma_{DL}(Z) + X_W \cdot \sigma_{WL,max}(Z)$

$\sigma_{c,min,j} = \sigma_{DL}(Z) + X_W \cdot \sigma_{WL,min}(Z)$

$f_{cfat} = \beta_{c,sus(t,t0)} \cdot \beta_{cc(t)} \cdot f_c \cdot (1 - f_c/400)$

$f_c = X_{f_c} \cdot f_{cm}$

Table 3: Stochastic parameters in limit-state-equation

Parameter	Dist* Type	Parameters Mean	Parameters Std. Dev.	Ref**
Δ	LN	1.0	0.30	SJ
X_{fc}	LN	1.00	0.14	Sec. 3.1
X_1	N	1.13	0.03	Sec 3.2
X_2	N	8.66	0.37	
ε	N	0.00	σ_ε	
σ_ε	N	0.88	0.07	
$\rho_{X_1,\sigma_\varepsilon}$	-	0.01		
$\rho_{X_2,\sigma_\varepsilon}$	-	-0.01		
ρ_{X_1,X_2}	-	-0.84		
X_W	LN	1.00	0.10	Sec 3.3

**: N-Normal, LN-Log-Normal*

*** SJ:* (Márquez-Domínguez & Sørensen, 2013)

6. STRESS CALCULATION AND MODELLING OF DESIGN PARAMETER

The stresses ($\sigma_{c,max}$ *and* $\sigma_{c,min}$) in the reinforced concrete section are obtained at the face of the embedded ring (at ground level, see red dot) considering the cantilever section of foundation as shown Figure 4.

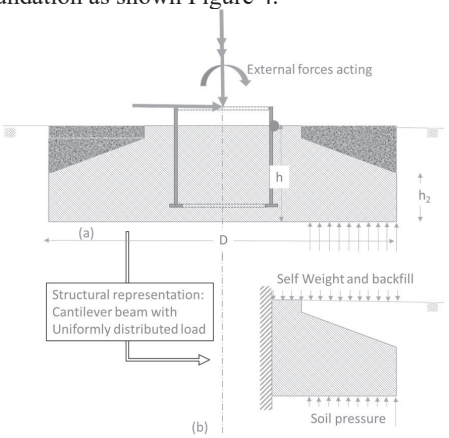

Figure 4: (a) geometry of foundation with external forces, (b) cantilever beam representative structure for (a).

The compressive stresses ($\sigma_{c,max}$ *and* $\sigma_{c,min}$) in the foundation concrete at the face of embedded

ring (at ground level where stresses in concrete in most cases are compressive) are obtained for various magnitudes of the reinforcement area (which is the design-parameter, Z).

The tensile reinforcement is chosen as the design-parameter, Z. since reinforcement area is a more costly material compared to concrete and optimizing amount of reinforcement is therefore more relevant than optimizing the quantity of concrete. The diameter (D) of the foundation is mostly governed by soil parameters or geotechnical aspects. The thickness of the foundation near the face of the embedded ring (h) and outer-thickness (h_2) is modelled as proportional to each other to keep the same slope of the foundation. The design value of thickness is obtained from the deterministic design equation (1).

Understanding and modelling the relationship between the design-parameter and the stresses in concrete is an important aspect as the design-parameter is the only connection between the design-equation and the limit-state-equation. The change of design-parameter may have different effects on mean level of stresses and amplitude of stresses. Such a relation is plotted in Figure 5.

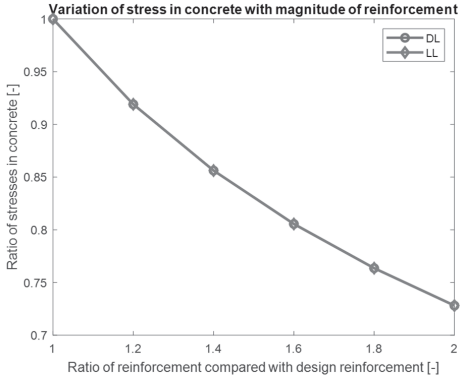

Figure 5: Stress variation as a funtion of variation in the design parameter.

The effect shown in Figure 5 reflects that increasing the magnitude of reinforcement increases bending stiffness that again reduces the dead-load-stress as well as live-load-stress, and thus the total-stress. The change in self-weight of the foundation when reinforcement area is changed is negligible, and hence not considered.

7. RELIABILITY ANALYSIS

A reliability analysis is performed using the limit-state-equation (3). The cumulative (accumulated) probability of failure in time interval $[0, t]$ is obtained by equation (5).

$$P_F(t) = P(g(t) \leq 0) \qquad (5)$$

The probability of failure is estimated by FORM, see (Sørensen J. D., 2011). The corresponding reliability index $\beta\ (t)$ is obtained by equation (6).

$$\beta(t) = -\phi^{-1}(P_F(t)\,) \qquad (6)$$

where, $\Phi(\,)$ is standardized normal distribution function.

The annual probability of failure conditional on survival up to year $t - \Delta t$ is obtained from:

$$\Delta P_F(t) = \frac{P_F(t) - P_F(t-\Delta t)}{1 - P_F(t-\Delta t)}, \quad t > 1\ year \qquad (7)$$

where Δt =1 year.

8. RESULTS

Results include comparison the annual-reliability-index ($\Delta\beta$) values obtained from analysis with international code requirements. Further an example of optimization of the design parameter is presented.

8.1. Code requirements of reliability

When designing the wind turbine foundation according to IEC 61400-1 ed. 4 a recommended target annual probability of failure throughout planned fatigue life should be 5.10^{-4} and corresponding annual reliability index is 3.3, see background document for safety factors in IEC 61400-1, (Sørensen & Toft, 2014). This reliability level corresponds to minor /moderate consequences of failure and moderate / high cost of safety measure. It is noted that this reliability level corresponds approximately to the reliability level for offshore structures that are unmanned or evacuated in severe storms and where other

consequences of failure are not very significant. The same conditions could also be assumed for an onshore wind turbine where these wind turbines are installed sufficiently away from inhabitants and consequence in terms of loss of human life due to failure of wind turbine are negligible.

When designing the wind turbine foundation according to DNVGL an annual target probability of failure should not exceed 10^{-4}, which corresponds to annual reliability index of 3.7, see DNV-OS-J101. However, this standard is superseded by (DNVGL-ST-0126, 2016) and this new standard recommends using target reliabilities for similar existing design solutions or internationally recognised codes and standards.

8.2. Optimal design parameter

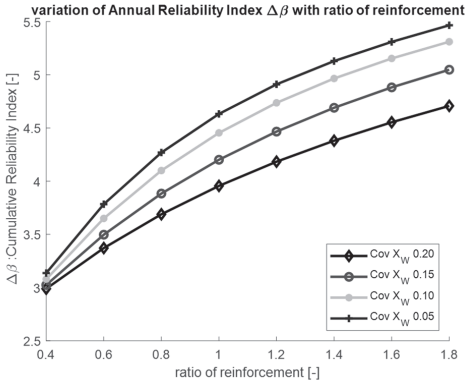

Figure 6: Annual reliability (Δβ) as function of design parameter

Figure 6 shows the annual reliability index $\Delta\beta$ as function of design parameter. To meet the target annual reliability indices $\Delta\beta$ set forth by codes in range of 3.3 to 3.7, the design-parameter (ratio of the reinforcement) to achieve this range of $\Delta\beta$ is 0.50-0.75. This shows that, only 50-75% (of 1540 mm^2/m) reinforcement is required to satisfy the reliability requirements with respect to fatigue failure of the concrete as compared to design requirements. Which means, in case of new structures these design requirements provide margin for life extension of the structures. It is noted that other design requirements may be governing for the design.

Figure 7 shows the annual reliability index $(\Delta\beta)$ as function of material partial safety factor (γ_C) for T_L of 25years. The partial safety factor for load is assumed equal to 1.0. It can be seen that for the case with CoV_X_W = 0.15, a material partial safety factor (γ_C) of around 1.3 together with a partial safety factor on the load γ_{ED} = 1.0 is sufficient to meet the target annual reliability index Δβ > 3.3. Next, for the case with CoV_X_W = 0.20 a partial safety factor on load (γ_{ED}) can be calibrated to 1.45/1.3 = 1.1, to be used together with γ_C = 1.3.

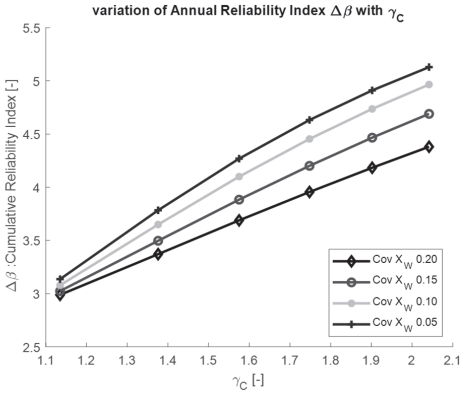

Figure 7: Annual reliability (Δβ) as function of γ_C

9. CONCLUSIONS AND FUTURE WORK

This paper presents a general approach for reliability assessment of wind turbine concrete foundations with respect to fatigue failure of the concrete. The approach can be used as basis for probabilistic design. The approach is illustrated in an example showing that the reliability level using present recommendations in standards is acceptable, and also that material savings could be possible. For future work an extension from component level reliability to system level reliability analysis is recommended. Further, combination with other limit states related to fatigue of reinforcement and ultimate failure due to extreme loads should be included.

ACKNOWLEDGEMENTS

Current work is carried out under the project INFRASTAR (infrastar.eu), which has received funding from the European Union's Horizon 2020 research and innovation programme under the Marie Skłodowska-Curie grant agreement No 676139. The grant is gratefully acknowledged.

10. REFERENCES

DNVGL-ST-0126. (2016). *Support structures for wind turbines.* DNV GL AS. doi:http://www.dnvgl.com

DS-INF 172. (2009). *Background Studies in connection with the preparation of National Annexes to EN 1990 and EN 1991.* København, Danmark: DS-publikationen er på dansk.

EN 1992-1. (2004). *Design of concrete structures - Part 1-1: General rules and rules for buildings.* Brussels: European committee for standardisation.

Görasson, F., & Nordenmark, A. (2011). *Fatigue Assessment of Concrete Foundations for Wind Power Plants.* Göteborg, Sweden.

ISO 1920. (2004). *Testing of Concrete.* International Organisation for Standardisation.

ISO 3893. (1977). *Concrete--Classification by compressive strength.* International Organization for Standardisation.

JCSS. (2000). *JCSS PROBABILISTIC MODEL CODE.* JCSS. doi:ISBN 978-3-909386-79-6

Lantsought, E. (2014). *Fatigue of Concrete under compression Database and proposal for high strength concrete.* TU, Design & Construction – Concrete Structures. Delft: TU-Delft.

Lohaus, L., Oneschkow, N., & Wefer, M. (2012). Design Model for fatigue behaviour of normal-strength, high-strength and ultra-high-strength concrete. *Structural Concrete*.

Mankar, A., Bayane, I., Sørensen, J. D., & Brühwiler, E. (2018). Probabilistic reliability framework for assessment of existing reinforced concrete bridge structures. *Engineering Structures*, Submitted.

Mankar, A., Rastayesh, S., & Sørensen, J. D. (2018). Sensitivity and Identifiability Study for Uncertainty Analysis of Material Model for Concrete Fatigue. *IRSEC 2018*, (p. B3). Shiraj.

Márquez-Domínguez, S., & Sørensen, J. D. (2013). Probabilistic Fatigue Model for Reinforced Concrete Onshore Wind Turbine Foundations. *Safety, Reliability and Risk Anaysis: Beyond the Horizon ESREL 2013.* Amsterdam: Taylor & Francis Group, London, UK.

MC2010. (2013). *FIB Model Code for concrete structures 2010* . Berlin Germany: Ernst & Sohn.

Sandia National Laboratories. (1999). *On the Fatigue Analysis of Wind Turbines.* New Mexico, US: Sandia National Laboratories.

Sørensen, J. D. (2011). *Notes in Structural Reliability Theory and Risk Analysis.* Aalborg University.

Sørensen, J. D., & Toft, H. S. (2006). Probabilistic Design of Wind Turbines. *Energies, 3(2)*, 241-257. doi:10.3390/en3020241

Sørensen, J. D., & Toft, H. S. (2014). *Safety Factors IEC 61400-1 background document.* Aalborg, Denmark: DTU Wind Energy. doi:ISBN nr.: 978-87-93278-08-0

Svensson, H. (2010). *Design of Foundation for Wind Turbines.* Lund, Sweden.

Thiele, M. (2016). *Experimentelle Untersuchung und Analyse der Schädigungsevolution in Beton unter hochzyklischen Ermüdungsbeanspruchungen.* Berlin: BAM.

Toft, H. S., Svenningsen, L., Sørensen, J. D., Moser, W., & Thøgersen, M. L. (2016). Uncertainty in wind climate parameters and their influence on wind turbine fatigue loads. *Renewable Energy*, 352–361.

Appendix E.

Paper 5

Probabilistic fatigue design of reinforced-concrete wind turbine foundations

John Dalsgaard Sørensen

Amol Mankar

This papar has been published online in

SMMS-2019 (Open Access policy)

e-ISBN: 978-2-35158-218-3

PROBABILISTIC DESIGN OF WIND TURBINE CONCRETE COMPONENTS SUBJECT TO FATIGUE

John D. Sørensen, Amol Mankar

Aalborg University, Denmark

Abstract

Wind turbines contribute significantly to the production of renewable energy. In order to minimize the Levelized Cost of Energy (LCOE) the cost of the wind turbine incl. tower and the foundation should be as low as possible but at the same time have a sufficient reliability. In this paper, focus is on wind turbine components which may be made of concrete such as tower and foundation. In traditional deterministic design based on design standards, partial safety factors are applied to obtain the design values. Improved design with a consistent reliability level for all components can be obtained by use of probabilistic design methods with explicit consideration of uncertainties connected to loads, strengths and numerical models / calculation methods. Wind turbines are basically designed based on IEC 61400-1:2019 which indicates a target reliability level that can be used for probabilistic design. In this paper, probabilistic fatigue models for concrete are presented based on the fatigue models in *fib* Model Code 2010, but extended within a stochastic modelling using a large dataset of fatigue tests. Generic uncertainty models for the fatigue load are applied. It is illustrated how reliability analyses can be performed within a probabilistic design framework.

Keywords: Wind turbines, Fatigue, Concrete, Reliability, Probabilistic design

1. INTRODUCTION

During the last decades, wind turbines for electricity production have increased significantly both in production capacity and in size; now with a rated power of 10MW, rotor diameters in the range of 160-200m and tower heights more than 100m; and even larger wind turbines are expected the next years to be installed offshore. Typically the tower and the substructure for offshore wind farms are made of structural steel, but concrete towers and substructures are been considered and also used as a cost-effective alternative to steel.

In traditional, deterministic design based on design standards, partial safety factors are applied to obtain the design values. Improved design with a consistent reliability level for all components can be obtained by use of probabilistic design methods with explicit consideration of uncertainties connected to loads, strengths and numerical models / calculation methods.

Furthermore, using a probabilistic design basis it is possible to design wind turbines such that site-specific information on climate parameters are applied. Wind turbines are basically designed based on the IEC 61400 series of standards where IEC 61400-1 ed. 4 [1] indicates a target reliability level which can be used for probabilistic design. In this paper, probabilistic fatigue models for concrete ae presented based on the basic, deterministic fatigue models in [2], but extended within a stochastic modelling framework and with parameters calibrated using a large dataset of fatigue tests. Generic uncertainty models for the fatigue load are applied.

The structural response of wind turbines is highly dependent on the wind turbulence, aerodynamics, dynamics of the structural system and of the control system applied. Further, wind turbines are manufactured in a series production based on many component tests, some subcomponent tests and a few prototype tests making it possible to update the knowledge through the design process, e.g. using a Bayesian approach.

In this paper, a general approach for probabilistic design is presented with focus on wind turbine components made of concrete such as tower and foundation, and especially the fatigue failure mode. It is illustrated how reliability analyses and probabilistic design can be performed within a probabilistic design framework considering a gravity based foundation for an offshore wind turbine.

2. PROBABILISTIC DESIGN

Structural components in wind turbines are designed considering a number of load combinations, see [1]:

- Failure during normal operation in extreme load or by fatigue (DLC 1)
- Failure under fault conditions (e.g. failure of electrical / mechanical components or loss of grid connection) due to extreme loads or by fatigue (DLC 2)
- Failure during start up, normal shut down or emergency shut down (DLC 3, 4 and 5)
- Failure when the wind turbine is idling / parked and does not produce electricity. Failure can be by extreme loads or by fatigue (DLC 6)
- Failure during transportation and installation (DLC 7)
- Failure during transport, assembly, maintenance and repair (DLC 8)

Wind turbine components can generally be divided in two groups:

1) Electrical and mechanical components modelled by the failure rate, λ. Further, the bath-tub model is often used to describe the time dependent behaviour of the failure rate / hazard rate, see e.g. [3] and [4]. Reliability of drivetrain components (e.g. the gear-box) has been considered in e.g. [5].

2) Structural components such as tower, main frame, blades and the support structure / foundation where failure modes can be described by limit state equations, $g_i(X)$. Parameters in the limit state equation $g(X)$ are assumed to be modelled by n stochastic variables $X = (X_1, \dots, X_n)$. The probability of failure, P_F can be estimated using Structural Reliability Methods, e.g. FORM / SORM / simulation methods, see e.g. [6] and [7].

For wind turbines, the risk of loss of human lives in case of failure of a structural element is generally very small. Further, it can be assumed that wind turbines are systematically reconstructed in case of collapse or end of lifetime. Therefore, an appropriate target reliability level corresponding to a minimum annual probability of failure, ΔP_F^{max} is considered be $5 \cdot 10^{-4}$

(annual reliability index equal to 3.3), see [1] and [8]. More details on probabilistic design and reliability assessment of wind turbines can be found in [9], [10], [11] and [12].

In probabilistic design, it has to be verified that $\Delta P_{F,i} \leq \Delta P_F^{max}$ or $\lambda_{F,i} \leq \Delta P_F^{max}$ for all components for all DLCs where $\Delta P_{F,i}$ and $\lambda_{F,i}$ are used where relevant. Some representative stochastic models and limit state equations can be found in e.g. [8].

3. GRAVITY BASED FOUNDATION (GBF) CASE STUDY

As a case study, a reinforced concrete GBF of an offshore wind turbine (OWT) is considered as shown in Figure 1, see [13] for details. Reliability assessment wrt. fatigue failure and ultimate strength failure in compression of the concrete shaft is considered. The critical section is assumed to be the section just above lower ring beam as shown in Figure 1.

The OWT is installed in water depth of 25m. The outer diameter of the shaft at critical section is 6.5m. The thickness of the shaft (t) is considered as a design parameter.

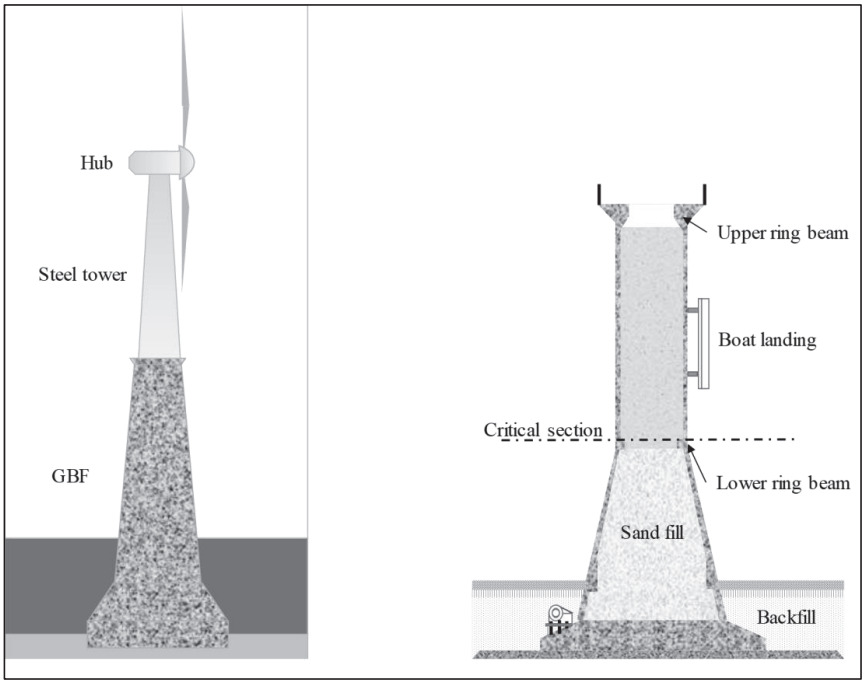

Figure 1: Typical GBF offshore wind turbine

Two limit states are considered in this paper, namely fatigue failure of the concrete in compression zone of the cross section (DLC 1.2) and extreme / ultimate strength failure of the concrete in compression (DLC 6.1). It is noted that it could also be very relevant to study yielding failure of the reinforcement in extreme storm conditions and tension fatigue failure of the concrete for cracked section given cracks in section due to extreme storm (multi-hazard scenario).

3.1 Fatigue limit state (DLC 1.2)

A probabilistic fatigue model for concrete is presented based on the basic, deterministic fatigue models in [2], but extended within a stochastic modelling framework and with parameters calibrated using a large dataset of fatigue tests, [14], [15] and [16].

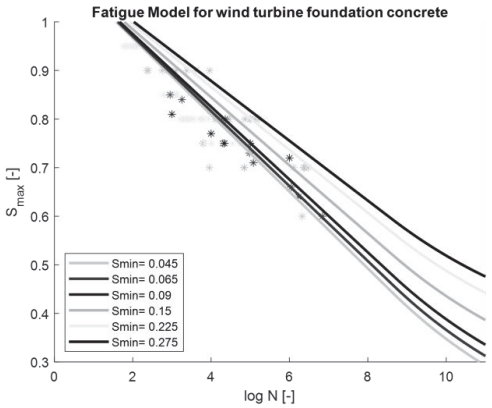

Figure 2: Fatigue strength model of concrete for GBF

Equation (1) shows a limit state equation based on Miner's rule where the number of cycles to failure is calculated based on [2] and [16]. Figure 2 shows graphical representation of fatigue strength model incl. fatigue test data while Table 1 shows the corresponding statistical parameters.

Table 1: Stochastic parameters

Parameter	Dist* Type	Parameters Mean	Parameters Std. Dev.	Ref**
X_1	N	1.13	0.03	Stochastic parameters associated with fatigue strength for compression-compression [16]
X_2	N	8.66	0.37	
ε	N	0.0	σ_ε	
σ_ε	N	0.88	0.07	
$\rho_{X_1,\sigma_\varepsilon}$	-	0.01		
$\rho_{X_2,\sigma_\varepsilon}$	-	-0.01		
ρ_{X_1,X_2}	-	-0.84		
X_W	LN	1.0	0.10	Uncertainty associated with wind loads
X_G	LN	1.0	0.05	Uncertainty associated with gravity loads
X_{PS}	LN	1.0	0.05	Uncertainty associated with pre-stressing loads
Δ	LN	1.0	0.30	[17]
X_{fc}	LN	1.0	0.14	Uncertainty in static strength of concrete
BM	G	186.7	40.4	Bending moment at critical section MN-m

$$g(t,z) = \Delta - \sum_{i=1}^{N_{\text{Windspeeds}}} \sum_{j=1}^{N_{\text{bins}}} \frac{n_{ij} t}{N_{S,ij}} \tag{1}$$

where

Δ model uncertainty associated with Miner's rule

t time in years $0 < t < T_L$

T_L design service life of the GBF structure

n_{ij} number of stress cycles per year in mean windspeed *i* in stress bin *j* (obtained by rainflow counting)

$N_{S,ij}$ number of stress cycles to failure of stress bin $S_{C,max,ij}$ and $S_{C,min,ij}$ modelled by

$$\log N_{S,ij} = \frac{X_2}{(Y - X_1)} \cdot \left(S_{c,max,ij} - X_1\right) + \epsilon \quad \text{if } \log N_{S,ij} \le X_2$$

$$\log N_{S,ij} = X_2 + \frac{X_2 \cdot \ln(10)}{(Y - X_1)} \cdot \left(Y - S_{c,min,ij}\right) \cdot \log\left(\frac{S_{c,max,ij} - S_{c,min,ij}}{Y - S_{c,min,ij}}\right) + \epsilon \quad \text{if } \log N_{S,ij} > X_2 \tag{2}$$

where

$S_{c,max,ij} = |\sigma_{c,max,ij}| / f_{cfat}$

$S_{c,min,ij} = |\sigma_{c,min,ij}| / f_{cfat}$

$\sigma_{c,max,ij}$ and $\sigma_{c,min,ij}$ are maximum and minimum stresses used to obtain $S_{c,max,ij}$ and $S_{c,min,ij}$

$\sigma_{c,max,ij}(z) = X_G \cdot \sigma_G(z) + X_{PS} \cdot \sigma_P(z) + X_w \cdot \sigma_{WL_{max,ij}}(z)$

$\sigma_{c,min,ij}(z) = X_G \cdot \sigma_G(z) + X_{PS} \cdot \sigma_P(z) + X_w \cdot \sigma_{WL_{min,ij}}(z)$

$f_{cfat} = \beta_{c,sus(t,t0)} \cdot \beta_{cc(t)} \cdot f_c \cdot (1 - f_c/400)$

$f_c = X_{f_c} \cdot f_{cm}$

z design parameter

3.2 Ultimate limit state (DLC 6.1)

The ultimate limit state (ULS) for extreme storm conditions is considered, [18] with the following limit state equation for compression failure of concrete:

$$g(z) = R - S = fc - \left(\frac{BM}{I_{Cr}(z)} \cdot y + \frac{X_G \cdot G}{A_{Eq}(z)} + \frac{X_{PS} \cdot A_P \cdot f_{pa}}{A_{Eq}(z)}\right) \tag{3}$$

where

R stochastic compression strength of concrete $= f_{cm} \cdot X_{fc}$

S action effects, e.g. lateral bending moment, gravity forces, and pre-stressing force

BM annual maximum storm bending moment at critical section due to lateral loads (wind and wave), Gumbel distributed, [18]

y extreme fibre distance (outer radius of concrete shaft)

G gravity forces on wind turbine, [18]

I_{Cr} moment of inertia of cracked section obtained using by considering rectangular stress block of concrete in compression zone

A_{Eq} $= A_c + A_R \cdot (m - 1)$, equivalent concrete area

A_c, A_R, A_P area of concrete, reinforcement and pre-stressing (m^2) respectively
f_{pa} maximum pre-stressing stress
m $= E_s/E_c$, modular ratio, ratio of modulus of elasticity of steel to concrete

3.3 Results and discussions

Reliability analyses as basis for probabilistic design are performed using the First Order Reliability Method (FORM), see [19] resulting in an estimate of the annual probability of failure P_F and the corresponding annual reliability index $\Delta\beta$.

The thickness of the GBF shaft (t) is considered as design parameter (denoted z in above section). Figure 3 shows the annual reliability index $(\Delta\beta)$ as function of thickness of the shaft (t) for different values of the reinforcement. It is noted that increase of the thickness of the shaft increases both fatigue and ultimate reliability indices increase, and also that an increase of the reinforcement (A_R) increases both fatigue and ultimate reliability indices. For all cases, ULS is governing.

Figure 4 shows the annual reliability index $(\Delta\beta)$as function of thickness of the shaft (t) with variation of pre-stressing. Increase in pre-stressing (A_P) induces additional pressure on concrete and thus reduces the reliability against fatigue as well ultimate strength failure. For all cases, ULS is governing. From Figure 3 and Figure 4 it is seen that to satisfy a minimum reliability requirement with an annual reliability index equal to 3.3, a design would require GBF shaft with thickness of 550 mm (minimum), reinforcement area of 0.2 m^2 (minimum) and pre-stressing area of 0.1 m^2 (maximum).

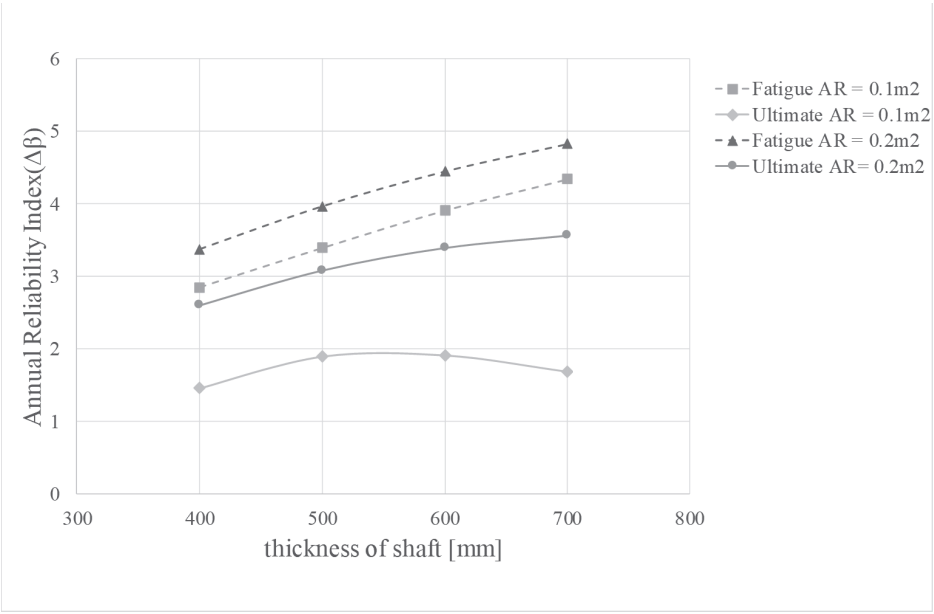

Figure 3: Sensitivity of reliability index to area reinforcement $A_P = 0.1\ m^2$

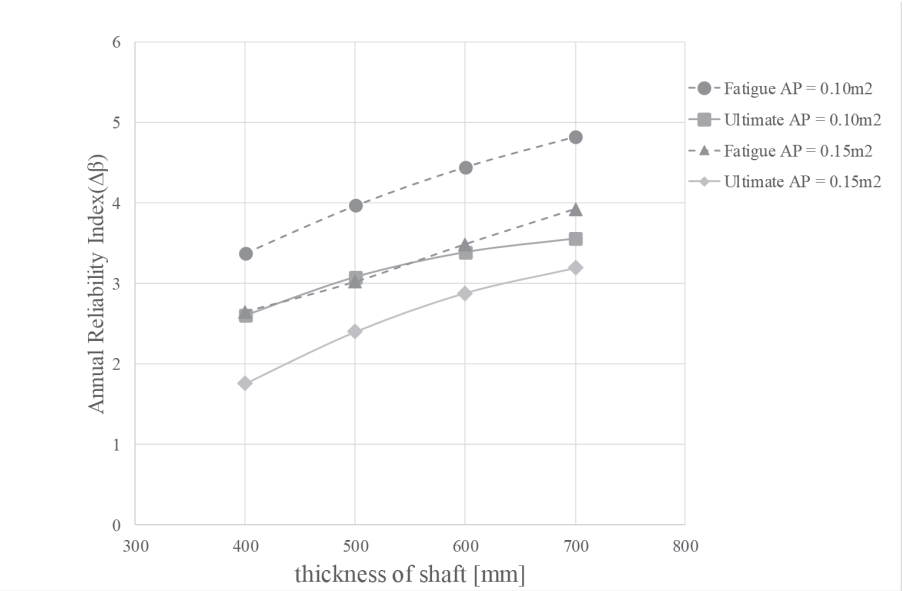

Figure 4: Sensitivity of reliability index to area of pre-stressing $A_R = 0.2\ \mathrm{m}^2$.

4. CONCLUSIONS AND FUTURE WORK

Probabilistic design of wind turbines has the potential to contribute significantly to reduction of the Levelized Cost of Energy and increased sustainability of wind turbines. The overall approach is presented in this paper and illustrated for offshore wind turbine tower and foundation made of concrete. The probabilistic design approach requires formulations of stochastic models for all uncertain parameters related to loads, strength and models, and development of limit state equation for the relevant design load cases. This paper only considers two of these limit states, but in future work stochastic models and limit state equations can be developed using the same principles for the remaining design load cases to be considered for design of wind turbines.

ACKNOWLEDGEMENTS

Current work is carried out under the project INFRASTAR (infrastar.eu), which has received funding from the European Union's Horizon 2020 research and innovation programme under the Marie Skłodowska-Curie grant agreement No 676139. The grant is gratefully acknowledged.

5. REFERENCES

[1] IEC 61400-1, Wind turbine generator systems – Part 1: Safety requirements, 4th edition ed., Geneva: International Electrotechnical Commission, 2019.

[2] fib MC2010, "FIB Model Code for concrete structures 2010," Ernst & Sohn, Berlin Germany, 2013.

[3] P. J. Tanver, J. Xiang and F. Spinato, "Reliability analysis for wind turbines," *Wind Energy,* vol. 10, pp. 1-18, 2007.

[4] P. Tanver, "Offshore Wind Turbines: Reliability, Availability and Maintenance," Institution of Engineering and Technology, 2012.

[5] W. Dong, T. Moan and Z. Gao, "Reliability-based gear contact fatigue analysis for wind turbines under stochastic dynamic conditions," in *ICOSSAR 2013*, New York, 2013.

[6] H. O. Madsen, S. Krenk and N. C. Lind, Methods of Structural Safety, New York: Dover Publications, 2006.

[7] JCSS, "JCSS PROBABILISTIC MODEL CODE," JCSS, 2002.

[8] J. D. Sørensen and H. S. Toft, "Safety Factors IEC 61400-1 background document," DTU Wind Energy, Denmark, 2014.

[9] J. D. Sørensen and H. S. Toft, "Probabilistic Design of Wind Turbines," *Energies,* vol. 3(2), pp. 241-257, 2006.

[10] J. D. Sørensen, "Reliability-based calibration of fatigue safety factors for offshore wind turbines," *International Journal of Offshore and Polar Engineering,* vol. 22, no. 3, pp. 234-241, 2012.

[11] H. S. Toft and , "Probabilistic Design of Wind Turbines," PhD thesis, Aalborg University, 2010.

[12] D. Veldkamp, "Chances in Wind Energy - A Probabilistic Approach to Wind Turbine Fatigue Design," PhD thesis, DUWIND Delft University, 2006.

[13] J. Velarde, A. Mankar, C. Kramhøft and J. D. Sørensen, "Uncertainty Modeling and Fatigue Reliability Assessment of Offshore Wind Turbine Concrete Structure," *IJOPE,* 2018.

[14] A. Mankar, S. Rastayesh and J. D. Sørensen, "Sensitivity and Identifiability Study for Uncertainty Analysis of Material Model for Concrete Fatigue". Proc. *IRSEC 2018*, Shiraj, 2018.

[15] A. Mankar, I. Bayane, J. D. Sørensen and E. Brühwiler, "Probabilistic reliability framework for assessment of existing reinforced concrete bridge structures," *Engineering Structures*. Submitted, 2018.

[16] A. Mankar and J. D. Sørensen, "Probabilistic fatigue design of reinforced-concrete wind turbine foundations". Submitted for *ICASP-13*, Seoul, South Korea, 2019.

[17] S. Márquez-Domínguez and J. D. Sørensen, "Probabilistic Fatigue Model for Reinforced Concrete Onshore Wind Turbine Foundations," in *Safety, Reliability and Risk Anaysis: Beyond the Horizon ESREL 2013*, Amsterdam, 2013.

[18] J. Velarde, C. Kramhøft and J. D. Sørensen, "Reliability-based Design Optimization of Offshore Wind Turbine Concrete Structures". Submitted for *ICASP-13*, Seoul, 2019.

[19] J. D. Sørensen, Notes in Structural Reliability Theory and Risk Analysis, Aalborg University, 2011.

Appendix F.

Paper 6

Reliability-based design optimization and inspection planning of wind turbine concrete structures subjected to fatigue

Amol Mankar

Joey Velarde

John Dalsgaard Sørensen

This papar is under review for publication

Engineering Structures Journal

ISSN: 0141-0296

Reliability-based design optimization and inspection planning of wind turbine concrete structures subjected to fatigue

Amol Mankar[a], Joey Velarde[b,a], John Dalsgaard Sørensen[a]

a. *Aalborg University, Thomas Manns Vej 23, 9220 Aalborg, Denmark*
b. *COWI A/S, Aarhus, Denmark*

ABSTRACT

Inspection of structures for assessing the level of fatigue damage in concrete is very challenging and available techniques are in nascent stage and needs more research. This paper presents a reliability-based approach for design optimization and updating the information about fatigue of concrete structures through inspections. A Gravity Based Foundation of an Offshore Wind Turbine is considered as case study. The Ultrasonic Technique (UT) is chosen to estimate the level of fatigue damage in concrete that is used to update the fatigue reliability of the reinforced-pre-stressed-concrete shaft of the structure. Finally, the current work provides a framework for reliability-based inspection planning and optimization of the structures in terms of fatigue damage of concrete with the decision-making process.

Keywords: concrete fatigue inspection, reliability updating, Offshore Wind Turbine (OWT), Gravity Based Foundation (GBF), Structural Health Monitoring (SHM)

1. INTRODUCTION

Traditionally, fatigue of reinforced concrete is often not considered for civil engineering structures since dead loads are very high (for normal strength concrete) while live loads are relatively small which lead to very small stress variations during the service life of the structure, [1], [2]. However, wind turbines structures push the limits of structural engineering and enter more into the mechanical domain, mostly due to the dynamic behaviour and the ratio of live loads to dead loads. With the use of concrete for support structure of the ever-increasing sizes of wind turbines, understanding the

*corresponding author +45-71634085
Email addresses: ama@civil.aau.dk (A. Mankar), jds@civil.aau.dk (J. D. Sørensen), jve@civil.aau.dk (J. Velarde),

fatigue process in concrete has gained attention [3]. In addition, with the trend of using mechanical properties of material to highest extent, the importance of studying fatigue in concrete is pronounced.

Understanding the level of fatigue damage in concrete is important to maintain the reliability of these structures above the acceptance throughout lifetime. Thus, the role of Structural Health Monitoring (SHM) systems becomes significant. In addition, concrete is a heterogeneous material having lots of micro-cracks by its nature. For the purpose, fatigue of concrete has to be treated on a global scale, where use of local crack growth models as for steel structures cannot be used to estimate the behaviour at the structure level. Instead, the modulus of elasticity of concrete $\left(E_c^{fat}\right)$ at time (T) can be used as an indicator claiming that the fatigue damage is assumed to be related to the Miner's fatigue damage (D) and the modulus of elasticity of concrete at start of life (E_{C_0}), see equation (1), [4]. Thus, a SHM technique that can estimate the modulus of elasticity $E_c^{fat}(T)$ of concrete would serve the purpose to estimate the fatigue damage in concrete $D(T)$.

$$E_c^{fat}(T) = E_{C_0} \cdot [1 - D(T)] \tag{1}$$

2. ULTRASONIC MEASUREMENT TECHNIQUES (UT)

The first use of velocity of mechanically generated pulses through concrete was in the USA in the mid-1940s, followed by more developments in France, Canada and the United Kingdom and later, more sophisticated modern UT were generated, [5, p. 51]. Techniques of UT of metals cannot be directly applied to concrete as concrete is heterogeneous with huge scattering. Thus, concrete testing is mainly based on the measurement of pulse velocity using transmission techniques. In such measurements, a signal is transmitted by an actuator through the material and run time for the signal to reach the receiver is measured. The velocity of the signal is then calculated, which is proportional to the elastic properties of the material (e.g. dynamic elastic modulus of concrete). Normally, pulses of frequency range 20-200 kHz are applied to concrete, which are very low compared to metals. In

concrete, high damping of signal occurs due to its heterogeneous nature and its high density of scattering sources such as aggregates and micro-cracks.

Speed of the UT signal decreases with load and life of the specimen. This velocity responds to changes in number of cracks in concrete and thus damage. At maximum load, cracks are compressed and less visible to UT signal whereas they remain open at minimum load and more visible to UT signal. Thus, Figure 1 represents two signals (shown as confidence bounds) for maximum and minimum loading. Ultrasonic velocity (V) is a very good indicator of modulus of concrete $\left(E_c^{fat}(T)\right)$, thus it indirectly indicates the level of damage. The relation between $E_c^{fat}(T)$ and V is given by equation (2):

$$V = \sqrt{\frac{K \cdot E_c^{fat}(T)}{\rho}} := E_c^{fat}(T) = \frac{V^2 \cdot \rho}{K} \tag{2}$$

where
V is the compression wave velocity in [m/s]
ρ is the unit weight of material$K = \frac{(1-\nu)}{(1+\nu)\cdot(1-2\nu)}$
ν is the dynamic Poisson's ratio

The relation between the dynamic modulus of concrete and UT velocity is established in section 3 and used for updating the fatigue reliability of the structure suggested as a case study, i.e. a Gravity Based Foundation (GBF) of an Offshore Wind Turbine (OWT).

3. RELATION BETWEEN US VELOCITY AND DAMAGE LEVEL

For the current case study, reliability updating is performed based on UT, as the data related to fatigue damage(D) and UT velocity are available, see [6]. A relation to the aforementioned data, between changes in Relative UT Velocity (R_V) and normalized-fatigue-damage (D), is originally proposed in [6] here it is re-obtained with corresponding uncertainty; see equation (4), Figure 1 and Figure 2.

When the structure is installed, an inspection is performed and velocity of UT wave at critical section is measured say V_{t_0}. Assuming another inspection is carried out at time t_{INSP}, which furnishes the UT velocity $V_{t_{INSP}}$, the relative velocity (R_V) at time t_{INSP}, can be obtained by normalizing $V_{t_{INSP}}$ with respect to V_{t_0}, see equation (3). Further, it is assumed that disturbances / noise on the measured velocities due to presence of reinforcement, pre-stressing and wet environment are of minor importance since only relative measurements are used. This approach can also be used even if no measurement is performed when the structure was installed. However, in such case, damage cannot be quantified, but relative damage can be assessed with respect to the two measurements campaigns.

$$R_{V_{t_{INSP}}} = \frac{V_{t_{INSP}}}{V_{t_0}} \tag{3}$$

The relation between the relative velocity and the normalized lifetime/ detected Damage (D_d) is given by a polynomial in equation (4), and shown in Figure 1. The polynomial is fitted using a least square fitting technique [7].

$$R_{V_D}(D_d) = p_1 \cdot D_d^5 + p_2 \cdot D_d^4 + p_3 \cdot D_d^3 + p_4 \cdot D_d^2 + p_5 \cdot D_d + X_u \tag{4}$$

where

X_u is the biased model uncertainty of fitted polynomial, modelled as normally distributed, see Figure 2.

$p_1 to\ p_5$ are polynomial constants

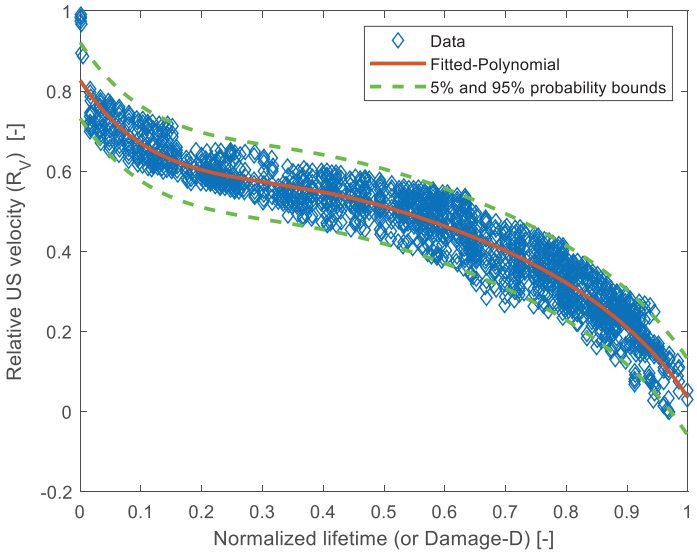

Figure 1 Relation between relative UT velocity and damage level.

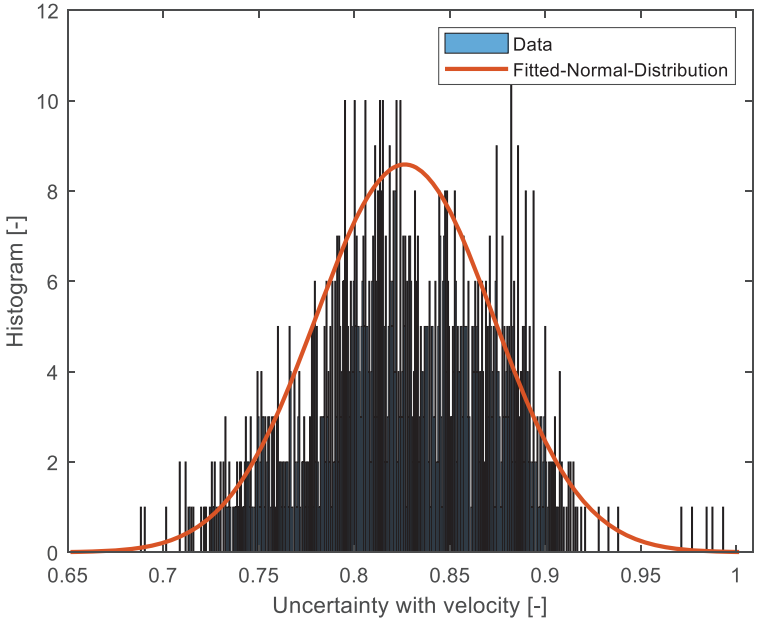

Figure 2 Fitted normal distribution for model uncertainty X_u

The speed of the UT signal decreases with the load and lifetime due to fatigue degradation of concrete. The propagation speed of ultrasound reacts to changes in the number and size of micro-cracks and damage in the concrete specimen. The measurement of the UT-transit time is performed during a running load program and can therefore be carried out at a random point of the load cycle. At maximum compressive stress, the cracks are compressed and are less visible to the signal, [6]. Therefore, this variation in (R_V) is attributed to the level of load on the specimen. However, for the current study, it is assumed that the variation is the uncertainty associated with the UT as it would be difficult to predict the level of load during inspection.

4. LIMIT-STATE-EQUATION FOR FATIGUE FAILURE EVENT

A probabilistic fatigue model for concrete is presented based on the basic, deterministic fatigue models in [8] and extended within a stochastic modelling framework. Stochastic parameters are calibrated using a large dataset of fatigue tests, see [9], [10] and [11].

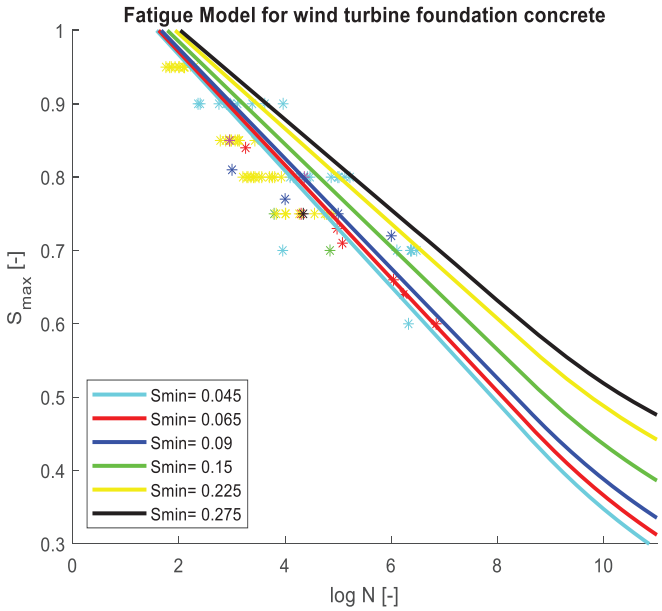

Figure 3: Fatigue strength model of concrete for GBF

Figure 3 shows the graphical representation of fatigue strength model including fatigue test data while Table *1* shows the corresponding statistical parameters.

A limit-state-equation is formulated for fatigue failure of concrete, see equation (5). Deterministically the failure is realized when the (D_C) reaches a value of 1.0. In stochastic domain, failure is realized when the (D_C) reaches a value of Δ, which is modelled accounting for the uncertainty associated with Miner's rule [12] and described by stochastic parameter with lognormal distribution with unit means and CoV of 0.3, [13], see Table *1*.

The damage (D_C) is calculated based on Miner's rule of linear damage accumulation, [8] and [10].

$$g(t,Z) = \Delta - D_C(t) \tag{5}$$

where,

$$D_C(t) = \sum_{i=1}^{N_{Smax}} \sum_{j=1}^{N_{Smin}} \frac{n_{ij} \cdot t}{N_{S,ij}}$$

$$\log N_{S,ij} = \frac{X_2}{(Y-X_1)} \cdot \left(S_{c,max,i} - X_1\right) + \epsilon, \text{ if } \log N_{S,ij} \le X_2$$

$$\log N_{S,ij} = X_2 + \frac{X_2 \cdot \ln(10)}{(Y-X_1)} \cdot \left(Y - S_{c,min,j}\right) \cdot \log\left(\frac{S_{c,max,i} - S_{c,min,j}}{Y - S_{c,min,j}}\right) + \epsilon, \text{if } \log N_{S,ij} > X_2$$

$$S_{c,max,ij} = |\sigma_{c,max,ij}|/f_{cfat}$$

$$S_{c,min,ij} = |\sigma_{c,min,ij}|/f_{cfat}$$

$\sigma_{c,max,ij}$ and $\sigma_{c,min,ij}$ are maximum and minimum stresses used to obtain $S_{c,max,ij}$ and $S_{c,min,ij}$

$$\sigma_{c,max,ij}(z) = X_G \cdot \sigma_G(z) + X_{PS} \cdot \sigma_P(z) + X_w \cdot \sigma_{WL_{max,ij}}(z)$$

$$\sigma_{c,min,ij}(z) = X_G \cdot \sigma_G(z) + X_{PS} \cdot \sigma_P(z) + X_w \cdot \sigma_{WL_{min,ij}}(z)$$

$$f_{cfat} = \beta_{c,sus(t,t0)} \cdot \beta_{cc(t)} \cdot f_c \cdot (1 - f_c/400)$$

$$f_c = X_{f_c} \cdot f_{cm}$$

Table 1: Stochastic parameters

Parameter	Dist* Type	Parameters Mean	Parameters Std. Dev.	Remark/reference
X_1	N	1.13	0.03	Stochastic parameters associated with fatigue strength for compression-compression, taken from [11]
X_2	N	8.66	0.37	
ε	N	0.0	σ_ε	
σ_ε	N	0.88	0.07	

$\rho_{X_1,\sigma_\varepsilon}$	-	0.01		
$\rho_{X_2,\sigma_\varepsilon}$	-	-0.01		
ρ_{X_1,X_2}	-	-0.84		
X_W	LN	1.0	0.10	Uncertainty associated with wind loads
X_G	LN	1.0	0.05	Uncertainty associated with gravity loads
X_{PS}	LN	1.0	0.05	Uncertainty associated with pre-stressing loads
Δ	LN	1.0	0.30	Uncertainty associated with Miner's rule
X_{fc}	LN	1.0	0.14	Uncertainty in static strength of concrete
Xu	N	0. 83	0.05	Uncertainty associated with US velocity measurement, given that damage is detected
U	N	0	1	Standard normal variable
PoD	E	0.04	0.04	Uncertainty associated with US velocity measurement, given no damage is detected**

* N-Normal, LN-LogNormal, E-Exponential

** Fitted distribution based on section 5.1 for chosen threshold of 75% of relative velocity

5. INSPECTION EVENT AND UNCERTAINTY

To model the observed events, an event function 'H' is introduced.

$$H = h(X) \tag{6}$$

The event function *h* corresponds to the limit state function. The actual observation of the relative velocity $R_{V_{INSP}}$ is the realization of stochastic variable *H*. When a structure has a high reliability, i.e. high fatigue life and very low fatigue damage, there is a small likelihood to see any changes in the relative velocity, and thus the event function *h* can be modelled as the following inequality $\{H \leq 0\}$, see section 5.1 for details. However, when the reliability of structure is low, there is a high possibility to see the change in relative velocity and the possible outcomes of the observation can be modelled as the equality $\{H = 0\}$, see section 5.2 for details.

5.1 Inspection event with no-damage information

When a structure has a high reliability and very low fatigue damage, the fatigue-damage observations can be modelled as the inequality $\{H \leq 0\}$, i.e. the observed fatigue-damage (D_{INSP}) is less than or equal to some limit. This limit can generally be evaluated from the reliability of the inspection method

in terms of the PoD. The PoD is estimated based on equation (7) and [14] using Monte-Carlo simulations of the fitted distribution of the signal (Equation (7) and Figure 1 & Figure 2) [15]. The Monte Carlo (MC) simulation is performed using the model in Equation (4) and the uncertainties are generated by the model uncertainty X_u, see Figure 2 and Table 1. The threshold of relative velocity of 75% is chosen to obtain the PoD, which is shown in blue in Figure 4. An exponential distribution, as shown in Figure 4 (red) and described in Equation (8) with an expected value of fatigue damage (D_{mean}) equal to 0.04, fits well and represents the obtained PoD (blue). Thus, inspection events (no damage detected) are modelled by the event margin as shown in equation (9).

$$P(I|D) = \int_{-\infty}^{t} f\left(R_{V_D}|D\right) dR_{V_D} \tag{7}$$

where

t is the threshold value chosen for relative velocity R_{V_D} for indication. Here chosen to 75%

$f\left(R_{V_D}|D\right)$ is the conditional distribution function of the relative velocity R_{V_D} given the damage size D, obtained from Equation (4)

$P(I|D)$ is the probability of indication or probability of detection for a given damage size D

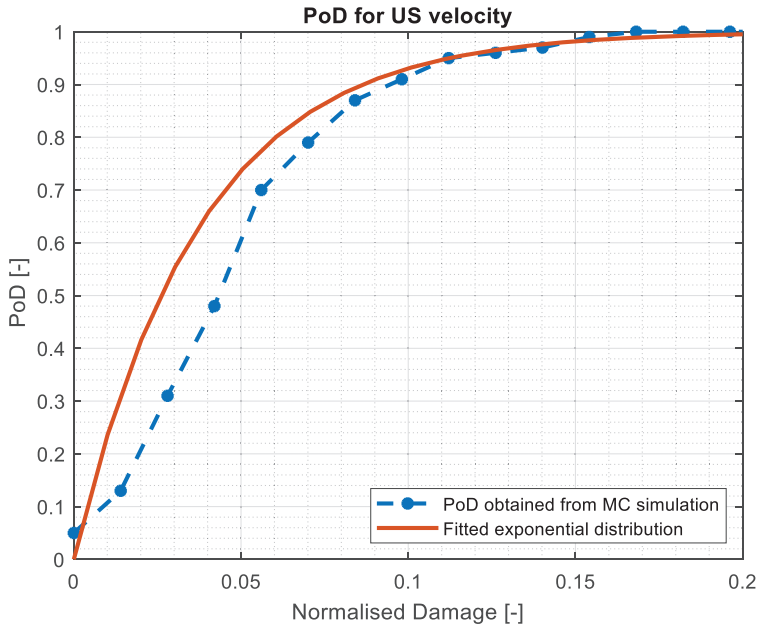

Figure 4 PoD for US velocity

$$PoD(D_{INSP}) = 1 - exp\left(-\frac{D_{INSP}}{D_{mean}}\right) \tag{8}$$

$$h = (D_C(t) - D_{INSP}) \leq 0 \tag{9}$$

5.2 Inspection event with damage information

When a structure has a relative low reliability and high fatigue-damage, the observations are modelled as the equality$\{H = 0\}$, i.e. the observed quantity is equal to some limit. However, when the information is of equality type, the a priori probability of the event is zero and most of the reliability methods are not directly applicable to compute the updated reliability, [16]. Therefore, a likelihood function is used to convert the equality information to inequality information based on [16]. As the failure limit state is defined in terms of damage, the observed relative velocity is converted to observed-damage by obtaining the root of polynomial defined in equation (4), imaginary roots are ignored to obtain real root. The mean value of the model uncertainty μ_{X_u} in equation (4) is updated using the measured value of the relative velocity $R_{V_{INSP}}$ along with the uncertainty associated with

the measurement (X_u). Equation (10) describes that damage value (D_{INSP}) can be obtained from inspected relative velocity ($R_{V_{INSP}}$)from the real root of the polynomial, where, $R_{V_D}^{-1}$ is the inverse polynomial function and indicates that the root of the polynomial has to be obtained:

$$D_{INSP} = R_{V_D}^{-1}(\mu_{X_u} = R_{V_{INSP}}) \tag{10}$$

For the fatigue critical detail under consideration is inspected at time, $T = t_{INSP}$. The inspection event is modelled as an in-equality event, see equation (11), [16].

$$h = U - \Phi^{-1}\big(\varphi(D_C(t) - D_{INSP})\big) \leq 0 \tag{11}$$

where,

U is the standard normal random variable
Φ^{-1} is the inverse standard normal cumulative distribution function
φ is the standard normal density function

6. RELIABILITY UPDATING USING INSPECTIONS

To maintain the reliability level, periodic inspections need to be performed in order to obtain information on the current health of the structure, but also to predict its future behaviour by updating the failure probabilities [17]. In both cases (no damage found, section 5.1 and damage found, section 5.2), the event margin is modelled as an inequality and it can be easily used to obtain updated failure probability.

The failure probability P_F after an inspection event is updated by calculating the conditional probability of failure given the inspection event is performed. Bayes' rule is used to obtain the updated failure probability P_F^U,

$$P_F^U = P(g(X,T) \leq 0 | h(X,T_{INSP}) \leq 0) = \frac{P(g(X,T) \leq 0 \cap h(X,T_{INSP}) \leq 0)}{P(h(X,T_{INSP}) \leq 0)} \tag{12}$$

The corresponding annual probability of failure and annual reliability index can be calculated, see equation (13)

$$\Delta\beta^{\mathrm{U}} = -\Phi^{-1}\left(\mathrm{P}\big(\mathrm{g(T)} \leq 0 \big| \mathrm{h}\big(\mathrm{T_{insp}}\big) \leq 0\big) - \mathrm{P}\big(\mathrm{g(T-1)} \leq 0 \big| \mathrm{h}\big(\mathrm{T_{insp}}\big) \leq 0\big)\right) \quad \mathrm{T} > \mathrm{T_{INSP}} \tag{13}$$

7. CASE STUDY OF A GRAVITY BASED FOUNDATION

A case study of a reinforced concrete GBF installed in the Belgian North Sea, about 30 km from the coast of Western Flanders, is considered. The GBF design for the Thornton Bank offshore wind farm, shown in Figure 5, supports a 5 MW wind turbine at a mean water depth of 25 m. A reliability assessment with respect to fatigue failure in compression of the concrete shaft is performed at a critical section just above the lower ring beam. Other limit states are not considered in this paper and may be critical e.g. fatigue failure of the reinforcement, or ultimate limit failure of the concrete in compression or tension failure of the steel reinforcement. The outer diameter of the shaft at the critical section is 6.5 m with a thickness of the shaft equals to 0.5 m. The total height of the structure is 44 m with ~25 m long shaft and ~19 m high cone. Diameter of the foundation cone tapers from 6.5 m at top to 23.5 m at the base. The layout of the post-tensioning strands along vertical section and layout of reinforcement within the shaft are shown in Figure 5 and Figure 6, respectively.

The Offshore Wind Turbine (OWT) loads are calculated using HAWC2 [18], an aero-hydro-servo-elastic tool for static and dynamic analysis of onshore and offshore wind turbines. Structural elements in HAWC2, such as wind turbine blades, tower, and foundation, are modelled as multibody elements, which are further represented by Timoshenko beam elements. The NREL 5 MW [19] reference wind turbine is used in load calculation.

Based on IEC 61400-3 [20] recommendations for the design of offshore wind turbines, fatigue loads are calculated based on time-domain simulations of relevant wind and wave conditions. Design load case (DLC) 1.2, which accounts for fatigue loads during power production, is considered. Twelve representative sea states, with correlated wind speeds (U_w) and significant wave heights (H_s) based on wind farm data, are simulated using six realizations per sea state. Hydrodynamic loads are based on linear irregular waves and Morison's equation, with calibrated drag (C_d) and inertia (C_m) coefficients to account for diffraction. For aerodynamic loads, normal turbulent wind fields were generated based on Mann turbulence model [21], and blade element momentum (BEM) theory is used

to estimate the wind loads. See [22] and [23] for further details on OWT modelling. Finally, rain-flow counting is performed to the resulting load histories to extract load cycle means, amplitudes and number of cycles. The loads are extrapolated to a design lifetime of 20 years.

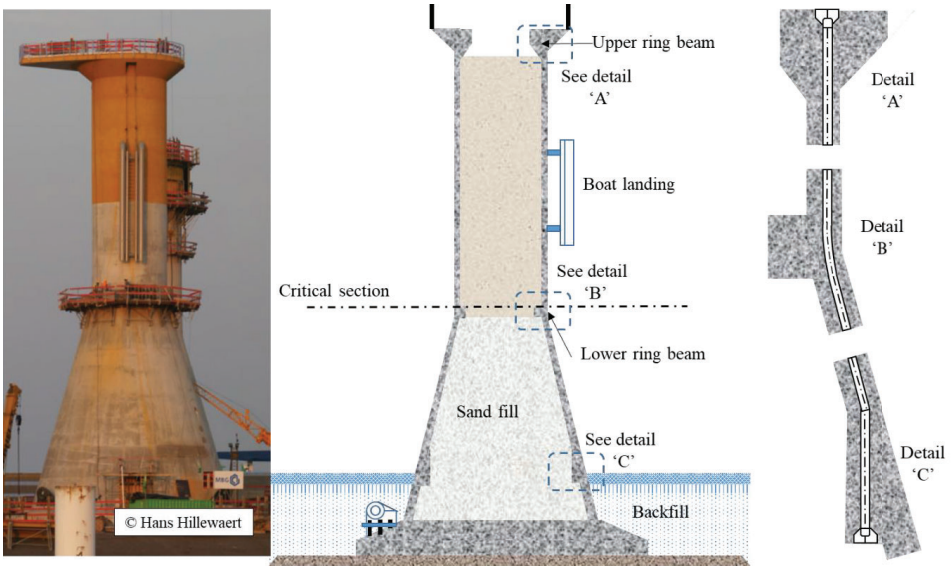

Figure 5 Gravity based foundation

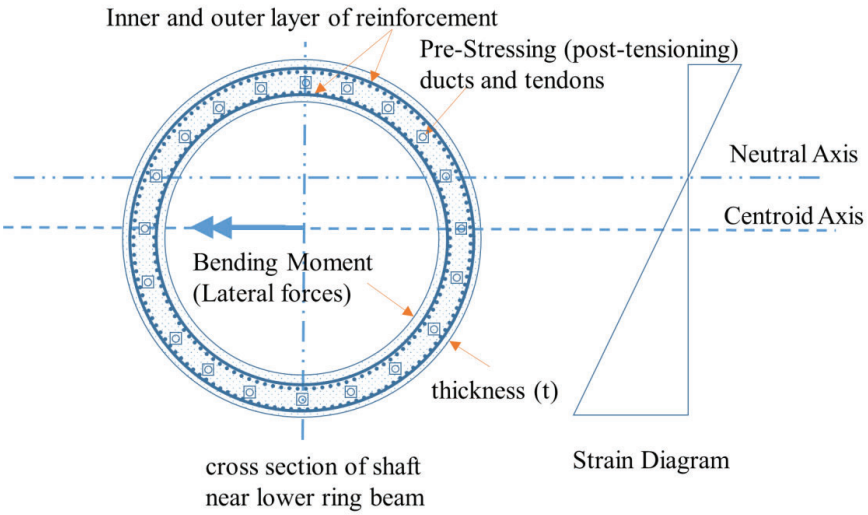

Figure 6 Conceptual reinforcement and stress calculations

8. RESULTS AND DISCUSSION

For wind turbines, the risk of loss of human lives in case of failure of a structural element is generally very small. Further, it can be assumed that wind turbines are systematically reconstructed in case of collapse or end of lifetime. Therefore, an appropriate target reliability level corresponding to a minimum annual probability of failure ΔP_F^{max} is considered to be $5 \cdot 10^{-4}$ (annual reliability index equals to 3.3), see [24], [3] and [25]. More details on probabilistic design and reliability assessment of wind turbines can be found in [26], [27], [28] and [29].

The following section presents two options of achieving the target annual reliability index of 3.3, with and without considerations of inspection planning, thus with and without reliability updating respectively. For a given level of pre-stressing force (A_p = 0.1 m^2), structural designer of the wind turbine can vary the thickness of the shaft or the amount of steel reinforcement in order to achieve the target reliability. The thickness of the shaft is governed mostly by parameters such as installation weight, construction of formwork, etc. Therefore, for the current case study, it is assumed as fixed and equal to 0.5 m. Thus, the design parameter considered here is steel reinforcement.

8.1 Case#1: Design without consideration of inspection

The case#1 consists of achieving the initial design such that there should not be any inspections required to maintain the target reliability during lifetime. Thus, the initial design parameter (amount of reinforcement) is determined in such a way that the annual reliability index at the end of design lifetime is 3.3; see Figure 7 & Figure 8.

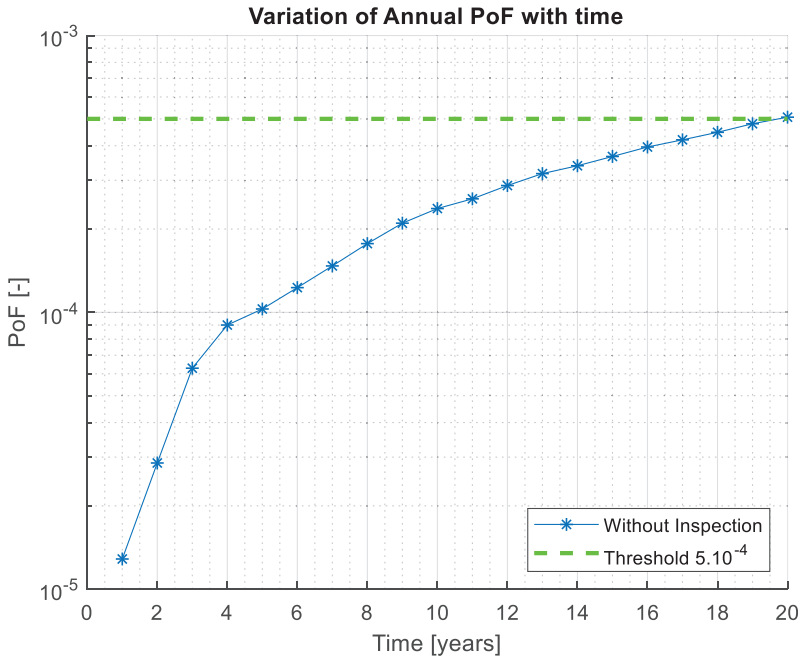

Figure 7 Variation of annual PoF with time

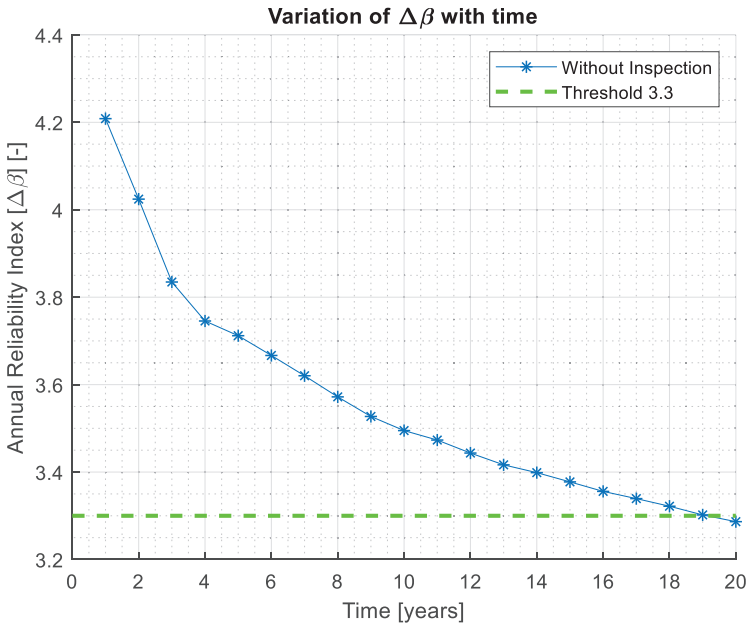

Figure 8 Variation of annual Reliability Index with time

8.2 Case#2: Design with consideration of inspection (damage detected)

Initially a lower design parameter (less steel reinforcement) compared to case#1 is here used. However, this implies inspections to be performed, and therefore some expenditures. Thus, updating of reliability is performed after each inspection, which leads to higher confidence on fatigue performance and thus higher reliability. Finally, a target annual reliability of 3.3 is again achieved; see Figure 9 & Figure 10. It should be noted that for the current study inspection, outcome is assumed as relative velocity of 0.7 for each inspection and thus the results are conditional to such assumed outcome. However, a sensitivity analysis of these assumptions shows a small influence on the final reliability results. Further, when a level of damage is detected, then a decision has to be taken on what to do, and generally it is advised to repair in order to achieve the original condition as close as possible. For concrete structures it is a difficult task to repair an alternative could be to lower the loads by operating the wind turbine at a lower power output or by parking the wind turbines for certain wind speeds. This is only efficient if a major part of the loading is from wind and not the waves. However, the current results are for illustration purpose only, focussing on how the reliability can be updated in case a damage is detected.

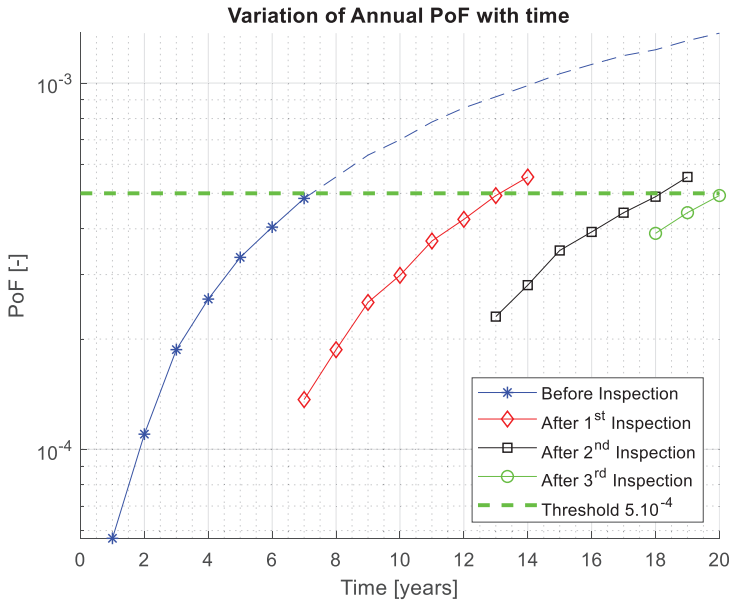

Figure 9 Variation of annual PoF with lifetime considering inspections

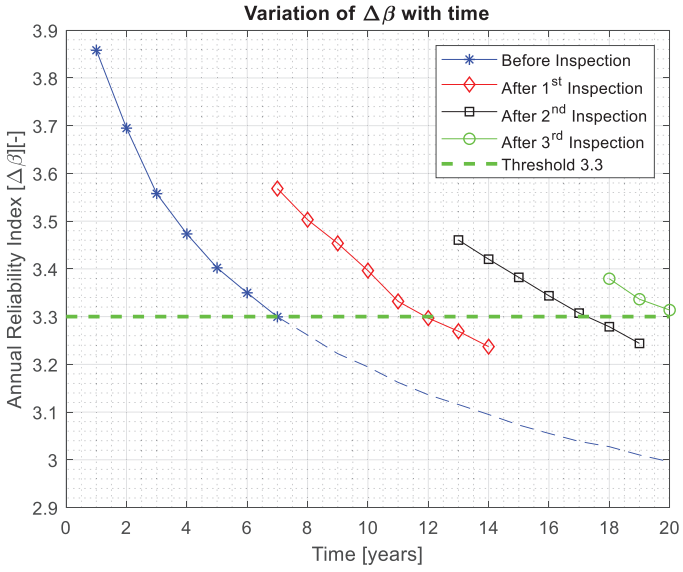

Figure 10 Variation of annual Reliability Index with lifetime considering inspections

8.3 Case#3: Design with consideration of inspection (no damage detected)

As the reliability of the structure is very high, the possibility of damage detection is very low. For the case#3, even less reinforcement is used compared to case#1 and case#2. Only one inspection is carried out during the lifetime. However, no damage is detected, which leads to higher confidence than the first two cases and thus a higher reliability; see Figure 11 & Figure 12. This outcome is again highly dependent on the accuracy of the information obtained from the performed inspection.

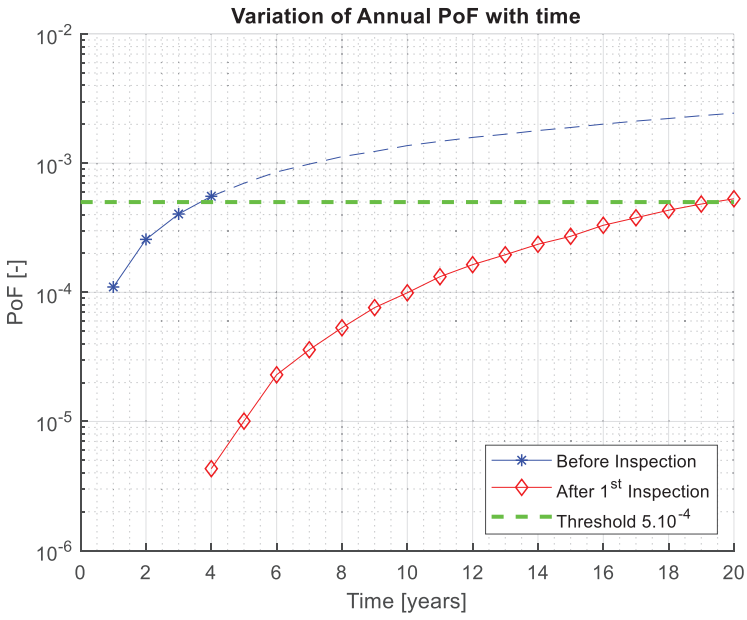

Figure 11 Variation of annual PoF with time considering inspections (no damage detected)

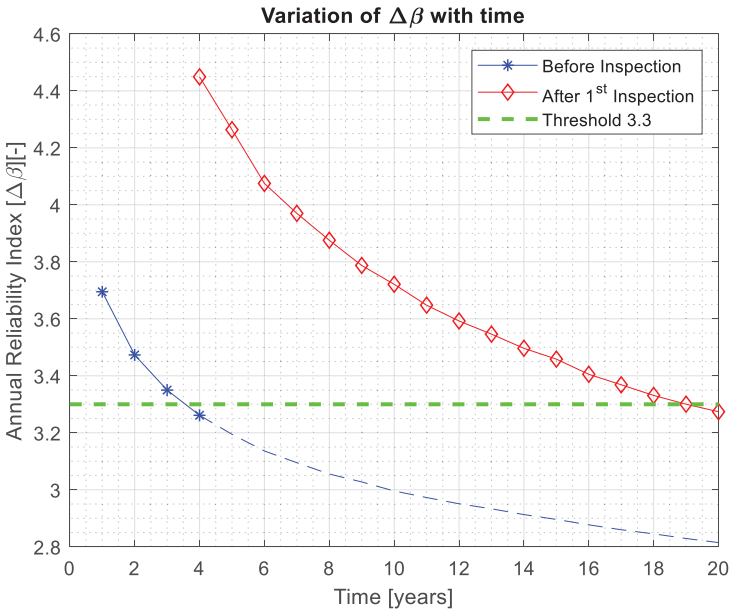

Figure 12 Variation of annual Reliability Index with lifetime considering inspections (no damage detected)

8.4 Comparison of Case#1, Case#2 and Case#3

The comparison of the three cases yields that the total cost to maintain the reliability of the structure above the target reliability throughout the lifetime is highly dependent on the amount of money spent on each inspection and the money spent on the cost of the materials used.

Table 2 Cost comparison

Item / Cost	Case # 1	Case # 2	Case # 3
Reinforcement (X_1/mm^2)	203 300 mm^2	168 500 mm^2	147 000 mm^2
Inspection (X_2/Inspection)	0	3	1
Total	XX_1	XX_2	XX_2

Table 2 compares the cost for all three cases. The conclusion is highly dependent on the cost of inspection and the cost of reinforcement, which may vary based on the geographical locations. In addition, it is important to note that the optimization of the structure in this case is performed just at the critical section, which can be exercised at a few more locations along the shaft or the conical section of the GBF OWT to reduce the reinforcement amount further. In addition, this optimization is based only on the fatigue limit state; other limit states could also be considered where relevant.

9. CONCLUSIONS

This paper presents a probabilistic framework for updating the reliability of concrete structures based on information obtained from inspections. UT is a very good indicator of fatigue damage of concrete claiming that the fatigue damage is assumed to be related to the Miner's fatigue damage (D) and the modulus of elasticity of concrete at start of life (E_{C_0}).

A relation between fatigue damage (D) and US velocity is re-developed based on available data; see [6], which can be used to quantify the damage, given that the damage is detected. The obtained damage can be treated as the equality information to update the probability of failure, see the case#2. If no damage is detected then the PoD of UT can be used to update failure probability, see case#3. Non-detection of the fatigue damage in case#3 shows a high fatigue performance and thus a very low updated probability of failure P_F^U as compared to case#2.

The presented framework helps designers to choose either an initial more costly design (with a relatively large amount reinforcement) with no inspections or initial lighter design (low amount of reinforcement) and frequent inspections achieving a total cost as low as possible.

Further, this framework is exercised only at the critical section and it is assumed that the same amount of reinforcement is used in other sections. However, for complete optimisation, more locations should be included and the reinforcement should be curtailed based on the results.

ACKNOWLEDGEMENTS

Current work is carried out under the project INFRASTAR (infrastar.eu), which has received funding from the European Union's Horizon 2020 research and innovation programme under the Marie Skłodowska-Curie grant agreement No 676139. The grant is gratefully acknowledged. We thank Hakim Ferria, INFRASTAR project manager, IFSTTAR for valuable editorial comments.

10. REFERENCES

[1] G. P. Mallet, Fatigue of Reinforced Concrete (State of the Art Review), Stationery Office Books (TSO), 1991.

[2] CEB 1988, "Fatigue of concrete structures - State of Art Report," CEB, Zurich, 1989.

[3] J. D. Sørensen and A. Mankar, "Probabilistic Design of WInd Turbine Concrete Components subject to fatigue," in *SMMS 2019 A RILEM spring convention and sustainable materials, systems and structures conference*, Rovinj, Croatia, 2019.

[4] A. Strauss, W. Macho, K. Bergmiester, C. Dehlinger and M. Reiterer, "Zyklisch belastete Betonstrukturen: Robustheits- und Redundanzbetrachtungen zur Optimierung der Restnutzungsdauer(Concrete structures under cyclic loading – robustness and redundancy considerations for residual lifetime optimization)," *Bautechnik,* pp. 737-753, 2012.

[5] J. H. Bungey, S. G. Millard and M. G. Grantham, Testing of Concrete in Structures, 4th Edition ed., Oxford: Taylor & Francis, 2006.

[6] S. Urban, A. Strauss, R. Schütz, K. Bergmeister and C. Dehlinger, "Dynamically loaded concrete structures - mointoring-based assessment of the real degree of fatigue deterioration," *Structural Concrete,* vol. 14, no. 4, 2014.

[7] D. C. Montgomery, Design and Analysis of Experiments, Westford, USA: John Wiley & Sons, Inc., 1013.

[8] fib MC2010, "FIB Model Code for concrete structures 2010," Ernst & Sohn, Berlin Germany, 2013.

[9] A. Mankar, S. Rastayesh and J. D. Sørensen, "Sensitivity and Identifiability Study for Uncertainty Analysis of Material Model for Concrete Fatigue," in *IRSEC 2018*, Shiraj, 2018.

[10] A. Mankar, I. Bayane, J. D. Sørensen and E. Brühwiler, "Probabilistic reliability framework for assessment of concrete fatigue of existing RC bridge deck slabs using data from monitoring," *Engineering Structures,* p. Submitted, 2018.

[11] A. Mankar and J. D. Sørensen, "Probabilistic fatigue design of reinforced-concrete wind turbine foundations," in *ICASP-13*, Seoul, South Korea, 2019.

[12] M. A. Miner, "Cumulative damage in fatigue," *American Society of Mechanical Engineers - Journal of Applied Mechanics,* vol. 12, no. 3, pp. 159-164, 1945.

[13] S. Márquez-Domínguez and J. D. Sørensen, "Probabilistic Fatigue Model for Reinforced Concrete Onshore Wind Turbine Foundations," in *Safety, Reliability and Risk Anaysis: Beyond the Horizon ESREL 2013*, Amsterdam, 2013.

[14] S. Thöns, M. Döhler and L. Long, "On damage detection system information for structural systems," *Structural Engineering International,* vol. 28, no. 3, pp. 255-268, 2018.

[15] MIL-HDBK-1823A, Nondestructive evaluation system reliability assessment, Department of Defence Handbook, 2009.

[16] D. Straub, "Reliability updating with equality information," *Probabilistic Engineering Mechanics,* pp. 254-258, 2011.

[17] DNVGL RP 0001, "Probabilistic methods for planning of inspection for fatigue cracks in offshore structures," DNVGL, Oslo, 2015.

[18] T. J. Larsen and A. M. Hansen, "How 2 HAWC2, the user's manual," Risø National Laboratory, 2007.

[19] J. Jonkman, S. Butterfield, W. Musial and G. Scott, "Definition of a 5-MW reference wind turbine for offshore system development," National Renewable Energy Laboratory (NREL), 2009.

[20] IEC 61400-3, "Wind Turbines—Part 3: Design Requirements for Offshore Wind Turbines," International Electrotechnical Commission, 2009.

[21] J. Mann, "Wind field simulation," *Probabilistic engineering mechanics,* vol. 13, no. 4, pp. 269-282, 1998.

[22] J. Velarde, A. Mankar, C. Kramhøft and J. D. Sørensen, "Uncertainty Modeling and Fatigue Reliability Assessment of Offshore Wind Turbine Concrete Structure," *IJOPE,* 2018.

[23] J. Velarde, C. Kramhøft and J. D. Sørensen, "Global sensitivity analysis of offshore wind turbine foundation fatigue loads," *Renewable Energy,* 2019.

[24] IEC 61400-1, Wind turbine generator systems – Part 1: Safety requirements, 4th edition ed., Geneva: International Electrotechnical Commission, 2019.

[25] J. D. Sørensen and H. S. Toft, "Safety Factors IEC 61400-1 background document," DTU Wind Energy, Aalborg, Denmark, 2014.

[26] J. D. Sørensen and H. S. Toft, "Probabilistic Design of Wind Turbines," *Energies,* vol. 3(2), pp. 241-257, 2006.

[27] J. D. Sørensen, "Reliability-based calibration of fatigue safety factors for offshore wind turbines," *International Journal of Offshore and Polar Engineering,* vol. 22, no. 3, pp. 234-241, 2012.

[28] H. S. Toft and , "Probabilistic Design of Wind Turbines," PhD thesis, Aalborg University, 2010.

[29] D. Velakamp, "Chances in Wind Energy - A Probabilistic Approach to Wind Turbine Fatigue Design," PhD thesis, DUWIND Delft University, Wind Energy Research Institute, Delft, 2006.

[30] J. D. Sørensen, Notes in Structural Reliability Theory and Risk Analysis, Aalborg University, 2011.

[31] J. Velarde, C. Kramhøft and J. D. Sørensen, "Reliability-based Design Optimization of Offshore Wind Turbine Concrete Structures," in *ICASP-13*, Seoul, 2019.

[32] V. M. Malhotra, "Testing of Hardened Concrete," in *Testing of Concrete in Structures*, Oxford, Tailor & Francis, 1976, pp. 251-252.

[33] M. Ohtsu, T. Isoda and Y. Tomoda, "ACOUSTIC EMISSION TECHNIQUES STANDARDIZED FOR CONCRETE STRUCTURES," *Acoustic Emission,* no. 25, pp. 21-32, 2007.

[34] NDIS 2421, "Recommended practice for in situ monitoring of concrete structures by acoustic emission," JSNDI, Tokyo, 2000.

[35] A. Bassil, X. Wang, X. Chapeleau, E. Niederleithinger, O. Abraham and D. Leduc, "Distributed Fiber Optics Sensing and Coda Wave Interferometry Techniques for Damage Monitoring in Concrete Structures," *Sensors,* p. 19, 2019.

[36] A. Bassil, X. Chapeleau, D. Leduc and O. Abraham, "Quantification of cracks in reinforced concrete structures using distributed fibre optic sensors," in *9th European Workshop on Structural Health Monitoring* , Manchester, United Kingdom, 2018.

[37] B. Glisic, D. L. Hubbell, D. H. Sigurdardottir and Y. Yao, "Damage detection and characterization using long-gauge and distributed fiber optic sensors," *Optical Engineering,* vol. 52, no. 8, p. 087101, 2013.

[38] G. Rodriguez, J. R. Casas Rius, S. Villalba Herrero and A. J. d. S. Barrias, "Monitoring of shear cracking in partially prestressed concrete beams by distributed optical fiber sensors," in *Maintenance, Monitoring, Safety, Risk and Resilience of Bridges and Bridge Networks*, CRC Press Taylor, 2016.

[39] X. Wang and E. Niederleithinger, "Coda Wave Interferometry used to detect loads and cracks in a concrete structure under field conditions," in *European Workshop on Structural Health Monitoring Series*, Manchester, UK, 2018.

[40] E. Niederleithinger, J. Wolf, F. Mielentz, H. Wiggenhauser and S. Pirskawetz, "Embedded ultrasonic transducers for active and passive concrete monitoring," *Sensors,* pp. 9756-9772, 2015.

[41] E. Niederleithinger, X. Wang, M. Herbrand and M. Müller, "Processing ultrasonic data by coda wave interferometry to monitor load tests of concrete beams," *Sensors,* p. 1971, 2018.

[42] F. Xie, L. Moreau, Y. Zhang and E. Larose, "A Bayesian approach for high resolution imaging of small changes in multiple scattering media," *Ultrasonics,* pp. 106-114, 2016.

[43] X. Wang and E. Niederleithinger, "Monitoring a concrete bridge girder with the coda wave interferometry method," in *International Conference on Smart Monitoring, Assessment and Rehabilitation of Civil Structures*, Postdam, 2019.

[44] M. Ohtsu and H. Watanabe, "Quantitative damage estimation of concrete by acoustic emission," *Construction Building Material,* vol. 15, no. 5, pp. 217-224, 2001.

[45] M. N. Noorsuhada, "An overview on fatigue damage assessment of reinforced concrete structures with the aid of acoustic emission technique," *Construction building Materials,* vol. 112, no. June 2016, pp. 424-439, 2016.

[46] "Nondestructive Testing Handbook, Third Edition: Volume 6, Acoustic Emission Testing (AE)," [Online]. Available: https://www.asnt.org/Store/ProductDetail?productKey=fab658bd-d953-431f-8143-b3cfb1164886.

[47] C. Wang, Y. Zhand and A. Ma, "Investigation into the Fatigue Damage Process of Rubberized Concrete and Plain Concrete by AE Analysis," *Journal of Materials in Civil Engineering,* vol. 23, no. 7, pp. 953-960, 2011.

[48] A. Benavent, E. Castro and A. Gallego, "Evaluation of low-cycle fatigue damage in RC exterior beam-column subassemblages by acoustic emission," *Construction and Building Materials,* vol. 24, no. 10, pp. 1830-1842, 2010.

[49] S. Shahidan, R. Pulin, N. Muhamad Bunnori and K. M. Holford, "Damage classification in reinforced concrete beam by acoustic emission signal analysis," *Construction Building Material,* vol. 45, no. Aug 2013, pp. 78-86, 2013.

[50] K. M. Holford, "Acoustic Emission in Structural Health Monitoring," *Key Engineering Materials,* 2009.

[51] R. Meltzer, K. Lieb, R. Horstman, I. Moore, J. Nielsen and D. Griffin, "Acoustic Emission of Plain Concrete," *Journal of Testing and Evaluation,* vol. 5, no. 6, p. 476, 1977.

[52] T. Shiotani, H. Ohtsu, S. Momoki, H. K. Chai, H. Onishi and T. Kamada, “Damage Evaluation for Concrete Bridge Deck by Means of Stress Wave Techniques,” *Journal of Bridge Engineering,* vol. 17, no. 6, pp. 847-856, 2012.

1
2

Appendix G.

Paper 7

Probabilistic Calibration of Fatigue Safety Factors for Offshore Wind Turbine Concrete Structures

Joey Velarde

Amol Mankar

Claus Kramhøft

John Dalsgaard Sørensen

This papar is published online in

Engineering Structures Journal

https://doi.org/10.1016/j.engstruct.2020.111090

Probabilistic Calibration of Fatigue Safety Factors for Offshore Wind Turbine Concrete Structures

Joey Velarde [a,b], Amol Mankar [b], Claus Kramhøft [a]
& John Dalsgaard Sørensen [b]

[a] *Marine and Foundation Engineering, COWI A/S, 8000 Aarhus, Denmark*
[b] *Department of Civil Engineering, Aalborg University, 9220 Aalborg, Denmark*

Manuscript submitted to *Engineering Structures*

Contents

Probabilistic Calibration of Fatigue Safety Factors for Offshore Wind Turbine Concrete Structures

Joey Velarde [a,b], Amol Mankar [b] , Claus Kramhøft [a]
& John Dalsgaard Sørensen [b]

[a] *Marine and Foundation Engineering, COWI A/S, 8000 Aarhus, Denmark*
[b] *Department of Civil Engineering, Aalborg University, 9220 Aalborg, Denmark*

Abstract

Current fatigue design rules for offshore concrete structures were adopted from the oil and gas industry. When better models or more information are available, partial safety factors can be re-calibrated according to target reliability levels for offshore wind turbines. This paper describes a framework for reliability-based calibration of fatigue partial safety factors for offshore wind turbine concrete structures. Offshore wind turbine loads accounting for the statistical distribution of turbulence intensity are estimated using a fully-integrated aeroelastic model. Based on available experimental fatigue tests, a fatigue reliability model for concrete is formulated and applied in two numerical examples. Results indicate that the recommended material partial safety factor in the DNV standard for *Offshore Concrete Structures* can be lowered without compromising structural safety. The proposed modification can potentially contribute to structural design optimization and further cost reduction in offshore wind energy.

Keywords: offshore wind turbines, fatigue reliability, concrete structures, code calibration, probabilistic design, gravity-based foundations

1 Introduction

The offshore wind energy industry has significantly matured during the last two decades in terms of rated capacities of offshore wind turbines (OWTs), relative scale of support structures and depth of installations. Today, OWTs with rated capacities of 9.5 MW to 12 MW are typically supported by up to 9 m diameter monopiles and installed at wind farm sites with up to 40 m water depth. Alternative to monopiles, concrete gravity-based foundations (GBF) are attractive solutions particularly at shallow to moderate water depths or at site conditions where piling of monopiles exhibit geotechnical challenges. Currently, applications of the GBF were demonstrated for up to 5 MW capacity installed at shallow to moderate water depths in Denmark, Sweden and Belgium [1, 2]. As wind turbine size increases and installations reach further offshore, concrete GBFs can potentially become more cost-effective solutions compared to traditional steel monopiles.

Continuous developments in the industry introduce uncertainties and changes in the loading environment, which make fatigue a more important issue in designing state-of-the-art support structures. Probabilistic methods can be applied to assess the structural reliability of OWT support structures. Most applications of reliability methods have been demonstrated in wind turbine blades [3, 4, 5, 6, 7] and wind turbine components [4, 8]. Fatigue reliability analyses of support

structures have also been demonstrated in several papers [9, 10, 11, 12, 13], mostly for assessment of wind turbine steel towers, monopiles and jacket foundations. Since current fatigue design rules for offshore concrete structures were adopted from the oil and gas industry, a re-assessment of these design rules for offshore wind turbines becomes important for structural design optimization.

This paper describes a framework for reliability-based calibration of fatigue safety factors for OWT concrete foundations. Fatigue design rules for offshore concrete structures are investigated by accounting for relevant load and resistance model uncertainties. Based on available experimental fatigue tests, a fatigue reliability model for concrete is formulated and applied in two numerical examples. The material partial safety factors are recommended based on target reliability levels for offshore wind turbines. Lastly, the sensitivity of concrete fatigue reliability to stochastic parameters are also presented.

2 Fatigue Design Factor Calibration

Structural design codes and standards recommend partial safety factors to account for load and resistance model uncertainties. These partial safety factors were traditionally selected based on sound judgement, accummulated experience or a combination of both. But during the last few decades, reliability-based methods have been applied to optimize structural design codes, which generally result to more rational and consistent reliability levels [14]. The procedure outlined in this section is based on the *Joint Committee on Structural Safety* (JCSS) [15] approach for calibration of safety factors.

2.1 Code calibration

Code calibration refers to the selection of code parameters to achieve a desired level of reliability. It is an optimization procedure, which requires both deterministic and probabilistic design approaches. A practical code calibration procedure can be summarized by the following steps [14, 16]:

1. Define the scope of the code
2. Define the code objectives
3. Define the code format
4. Identify the typical failure modes and related stochastic models
5. Define a measure of closeness between code realization and its objective
6. Determine the optimal partial safety factors for the chosen code format
7. Verify the code and the partial safety factors

The (1) scope of the code refers to the class of the structure and critical failure modes to be considered, while the (2) objectives can be defined by the target reliability indices or target probabilities of failure (refer to sec. 2.2). The (3) code format deals with the number of partial safety factors and load combination factors, if any. In some instances, re-writing of the code format is performed to reflect a more correct design philosophy, to align with other international standards, or to simplify code formulation [14]. Step (4) deals with the identification of the relevant failure modes and the corresponding design and limit state equations. The stochastic models representing

the loads and resistance parameters are also defined, including statistical correlations. Recommendations related to stochastic modeling of load, resistance and model uncertainties can be found in the *JCSS Probabilistic Model Code* [15].

The partial safety factors $\gamma = [\gamma_1, \gamma_2, .., \gamma_n]$ are calibrated considering $j = 1, 2, .., L$ number of relevant failure modes. The measure of closeness defined in step (5), normally expressed as the square of the difference between the target reliability index (β_t) and the actual reliability index (β_j) for failure mode j, is included in a general optimization problem defined by Eq. 1.

$$\min_{\gamma} W(\gamma) = \sum_{j=1}^{L} w_j \left(\beta_j(\gamma) - \beta_t\right)^2 \tag{1}$$

where w_j is the weighting factor indicating the relative importance of design situation j. Based on Eq. 1, the optimal set partial safety factors (γ) can be obtained. It is noted that an alternative optimization problem can be formulated using probabilities of failure instead of reliability indices. The target reliability level could also be different for different failure modes, depending on the consequences of failure.

In step (6), the reliability index (β_j) is normally estimated by FORM/SORM [14] based on the limit state equations and stochastic parameters defined in Step (4). Note that the target reliability level is given with a reference period (typically 1 year). Lastly, the verification (step 7) involves taking into account engineering judgement, practical considerations and accummulated experience.

The scope of the calibration exercise demonstrated in this study considers a concrete GBF for offshore wind turbines. Failure of the concrete foundation due to fatigue damage accummulation is considered, following the DNV code [17] for *Offshore Concrete Structures*. Other relevant design codes for fatigue design of concrete structures, such as the *fib Model Code* [18] and *Eurocode (EN 1990)* [19] are based on a different design format that does not employ *FDF*. This study employs the DNV [17] format. The resistance model for concrete fatigue is further discussed in sec. 5.

2.2 Target reliability level

For unmanned offshore wind turbines, the risk of fatality due to failure of a structural element is not significant. OWTs are therefore classified as having minor consequences of failure with large relative costs of safety measures. Based on Table 1 [15, 20], a target reliability level corresponding to an annual probabilities of failure, $P_f = 10^{-3}$ to $5 \cdot 10^{-4}$ $(\beta = 3.1 - 3.3)$, are normally used in developing design rules for OWTs [21, 22, 23]. This value can vary depending on the possibility of inspection and repair, and on the consequence of fatigue failure (e.g. due to structural redundancy).

Table 1: Tentative target reliability levels related to one year reference period [15]

Relative cost of safety measure	Consequences of failure		
	Minor	Moderate	Large
Large	$\beta = 3.1$ $(P_F \approx 10^{-3})$	$\beta = 3.3$ $(P_F \approx 5 \cdot 10^{-4})$	$\beta = 3.7$ $(P_F \approx 10^{-4})$
Medium	$\beta = 3.7$ $(P_F \approx 10^{-4})$	$\beta = 4.2$ $(P_F \approx 10^{-5})$	$\beta = 4.4$ $(P_F \approx 5 \cdot 10^{-6})$
Small	$\beta = 4.2$ $(P_F \approx 10^{-5})$	$\beta = 4.4$ $(P_F \approx 5 \cdot 10^{-6})$	$\beta = 4.7$ $(P_F \approx 10^{-6})$

2.3 Calibration approach

For fatigue design of offshore steel structures, partial safety factors related load (γ_f) and resistance (γ_Q) models are traditionally expressed in terms of *fatigue design factor*, which is the product of both partial safety factors ($FDF = \gamma_f \gamma_Q$). This is also commonly referred to as *design fatigue factor (DFF)*. The required FDF depends on the possibility of inspection, on the level of exposure and on whether the structural detail is a critical component. A range of FDF values from 1.5 to 3 for steel welded details are recommended by DNVGL [24].

For offshore concrete structures, fatigue design based on FDF has also been adapted, particularly in the DNVGL standard for offshore concrete structures [17]. In addition to safety margin provided by FDF, additional partial safety factor (γ_m) on the concrete material strength is recommended by the code. Proper calibration of these safety factors is essential for cost-effective foundations. A case study [25] on a concrete bridge showed that resistance partial safety factor for fatigue can be lowered without compromising fatigue reliability.

As shown in a previous study [26], the uncertainty related to the concrete fatigue damage model governs the fatigue reliability of OWT concrete structures. This suggests that calibration of material partial safety factor (γ_m) is more rational, and can lead to more profound effects than calibration of FDF. Fig. 1 illustrates the calibration approach performed in this study. Deterministic calculations are performed for a chosen design parameter $\mathbf{z}$. Based on the wind turbine design fatigue load and design resistance models, a set of design parameters ($\mathbf{z}^*$) corresponding to selected partial safety factors (γ_m, FDF) can be derived such that the design equation is satisfied ($G(x_d, \mathbf{z_i}) = 0$). Probabilistic analysis is then carried out using these design parameters to evaluate the reliability level. Finally, a set of material partial safety factors conditional to FDF ($\gamma_m | FDF$) are recommended based on how the code realizations ($\beta(\mathbf{z}^*)$) compare with the target reliability (β_t). The deterministic and probabilistic load and resistance models are discussed in the succeeding sections.

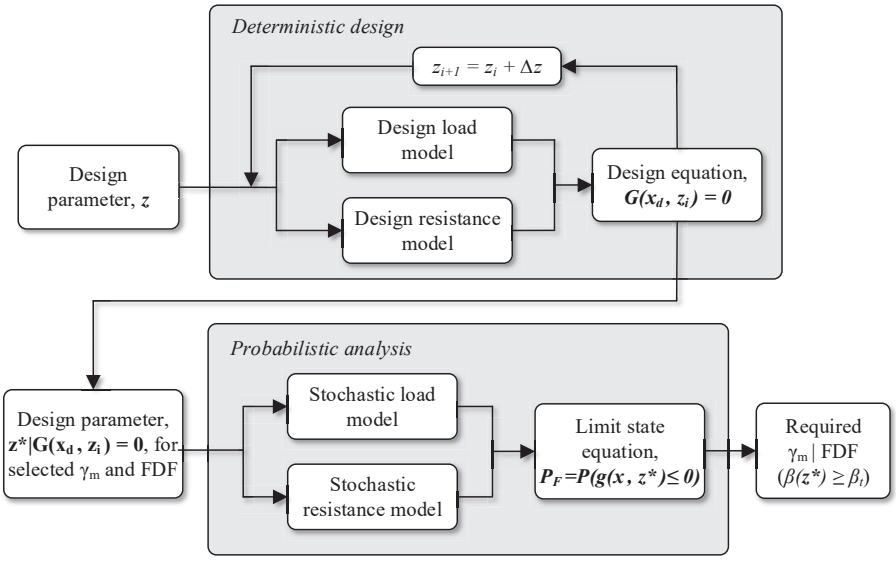

Figure 1: Reliability-based approach for calibration of materal partial safety factor, γ_m

3 Uncertainties in Fatigue Design

Uncertainties can generally be classified into (1) aleatory or (2) epistemic uncertainties. Aleatory uncertainties refer to the physical or inherent randomness, which are found in environmental conditions and material properties. Epistemic uncertainties refer to having limited information or knowledge about a system, and covers statistical, measurement and model uncertainties. Unlike aleatory uncertainties, epistemic uncertainties can be further reduced by increasing the amount of data, improving the quality of data, or developing better mathematical models to describe a physical phenomena. Both aleatory and epistemic uncertainties need to be accounted for when calibrating partial safety factors [16, 6].

Uncertainties are normally modelled by using stochastic parameters defined by a distribution function and distribution parameters. The *JCSS Probabilistic Model Code* [15] recommends probabilistic load and resistance models, which covers a wide range of practical engineering applications. For fatigue assessment of offshore wind turbines, general sources of uncertainty related to the loads include assessment of metocean conditions, aerodynamic models, hydrodynamic models, structural modelling and wind turbine control. On the fatigue resistance side, the primary sources of uncertainties include material fatigue strength and fatigue model—e.g., cumulative linear damage model or fracture mechanics model [4, 15, 27].

4 Wind Turbine Load Effects

Current industry practice for estimation of offshore wind turbine responses is based on running an extensive set of time-domain simulations. A fully integrated OWT model is normally used, where aerodynamic loads, hydrodynamic loads, wind turbine control and soil-structure interaction are considered in each time step (Δt). A case of a concrete GBF is investigated in this study, where the fatigue reliability of the foundations is evaluated for both 5 MW and 10 MW reference wind turbine cases.

4.1 Case study: Thornton Bank GBF concept

The GBF concept based on the Thornton Bank offshore wind farm (Phase 1) considered in this study is shown in Fig. 2. The foundation is approximately 44 m high and has a 23.5 m base diameter, which tapers to 6.5 m diameter at the shaft. The post-tensioned reinforced concrete GBF is originally designed to support a 5 MW OWT at a mean water depth of 25 m in the North Sea.

Figure 2: Thornton bank gravity-based foundation concept © C-Power

4.2 Long-term metocean conditions

The assumed metocean conditions are based on the site characteristics of *Vesterhav Nord* offshore wind farm, which is located at the Danish North Sea. The long-term metocean condtions were generated from the Danish Meteorological Insitute's (DMI) hindcast models, which were validated against 11 years of available measurements. The representative mean wind speeds at hub height (U_{hub}) and turbulence intensities at different fractiles are summarized in Table 2. The U_{hub} is assumed to follow a Weibull distribution, with scale parameter, $A = 10.67\ m/s$ and shape parameter, $k = 2.23$.

Fatigue design loads are calculated using the characteristic value of the turbulence intensity TI_{90}, which is given by the 90% quantile of the turbulence standard deviation (σ_1) as shown in Eq. 2 and Eq. 3, respectively [21]. Design fatigue factors are calibrated based on the safety margin resulting from this design principle.

$$TI_{90} = \sigma_1 / U_{hub} \tag{2}$$

$$\sigma_1 = I_{ref}(0.75U_{hub} + b); \quad b = 5.6\ m/s \tag{3}$$

For probabilic fatigue analysis, it is important to account for the turbulence intensity distribution to avoid hidden safety. A Weibull distribution (Eq. 4) can be assumed for other turbulence standard deviation quantiles (σ_0), with scale (k) and shape (C) parameters defined by Eq. 5 and Eq. 6, respectively [21].

$$F(\sigma_0|U_{hub}) = 1 - \exp\left[-\left(\frac{\sigma_0}{C}\right)^k\right] \tag{4}$$

$$k = 0.27U_{hub} + 1.4 \tag{5}$$

$$C = I_{ref}\,(0.75U_{hub} + 3.3\ m/s) \tag{6}$$

Table 2: Representative U_{hub} and turbulence intensities at different fractiles from wind farm data [28]

Sea state	Wind direction: $0-360$ deg	U_{hub} [m/s]	Occ. [-]	Turbulence Intensity [-]							
				Char.	Other fractiles						
				0.90	0.05	0.20	0.35	0.50	0.65	0.80	0.95
1	4-6	5	0.053	0.262	0.067	0.114	0.145	0.173	0.201	0.235	0.294
2	6-8	7	0.104	0.217	0.069	0.108	0.132	0.153	0.174	0.198	0.239
3	8-10	9	0.152	0.192	0.072	0.106	0.126	0.142	0.158	0.177	0.208
4	10-12	11	0.179	0.176	0.075	0.104	0.121	0.135	0.149	0.164	0.189
5	12-14	13	0.171	0.165	0.077	0.104	0.118	0.130	0.142	0.155	0.176
6	14-16	15	0.130	0.157	0.079	0.103	0.116	0.127	0.137	0.148	0.166
7	16-18	17	0.092	0.151	0.081	0.103	0.115	0.124	0.133	0.143	0.159
8	18-20	19	0.055	0.146	0.082	0.103	0.114	0.122	0.130	0.139	0.153
9	20-22	21	0.030	0.142	0.083	0.103	0.113	0.121	0.128	0.136	0.148
10	22-24	23	0.016	0.139	0.085	0.103	0.112	0.119	0.126	0.133	0.145
11	24-26	25	0.007	0.136	0.086	0.103	0.111	0.118	0.124	0.131	0.141
Total occ. [%]			**98.9**	-	12.5	15.0	15.0	15.0	15.0	15.0	12.5

The lumped representative sea states for fatigue analysis are summarized in Table 3, with the mean significant wave height (H_s) and mean wave period (T_p) derived from wind and wave correlation. Based on the global sensitivity analysis [29] performed on the same case study, it can be assumed that the variation in the predicted fatigue loads is governed by the uncertainty related to the turbulence intensity. For simplicity, the effects of wind and wave directionality are ignored.

Table 3: Representative sea states for fatigue analysis based on wind farm data [28]

Sea state	U_{hub} range	U_{hub} $[m/s]$	Occ. [-]	Mean H_s $[m]$	Mean T_p $[s]$
1	4-6	5	0.053	0.82	6.8
2	6-8	7	0.104	1.01	7.0
3	8-10	9	0.152	1.24	7.1
4	10-12	11	0.179	1.55	7.4
5	12-14	13	0.171	2.01	7.8
6	14-16	15	0.130	2.53	8.2
7	16-18	17	0.092	3.07	8.9
8	18-20	19	0.055	3.65	9.9
9	20-22	21	0.030	4.08	10.4
10	22-24	23	0.016	4.76	11.4
11	24-26	25	0.007	5.40	12.9
Sum			**0.989**		

4.3 Wind turbine load model

The aeroelastic simulation tool, *HAWC2* [30], is used to develop the OWT integrated models where both wind and wave loads are included. *HAWC2* is based on a multibody formulation, where each structural component is modelled by Timoshenko beam elements with six degrees of freedom (6 DOF), x. For a given mass matrix $[M]$, damping matrix $[D]$ and stiffness matrix $[K]$ representing the OWT, the general equation of motion can be written as shown in Eq. 7.

$$[M]\,\ddot{x} + [D]\,\dot{x} + [K]\,x = F_{aero} + F_{hydro} \tag{7}$$

where F_{aero} and F_{hydro} are the aerodynamic and hydrodynamic forces, respectively.

The *HAWC2* model of the Thornton bank GBF supporting a 5 MW reference wind turbine is illustrated in Fig. 3. A combined soil and structural damping ratio, $\zeta_{soil+struc} = 1\%$, is assumed for the first fore-aft and side-side modes. In addition, the aerodynamic and hydrodynamic damping contributions are also considered in the simulations based on the wind and wave input parameters, respectively. Table 4 summarizes the key elevations and reference wind turbine properties used in the simulations.

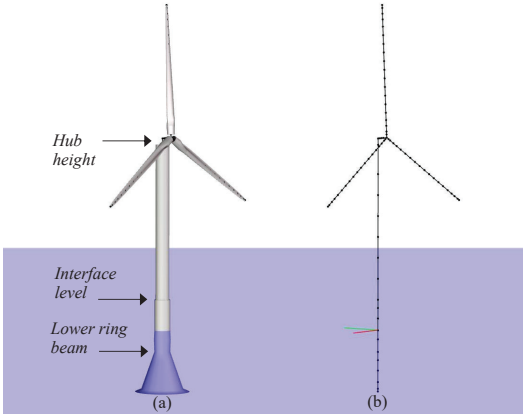

Figure 3: *HAWC2* model of a GBF supporting a 5 MW reference wind turbine: (a) surface model; (b) beam elements

Table 4: Key elevations and reference wind turbine properties [31, 32]

Parameter	NREL 5 MW	DTU 10 MW
Rating $[MW]$	5	10
Rotor diameter $[m]$	126	178.3
Number of blades $[-]$	3	3
Cut-in, rated, cut-out U_w $[m/s]$	3.0, 11.4, 25.0	4.0, 11.4, 25.0
Dynamic rotor speed range $[rpm]$	6.9, 12.1	6.0, 9.6
Hub height $[m]$	91.7	114
Interface elevation $[m]$	14.7	14.7
Mean water depth $[m]$	25	25

For all wind conditions summarized in Table 2, turbulent wind fields were generated based on the *Mann* turbulence model [33]. The Normal Turbulence Model (NTM) [22] is assumed for fatigue analysis. Based on metocean data, metocean data, a power law wind profile is assumed with a shear exponent, $\alpha = 0.08$ (0.14 for characteristic fatigue load). The aerodynamic loads (F_{aero}) were calculated based on the *Blade Element Momentum* (BEM) theory [34, 35].

For all sea states summarized in Table 3, linear irregular waves were generated based on the JONSWAP spectrum. The hydrodynamic loads (F_{hydro}) were calculated based on Morsion's equation [36], where the total force per unit length is defined as the sum of the drag and inertia components. Both load components can be expressed as a function of water density (ρ), sectional area (A), and wave particle velocity (U) and acceleration $(\dot{U})$ as defined by Eq. 8. The drag (C_D) and inertia (C_M) coefficients were calibrated to account for diffraction and secondary steel.

$$F_{hydro} = \rho C_D D U|U| + \rho C_M A \dot{U} \tag{8}$$

Based on modified IEC [22] design load cases (DLC), time-domain fatigue simulations covering power production (DLC 1.2) and idling situations (DLC 6.4) were performed. Each simulation corresponding to the sea states defined in Table 2 and Table 3 has a 10- minutes duration and six independent realizations. The loads are scaled assuming a 95% wind turbine availability and 25 years of design lifetime. For simplicity, wind and wave misalignment is considered not important for this study, and thus unidirectional loading is assumed for both 5 MW and 10 MW cases.

The resulting load time histories are used to estimate the stresses at a critical concrete section. The lower ring beam, located at 14.5 m above the mudline (see Fig. 3), is assumed to be most critical. Using a standard rainflow count algorithm, the number of load cycles for predefined stress bins are derived. Fig. 4 shows the distribution of load cycles (n_{cycles}) according to the mean stress (σ_{mean}) and stress amplitude (σ_{amp}), which is also referred to as the *Markov* matrix. The *Markov* matrices are evaluated together with the design and probabilistic fatigue resistance models, which are presented in the next section.

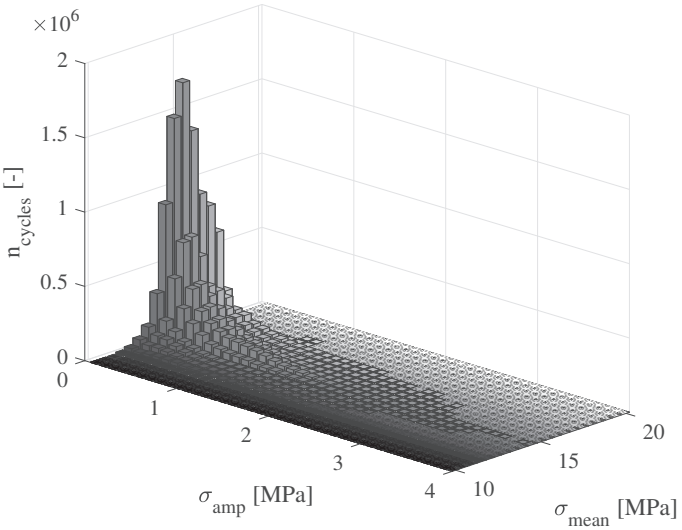

Figure 4: Markov matrix showing annual number of cycles for probabilistic analysis (5 MW OWT) accounting for wind speed and turbulence intensity distribution

5 Concrete Fatigue Reliability Model

During code optimization, it is important to account for the hidden safety margins included in the code format. The following fatigue resistance model formulations are based on recommendations in the DNV standard for *Offshore Concrete Structures* [17].

5.1 Deterministic design

A cumulative linear damage theory [37, 38] is assumed for fatigue assessment. Given the number of stress cycles $(n_{i,j,k})$ and the corresponding number of cycles $(N_{j,k})$ in each sea state bin i, mean stress

bin j and stress amplitude bin k, the damage can be quantified by integrating over the total number of representative sea states (N_{U_w}), mean stress bins $(N_{\sigma_{mean}})$ and stress amplitude bins $(N_{\sigma_{amp}})$. The design equation can be written as shown in Eq. 9. A *Markov* matrix is obtained for each sea state, which is defined according to the mean wind speed (U_w) distribution.

$$G(t,\mathbf{z}) = 1 - \sum_{i=1}^{N_{U_w}} \sum_{j=1}^{N_{\sigma_{mean}}} \sum_{k=1}^{N_{\sigma_{amp}}} \frac{n^d_{i,j,k}\ p_i\ FDF\ T_L}{N^d_{j,k}} = 0 \tag{9}$$

where:

$n^d_{i,j,k}$ is the design number of stress cycles per year at bin i,j,k

$N^d_{j,k}$ is the number of stress cycles to failure at stress bin j,k calculated from the design resistance as a function of the material partial safety factor (γ_m)

p_i is the occurrence probability of design sea state i $(\sum p_i = 1)$

T_L is the design lifetime (25 years)

In addition to the stress cycle amplitude, the mean stress is an important parameter in defining the concrete resistance against fatigue. The S-N curves for concrete are normally expressed in terms of the maximum (σ_{max}) and minimum (σ_{min}) compressive stress within each stress block, which are calculated from the mean (σ_{mean}) and amplitude (σ_{amp}) of each stress cycle as illustrated in Fig. 5. Both σ_{max} and σ_{min} are obtained from the *Markov* matrix.

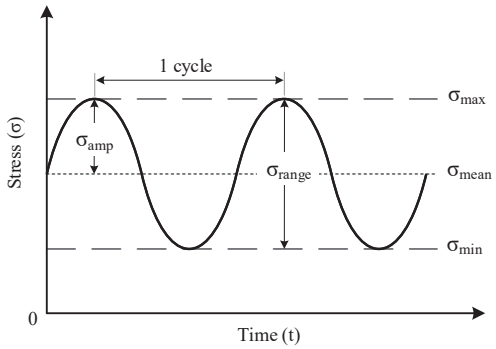

Figure 5: Defintion of a stress cycle mean, amplitude and range

The design number of cycles to failure $(N^d_{j,k})$, with superscript *"d"* indicating design value, is calculated based on Eq. 10. The factor $C_1 = 10$ for structures in water having stress variation in the compression-compression range is used, while the fatigue strength parameter $C_5 = 1$ for concrete [17]. If the calculated design life $(\log_{10} N^d)$ is greater than X^d, this value can be increased by a factor C_2^d. The parameters X^d and C_2^d are expressed as shown in Eq. 11 and Eq. 12, respectively.

$$\log_{10} N^d = \begin{cases} C_1 \dfrac{1 - \dfrac{\sigma_{max}}{C_5 f_{rd}}}{1 - \dfrac{\sigma_{min}}{C_5 f_{rd}}}, & \log_{10} N^d \leq X^d. \\ C_1 C_2^d \dfrac{1 - \dfrac{\sigma_{max}}{C_5 f_{rd}}}{1 - \dfrac{\sigma_{min}}{C_5 f_{rd}}}, & \log_{10} N^d > X^d. \end{cases} \tag{10}$$

$$X^d = \frac{C_1}{1 - \dfrac{\sigma_{min}}{C_1\ f_{rd} + 0.1\ C_1}} \tag{11}$$

$$C_2 = \Big(1 + 0.2(\log_{10} N^d - X)\Big) > 1.0 \tag{12}$$

The design fatigue compressive strength ($f_{rd}\ [MPa]$) is related to the characteristic compressive cylinder strength($f_{cck}\ [MPa]$) by Eq. 13, where $\alpha = 1$ for concrete in compression. Eq. 13 is valid for concrete grades C25 to C90 [17]. Assuming a C45 concrete grade with $f_{cck} = 45\ MPa$ and using a recommended material partial safety factor of $\gamma_m = 1.50$ for concrete fatigue, $f_{rd} \approx\ 27.75\ MPa$.

$$f_{rd} = \alpha \frac{f_{cck}(1 - f_{cck}/600)}{\gamma_m} \tag{13}$$

Concrete design S-N curves are normally expressed as a function of S^d_{max} and S^d_{min}, which are equivalent to the σ_{max} and σ_{min} normalized to the design compressive strength f_{rd} as shown in Eq. 14. The design S-N curve is illustrated in Fig. 6, which also shows the design code safety margin relative to the mean and characteristic curves. The mean curve is derived based the Maximum Likelohood Method (MLM), applied on a database of experimental fatigue tests [39, 40, 41, 42]. In particular, test results with $S_{max} \geq 0.6$ covering $f_{cck} = 20$ to $60\ MPa$ are considered in the MLM fit.

$$S^d_{max} = \frac{\sigma_{max}}{C_5 f_{rd}}, \quad S^d_{min} = \frac{\sigma_{min}}{C_5 f_{rd}} \tag{14}$$

Creep, shrinkage and size effects are not considered in design load calculation, since these effects are not covered by the fatigue test results. The probabilistic analysis covers the uncertainty related to the linear damage accummulation model. In addition, fatigue tests used to evaluate the uncertainty were performed under in-air conditions. For simplicity, the same level of uncertainty is assumed for both air and seawater exposures. The factor C_1 in Eq. 10 adapts the curve for either in-air $(C_1 = 12)$ or seawater $(C_1 = 10)$ conditions.

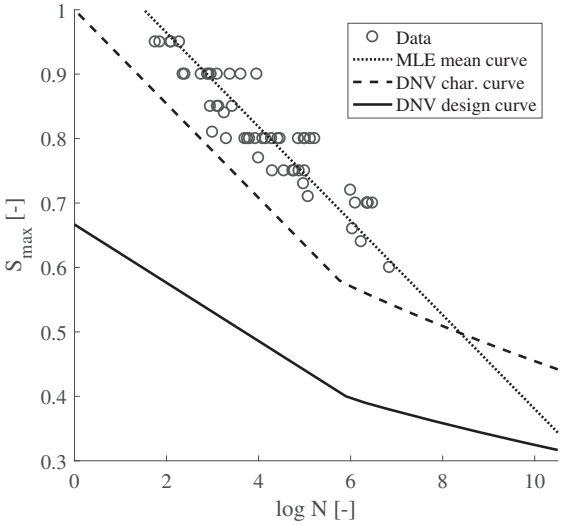

Figure 6: Concrete S-N curve based on available fatigue tests ($S_{min} = 0.12$) and DNV code [17]. All curves are plotted against $S_{max} = \sigma_{max}/f_c$

.

5.2 Probabilistic design

The limit state equation for fatigue failure of concrete is written as shown in Eq. 15. The resistance is represented by the stochastic parameter Δ, which represents the Miner's rule (linear damage accummulation) model uncertainty. In addition to the wind speed (U_w) distribution, the load model also accounts for the statistical distribution of turbulence intensity (TI), which is the governing source of load uncertainty during power production [29]. It is assumed that the uncertainty in the calculated number of cycles ($n_{i,j,k}$) is relatively small.

$$g(\mathbf{z}, t) = \Delta - \sum_{i=1}^{N_{U_w,TI}} \sum_{j=1}^{N_{\sigma_{mean}}} \sum_{k=1}^{N_{\sigma_{amp}}} \frac{n_{i,j,k}\ p_i\ t}{N_{j,k}} \tag{15}$$

where:

$n_{i,j,k}$ is the number of stress cycles per year at bin i, j, k

p_i is the occurrence probability of wind speed and turbulence intensity ($\sum p_i = 1$)

t is the time in years ($0 < t \leq T_L$)

The uncertain parameters in the fatigue resistance model are represented by stochastic variables. Following the same equations used in the design design, the number of stress cycles to failure (N) is calculated using Eq. 16 to 19. In general, predictions of stress amplitudes have higher uncertainties compared to the mean stress estimates. This is accounted for by separately modelling the uncertainties for both mean and amplitude stress components as shown in Eq. 18 and Eq. 19. It is noted that the mean S-N curve illustrated in Fig. 6) is defined without accounting for the asymptotic second slope at the lower maximum stress ranges ($S_{max} < 0.6$) due to lack of experimental tests covering lower stress cycle fatigue supporting this assumption.

$$\log_{10} N = C_1 \frac{1 - \frac{\sigma_{max}}{C_5\, f_{ns}}}{1 - \frac{\sigma_{min}}{C_5\, f_{ns}}} + X_m \tag{16}$$

$$f_{ns} = X_{fc}\, f_{cm} \left(1 - X_{fc}\, f_{cm}/600\right) \tag{17}$$

$$\sigma_{max} = X_{S2}\, X_{stress}\, \sigma_{mean} + X_{S1}\, X_{stress}\, X_{dyn}\, \sigma_{amp} \tag{18}$$

$$\sigma_{min} = X_{S2}\, X_{stress}\, \sigma_{mean} - X_{S1}\, X_{stress}\, X_{dyn}\, \sigma_{amp} \tag{19}$$

where:
X_m models the resistance model uncertainty related to concrete S-N curve
X_{fc} models the concrete strength uncertainty
f_{cm} models the mean static compressive strength in MPa
f_{ns} models the stochastic in-situ compressive strength in MPa
X_{S1} models the load model uncertainty related to the amplitude stress (σ_{amp})
X_{S2} models the load model uncertainty related to the mean stress (σ_{mean})
X_{stress} models the uncertainty related to the stress calculation
X_{dyn} models the uncertainty related to the dynamic response

5.3 Reliability assessment

The limit state equation (Eq. 15) involves the stochastic parameters summarized in Table 5. It is possible that a correlation exists between the load uncertainties X_{S1} and X_{S2}. Statistical indepence is assumed in this case study since the uncertainty sources for the the mean stress (driven by prestressing) and the stress range (driven by wind and wave loads) can be considered partly independent.

Based on Eq. 15, the accumulated probability of failure at time t, $P_F(\mathbf{z}, t) = P(g(\mathbf{z}, t) \leq 0)$, is estimated using First Order Reliability Method (FORM) [14]. Hence, the corresponding reliability index can be estimated as $\beta(\mathbf{z}, t) = -\Phi^{-1}(P_F(\mathbf{z}, t))$, where Φ is the standard normal distribution function. The annual probability of failure (ΔP_F) and annual reliability index $(\Delta\beta)$ is obtained by Eq. 20 and Eq. 21, respectively.

$$\Delta P_F(\mathbf{z}, t) = \frac{P_F(\mathbf{z}, t + \Delta t) - P_F(\mathbf{z}, t)}{(1 - P_F(\mathbf{z}, t))\, \Delta t} \tag{20}$$

$$\Delta\beta(\mathbf{z}, t) = -\Phi^{-1}(\Delta P_F(\mathbf{z}, t)) \tag{21}$$

where $t > \Delta t$ and Δt is the time interval taken as 1 year.

This study investigates two design parameters, namely the prestressing force (F_{PT}) and concrete shaft thickness (t). For simplicity, these parameters are expressed in terms of the ratio of the design parameter value to the default value of prestressing force (z_1) and shaft thickness (z_2) based on the Thornton bank GBF design. Based on the reliability-based calibration approach illustrated in Fig. 1, a relationship between selected safety factors $(\gamma_m,\ FDF)$, design parameters $(z_1,\ z_2)$ and fatigue reliabilty can be derived using the same design equation $(Eq.\ 9)$.

Table 5: Stochastic model parameters for the concrete fatigue; LN: LogNormal; N: Normal; Values inside () applies for the 10 MW case

Parameter	Distribution	Mean	Std.	Remark	Reference
Δ	LN	1.00	0.30	Linear damage accummulation model uncertainty	[43, 44]
X_{S1}	LN	1.00	0.10	Load amplitude uncertainty	[44]
X_{S2}	LN	1.00	0.10	Mean load uncertainty	[44]
X_{dyn}	LN	1.00	0.05 (0.10)	Dynamic response uncertainty	[6]
X_{stress}	LN	1.00	0.05	Stress calculation uncertainty	[6]
X_{fc}	LN	1.00	0.14	Concrete compressive strength uncertainty	[15]
X_m	N	1.52	0.75	Resistance model uncertainty estimated from data	[26]

6 Numerical Examples

The results summarized in this section only considers fatigue failure mode. In addition, no system effects are taken into account. A minimum $\Delta\beta = 3.1$ $\left(P_F \approxeq 10^{-3}\right)$ is assumed acceptable for design of OWT support structures.

6.1 Comparison between γ_m and FDF

The fatigue design equation is formulated with two safety factors, namely the material partial safety factor (γ_m) and fatigue design factor (FDF). Based on the 5 MW OWT case study, an investigation of how variations in both γ_m and FDF affects the annual reliability index $(\Delta\beta)$ is illustrated in Fig. 7.

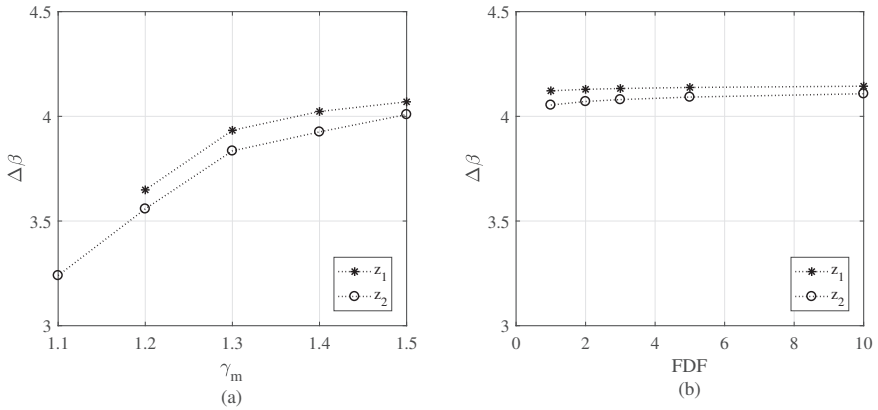

Figure 7: Calculated annual reliability index $(\Delta\beta)$ for the 5 MW case as a function of (a) material partial safety factor, γ_m ($FDF = 3$) and (b) FDF ($\gamma_m = 1.5$) given design parameters z_1 and z_2

For both design parameters, z_1 and z_2, a higher sensitivity on $\Delta\beta$ is observed for variations in γ_m conditional to $FDF = 3$. Alternatively, it can be concluded that the design parameters are not sensitive to changes in FDF conditional to fixed $\gamma_m = 1.5$.

The sensitivity analyses presented in the following sections verify that the uncertainties related to the material resistance model have the highest influence on the fatigue reliability. Hence the following investigation of fatigue reliability is performed for different values of γ_m conditional to $FDF = 3$.

6.2 Example 1: 5 MW Offshore Wind Turbine

Using the design equation (Eq. 9), relationships between material partial safety factor (γ_m) and design parameters z_1 and z_2 are derived as shown in Fig. 8a and Fig. 8b, respectively. The relation between γ_m and z_1 is derived for a fixed value of $z_2 = 1.0$, and vice versa. A lower γ_m allows for higher prestressing force, which is directly related to the mean stress on the concrete section. Similarly, a lower γ_m results to a decrease in the required concrete shaft thickness. The derived relationship only considers concrete fatigue safety.

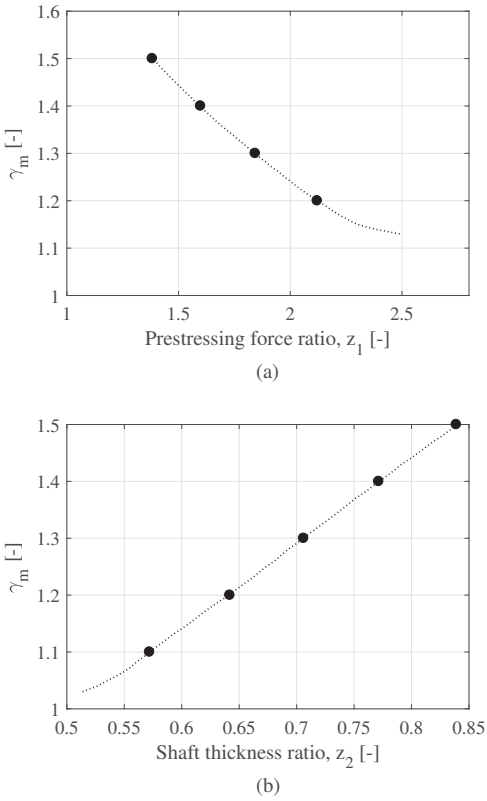

Figure 8: Relationship between material partial safety factor (γ_m) and design parameters (a) z_1 (with $z_2 = 1.0$) and (b) z_2 (with $z_1 = 1.0$) for a 5 MW offshore wind turbine

The reliability indices are calculated based on the relationship between γ_m and design parameters (z_1 z_2). Fig. 9 illustrates the reliability indices as a function of service life in years. The $\Delta\beta$ at end of a 25-year service life are calculated and summarized in Table 6. All design combinations resulted in acceptable $\Delta\beta \geq 3.1$. The results of the reliability analysis indicates that a higher prestressing force (lower γ_m) can be applied on the section if necessary for design optimization. For design parameter z_2, results indicate that the shaft thickness of the original concept design can be reduced without compromising fatigue safety.

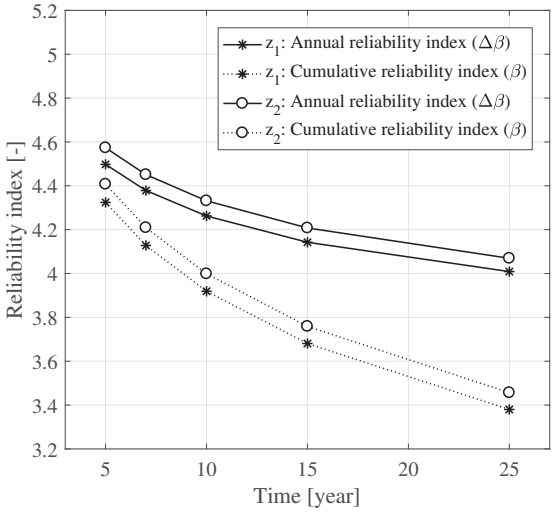

Figure 9: Reliability indices $(\Delta\beta, \beta)$ for z_1 (with $z_2 = 1.0$) and z_2 (with $z_1 = 1.0$) for the 5 MW case as a function of service life $(\gamma_m = 1.5)$

Table 6: Annual reliability index $(\Delta\beta)$ for different combinations of material partial safety factor (γ_m) and design parameters $(z_1,\ z_2)$ conditional to $FDF = 3$ for a 5 MW OWT

γ_m $[-]$	Prestressing force		Shaft thickness		$\Delta\beta$
	z_1	F_{PT} $[MN]$	z_2	t $[mm]$	
1.1	-	-	-	-	-
1.2	2.12	197	1.00	500	3.65
1.3	1.84	171	1.00	500	3.93
1.4	1.60	149	1.00	500	4.02
1.5	1.38	129	1.00	500	4.07
1.1	1.00	93	0.57	286	3.24
1.2	1.00	93	0.64	321	3.56
1.3	1.00	93	0.71	353	3.83
1.4	1.00	93	0.77	386	3.93
1.5	1.00	93	0.84	419	4.01

6.3 Example 2: 10 MW Offshore Wind Turbine

Numerical example 2 considers the same GBF concept to support a 10 MW offshore wind turbine. Fig. 10a and Fig. 10b show the derived relationships between γ_m and design parameters z_1 and z_2, respectively, following the same trend as example 1. To accommodate higher mean and amplitude loads and to satisfy the design equation at different values of z_1, the shaft thickness is increased by 50% ($z_2 = 1.5$). The same amount of prestressing force ($z_1 = 1.0$) can be assumed for variations in design parameter z_2.

The resulting reliability indices as a function of service life in years are shown in Fig. 11. The $\Delta\beta$ at end of a 25-year service life are calculated and summarized in Table 7. All design combinations resulted in acceptable $\Delta\beta \geq 3.1$, except for the design configuration with $\gamma_m = 1.1$, $z_1 = 1.00$ and

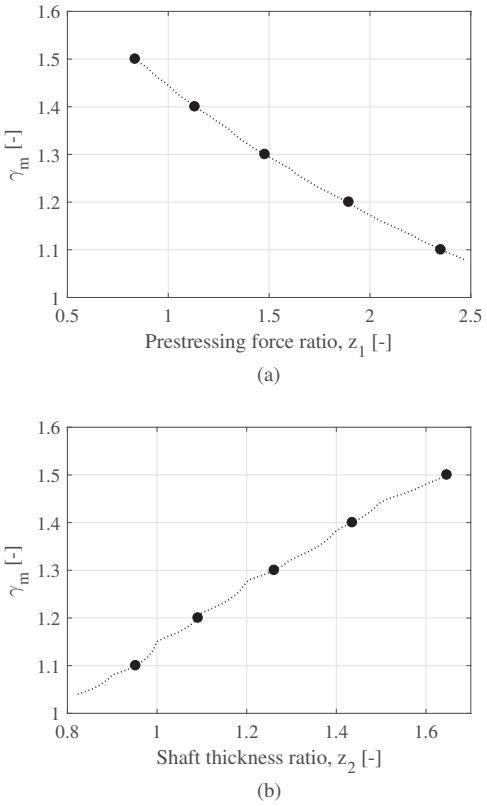

Figure 10: Relationship between material partial safety factor (γ_m) and design parameters (a) z_1 (with $z_2 = 1.5$) and (b) z_2 (with $z_1 = 1.0$) for a 10 MW reference case.

$z_2 = 0.95$. The results indicate that the same GBF concept initially design for a 5 MW OWT can be used to support a 10 MW OWT, with minor modifications in design parameters. Similar to example 1, it can also be concluded that a lower γ_m can be recommended without compromising fatigue safety, even for large wind turbines whose support structure design can be driven by fatigue.

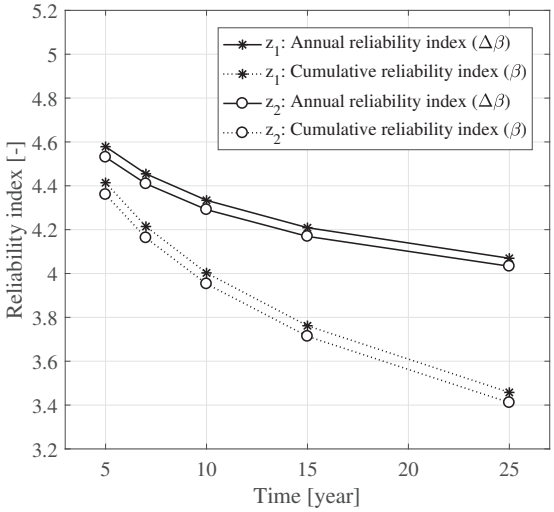

Figure 11: Reliability indices $(\Delta\beta, \beta)$ for z_1 (with $z_2 = 1.0$) and z_2 (with $z_1 = 1.0$) for the 10 MW case as a function of service life $(\gamma_m = 1.5)$

Table 7: Annual reliability index $(\Delta\beta)$ for different combinations of material partial safety factor (γ_m) and design parameters $(z_1,\ z_2)$ conditional to $FDF = 3$ for a 10 MW OWT

γ_m $[-]$	Prestressing force		Shaft thickness		$\Delta\beta$
	z_1	F_{PT} $[MN]$	z_2	t $[mm]$	
1.1	2.35	219	1.50	750	3.31
1.2	1.90	176	1.50	750	3.58
1.3	1.48	138	1.50	750	3.87
1.4	1.13	105	1.50	750	3.99
1.5	0.84	78	1.50	750	4.03
1.1	1.00	93	0.95	476	3.08
1.2	1.00	93	1.09	546	3.38
1.3	1.00	93	1.26	631	3.76
1.4	1.00	93	1.44	718	3.98
1.5	1.00	93	1.65	823	4.07

6.4 Proposed material safety factor (γ_m)

The DNV standard for *Offshore Concrete Structures* [17] currently recommends a $\gamma_m = 1.5$. Table 8 summarizes the corresponding reduction in concrete shaft thickness and $\Delta\beta$ as a function of γ_m. Results from the 5 MW case indicate that a $\gamma_m = 1.1$ can be used, which leads to about 32% reduction in the required shaft thickness. Similarly, results from the 10 MW case indicate that a $\gamma_m = 1.2$ can be used, which leads to about 34% reduction in the required shaft thickness. Based on the two numerical examples presented above, a lower value of $\gamma_m = 1.1$ to 1.2 can be used while still satisfying the required safety level $(\Delta\beta \geq 3.1)$. This reduction can significantly lead to a more optimal concrete foundation design.

Table 8: Reduction in shaft thickness (%) and reliability index ($\Delta\beta$) as a function of material partial safety factor (γ_m) for both 5 MW and 10 MW cases

γ_m	5 MW		10 MW	
	Reduction [%]	$\Delta\beta$	Reduction [%]	$\Delta\beta$
1.1	31.8	3.24	42.2	3.08
1.2	23.5	3.56	33.7	3.38
1.3	15.8	3.83	23.4	3.76
1.4	8.0	3.93	12.8	3.98
1.5	0.0	4.01	0.0	4.07

6.5 Sensitivity to input parameters

The sensitivity of the reliability index to each stochastic input parameter (i) can be expressed in terms of the square of the alpha factors (α_i^2), which are determined by FORM. Table 9 and Table 10 summarize the calculated α_i^2 factors for both 5 MW and 10 MW offshore wind turbine cases, respectively.

The relative importance of stochastic parameters vary according to the assumed γ_m and correspoding design parameters. In general, the uncertainty related to concrete compressive strength (X_{fc}) is the governing parameter at lower γ_m values ($\gamma_m = 1.1,\ 1.2,\ 1.3$). These are associated with design configurations with high prestressing force or low shaft thickness, where the most likely fatigue failure is due to the relatively high mean stresses that result to lower resistance or number of cycles. On the other hand, design configurations at higher γ_m values ($\gamma_m = 1.4,\ 1.5$) have lower magnitudes of stress cycles. These designs are governed by the fatigue resistance model uncertainty (X_m). The variations in α_i^2 factors for the 5 MW case are illustrated in Fig. 12 and Fig. 13. Comparable results are found for the 10 MW case as illustrated in Fig. 14 and Fig. 15.

Table 9: Sensitivity factors (α_i^2) of stochastic input parameters for the 5 MW case at different values of design parameters, $z_1|\gamma_m$ and $z_2|\gamma_m$

Parameter	Prestressing force ratio, $z_1\|\gamma_m$				Shaft thickness ratio, $z_2\|\gamma_m$				
	1.2	1.3	1.4	1.5	1.1	1.2	1.3	1.4	1.5
Δ	0.002	0.003	0.029	0.030	0.004	0.005	0.007	0.028	0.030
X_{S1}	0.013	0.017	0.008	0.004	0.030	0.032	0.035	0.013	0.006
X_{S2}	0.235	0.216	0.007	0.002	0.171	0.157	0.137	0.009	0.003
X_{fc}	0.599	0.592	0.047	0.020	0.567	0.551	0.520	0.072	0.027
X_{stress}	0.091	0.089	0.007	0.003	0.086	0.083	0.078	0.011	0.004
X_{dyn}	0.003	0.004	0.002	0.001	0.007	0.008	0.009	0.003	0.002
X_m	0.057	0.079	0.901	0.939	0.134	0.164	0.215	0.864	0.929
$\sum_{i=1} \alpha_i^2$	1.000	1.000	1.000	1.000	1.000	1.000	1.000	1.000	1.000

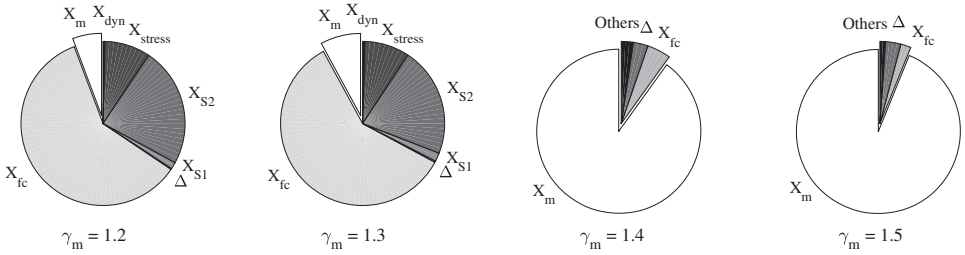

Figure 12: Sensitivity (α_i^2) of fatigue reliability $(\Delta\beta)$ to stochastic input parameters for the 5 MW case at different values of design parameter, $z_1|\gamma_m = 1.2,\ 1.3,\ 1.4,\ 1.5$

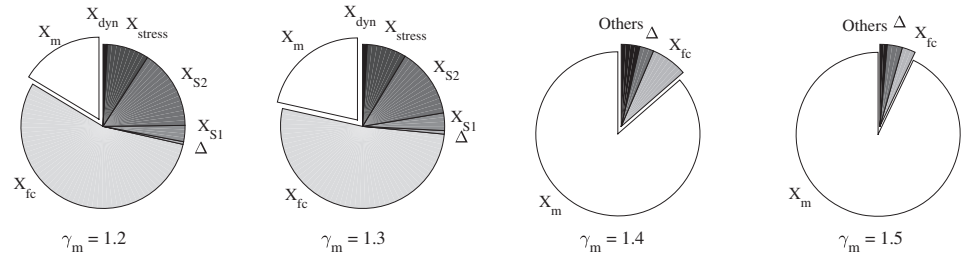

Figure 13: Sensitivity (α_i^2) of fatigue reliability $(\Delta\beta)$ to stochastic input parameters for the 5 MW case at different values of design parameter, $z_2|\gamma_m = 1.2,\ 1.3,\ 1.4,\ 1.5$

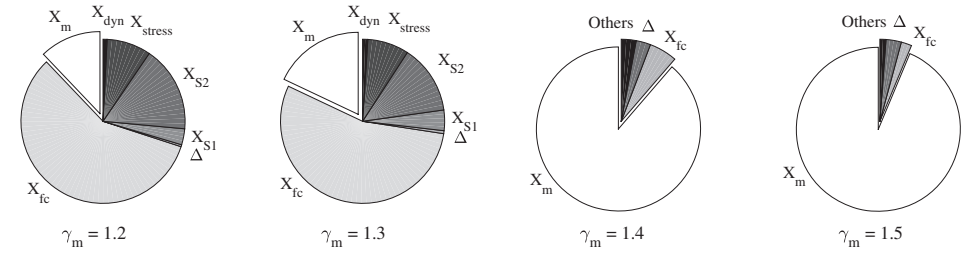

Figure 14: Sensitivity (α_i^2) of fatigue reliability $(\Delta\beta)$ to stochastic input parameters for the 10 MW case at different values of design parameter, $z_1|\gamma_m = 1.2,\ 1.3,\ 1.4,\ 1.5$

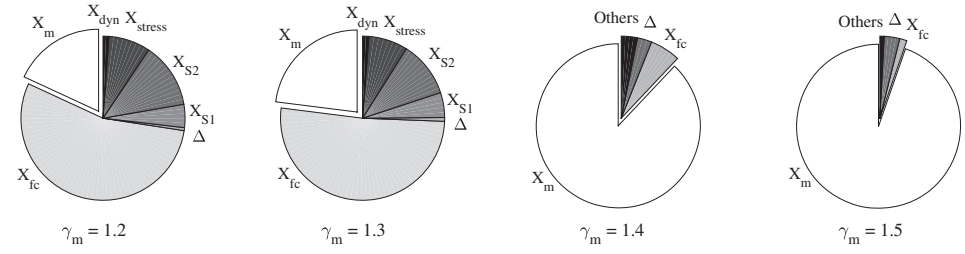

Figure 15: Sensitivity (α_i^2) of fatigue reliability $(\Delta\beta)$ to stochastic input parameters for the 10 MW case at different values of design parameter, $z_2|\gamma_m = 1.2,\ 1.3,\ 1.4,\ 1.5$

Table 10: Sensitivity factors (α_i^2) of stochastic input parameters for the 10 MW case at different values of design parameters, $z_1|\gamma_m$ and $z_2|\gamma_m$

Parameter	Prestressing force ratio, $z_1\|\gamma_m$					Shaft thickness ratio, $z_2\|\gamma_m$				
	1.1	1.2	1.3	1.4	1.5	1.1	1.2	1.3	1.4	1.5
Δ	0.003	0.004	0.006	0.029	0.030	0.005	0.006	0.007	0.028	0.031
X_{S1}	0.025	0.032	0.040	0.012	0.006	0.041	0.046	0.049	0.013	0.004
X_{S2}	0.194	0.169	0.136	0.005	0.001	0.145	0.129	0.110	0.006	0.001
X_{fc}	0.592	0.579	0.546	0.055	0.021	0.561	0.545	0.514	0.060	0.014
X_{stress}	0.090	0.087	0.082	0.009	0.003	0.086	0.082	0.077	0.009	0.002
X_{dyn}	0.006	0.008	0.010	0.003	0.001	0.010	0.011	0.012	0.003	0.001
X_m	0.089	0.121	0.180	0.887	0.937	0.152	0.181	0.230	0.880	0.947
$\sum_{i=1} \alpha_i^2$	1.000	1.000	1.000	1.000	1.000	1.000	1.000	1.000	1.000	1.000

The results above are based on a resistance model uncertainty X_m with COV $X_{m\ COV} = 0.50$, which is estimated from available fatigue tests. A simple sensitivity study to investigate the importance of this COV is performed for the 5 MW case by assuming $X_{m\ COV} = 0.25$. The results are summarized in Table 11 and Fig. 16. Note that the lower COV could probably be obtained in a narrow subset of the fatigue test data, covering only the application for this type of substructure.

Table 11: Calculated sensitivity factors (α_i^2) of stochastic input parameters assuming $X_{m\ COV} = 0.50$ ($\Delta\beta = 4.01$) and $X_{m\ COV} = 0.25$ ($\Delta\beta = 4.72$)

Sensitivity ranking	$X_{m\ COV} = 0.50$		$X_{m\ COV} = 0.25$	
	Parameter	α_i^2	Parameter	α_i^2
1	X_m	0.9294	X_{fc}	0.6409
2	Δ	0.0300	X_{S2}	0.2024
3	X_{fc}	0.0265	X_{stress}	0.0941
4	X_{S1}	0.0059	X_{S1}	0.0264
5	X_{stress}	0.0041	X_m	0.0261
6	X_{S2}	0.0026	X_{dyn}	0.0066
7	X_{dyn}	0.0015	Δ	0.0034
$\sum \alpha_i^2$		1.00		1.00

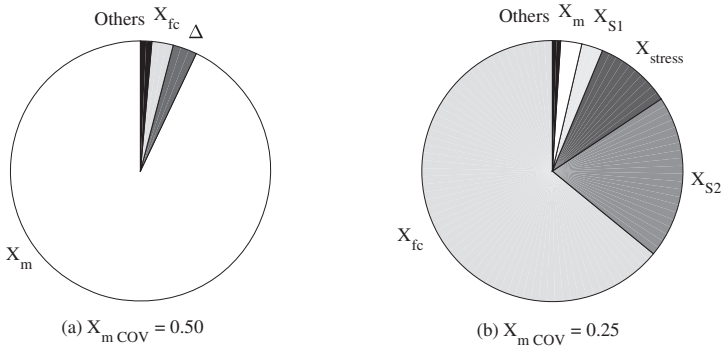

Figure 16: Sensitivity (α_i^2) of fatigue reliability $(\Delta\beta)$ to stochastic input parameters assuming (a) $X_{m\ COV} = 0.50$ and (b) $(b) X_{m\ COV} = 0.25$ for $\gamma_m = 1.5$ $(z_1 = 1.0,\ z_2 = 0.84)$

7 Summary and Conclusions

This paper demonstrates a probabilistic approach for reassessment of fatigue design rules for offshore wind turbine concrete structures. Offshore wind turbine loads accounting for the statistical distribution of turbulence intensity are estimated based on a fully-integrated model. Using available concrete fatigue tests, a fatigue reliability model is formulated based on the DNV code [17]. Reliability-based calibration of the material partial safety factor (γ_m) is demonstrated, while accounting for the relevant sources of uncertainties in both load and resistance models.

Safety margins in fatigue design of offshore concrete structures can be incorporated in terms on FDF and γ_m. The study showed that fatigue reliability is more sensitive to changes in γ_m. Two numerical examples of a concrete GBF supporting a 5 MW and 10 MW OWTs also showed that a lower γ_m can be used without compromising fatigue safety. Reducing the recommended value from $\gamma_m = 1.5$ to $\gamma_m = 1.1$ to 1.2 can lead to about 33% reduction in the required shaft thickness for both 5 MW and 10 MW cases. Lastly, the relative importance of stochastic input parameters are investigated. Depending on the assumed γ_m, reliability indices can be very sensitive to uncertainties related to concrete compressive strength (X_{fc}) and resistance model uncertainty (X_m).

A major limitation of the study is the lack of experimental concrete fatigue test data at lower stress amplitude cycles (high cycle fatigue tests). It is currently assumed that the same amount of uncertainty exists with concrete exposed to moderate stress levels. In addition, the study is limited to compression-compression fatigue cycles as assured by the prestressing, and does not take into account the effect of inspection which are difficult to perform and model in a probabilistic framework. Nonetheless, the presented framework can be applied to investigate fatigue reliability of other foundation concepts. Based on the main results presented, this study opens opportunities for life extension or repowering of offshore wind turbine concrete foundations approaching the end of their service lives.

Acknowledgements

This research work was performed within the European project INFRASTAR, which has received funding from the European Union's Horizon 2020 research and innovation programme under the Marie Skłodowska-Curie grant agreement No 676139.

References

[1] M. D. Esteban et al. "Gravity based support structures for offshore wind turbine generators: Review of the installation process". eng. In: *Ocean Engineering* 110 (2015), pp. 281–291. ISSN: 18735258, 00298018. DOI: 10.1016/j.oceaneng.2015.10.033.

[2] M Dolores Esteban, José-Santos López-Gutiérrez, and Vicente Negro. "Gravity-Based Foundations in the Offshore Wind Sector". In: *Journal of Marine Science and Engineering* 7.3 (2019), p. 64.

[3] Knut O Ronold, Jakob Wedel-Heinen, and Carl J Christensen. "Reliability-based fatigue design of wind-turbine rotor blades". In: *Engineering structures* 21.12 (1999), pp. 1101–1114.

[4] Dick Veldkamp. "A probabilistic evaluation of wind turbine fatigue design rules". In: *Wind Energy* 11.6 (2008), pp. 655–672.

[5] John D Sørensen and Henrik S Toft. "Probabilistic design of wind turbines". In: *Energies* 3.2 (2010), pp. 241–257.

[6] Henrik Stensgaard Toft and John Dalsgaard Sørensen. "Reliability-based design of wind turbine blades". In: *Structural Safety* 33.6 (2011), pp. 333–342.

[7] Henrik Stensgaard Toft et al. "Uncertainty modelling and code calibration for composite materials". In: *Journal of Composite Materials* 47.14 (2013), pp. 1729–1747.

[8] Amir Rasekhi Nejad, Zhen Gao, and Torgeir Moan. "On long-term fatigue damage and reliability analysis of gears under wind loads in offshore wind turbine drivetrains". In: *International Journal of Fatigue* 61 (2014), pp. 116–128.

[9] John Dalsgaard Sørensen. "Reliability-Based Calibration of Fatigue Safety Factors For Offshore Wind Turbines". In: *International Journal of Offshore and Polar Engineering* 22.03 (2012).

[10] Sergio Márquez-Domínguez and John D Sørensen. "Fatigue reliability and calibration of fatigue design factors for offshore wind turbines". In: *Energies* 5.6 (2012), pp. 1816–1834.

[11] Wenbin Dong, Torgeir Moan, and Zhen Gao. "Fatigue reliability analysis of the jacket support structure for offshore wind turbine considering the effect of corrosion and inspection". In: *Reliability Engineering & System Safety* 106 (2012), pp. 11–27.

[12] Quang A. Mai et al. "Prediction of remaining fatigue life of welded joints in wind turbine support structures considering strain measurement and a joint distribution of oceanographic data". In: *Marine Structures* 66 (2019), pp. 307 –322. ISSN: 0951-8339. DOI: https://doi.org/10.1016/j.marstruc.2019.05.002. URL: http://www.sciencedirect.com/science/article/pii/S095183391830217X.

[13] Jan-Tore Horn and Bernt J Leira. "Fatigue reliability assessment of offshore wind turbines with stochastic availability". In: *Reliability Engineering & System Safety* (2019), p. 106550.

[14] Henrik O Madsen, Steen Krenk, and Niels Christian Lind. *Methods of structural safety*. Courier Corporation, 2006.

[15] JCSS JCSS. "Probabilistic model code". In: *Joint Committee on Structural Safety* (2001).

[16] MH Faber and John Dalsgaard Sørensen. "Reliability-Based Code Calibration: The JCSS Approach". In: *9th International Conference on Applications of Statistics and Probability in Civil Engineering*. Millpress. 2003, pp. 927–935.

[17] Det Norsk Veritas. "Offshore Concrete Structures–DNV OS-C502". In: *Det Norsk Veritas, Norway* (2012).

[18] fib. *FIB Model Code for concrete structures 2010*. 2010.

[19] Eurocode No. "2, Design of concrete structures". In: *European Committee for Standardization* (1992).

[20] International Standards Organization. *ISO 2394: 2015: General principles on reliability for structures*. 2015.

[21] International Electrotechnical Commission et al. “IEC 61400-1”. In: *Wind Turbines—Part 1: Design Requirements* (2019).

[22] International Electrotechnical Commission et al. “IEC 61400-3”. In: *Wind Turbines—Part 3: Design Requirements for Offshore Wind Turbines* (2009).

[23] GL DNV. “Support structures for wind turbines”. In: *Standard DNVGL-ST-0126* (2018).

[24] GL DNV. “Fatigue design of offshore steel structures”. In: *Recommended Practice DNVGL-RP-C203* 20 (2016).

[25] Amol Mankar et al. “Probabilistic reliability framework for assessment of concrete fatigue of existing RC bridge deck slabs using data from monitoring”. In: *Engineering Structures* 201 (2019), p. 109788. ISSN: 0141-0296. DOI: https://doi.org/10.1016/j.engstruct.2019.109788. URL: http://www.sciencedirect.com/science/article/pii/S0141029619300045.

[26] Joey Velarde et al. “Uncertainty Modeling and Fatigue Reliability Assessment of Offshore Wind Turbine Concrete Structures”. In: *International Journal of Offshore and Polar Engineering* 29.02 (2019), pp. 165–171.

[27] JD Sørensen and HS Toft. “Safety Factors—IEC 61400-; 4—Background Document”. In: *DTU Wind Energy-E-Report-0066 (EN)* (2014).

[28] Joey Velarde et al. “Fatigue reliability of large monopiles for offshore wind turbines”. English. In: *International Journal of Fatigue* (2019). ISSN: 0142-1123.

[29] Joey Velarde, Claus Kramhøft, and John Dalsgaard Sørensen. “Global sensitivity analysis of offshore wind turbine foundation fatigue loads”. In: *Renewable Energy* (2019). ISSN: 0960-1481. DOI: https://doi.org/10.1016/j.renene.2019.03.055. URL: http://www.sciencedirect.com/science/article/pii/S096014811930360X.

[30] Torben Juul Larsen and Anders Melchior Hansen. “How 2 HAWC2, the user’s manual”. In: *target* 2 (2015), p. 2.

[31] Jason Jonkman et al. *Definition of a 5-MW reference wind turbine for offshore system development*. Tech. rep. National Renewable Energy Laboratory (NREL), Golden, CO., 2009.

[32] Christian Bak et al. “Description of the DTU 10 MW reference wind turbine”. In: *DTU Wind Energy Report-I-0092* 5 (2013).

[33] Jakob Mann. “Wind field simulation”. In: *Probabilistic engineering mechanics* 13.4 (1998), pp. 269–282.

[34] Hermann Glauert. “Airplane propellers”. In: *Aerodynamic theory*. Springer, 1935, pp. 169–360.

[35] Martin OL Hansen and Helge Aagaard Madsen. “Review paper on wind turbine aerodynamics”. In: *Journal of fluids engineering* 133.11 (2011), p. 114001.

[36] JR Morison, JW Johnson, SA Schaaf, et al. “The force exerted by surface waves on piles”. In: *Journal of Petroleum Technology* 2.05 (1950), pp. 149–154.

[37] Arvid Palmgren. “Die lebensdauer von kugellagern”. In: *Zeitschrift des Vereins Deutscher Ingenieure* 68.14 (1924), pp. 339–341.

[38] Milton A Miner et al. “Cumulative damage in fatigue”. In: *Journal of applied mechanics* 12.3 (1945), pp. 159–164.

[39] Eigil V Sørensen. “Fatigue life of high performance grout in dry and wet environment for wind turbine grouted connections”. In: *Nordic Concrete Research* 44 (2011), pp. 1–10.

[40] Ludger Lohaus, Nadja Oneschkow, and Maik Wefer. “Design model for the fatigue behaviour of normal-strength, high-strength and ultra-high-strength concrete”. In: *Structural Concrete* 13.3 (2012), pp. 182–192.

[41] EOL Lantsoght. “Fatigue of concrete under compression: Database and proposal for high strength concrete”. In: *Report nr. 25.5-14-04* (2014).

[42] Marc Thiele. “Experimentelle Untersuchung und Analyse der Schädigungsevolution in Beton unter hochzyklischen Ermüdungsbeanspruchungen”. In: (2016).

[43] Rasmus Folsø, Sven Otto, and Guy Parmentier. “Reliability-based calibration of fatigue design guidelines for ship structures”. In: *Marine Structures* 15.6 (2002), pp. 627–651.

[44] Henrik Stensgaard Toft et al. “Uncertainty in wind climate parameters and their influence on wind turbine fatigue loads”. In: *Renewable Energy* 90 (2016), pp. 352–361.

ISSN (online): 2446-1636
ISBN (online): 978-87-7210-551-2

AALBORG UNIVERSITY PRESS